

**Study on biomedical and chemical reactions
in culture medium irradiated with
non-equilibrium atmospheric pressure plasmas**

Naoyuki KURAKE

2017

Nagoya University

Department of Electrical Engineering and Computer Science

Chapter 1 Introduction

§ 1.1 Non-equilibrium atmospheric pressure plasma	
§ 1.1.1 Characteristic	1
§ 1.1.2 Mechanism of NEAPP effects	3
§ 1.1.3 Current applications	8
§ 1.2 Plasma cancer therapy	
§ 1.2.1 Cancer therapy	14
§ 1.2.2 Direct NEAPP irradiation	17
§ 1.2.3 Plasma activated medium (PAM)	21
§ 1.2.4 Reactive oxygen and nitrogen species (RONS)	25
§ 1.3 Plasma organic synthesis and crystallization	
§ 1.3.1 Oxalic acid generation	27
§ 1.3.2 Interactions between plasma and organic species	29
§ 1.3.3 Plasma inducing organic crystallization	30
§ 1.3.4 Plasma inducing oxalic acid synthesis	31
§ 1.4 Objective of this study	32
§ 1.5 Chapters in the thesis	35
References for Chapter 1	37

Chapter 2 Experimental setup and evaluation methods of

PAM and crystals

§ 2.1 Plasma source	42
§ 2.2 Cell culture medium	44
§ 2.3 Method of plasma treatments	
§ 2.3.1 Making PAM	46
§ 2.3.2 Calcium oxalate crystal synthesis	49
§ 2.4 Optical emission spectroscopy (OES)	
§ 2.4.1 Theory	50
§ 2.4.2 Measurement	52
§ 2.5 Electron spin Resonance (ESR)	
§ 2.5.1 Theory	54
§ 2.5.2 Spin-trapping method	57

Contents

§ 2.6 Chemical probe method	
§ 2.6.1 Theory	61
§ 2.6.2 Micro plate reader	63
§ 2.6.3 Hydrogen peroxide (H ₂ O ₂)	64
§ 2.6.4 nitrite and nitrate ion (NO ₂ ⁻ / NO ₃ ⁻)	67
§ 2.7 Gas chromatography and mass spectrometry (GC-MS)	
§ 2.7.1 Theory	70
§ 2.7.2 Derivatization method	75
§ 2.8 Microscope observation	78
§ 2.9 Analysis using cells	
§ 2.9.1 Cell passaging	80
§ 2.9.2 Cell survival assay	82
§ 2.9.3 Fluorescence probe	85
§ 2.10 Metabolomics	
§ 2.10.1 Theory	87
§ 2.10.2 Capillary electrophoresis and mass spectrometry (CE-MS)	89
§ 2.10.3 Principal component analysis (PCA)	91
§ 2.11 X-ray diffraction (XRD)	
§ 2.11.1 Theory	92
§ 2.11.2 Rietveld analysis	94
§ 2.12 Scanning electron microscope and energy dispersive X-ray spectrometry (SEM-EDX)	95
§ 2.13 Fourier Transform infrared (FT-IR)	96
§ 2.14 Statistics	99
References for Chapter 2	100

Chapter 3 Quantitative measurement of RONS in the PAM

§ 3.1 Introduction	104
§ 3.2 Short-lived RONS	105
§ 3.3 Long-lived RONS	111
§ 3.4 Reactive organic species	118
§ 3.5 Summary	122
References for Chapter 3	123

Chapter 4 H₂O₂ and NO₂⁻ generation mechanism in the PAM

§ 4.1 Introduction	125
§ 4.2 Hydroxyl peroxide (H ₂ O ₂)	
§ 4.2.1 H ₂ O ₂ generation in gaseous phase	126
§ 4.2.2 H ₂ O ₂ generation in liquid phase	131
§ 4.3 Nitrite ion (NO ₂ ⁻)	
§ 4.3.1 NO ₂ ⁻ generation in gaseous phase	136
§ 4.3.2 NO ₂ ⁻ generation in liquid phase	140
§ 4.4 Summary	143
References for Chapter 4	146

Chapter 5 H₂O₂ and NO₂⁻ contribution to antitumor effect of the PAM

§ 5.1 Introduction	147
§ 5.2 Selective antitumor effect of the PAM	148
§ 5.3 Intracellular RONS	152
§ 5.4 Antitumor effect of antitumor species generated by the NEAPP	
§ 5.4.1 Nitrate ion (NO ₃ ⁻)	154
§ 5.4.2 Synergistic antitumor effect of H ₂ O ₂ and NO ₂ ⁻	156
§ 5.5 Summary	160
References for Chapter 5	161

Chapter 6 Intracellular metabolism pathways disordered by the PAM

§ 6.1 Introduction	162
§ 6.2 Sample preparation	163
§ 6.3 Statistical analysis	165
§ 6.4 Adenosine triphosphate (ATP) decreasing by the PAM	173
§ 6.5 Summary	182
References for Chapter 6	184

Chapter 7 Analysis of calcium oxalate crystals synthesized by the NEAPP

§ 7.1 Introduction	186
§ 7.2 Synthesis of crystals in NEAPP irradiated medium	187
§ 7.3 Analysis of those particles structure	
§ 7.3.1 Analysis of XRD	189
§ 7.3.2 Analysis of SEM-EDX	197
§ 7.3.3 Analysis of FT-IR	199
§ 7.4 Dynamics of the crystal growth	201
§ 7.5 Summary	207
References for Chapter 7	208

Chapter 8 Essential components of the oxalate crystal synthesis by the NEAPP

§ 8.1 Introduction	210
§ 8.2 Screening of essential components for the crystal synthesis	211
§ 8.3 Roles of essential components for the crystal synthesis	
§ 8.3.1 Glucose	214
§ 8.3.2 Calcium chloride (CaCl ₂)	218
§ 8.3.3 Sodium hydrogen carbonate (NaHCO ₃)	220
§ 8.4 Summary	221
References for Chapter 8	223

Chapter 9 Conclusions

§ 9.1 Conclusion	224
§ 9.2 Scope of future works	230
Acknowledgement	233
List of papers related to this thesis	237

Chapter 1

Introduction

§ 1.1 Non-equilibrium atmospheric pressure plasma

§ 1.1.1 Characteristics

Recently, non-equilibrium plasma process is putted into practice. As compared to low pressure plasmas, non-equilibrium atmospheric pressure plasma (NEAPP) is appropriate to apply to materials being easily affected by heat or a living body, since it can be driven in ambient air and the temperature is almost room temperature. The highly reactive process is given because the electron temperature is high nevertheless the low gas temperature.¹⁾ Examples of NEAPP are shown in Figure 1.1.1.

There are many reports of NEAPPs for bio applications not only cancer therapy and organic synthesis. For example, kINPen® (a kind of Ar plasma jet),²⁾ dielectric barrier discharge (DBD)³⁾ and water electro spray⁴⁾, are shown in § 1.1.3.

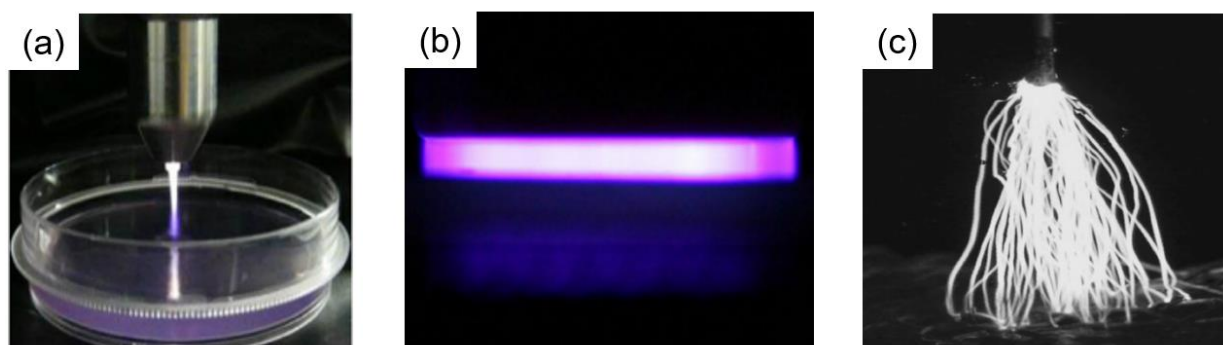


Figure 1.1.1 Examples of NEAPPs, (a) kINPen,²⁾ (b) Dielectric barrier discharge (DBD)³⁾ and (c) water electro spray.⁴⁾

§ 1.1.2 Mechanism of NEAPP effects

Various unique reactions are induced by NEAPPs and the acting mechanism is partly elucidated. It is generally known that various reactive species are generated by ignition of NEAPPs in the ambient air.

“Non-equilibrium” of NEAPPs mean relative high energy electrons compared with the gas temperature ($T_e \gg T_g$). The characteristic has been achieved by using a fast carrier gas flow or pulsed power sources. In addition, various wavelength lights are also emitted from molecules or atoms excited by NEAPPs. Especially, 10-400 nm of wavelength light called as ultra violet / vacuum ultra violet light (UV/VUV) gives very high energy to an irradiation target and induces excitation, ionization and dissociation. Examples of energy for dissociation are shown in Table 1.1.1.

Table 1.1.1 Examples of energies and wavelengths for dissociation.

	Binding energy		Wavelength (nm)
	(eV)	(kJ/mol)	
$\text{N}\equiv\text{N}$ (N_2)	9.794	945.0	126.6
$\text{C}=\text{O}$ (CO_2)	8.243	795.3	150.4
$\text{N}=\text{O}$ (NO)	6.550	632.0	189.3
$\text{O}=\text{O}$ (O_2)	5.098	491.9	243.2
$\text{H}-\text{O}$ (H_2O)	4.742	457.5	261.5
$\text{H}-\text{H}$ (H_2)	4.519	436.0	276.3
$\text{H}-\text{N}$ (NH_3)	3.987	384.7	311.0
$\text{O}-\text{O}$ (H_2O_2)	1.503	145.0	824.9
$\text{C}-\text{C}$ (organic)	3.658	352.9	339.0

Chapter 1 Introduction

Reactive Oxygen and Nitrogen Species (RONS) such as NO, H₂O₂, NO₃⁻ are also generated by activation of oxygen and nitrogen in the ambient air involved in NEAPPs. As shown in the above, NEAPP generates chemical reactive species and induces chemical reactions.

Inducing reactions depend on a way of applying NEAPPs. Reactive species generated by NEAPPs affect directly in one of simple ways, which is direct NEAPP irradiation to a dry target. Hydrophilization of material surface is one of the examples.

However, targets of biological NEAPP applications, which is one of the most important application of NEAPPs, have usually wet surface, so that gaseous reaction, gaseous-liquid surface reaction and liquid reaction should be considered.

In the NEAPP region, ions, radicals, high energy electron and VUV/UV are generated from discharge gas, which is mainly composed of rare gas (e.g. He, Ar), and RONS deriving from involving ambient air. Almost constituents of the ambient air are constant except humidity. Especially, H₂O₂ generation by He plasma jet was greatly increased by humidity increasing.⁵⁾

The gas-liquid interface region is very reactive because reactive gaseous NEAPP species injected to dense liquid region. There are not only chemical reaction but also dissolving gaseous species, which efficiency is decided by Henry's law constant shown in Table 1.1.2.^{6,7)}

Table 1.1.2 Dimensionless Henry's law constants for various RONS at 300K and 1 atm.^{6,7)}

RONS	Henry's law constant
NO	4.4×10^{-2}
NO ₂	2.8×10^{-1}
HNO ₂	1.15×10^3
HNO ₃	4.8×10^6
OH	6.92×10^2
H ₂ O ₂	1.92×10^6

A NEAPP irradiation distance is also important parameter because reactive species transmission depends on the distance. Relative short-lived species such as electron, VUV and unstable RONS (e.g. $\cdot\text{OH}$, $\cdot\text{O}_2^-$) don't reach to the remote region from NEAPP. Therefore, reactions induced by NEAPP irradiation also differ by the distance and generally reactivity is higher with shorter irradiation distance.

Actually, selective cancer cell killing against normal cell for a new cancer therapy is reported *in vivo* by using a remote irradiation.⁸⁾ The introduction and results of related application study is shown in § 1.2 and chapter 3 to 6. On the other hand, the interaction between NEAPP and organic species such as treatment of waste liquid,⁹⁾ and enhancement of protein crystallization¹⁰⁾ were reported by using a close irradiation. The introduction and results of related study is shown in § 1.3 and chapter 7 to 8.

Since reactions between NEAPP and liquid components also occurred in the NEAPP irradiated liquid phase, the analysis of liquid phase reactions become difficult. For example, since Dulbecco's Modified Eagle's Medium (DMEM), which is one of cell culture mediums often irradiated with NEAPPs, is composed of over 30 kinds of glucose, amino acids, vitamins and inorganics, the reaction mechanism is complex and only partly analysis have been done. Even the reaction mechanism between solutions composed of individual amino acid and NEAPPs has not been analyzed.¹¹⁾

§ 1.1.3 Current applications

There are many reports about applications of NEAPPs because of the inducing various reactive reactions against the low process temperature and the simple device configuration.

When NEAPPs are applied to targets in liquid phase, methods can be divided into two types, which are direct and indirect, as shown in Figure 1.1.2. The NEAPP treatment targets are in the liquid phase in the case of a direct irradiation, or the targets are poured with a NEAPP treated liquid in the case of indirect. In this study, cancer therapy and oxalic acid synthesis were successfully performed by the indirect and direct irradiation, respectively.

In the direct NEAPP irradiation, all reactive species from NEAPPs, shown in § 1.1.2, can affect samples. On the other hand, in the indirect NEAPP irradiation, only long-lived species remain in the liquid phase and affect to targets. To elucidate those mechanisms and establish a theory applicable to whole NEAPP application, the author studied those 2 types of applications, respectively.

Previously, indirect NEAPP treatments have been applied to sterilization, hemostasis, growth enhancement, surface modification, gene injection and so forth. A sterilization of *Penicillium digitatum* by a NEAPP irradiation was reported as shown in Figure 1.1.3.¹²⁾ The NEAPP sterilization can be applied to farm products and medical equipment, and contribute for storing foods cleanly and fleshly.

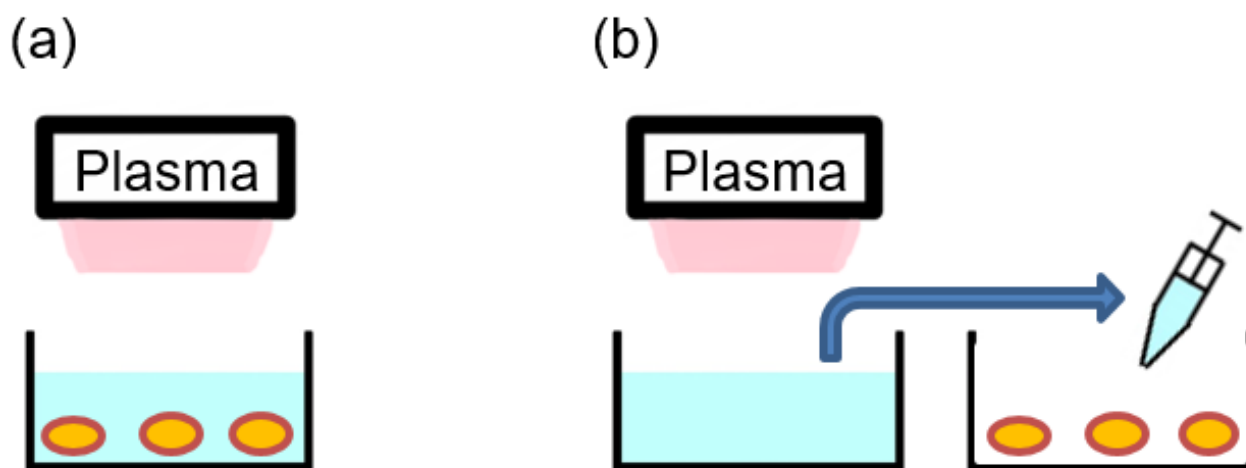


Figure 1.1.2 Schematic illustrations of (a) direct and (b) indirect NEAPP irradiation methods.

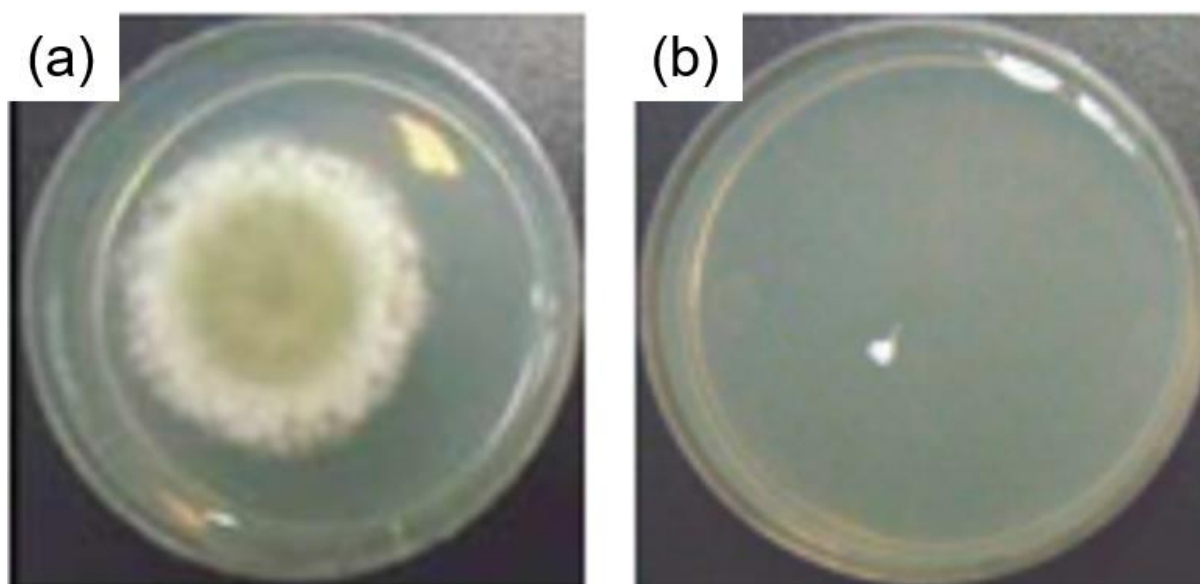


Figure 1.1.3 Observation images of *Penicillium digitatum* (a) without or (b) with NEAPP irradiation.¹²⁾

Chapter 1 Introduction

The sterilization was clearly explained by the dose of triplet oxygen atom, which is a kind of RONS. The triplet oxygen atom dose was controlled by several % of O₂ mixture to the discharge Ar gas and more efficient sterilization was implemented than without O₂ mixture.¹²⁾

A vital signal of *Penicillium digitatum* was measured by Electron Spin Resonance (ESR) with the lapse of time.¹³⁾ It was elucidated that gaseous reactive species dominantly contribute for the NEAPP sterilization because the sterilization was not occurred when only lights from the NEAPP was passed by a covering.¹³⁾

Noninvasive hemostasis induces a fast and fine injury cure. A hemostasis induced by an Ar plasma jet irradiation was also reported.¹⁴⁾ As shown in Figure 1.1.4, a faster coagulation and a fine fibril construction were observed in only the plasma-induced coagulation (PIC) region against the natural coagulation (NC). This result indicates fine hemostasis was induced by a NEAPP-characteristic coagulation with the high reactive species.¹⁴⁾

Shortage of food is a big issue because of the world population increasing. Growth enhancement of a sprout was reported by the irradiation of oxygen molecule dosed NEAPP to the seeds as shown in Figure 1.1.5.¹⁵⁾ It is also elucidated that an oxygen atom, which deriving from oxygen molecules, irradiation enhances a growth of plants.¹⁵⁾

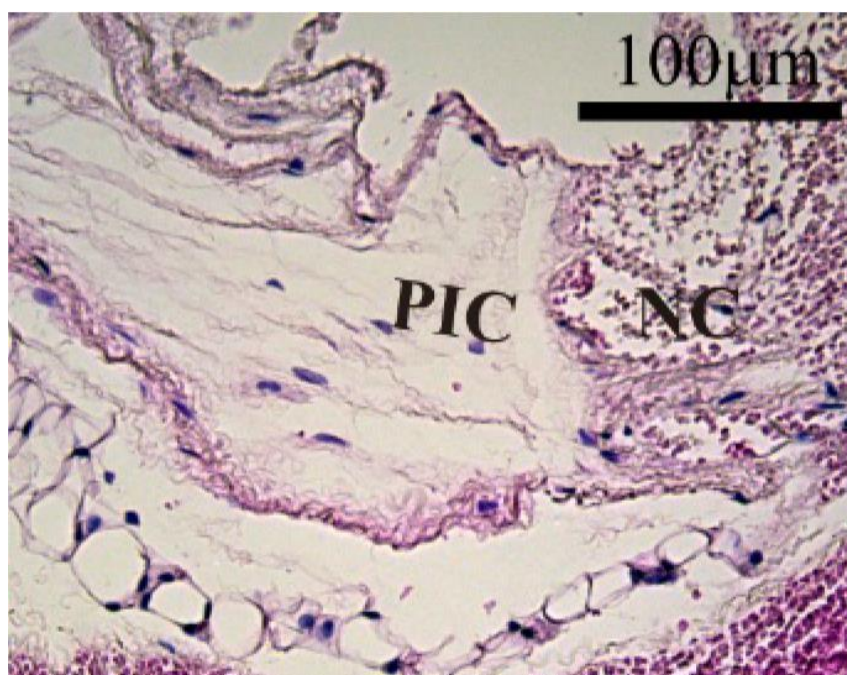


Figure 1.1.4 Histological analysis of blood clots generated by plasma-induced coagulation (PIC) and natural coagulation (NC).¹²⁾

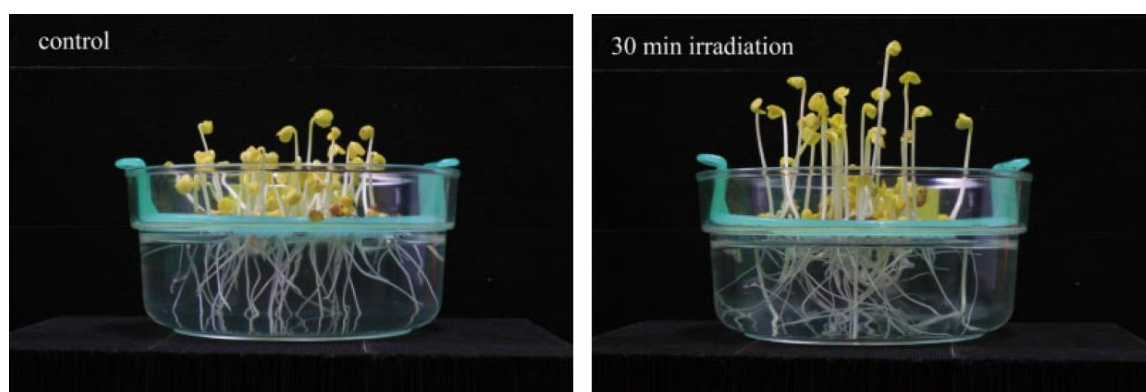


Figure 1.1.5 Typical images of sprouts with or without O₂ plasma irradiation.¹⁵⁾

Surface hydrophilization and hydrophobization are important in industrial processes such as adhesion processes. A glass surface became hydrophilic by a NEAPP irradiation.¹⁶⁾ An etching of contaminations, which are mainly organic compounds, on the glass surface by oxygen atoms from the NEAPP is a main mechanism of the hydrophilic treatment since the effect of the treatment increased with increasing the dose of oxygen atoms.¹⁶⁾ The NEAPP hydrophilic process widely attracted attention because it is simple and a low temperature process.

Even carbon nano-wall (CNW) grew on a glass surface, which is hydrophobic, became ultra-hydrophilic by the NEAPP irradiation.¹⁷⁾ It was also elucidated that decrease of the surface free energy induced the ultra-hydrophilic by reducing fluorine on CNW, oxidizing and cleaning the CNW.¹⁷⁾

Gene injection is a next generation technology for genetic engineering. Recently, a report of induced pluripotent stem (iPS) cells gives great impact.¹⁸⁾ The iPS cells can differentiate on various tissues by a noninvasive gene injection.¹⁸⁾ Very recently, the noninvasive and efficient gene injection compared with conventional processes, which are methods using liposome, a electroporation and a viral vector, was reported by using a NEAPP irradiation.¹⁹⁾

The indirect applications, such as disinfection, therapy of human disease and so forth, also previously have been reported. In addition, the indirect NEAPP treatment is easier to be applied to inside of targets by an injection and so on since it use activated liquids.

For a disinfection reagent, plasma irradiated water (PAW) was used, for example, to disinfect a teeth after a dental therapy.²⁰⁾ PAW also showed a sterilization effect, and hydroperoxy radical ($\text{HOO}\cdot$) in the PAW is a key species.²¹⁾

The plasma activated medium (PAM), which also described in detail at § 1.2.3,

Chapter 1 Introduction

showed a promise as a novel therapeutic agent for suppressing choroidal neovascularization,²²⁾ and can reduce the number of viable human retinal endothelial cells aggregated by therapeutic laser irradiation.

From the above, recently many applications of NEAPPs have been reported and attracted considerable attentions for next-generation reactive processes.

In this dissertation, the author studied both indirect and direct NEAPP applications, which are cancer therapy and oxalic acid synthesis, and tried to comprehensively understand the interaction mechanism between NEAPPs and target solutions.

§ 1.2 Plasma cancer therapy

§ 1.2.1 Cancer therapy

Recently, studies of medical field has attracted attentions of the world because of the increasing of aging population combined with the low birth rate especially in Japan. Especially, the number of death caused by cancer (malignant neoplasm) is increasing in countries with large percent of the aged population such as Japan. As shown in Figure 1.2.1, since cancer deaths (“malignant neoplasm” in Figure 1.2.1) have been the most common cause of death in Japan from 1981 until now, Establishment of cancer therapy is greatly needed.²³⁾

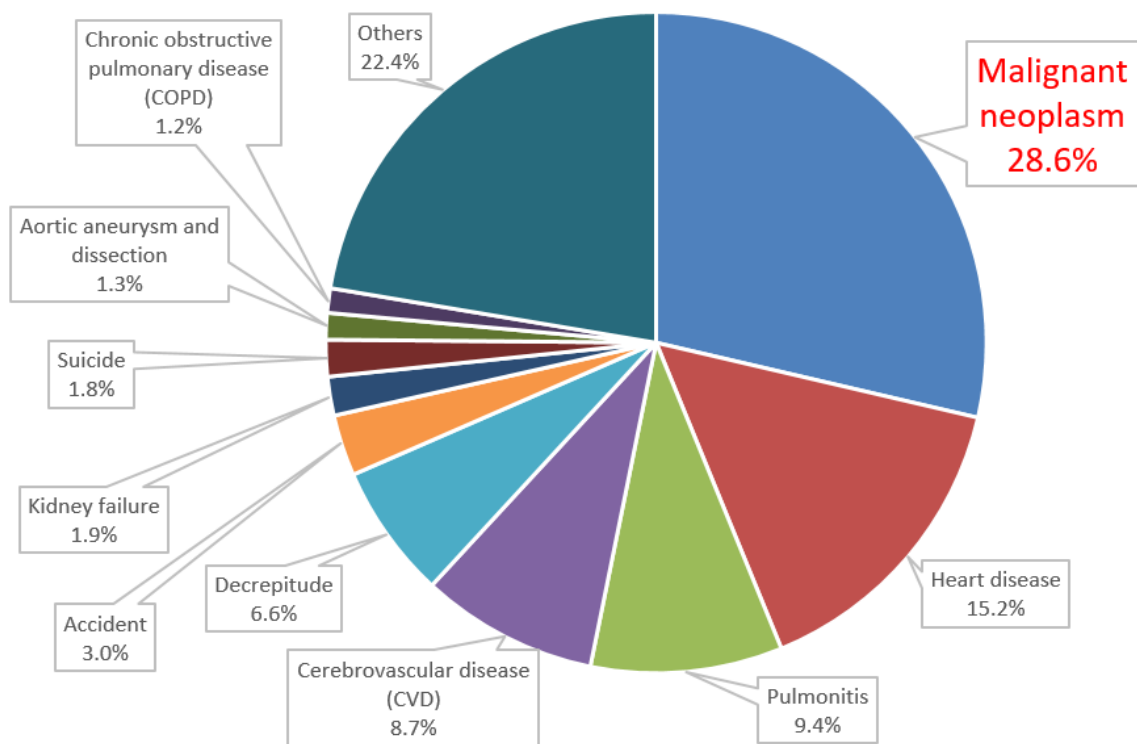


Figure 1.2.1 Cause of deaths in Japan (2015)²³⁾

Conventionally, 3 types of cancer therapy are commonly used; these are radiation therapy, anticancer drug and surgery.

Radiation therapy has small side-effect unless overdosed. However, the limited amount of radiation is generally irradiated to cancer when doing the therapy and the damage of radiation remains in body for a long time. Therefore, recurring re-irradiation is unavailable.²⁴⁾

Anticancer drug gives fatal damages for deoxyribonucleic acid (DNA) in cancer cells and kills the cancer cells. Since the drug is more effective to cells which has faster proliferation speed, cancer cells, which generally have abnormal fast proliferation speed, are killed selectively. However, anticancer drugs also affect to normal cells, which have relative high proliferation speed, such as hematopoietic cell, mouth mucosa, gastrointestinal tract mucosa and hair root cell and then side-effects such as gagging, alopecia and decreasing of leucocyte occur.²⁵⁾

Cancer tissue inside of the body can be excised by surgery. The surgery is especially effective for tumor in an early stage. The possibility of a completely recovery is highest in those therapies. However, the surgery is not valid for metastatic tumor. Moreover, sometimes not only tumor but also the surrounded tissues are excised so that it has a risk of a body function loss.²⁶⁾

As mentioned, however those conventional therapies have been contributed to a cancer therapy. These therapies have some drawbacks and complement each other. Therefore, the 4th cancer therapy is greatly needed for increasing the curing probability. The author suggest a new cancer therapy by using NEAPPs.

§ 1.2.2 Direct NEAPP irradiation

Recently, a NEAPP application for a cancer therapy is studied actively in throughout the world. It was reported that ovarian cancer cells (SKOV3, HRA) was killed by a direct NEAPP irradiation as shown in Figure 1.2.2.²⁷⁾ Moreover, the mechanism of killing was an apoptosis, which is programmed cell death induced by an intracellular signaling, not a necrosis, which is induced by physical damage such as a destruction of cell membrane or tissues.

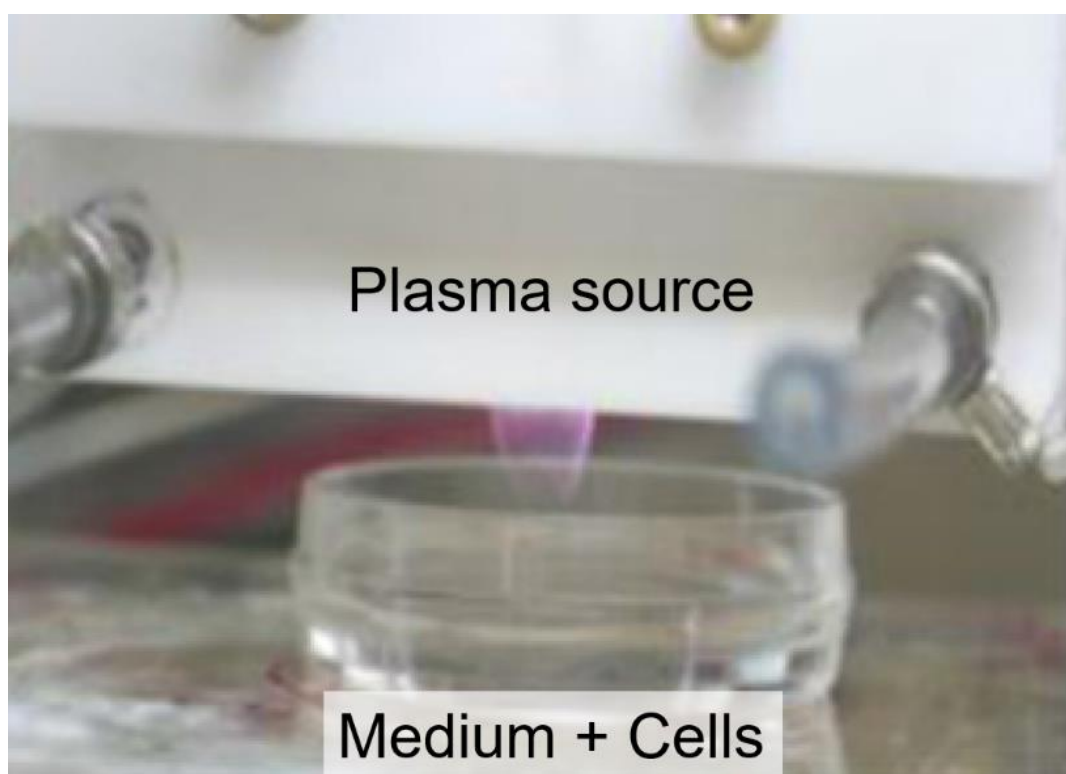


Figure 1.2.2 Direct NEAPP irradiation to a cell suspension.²⁷⁾

One of characteristics of the NEAPP cancer therapy is selective killing of cancer cells against normal cells. Figure 1.2.3 shows 24 h after morphologies of (a,b) ovarian cancer cells and (c,d) fibroblast, which constitute muscle and bones, (a,c) with or (b,d) without the NEAPP irradiation. Ovarian cancer cells were induced apoptosis, which is shown as shrinking shape against normal cells, which hardly changed the shape. It means that influences on the surrounding cells is smaller than a necrosis because the keeping intracellular components into dead cells.²⁷⁾ As shown in those result, the direct irradiation of the NEAPP can kill cancer cells without injuring normal cells. The selectivity of killing is essential for cancer therapies.²⁷⁾

From the above, one of essential characteristics, the selective killing, was induced by an irradiation of the NEAPP. However, the acting mechanism has not been elucidated yet. The investigation is urgently needed.

However those fine results have been reported, radically the direct irradiation is difficult to apply to a cancer therapy because tumors generally occur inside of human body.

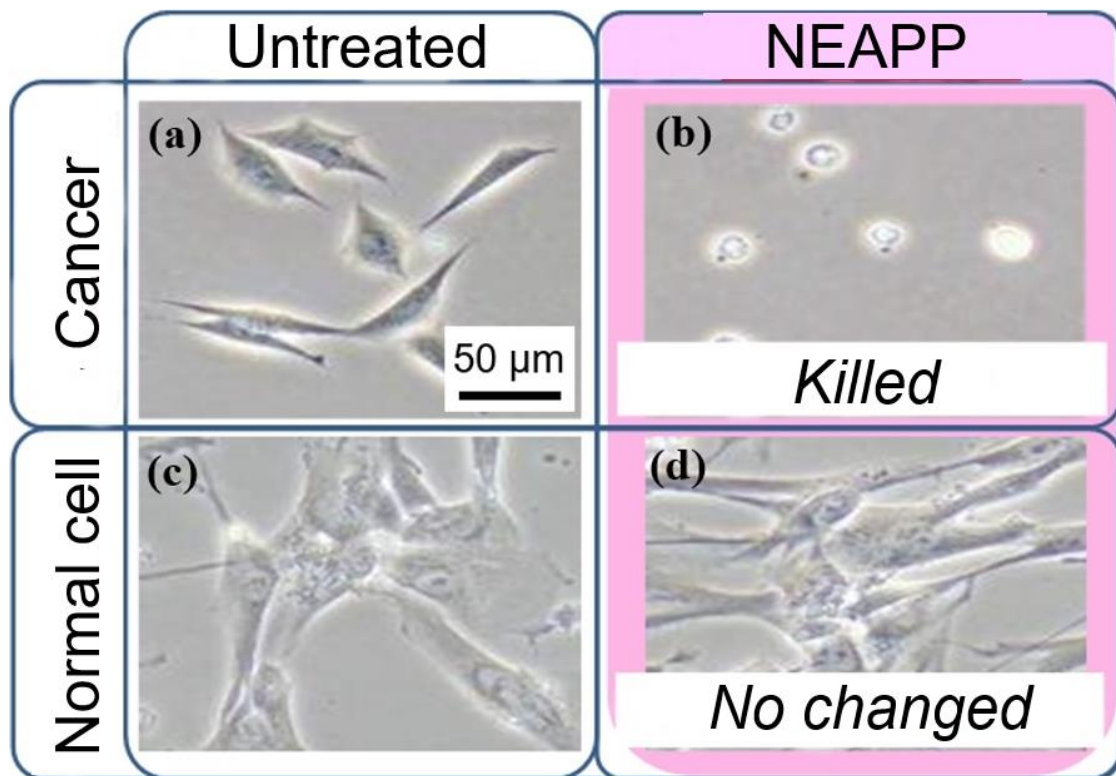


Figure 1.2.3 24 h after morphologies of (a,b) ovarian cancer cells and (c,d) fibroblast, which constitute muscle and bones, (a,c) with or (b,d) without the NEAPP irradiation.²⁷⁾

§ 1.2.3 Plasma-Activated-Medium (PAM)

The direct NEAPP irradiation is difficult to be applied for a cancer therapy. Therefore, a new therapy method using a solution activated by a NEAPP irradiation is attracted attention.

Recently, many researchers report about a cancer therapy using Plasma Activated Medium (PAM), which is a cell culture medium irradiated with NEAPPs. Appearance of a making the PAM is shown in Figure 1.2.4. Unlike the direct irradiation method, the NEAPP was irradiated to a medium, then PAM was applied to cells. The method using the NEAPP irradiated liquid is effective to a tumor inside body since it can be induced by an injection.

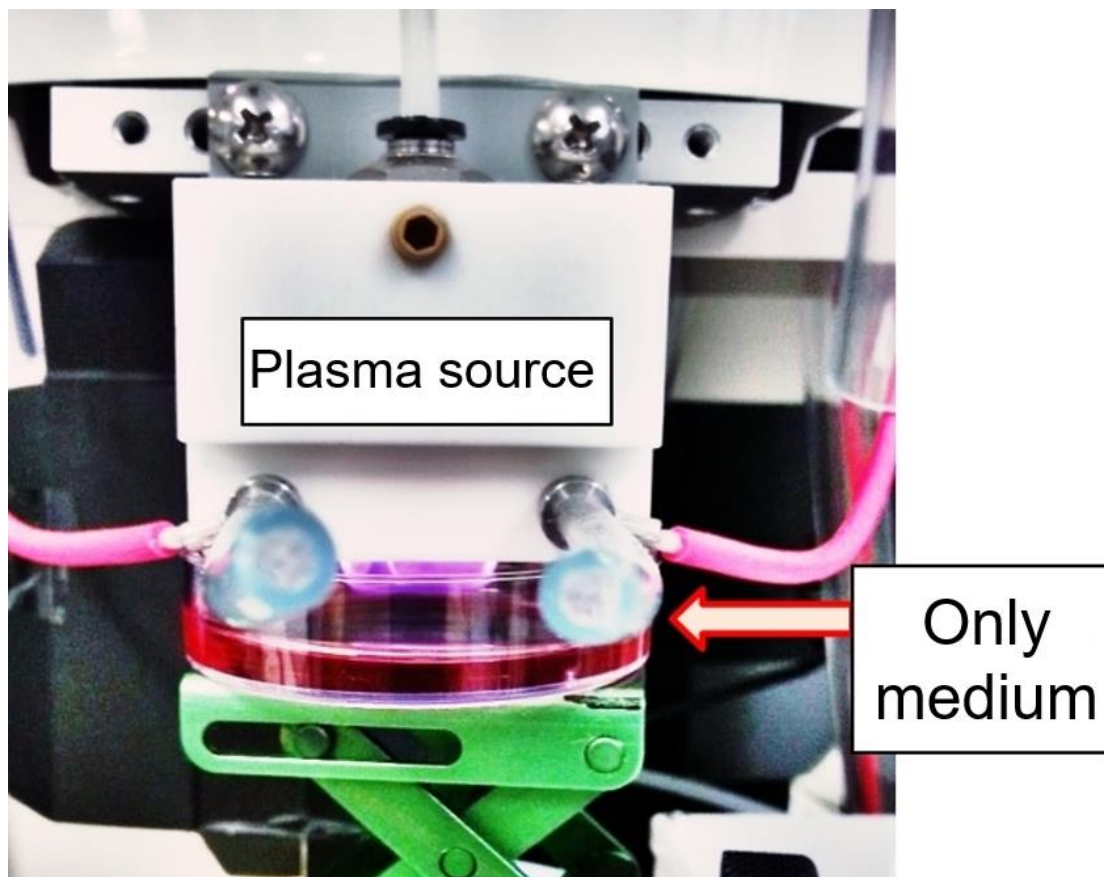


Figure 1.2.4 Appearance of a making the PAM by the NEAPP source.

It was recently reported that the culture of glioblastoma cells and normal astrocyte cells in PAM resulted in the selective apoptotic death of the glioblastoma cells.⁸⁾ This approach may be applicable to target cancer cells inside the body. The cell killing effect of PAM against several cancer cell types *in vitro* has been widely reported, including against gastric cancer cells,²⁸⁾ human lung adenocarcinoma, human liver hepatocellular carcinoma, non-small-cell lung carcinoma,²⁹⁾ human colorectal carcinoma,³⁰⁾ and ovarian clear-cell carcinoma (CCC).³¹⁾

Very recently, it was reported that an *in vivo* PAM antitumor effect using a nude mouse xenograft model of human ovarian cancer cells.³²⁾ An intraperitoneal injection of PAM reduced the volume of the xenograft tumors.³²⁾ Additionally, PAM has been shown to be effective towards anticancer agent resistant ovarian cancer cells.³²⁾

Despite the many benefits of NEAPP for the cancer therapy, the mechanism underlying its selective killing effect is not fully understood. There are some reports of the intracellular antitumor mechanism induced by the PAM with measuring a cell survival signals such as proteins.

An analysis of intracellular proteins of cancer cells incubated with the PAM was reported.³³⁾ The result indicated that PAM downregulated the AKT, ERK and mTOR intracellular signaling pathways, which mediated survival and proliferation by inhibiting apoptosis.³³⁾ Thus, the incubation of cancer cells in PAM causes their apoptotic death. However, other intracellular components have been not elucidated. The elucidation help more accurate understanding of the cancer death mechanism or discovering another mechanism. In this study, metabolomes in cancer cells incubated with the PAM was investigated in Chapter 6.

In addition, PAM-triggered cell injury was characteristically induced following the

activation of the caspase 3/7 signaling pathway, the down-regulation of the expression of the anti-apoptotic protein Bcl₂, by the activation of poly(ADP-ribose) polymerase-1, and by the release of apoptosis-inducing factors from mitochondria exposed to endoplasmic reticulum stress.²⁹⁾

From another aspect, it was reported that lipid peroxidation generated 4-hydroxy-2-nonenal (4-HNE) which induced selective apoptosis in malignant cells. 4-HNE was accumulated in tumor cells due to inactivation of the protection mechanism.³⁴⁾ The protection typically guarded against extracellular superoxide anions.³⁴⁾ It has been hypothesized that the selective apoptosis of tumor cells is triggered by intercellular signaling through the NO/peroxynitrite and HOCl pathways, followed by the mitochondrial apoptosis pathway.³⁴⁾

Those studies of cell survival signaling gave a knowledge directly linked to the cell apoptosis and contributed for understanding the PAM. However the intracellular mechanism has not been fully understood yet because of unclear other cell components such as metabolome, genome and so forth. Especially, metabolomes changed by the PAM has been not elucidated yet and preferred to analysis of a transitional PAM effect because it has the fastest response in the cell components and reflects well the phenotype.

As described in § 1.2.4 in detail, NEAPPs interact with the liquid surrounding cells and the reactive oxygen and nitrogen species (RONS) generated in these liquids are important intermediates in biological reactions. RONS are generated when the atmospheric air is entrained in the discharged region.³⁵⁾

§ 1.2.4 Reactive Oxygen and Nitrogen Species (RONS)

In the case of the NEAPP cancer therapy, a NEAPP affects cancer cells through a medium. As described in § 1.2.3, it is considered that the antitumor effect was induced by relatively long-lived species remaining in the PAM, for example, long-lived RONS such as H_2O_2 , NO_2^- , NO_3^- and so forth.

There have been many studies on the effects of plasma activated water (PAW) for medical applications such as sterilization. It has been reported that chemical species such as H_2O_2 and NO_2^- are generated in PAW.³⁶⁾ It has been suggested that H_2O_2 is generated by a chemical reaction cascade: the $\cdot\text{OH}$ radical is generated by the photo-dissociation of water by ultraviolet (UV) and vacuum ultraviolet (VUV) radiation, and then H_2O_2 is produced mainly through the $\cdot\text{OH} + \cdot\text{OH} \rightarrow \text{H}_2\text{O}_2$ reaction.³⁵⁾ The predominant reactions for the generation of nitrites and nitrates are $\cdot\text{NO} + \cdot\text{OH} \rightarrow \text{HNO}_2$, $\text{NO}_2 + \text{HO} \rightarrow \text{HNO}_3$ and $\text{HO}_2 + \cdot\text{NO} \rightarrow \text{HNO}_3$, respectively.^{31,35)} The acidity of HNO_3 (pKa -1.4) and HNO_2 (pKa 3.38) results in a higher concentration of HNO_3 in water at lower pH. It has been reported that PAW is acidic and the acidification supports the significant formation of super oxide anion (O_2^-), in particular of acidic solutions.^{37,38)} In conclusion, these results suggest that the chemical composition of PAW strongly depends on its pH value.

It was reported that the generation of high concentrations of H_2O_2 , NO_2^- and NO_3^- in Dulbecco's phosphate buffered solutions (DPBS) and culture media when exposed to spark-discharges at the liquid-air interface.⁴⁾ It was also reported that the detection of $\cdot\text{OH}$ and O_2^- radicals in Ar plasma-jet-irradiated DPBS, whereas only $\cdot\text{OH}$ was detected in Roswell Park Memorial Institute medium (RPMI) following irradiation.³⁹⁾ It

has been suggested that the dissolution of gaseous H_2O_2 , which is generated through gas-plasma reactions, plays a dominant role in determining the aqueous H_2O_2 concentrations generated in RPMI.⁴⁰⁾

However RONS are likely to contribute for the antitumor effect of the PAM, RONS generated in the PAM has not been measured quantitatively and the generation mechanism also has been unclear.

There is some report of discussions on RONS contribution to the PAM antitumor effect. In this study, RONS generation, especially H_2O_2 and NO_2^- , were obviously detected as described in Chapter 3.

NEAPPs initiates the dissociation of H_2O molecules to form H_2O_2 as RONS in the aqueous medium, and H_2O_2 acts as a key intermediate in killing cells.⁴¹⁾ Nitrite ion (NO_2^-), which is also one of RONS, kills bacterial not but mammalian cells.^{36,42)} The effects of H_2O_2 and nitrite produced by plasmas have been studied in biological reactions.^{42,43)} To date, no study has focused on understanding the mechanism underlying the selective cancer cell killing effect of H_2O_2 and NO_2^- present in the PAM.

From the above, it is generally reported the RONS generation in a NEAPP irradiated solution and it likely to contribute to the antitumor effect of the PAM. However, there is not enough study of individual RONS effect and no study of a synergistic effect of two or more kinds of RONS.

§ 1.3 Plasma organic synthesis and crystallization

§ 1.3.1 Oxalic acid generation

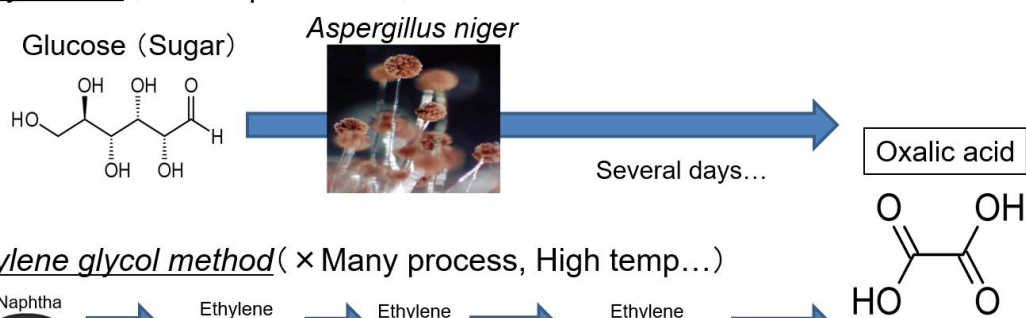
Oxalic acid is widely used in a variety of industries for purposes such as ablent for ships or large vehicles, pharmaceutical productions, oil refinery for vegetables and so on.⁴⁴⁾

Conventionally, the oxalic acid is synthesized by means of biosynthetic sugar fermentation or industrial synthesis from ethylene glycol as ingredients.^{45,46)} Conventional methods are schematically shown in Figure 1.3.1.

The biosynthesis method consumes several days at least because of a slow reaction of yeasts such as *Aspergillus niger* ferment a sucrose.⁴⁵⁾ The ethylene glycol method consists of four processes for synthesizing oxalic acid; starting material is naphtha, and then there are three intermediates synthesized oxidatively at high temperature with catalysts such as Ag.⁴⁶⁾

Those methods are likely time-consuming or high-cost to processes. Therefore, a fast and simple alternative method is necessary.

Biosynthesis (× Slow production)



Ethylene glycol method (× Many process, High temp...)

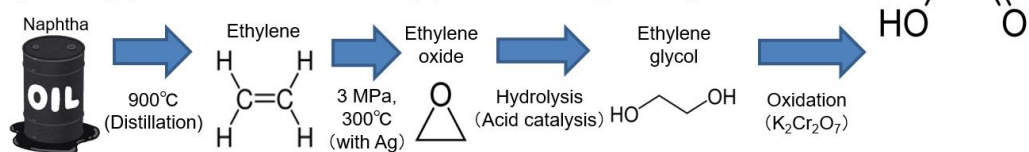


Figure 1.3.1 Conventional oxalic acid synthesis methods, which are Biosynthesis,⁴⁵⁾ and ethylene glycol method.⁴⁶⁾

§ 1.3.2 Interactions between plasma and organic species

Conventionally, interactions between plasma and organic species have been widely applied to a decomposition of organic waste to carbon dioxide or water, and there are many reports about the NEAPP organic decomposition.⁴⁷⁻⁵⁴⁾ In this study, a chemical synthesis by a NEAPP treatment was examined.

The chemical effects of NEAPP treatment in aqueous solution on 20 amino acids which comprise proteins were reported.¹¹⁾ The side chains of 14 amino acids were oxidized to form various products, and sulfur-containing and aromatic amino acids were preferentially decreased in a plasma treatment experiment. Amino acids showing chemical modification likely resulted from the chemical reaction with reactive species generated by a NEAPP.¹¹⁾

However the NEAPP synthesis of organic species is attracted attention as a new way in industry, the mechanism of the chemical synthesis reactions induced by NEAPPs has been not fully elucidated yet.

§ 1.3.3 Plasma inducing organic crystallization

There are a lot of reports about a crystallization of organic components. Organic crystallization is used for purification or separation.⁵⁵⁾ The crystallized products are used to carry out identification of the crystal structure by X-ray diffraction. or X-ray scattering.

Recently, the NEAPP have successfully aided the organic crystallization. For example, a crystallization of proteins was reported. The protein crystallization is useful for identification of their molecular structural information, especially for drug development. The protein crystallization was conventionally conducted by only standing a protein solution for several days. Surprisingly, the crystallization of lysozymes was enhanced by a NEAPP irradiation to the solution.¹⁰⁾ Indeed, by the standing method, only 10% of lysozyme was crystallized after 200 h of incubation, on contrary by the plasma-treated lysozyme solutions, 90% crystallization was obtained within shorter periods.¹⁰⁾ Moreover, there is other similar report about the crystallization within only one hour in the lysozyme solution irradiated with the electrically-driven mono-dispersed micro-bubble knife.⁵⁶⁾

Since the crystallization of oxalates was reported for the first time in this study, an accurate understanding of the phenomenon was needed.

§ 1.3.4 Plasma inducing oxalic acid synthesis

In this study, crystals mainly composed of calcium oxalate were successfully synthesized in the NEAPP irradiated medium. Then, the synthesis of oxalic acid is suggested by the extraction on production of calcium oxalate. Oxalic acid ((COOH)₂) is easily purified by dissolution of calcium oxalate crystal in high concentration of sulfuric acid at temperature ranging from 323 to 333 K by a precipitate formation reaction of $\text{Ca}(\text{COO})_2 + \text{H}_2\text{SO}_4 \rightarrow (\text{COOH})_2 + \text{CaSO}_4 \downarrow$.⁵⁷⁾

There is some possibility that the method is more useful than conventional methods described in § 1.3.1. Namely, the NEAPP synthesis is faster than the conventional bio-synthesis method because it takes only several minutes of the NEAPP irradiation to sulfuric acid. In addition the method is simpler than the conventional ethylene glycol method because the method is composed of only 2 processes, the NEAPP irradiation and a sulfuric acid treatment.

Therefore the oxalic acid generation by using the NEAPP is a challenge for the first time, a fundamental knowledge and an accurate understanding of the phenomenon was needed.

§ 1.4 Objective of this study

NEAPP gives characteristic reactions and applied to various applications. When NEAPPs apply, methods can be divided into two types, which are direct and indirect, as shown in Figure 1.1.2. In the direct NEAPP irradiation, all reactive species from NEAPPs affect irradiated targets. Therefore, relative strong treatment can be performed for various applications such as waste treatment, hemostasis, sterilization and so on. On the other hand, in the indirect NEAPP irradiation, only long-lived species will remain in the liquid phase and affect targets. In addition, because it uses reactive liquid, an applicability is better than direct irradiation in cases of disease therapies, dental sterilization and so forth. From the above, the two of applying way have been used for different purposes, both of those mechanisms should be understood, respectively.

As mentioned in § 1.2, the NEAPP has been applied to cancer therapy with the indirect method, which is called as plasma activated medium (PAM). Fine results have been obtained by testing cells and mice. In making PAM, (1) gaseous reactive species generate in the NEAPP, (2) those reactive species reach to a medium and change into stable RONS, and (3) the relative stable species kill cancer cells. For elucidating the mechanism of NEAPP cancer therapy, whole of those reactions of (1) gaseous phase, (2) liquid phase and (3) biological phase.

In understanding gaseous phase, a measurement method of gaseous species in NEAPPs has been established. However, the generation mechanism and contribution for generating liquid species were unclear. In this thesis, the gaseous reactions were examined by measuring gaseous reactive species in the NEAPP. Moreover, the ambient gas and carrier gas were changed for controlling reactive species generation.

In understanding liquid phase, RONS generation mechanisms in a plasma irradiated water have been partly investigated. However, there are not enough elucidation of reactions in a plasma irradiated medium. In this thesis, short-lived and long-lived RONS in the PAM were measured and the generation mechanism of long-lived RONS was examined.

In understanding biological phase, it has been considered that long-lived reactive species generated in the PAM have induced the antitumor effect of the PAM. However RONS are likely to contribute for the antitumor effect of the PAM, RONS generated in the PAM has not been measured quantitatively. The generation mechanism also has been unclear. Moreover, there are not enough study of individual RONS effect and no study of a synergistic effect of two or more kinds of RONS. In addition, however previous study of cell survival signaling gave a knowledge directly linked to the cell apoptosis and contributed for understanding the PAM, the intracellular mechanism has been not fully understood yet because of unclear other cell pathway such as metabolome. Therefore, the author investigated metabolome in dying cancer cells by incubating with the PAM.

As mentioned in § 1.3, in the case of the irradiation to a medium, interactions between the NEAPP and organic species composed of a medium also occur. However there are many reports about organic decomposition in a solution of organic species by using a direct irradiation of plasmas, the calcium oxalate synthesis by using a direct irradiation of NEAPPs to a medium may be a challenge for the first time. Therefore, a fundamental knowledge and an accurate understanding of the phenomenon were needed.

In this study, the structure and synthesizing dynamics of crystal-like particles synthesized in the plasma irradiated medium were analyzed by structural analysis methods and an observation with time lapse. The essential components for the calcium

oxalate synthesis were identified from 32 kinds of the medium components.

From the above, the objective of the thesis is an elucidation of reactive species generation mechanism and those effect in NEAPP irradiated medium from both aspects of the direct and indirect NEAPP irradiations, which applied to calcium oxalate crystals synthesis and cancer therapy, respectively.

The RONS generation mechanism in a medium irradiated with NEAPP was elucidated by measuring both short and long-lived RONS generated in the PAM. The antitumor effect of the PAM was elucidated with cell culturing method, especially focused on H_2O_2 and NO_2^- which are dominantly generated RONS in the PAM. Metabolism of cancer cells was also measured after an incubation with the PAM.

§ 1.5 Chapters in the thesis

This thesis is constructed by 9 chapters. This chapter is Chapter 1 describing introductions. Details of all experimental methods are described in Chapter 2. The study for cancer therapy is mainly described in Chapter 3 to 6. The study for oxalic acid generation is also described in Chapter 7 to 8. A whole study is summarized in Chapter 9.

Materials and methods used in this study is described in Chapter 2. The author used a plasma source developed in their laboratory. Experimental conditions and theories of 11 kinds of engineering and biochemical methods used in this study were described in this chapter.

Both short-lived and long-lived RONS in the PAM measured in this study is described in Chapter 3. The generation mechanism of long-lived RONS could be elucidated by measuring short-lived species, which was the precursor. Long-lived RONS is directly contribute for the antitumor effect of the PAM.

The long-lived RONS, which contributes for the antitumor effect of the PAM, generation mechanism is discussed in Chapter 4. H_2O_2 and NO_2^- generation in both gaseous and liquid phase is discussed with his data and some referenced data.

Contributions of RONS to the antitumor effect are described in Chapter 5. The author elucidated the synergistic antitumor effect of H_2O_2 and NO_2^- occurring in the PAM. Moreover, the unknown mechanism was also discovered except the synergistic antitumor effect.

A result of investigation of a metabolism of cancer cells incubated with the PAM is described in Chapter 6. An adenosine triphosphate (ATP), which is a store of an energy,

in cancer cells was decreased as a result of disordering the *glycolysis* induced by an incubation with the PAM.

Properties and synthesis dynamics of crystalline particles synthesized in a directly plasma irradiated medium were described in Chapter 7. The accidentally observed particles were identified as a crystal mainly composed of calcium oxalate, which is not involved in the initial medium. Moreover, the crystallization speed might be also enhanced by the NEAPP irradiation.

Essential components of the solution irradiated the NEAPP for calcium oxalate crystal synthesis is described in Chapter 8. The author identified 3 kinds of essential components, glucose, CaCl_2 , NaHCO_3 , and roles from over 30 kinds of components of the medium.

The dissertation is summarized in Chapter 9. Contribution of the study for NEAPP biochemical applications and the future scope are described.

References for Chapter 1

- 1) The 153rd Committee on Plasma Materials Science, Japan Society for the Promotion of Science, Taikiatsu Plasma -Kiso to Ouyo- [Atmospheric pressure plasma fundamental and application], Tokyo, Ohmsha (2009).
- 2) S. Bekeschus, J. Kolata, C. Winterbourn, A. Kramer, R. Turner, K.D. Weltmann, B. Broker, and K. Masur, *Free Radical Research*. **48**, 542-549 (2014).
- 3) N. Mertens, M. Mahmoodzada, A. Helmke, P. Grunig, P. Laspe, S. Emmert, and W. Viol, *Plasma Process. Polym.* **11**, 910-920 (2014).
- 4) Z. Machala, B. Tarabova, K. Hensel, E. Spetlikova, L. Sikurova, and P. Lukes, *Plasma Process. Polym.* **10**, 649-659 (2013).
- 5) J. Winter, H. Tresp, M.U. Hammer, S. Iseni, S. Kupsch, A.S. Bleker, K. Wende, M. Dunnbier, K. Masur, K.D. Weltmann, and S. Reuter, *J. Phys. D: Appl. Phys.* **47**, 285401 (2014).
- 6) R. Sander, *Atmos. Chem. Phys.*, **15**, 4399-4981, (2015).
- 7) D. Mackay, and W. Y. Shiu, *J. Phys. Chem. Ref. Data*. **10**, 1175 (1981).
- 8) H. Tanaka, M. Mizuno, K. Ishikawa, K. Nakamura, H. Kajiyama, H. Kano, F. Kikkawa, and M. Hori, *Plasma Medicine*. **1**, 265-277 (2011).
- 9) J. Li, T. Wang, N. Lu, D. Zhang, Y. Wu, T. Wang, and M. Sato, *Plasma Sources Sci. Technol.* **20**, 034019 (2011).
- 10) T. Ito, T. Ito, and S. Yokoyama, *Applied Physics Express*. **4**, 026201 (2011).
- 11) E. Takai, T. Kitamura, J. Kuwabara, S. Ikawa, S. Yoshizawa, K. Shiraki, H. Kawasaki, R. Arakawa, and K. Kitano, Chemical modification of amino acids by atmospheric-pressure cold plasma in aqueous solution. *J. Phys. D: Appl. Phys.* **47**, 285403 (2014).

- 12) S. Iseki, H. Hashizume, F. Jia, K. Takeda, K. Ishikawa, T. Ohta, M. Ito, and M. Hori, *Appl. Phys. Exp.* **4**, 116201 (2011).
- 13) K. Ishikawa, H. Mizuno, H. Tanaka, K. Tamiya, H. Hashizume, T. Ohta, M. Ito, S. Iseki, K. Takeda, H. Kondo, M. Sekine, and M. Hori, *Appl. Phys. Lett.* **101**, 013704 (2012).
- 14) Y. Ikehara, H. Sakakita, N. Shimizu, S. Ikehara, and H. Nakanishi, *J. Photopolym. Sci. Technol.* **26**, 555-557 (2013).
- 15) S. Kitazaki, K. Koga, M. Shiratani, and N. Hayashi, *Jpn. J. Appl. Phys.* **51**, 01AE01 (2012).
- 16) M. Iwasaki, H. Inui, Y. Matsudaira, H. Kano, N. Yoshida, M. Ito, and M. Hori, *J. Appl. Phys.* **92**, 081503 (2008).
- 17) H. Watanabe, H. Kondo, M. Sekine, M. Hiramatsu, and M. Hori, *Jpn. J. Appl. Phys.* **51**, 01AJ07 (2012).
- 18) K. Takahashi, and S. Yamanaka, *Cell.* **126**, 663-676 (2006).
- 19) S. Sasaki, M. Kanzaki, and T. Kaneko, *Appl. Phys. Exp.* **7**, 026202 (2014).
- 20) K. Kitano, S. Ikawa, A. Tani, Y. Nakashima, H. Yamazaki, T. Ohshima, K. Kaneko, M. Ito, T. Kuwata, and A. Yagishita, *Proceedings of the 21st International Symposium on Plasma Chemistry.* 4-7 (2013).
- 21) E. Takai, S. Ikawa, K. Kitano, J. Kuwabara, and K. Shiraki, *J. Phys. D: Appl. Phys.* **46**, 295402 (2013).
- 22) F. Ye, H. Kaneko, Y. Nagasaka, R. Ijima, K. Nakamura, M. Nagaya, K. Takayama, H. Kajiyama, T. Senga, H. Tanaka, M. Mizuno, F. Kikkawa, M. Hori, and H. Terasaki, *Sci. Rep.* **5**, 7705 (2015).
- 23) Ministry of Health,

(<http://www.mhlw.go.jp/toukei/saikin/hw/jinkou/geppo/nengai15/dl/gaikyou27.pdf>)

(2016).

24) T. Sugita, *Journal of Niigata Cancer Center Hospital*. **44**, 6-9 (2005).

25) Saitama medical university International medical Center,

(http://www.saitama-med.ac.jp/kokusai/division_info/anticancer_drug-4.html).

(2009).

26) M. Kanada, Y. Takeuchi, T. Sakai, S. Namikawa, H. Yuasa, and M. Kusagawa, *The Japanese Journal of Thoracic Diseases*. **22**, 468-473 (1984).

27) S. Iseki, K. Nakamura, M. Hayashi, H. Tanaka, H. Kondo, H. Kajiyama, H. Kano, F. Kikkawa, and M. Hori, *Appl. Phys. Lett.* **100**, 113702 (2012).

28) K. Torii, S. Yamada, K. Nakamura, H. Tanaka, H. Kajiyama, K. Tanahashi, N. Iwata, M. Kanda, D. Kobayashi, C. Tanaka, T. Fujii, G. Nakayama, M. Koike, H. Sugimoto, S. Nomoto, A. Natsume, M. Fujiwara, M. Mizuno, M. Hori, H. Saya, and Y. Kodera, *Gastric Cancer* **18**, 635-643 (2015).

29) T. Adachi, H. Tanaka, S. Nonomura, H. Hara, S. Kondo, and M. Hori, *Free Radical Biol. Med.* **79**, 28-44 (2014).

30) M. Vandamme, E. Robert, S. Lerondel, V. Sarron, D. Ries, S. Dozias, J. Soblio, D. Gosset, C. Kieda, B. Legrain, J.M. Pouvesle, and A.L. Pape, *International Journal of Cancer*. **130**, 2185-2194 (2012).

31) F. Utsumi, H. Kajiyama, K. Nakamura, H. Tanaka, M. Hori, and F. Kikkawa, *Springer Plus* **3**, 398 (2014).

32) F. Utsumi, H. Kajiyama, K. Nakamura, H. Tanaka, M. Mizuno, K. Ishikawa, H. Kondo, H. Kano, M. Hori, and F. Kikkawa, *PLoS One* **8**, e81576 (2014).

33) H. Tanaka, M. Mizuno, K. Ishikawa, K. Nakamura, F. Utsumi, H. Kajiyama, H. Kano,

- S. Maruyama, F. Kikkawa, and M. Hori, *Plasma Medicine* **2**, 207-220 (2012).
- 34) G. Bauer, and N. Zarkovic, *Free Radical Biol. Med.* **81**, 128-144 (2015).
- 35) W. Tian, and M.J. Kushner, *J. Phys. D: Appl. Phys.* **47**, 165201 (2014).
- 36) C.A.J van Gils, S. Hofmann, B.K.H.L. Boekema, R. Brandenburg, and P.J. Bruggeman, *J. Phys. D: Appl. Phys.* **46**, 175203 (2013).
- 37) S. Ikawa, K. Kitano, and S. Hamaguchi, *Plasma Process. Polym.* **7**, 33-42 (2010).
- 38) A. Tani, Y. Ono, S. Fukui, S. Ikawa, and K. Kitano, *Appl. Phys. Lett.* **100**, 254103 (2012).
- 39) H. Tresp, M.U. Hammer, J. Winter, K.D. Weltmann, and S. Reuter, *J. Phys. D: Appl. Phys.* **46**, 435401 (2013).
- 40) J. Winter, H. Tresp, M.U. Hammer, S. Iseni, S. Kupsch, A. Schmidt-Bleker, K. Wende, M. Dunnbier, K. Masur, K.D. Weltmann, and S. Reuter, *J. Phys. D: Appl. Phys.* **47**, 285401 (2014).
- 41) T. Sato, M. Yokoyama, and K. Johkura, *J. Phys. D: Appl. Phys.* **44**, 372001 (2011).
- 42) Z. Machala, B. Tarabova, K. Hensel, E. Spetlikova, L. Sikurova, and P. Lukes, *Plasma Process. Polym.* **10**, 649-659 (2013).
- 43) S. Bekeschus, J. Kolata, C. Winterbourn, A. Kramer, R. Turner, K.D. Weltmann, B. Broker, and K. Masur, *Free Radical Research* **48**, 542-549 (2014).
- 44) http://www.ryoko.co.jp/products/oxalic/oxalic_01.pdf
- 45) H. Strasser, W. Burgstaller, and F. Schinner, *FEMS Microbiol. Lett.* **119**, 345-370 (1994).
- 46) E. Yonemitsu, T. Isshiki, T. Suzuki, and Y. Yashima, U.S. Patent 3,678,107, priority date March 15, (1969).
- 47) M. Iwabuchi, K. Takahashi, K. Takaki, and N. Satta, *Jpn. J. Appl. Phys.* **55**, 07LF02

- (2016).
- 48) H. Katayama, H. Honma, N. Nagawara, and K. Yasuoka, *IEEE T. Plasma. Sci.* **37**, 897-904 (2009).
- 49) N. Takeuchi, M. Ando, and K. Yasuoka, *Jpn. J. Appl. Phys.* **54**, 116201 (2015).
- 50) Y. Matsui, N. Takeuchi, K. Sasaki, R. Hayashi, and K. Yasuoka, *Plasma Sources Sci. Technol.* **20**, 034015 (2011).
- 51) H. Yang, and M. Tezuka, *J. Phys. D: Appl. Phys.* **44**, 155203 (2011).
- 52) G.H. Ni, Y. Zhao, Y.D. Meng, X.K. Wang, and H. Toyoda, *EPL*. **101**, 45001 (2013).
- 53) M.A. Malik, *Plasma Sources Sci. Technol.* **12**, S26-S32 (2003).
- 54) J. Li, T. Wang, N. Lu, D. Zhang, Y. Wu, T. Wang, and M. Sato, *Plasma Sources Sci. Technol.* **20**, 034019 (2011).
- 55) H. Tung, E.L. Paul, M. Midler, and J.A. McCauley, "Crystallization of Organic Compounds: An Industrial Perspective", John Wiley and Sons, Inc. (2009).
- 56) H. Kuriki, S. Takasawa, S. Sakuma, K. Shinmura, G. Kurisu, F. Arai, and Y. Yamanishi, *17th International Conference on Miniaturized Systems for Chemistry and Life Sciences*, 3B1-3 (Germany, 2013).
- 57) G. Bredig, and D.M. Lichty, and Z. Elehirochem. *Angew. Phys. Chem.* **12**, 459 (1906).

Chapter 2

Experimental setup and evaluation methods of PAM and crystals

§ 2.1 Plasma source

In all of the studies described in the paper, the same NEAPP source was used. The NEAPP source was connected to a 60 Hz ac high voltage power-source driven by 7 kV_{0-p} for making PAM or 13 kV_{0-p} for a synthesizing calcium oxalate crystals with an Ar gas flow (flow rate: 2 slm).¹⁾

Figure 2.1.1 shows a schematic illustration and a photograph of (a) the bottom and (b) the side of the NEAPP source set above medium. The NEAPP source is same as a NEAPP used in previous reports.^{2,3)}

The plasma plume extended about 6 mm from the exit and the exit slit was 20×1 mm. The characteristics of the source were analyzed by vacuum ultraviolet absorption spectroscopy, as previously reported.¹⁾ The plasma density was approximately 2×10¹⁶ cm⁻³ and the O atom density was approximately 4×10¹⁵ cm⁻³.¹⁾

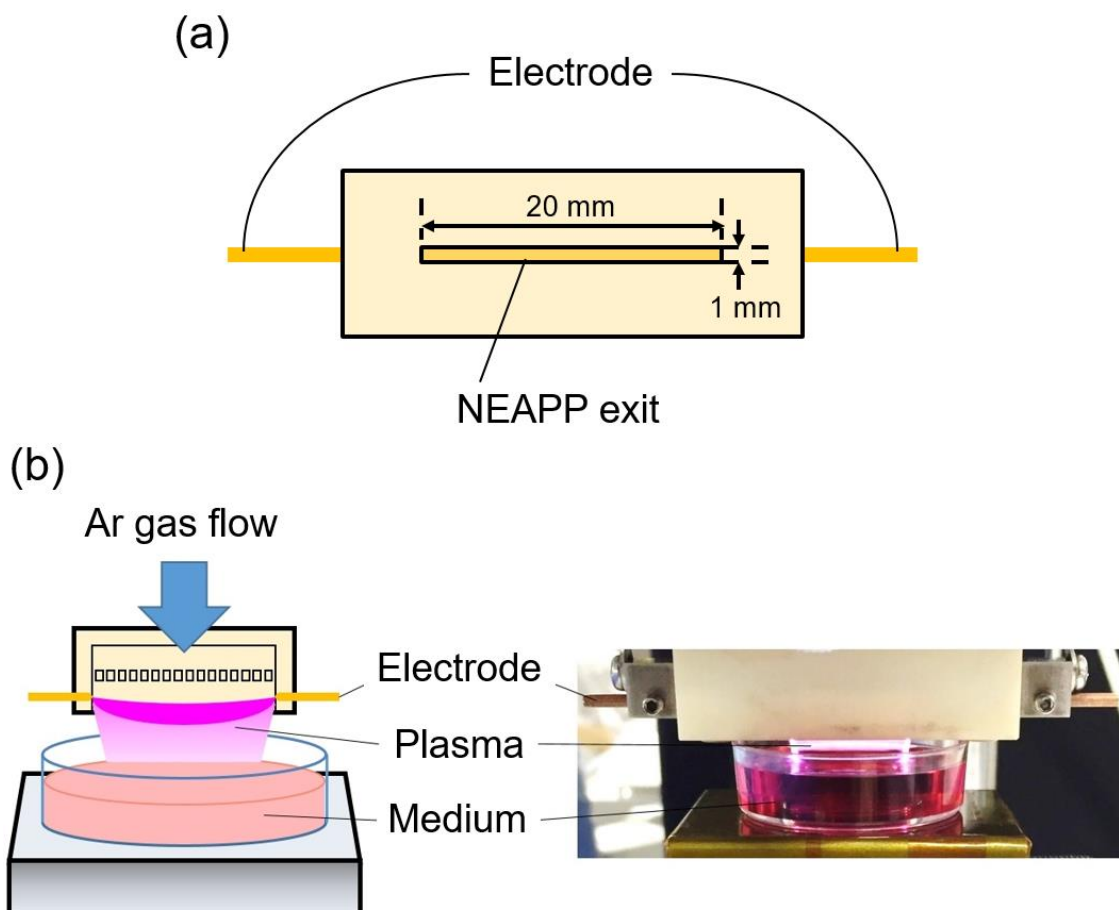


Figure 2.1.1 Schematic illustration and a photograph of (a) the bottom and (b) the side of the NEAPP source set above medium.

§ 2.2 Cell culture medium

A cell culture medium is the target of the NEAPP irradiation in this study. There are many kinds of products of prepared cell culture medium. The preferred medium depends on the kind of culturing cells. Sometime some additives are needed.

In this study, Dulbecco's modified Eagle's medium (DMEM) (cat. no. D5796; Sigma) was used for the irradiation target. The medium has been used for culturing U251SP and MCF10A in previous studies.^{2,4)} The medium is composed of 32 kinds of inorganics, amino acids, vitamins, glucose and so forth shown in Table 2.1.1.⁵⁾

10% fetal bovine serum (FBS; Sigma) and 1% penicillin and streptomycin (P/S) were added to the medium for only usual subcultures. FBS is composed of some growth hormone, antibiotics and so forth. P/S works as an antibiotics. Penicillin impedes a synthesis catalyst of peptide glucan, which is major component of a cell wall of bacteria. Streptomycin impedes a protein synthesis in ribosomes and kills various bacteria.

Table 2.2.1 List of the components of the DMEM (cat. no. 5796).⁵⁾

Inorganics	Organics		
	Amino acids	Vitamins	Others
NaCl	Arginine	Choline chloride	D-glucose
[Fe(H ₂ O) ₆](NO ₃) ₃ · 3H ₂ O	Cystine	Folic acid	Phenol red · Na
MgSO ₄	Glutamine	Myo-inositol	
KCl	Glycine	Niacin amide	
NaHCO ₃	Histidine	D-pantothenic acid	
NaPO ₄	Isoleucine	Pyridoxine · HCl	
	Leucine	Riboflavin	
	Lysine	Thiamine · HCl	
	Methionine		
	Phenylalanine		
	Serine		
	Threonine		
	Tryptophan		
	Tyrosine		
	Valine		

§ 2.3 Method of plasma treatments

§ 2.3.1 Making PAM

3 mL of the medium in each well of 6 well plate with or without penicillin streptomycin (P/S) and fetal bovine serum (FBS) was typically positioned 13 mm below the plasma source and irradiated down-stream of the plasma plume from the NEAPP source for between 30 s and 300 s. The NEAPP irradiation method has been employed by previous studies of the PAM.^{2,3)}

In the case of metabolomic analysis, 8 mL of a cell culture medium (Dulbecco's Modified Eagle's Medium (DMEM), cat. no. 5796, Sigma) in 60-mm culture dishes (430166; Corning) was fixed at 3 mm under of the exit slit of the NEAPP source. Since the NEAPP plume extended approximately 10 mm, the NEAPP plume was contacted to the medium surface. The duration for PAM irradiation was 10 min.

As mentioned in § 1.1, NEAPP contains electrons, ions, and radicals and emits photons in the UV and visible ranges. A variety of effects due to each of these species and their synergistic interactions occur simultaneously within the liquid. Here, the effect of light alone was evaluated by employing the palette for plasma evaluation (PAPE) method.⁶⁾

For some experiments, the dish containing 250 μ L of medium to be irradiated with NEAPP was covered with a 1-mm-thick transparent window made of magnesium fluoride (MgF_2), which transmitted only that light emitted from the NEAPP source at wavelengths >115 nm as shown in Figure 2.3.1. Thus, the contribution of light alone could be

examined without interference from electrons, ions, and radicals. The aim was similar to the PAPE method.⁶⁾

As also mentioned in § 1.2.4, reactive species in NEAPPs are influenced by the ambient air mixture. For elucidate the contribution of air mixing, the ambience is purged with Ar gas as shown in Figure 2.3.2. The plasma source and 3 mL of the medium was putted into a desiccator, which has 2 liter of capacity. Then the initial ambient air was exhausted 3 times by a rotary pump with 2 slm of Ar gas flowing until the oxygen level reached lower than 0.5%.

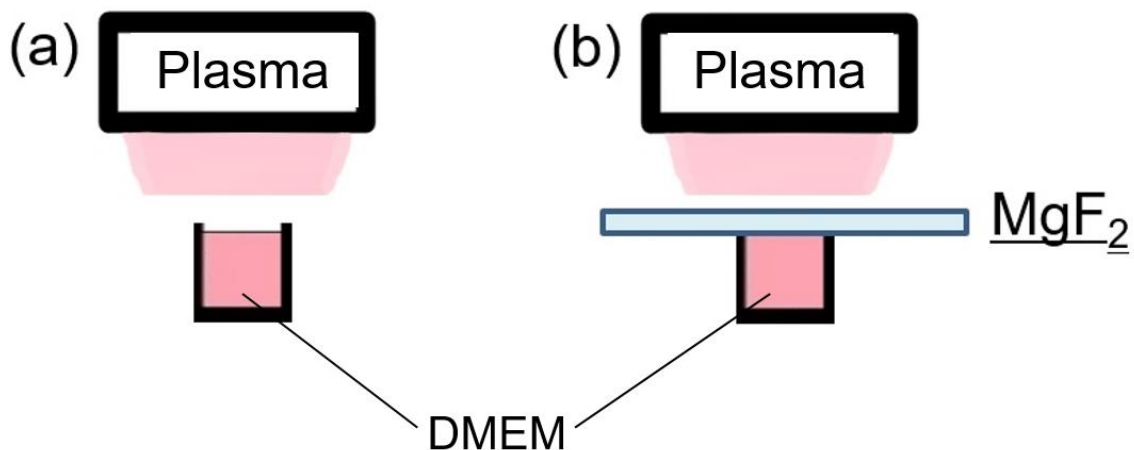


Figure 2.3.1 NEAPP irradiation (a) with or (b) without the MgF₂ covering.

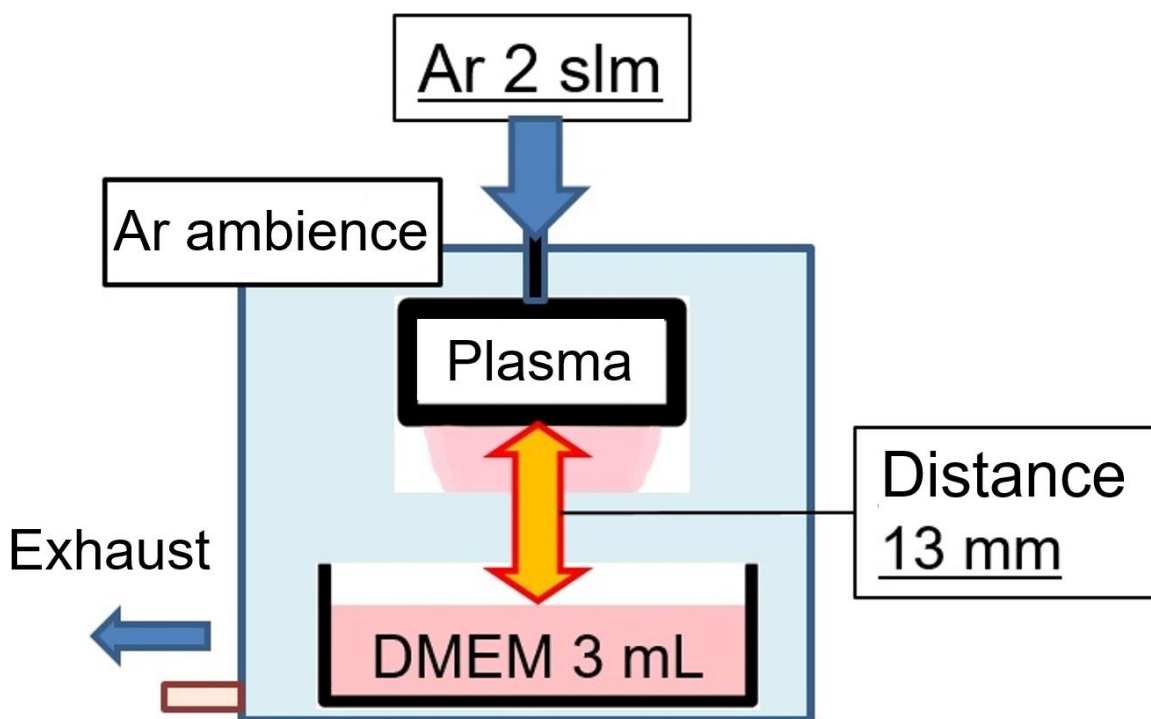


Figure 2.3.2 Schematic illustration of a NEAPP irradiation with purging the ambience by Ar gas.

§ 2.3.2 Calcium oxalate crystal synthesis

The oxalate synthesis was accidentally observed 24 h after the NEAPP irradiated to a medium with the plasma plume attaching to the medium surface. 6 mL of the medium was added to a 35-mm glass-bottom dish (Matsunami, Japan) and irradiated for 10 min with the distance from the NEAPP exit slit to the medium surface set to 3 mm. On the other hand, no particles were synthesized by a remote NEAPP irradiation. Therefore, the phenomenon was discussed with separated from the PAM used for cancer therapy described in § 2.3.1.

After that, an observation and an analysis of the properties of synthesized particles were done. For an observation of the particles, the treated medium was left to stand at room temperature for 24 h, then particles synthesized on the bottom of the dish were observed by a microscope with the lapse of time.

For an analysis of the particles properties, immediately after the plasma irradiation, the treated medium was aliquoted into 1.5-mL micro-tubes, which were then rotated slowly (approximately 10 rpm) for 24 hours at room temperature using a rotator (RT-30mini, Taitec). At the beginning of the rotation period, only perfectly clear solution was observed.

The particulates were washed twice by replacing the supernatant fluid with 1.5 mL of pure water (milliQ) followed by centrifugation, after which the final supernatant was removed and the particulates were dried under a stream of dry ambient air at room temperature, then some analysis methods were performed.

§ 2.4 Optical Emission Spectroscopy (OES)

§ 2.4.1 Theory

Optical emission spectroscopy (OES) is one of the famous for optical analysis of gaseous species in NEAPPs.⁷⁻¹³⁾

Some species composed of NEAPPs are excited by the NEAPP. Especially, electron impacts mainly contribute for the excitation with a reaction of (2.4.1),



Where X represents some molecules or atoms in the NEAPP and X* represents the excited specie. Then, a photon from the excited state is emitted with a reaction of (2.4.2),



The kind of the light emitting species is identified from the wavelength depending on the energy states.

The intensity of the optical emission is followed by an equation of (2.4.3),

$$I_x \propto n_e n_X \int \sigma_X(\varepsilon) \nu(\varepsilon) f_e(\varepsilon) d\varepsilon = k_{eX} n_e n_X, \quad (2.4.3)$$

where n_e is the electron density, n_X is the concentration of X, $\sigma_X(\varepsilon)$ is the collision cross section for the electron impact excitation of X as a function of electron energy ε ,

$v(\varepsilon)$ is the electron velocity and $f_e(\varepsilon)$ is the electron energy distribution function. $k_{eX}(\varepsilon)$ is the excitation rate coefficient for X^* by the electron impact on X .

Under a condition where k_{eX} and n_e values unchanging, the obtained emission intensity is proportion to its density. However, those values depends on experimental conditions and are generally difficult to be kept constant because an external parameters such as power, pressure, are varied in types of plasmas.

§ 2.4.2 Measurement

As mentioned in § 2.4.1, the method identify the gaseous components of NEAPPs by an observation of the wavelength of light emissions from NEAPPs indigenous to exciting gaseous species (e.g. O: 844.6 nm, Ar: 750.3 nm). The observation mechanism is schematically illustrated in Figure 2.4.1.

In this study, light spectrum emitted from the NEAPP of VUV region (115-200 nm) and UV region (200-400 nm) were measured by using the spectrometers (Shamrock500i, Andor). The exposure time was 0.1 s with a frequency of 8.475 Hz and 50 times of accumulation was done. The distance from the NEAPP to a window to the spectrometer was about 150 mm and the observed light spectrum with the NEAPP turning off was subtracted from the NEAPP emission spectrum as a background.

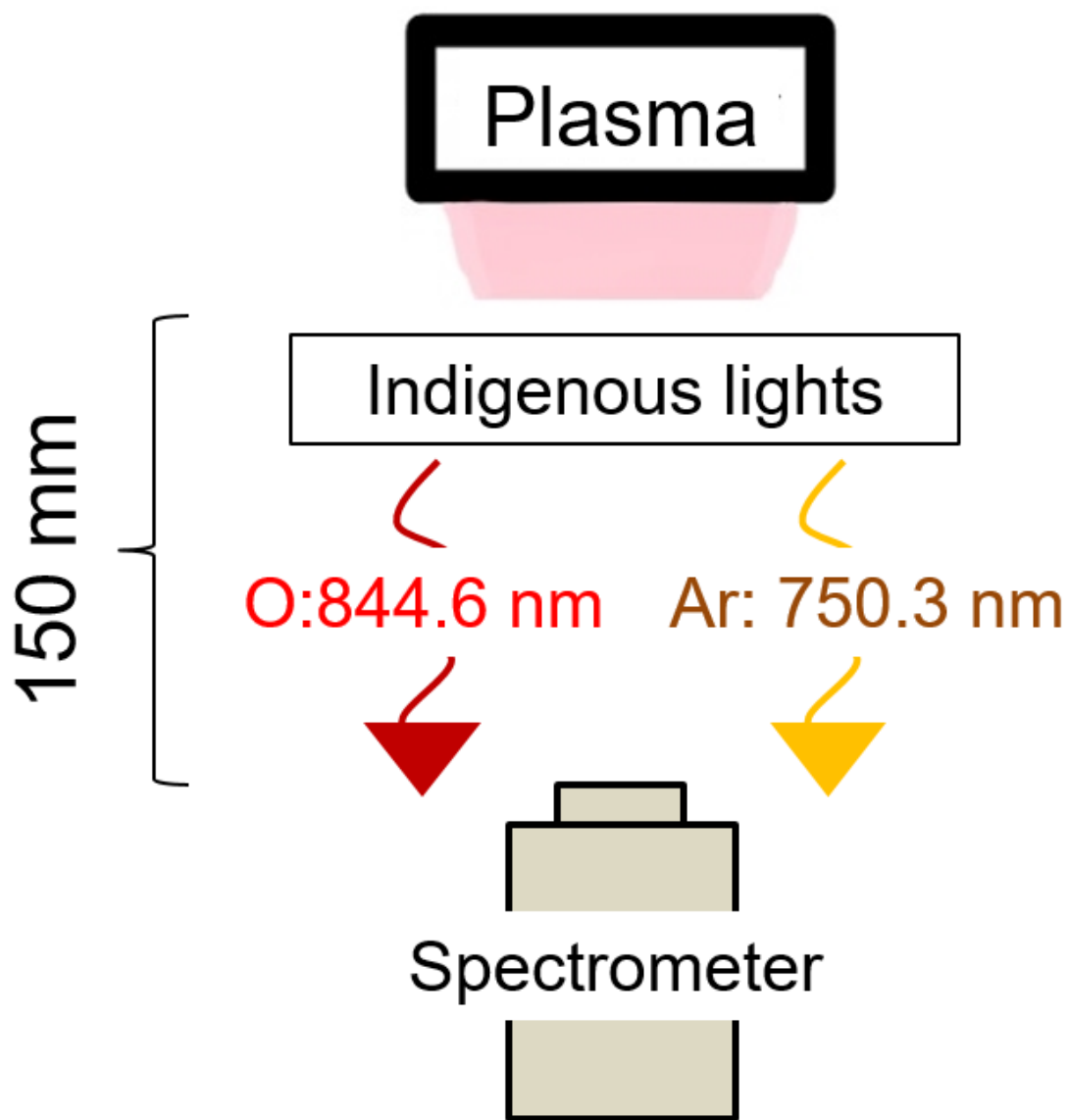


Figure 2.4.1 Schematic illustration of the mechanism of an OES analysis for the NEAPP.

§ 2.5 Electron Spin Resonance (ESR)

§ 2.5.1 Theory

A radical generation is one of the important characteristic of NEAPPs and the measurement is essential for analyzing the mechanism of reactive reactions induced by NEAPPs.

In this study, relative short-lived radicals in the PAM was measured by electron spin resonance (ESR). Radical means species having unpaired electron(s). ESR is prefer to measuring radicals because it detects an unpaired electron in a sample. Short-lived radicals were measured with the lapse of time and the process of those generation and disappearance was analyzed.

Figure 2.4.1 shows the system of the ESR measurement.¹³⁾

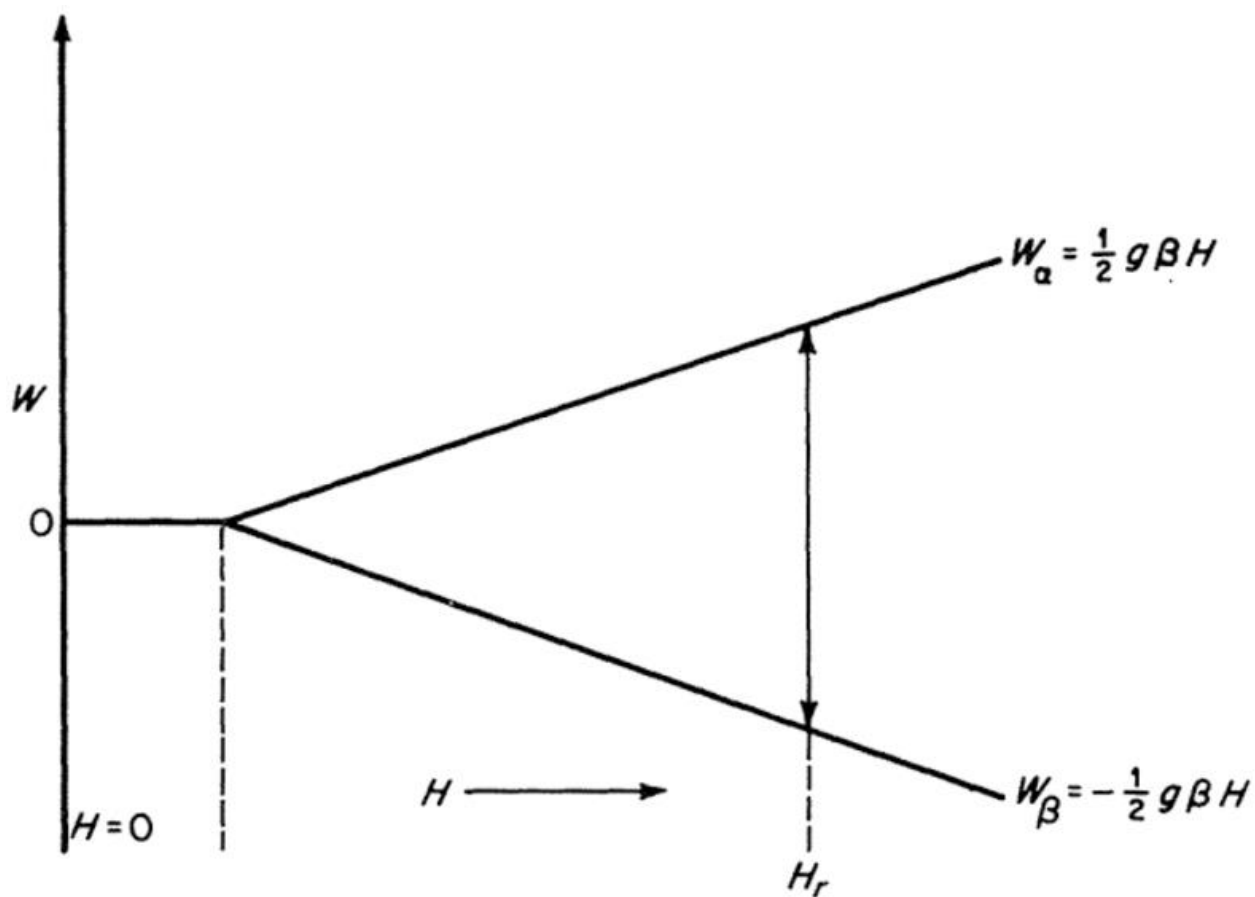


Figure 2.5.1 Energy-level scheme for ESR absorption; W_{α} and W_{β} indicate energies of the $M_s = +1/2$ and the $M_s = -1/2$ states.

In Figure 2.5.1, g represents g value, which value is specific to individual radicals and reflects a surrounding nucleus of an unpaired electron. β represents Bohr magnetron constant, which value is $9.274 \times 10^{-28} \text{ J}\cdot\text{T}^{-1}$ and H represents a sweeping magnetic field.

Degenerated energy levels are divided to the $M_s = +1/2$ and the $M_s = -1/2$ states by sweeping of a magnetic field. The division is named as the *Zeeman effect* and the dividing width follow a formula (2.5.1).¹⁴⁾

$$\Delta W = g \cdot \beta \cdot H \quad (2.5.1)$$

Microwave is also entering to the sample cavity except of the sweeping magnetic field. When a microwave power, $\Delta E_{\mu} = h\nu$, becomes the same as the dividing width, the microwave is absorbed by the unpaired electron and the electron is excited from lower to upper state. In an ESR system, the unpaired electron is detected by measuring a “valley” of a reflected microwave power from the sample cavity.¹⁴⁾

A quantitative measurement is performed by making a standard curve with some stable radicals such as 2,2,6,6-tetramethylpiperidine 1-oxyl (TEMPO) since an absorbance of the microwave is proportional to the unpaired electron density.

§ 2.5.2 Spin-trapping method

Generally, a direct detection of short-lived reactive species generated in the PAM is difficult since the lifetimes of those reactive species are too short to detect. For example, the half-life of hydroxyl radical ($\cdot\text{OH}$) in water is only about several tens of microseconds. In this study, such short-lived species were measured by an ESR with employing a spin-trapping method.

Spin-trapping method have been widely used and there are many products of spin-trapping reagent. Spin-trapping reagents dissolving in measuring liquid rapidly and specifically reacts with a radical and generates a stable adduct. The scheme of the trapping reaction in the case of using a kind of trapping reagent, 5,5-dimethyl-1-pyrroline-N-oxide (DMPO), is shown in Figure 2.5.2. High selectivity is done with the method because ESR signals from those adducts are specific to trapped radicals, respectively.¹⁵⁾

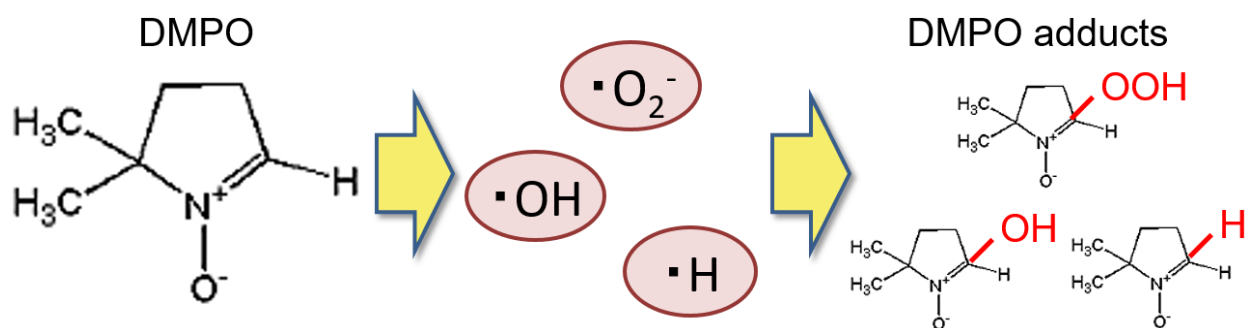
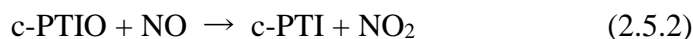


Figure 2.5.2 Scheme of the trapping reaction in the case of using a kind of trapping reagent, DMPO.

Even in analysis of a solution irradiated with a NEAPP, many studies using spin-trapping method have been reported. For example, hydrogen radical ($\cdot\text{H}$), hydroxyl radicals ($\cdot\text{OH}$) and super oxide anion ($\cdot\text{O}_2^-$) were measured by using a trapping reagent of DMPO.¹⁶⁾ 5-(2,2-dimethyl-1,3-dioxaphosphoryl)-5-methyl-1-pyrroline N-oxide (CYPMPO) is also trapping both of $\cdot\text{OH}$ and $\cdot\text{O}_2^-$. However, the reagent is better at the $\cdot\text{O}_2^-$ detection than the DMPO.¹⁷⁾ In addition, 2,2,6,6-tetramethylpiperidine (TEMP) for singlet oxygen ($^1\text{O}_2$),¹⁸⁾ and 2-(4-carboxyphenyl)-4,4,5,5-tetramethylimidazoline-1-oxyl-3-oxide (c-PTIO) for nitric oxide (NO),¹⁹⁾ have been also used.

The trapping mechanism of CYPMPO and TEMP is similar as DMPO. In the case of c-PTIO, it should be noticed that the reagent introduce ESR peaks by itself. The c-PTIO reacts with aqueous NO and generates c-PTI with a reaction of (2.5.2).



In this study, 250 μL of the medium put the surface 7 mm under from the NEAPP slit was irradiated with the NEAPP. 70 mM of DMPO or 500 μM of c-PTIO were added before a NEAPP irradiation or 100 mM of CYPMPO was added immediate after a NEAPP irradiation to prepare samples for the ESR analysis. 32 μL of sample was poured to a test tube made of synthetic quartz.

In the measurement by using c-PTIO, 20 mM of 4-(2-hydroxyethyl)-1-piperazineethanesulfonic acid (HEPES, pH 7.4; Wako) buffer mixed with an NO generation reagent, 1-hydroxy-2-oxo-3-(N-methyl-3-aminopropyl)-3-methyl-1-triazene

(NOC7; Dojindo), was also measured as a positive control sample.

§ 2.6 Chemical probe method

§ 2.6.1 Theory

The chemical probe method is extremely precise and quantitative even though the method is relative simple. Therefore, the author employed the method for measuring long-lived RONS in the PAM.

Various kinds of chemical probe reagents are on market. The reagent reacts with measurement target species and a product has absorbance of a specific wavelength, which is visible light wavelength in many cases. After finished the reaction, an absorbance of the sample at the wavelength is measured.

In this study, the author measured only absorbance for the quantitative analysis however some reagents can detected by a fluorescence. Solutions composed of known concentration of detection target were also measured to draw a standard curve for quantitative analysis.

Actual examples of detection reagents are shown in § 2.6.3 and § 2.6.4.

§ 2.6.2 Micro plate reader

The absorbance of all samples, background and standard curve are preferred to be measured at the same time since absorbance of some chemical reagents are changed with the reaction time. Therefore, a micro plate reader was used for the absorbance measurement instead of an absorption spectrometer.

The micro plate reader can measure 96 samples at the almost same time at most in the case of using 96 well cell culture plate however an absorbance of only single wavelength light can measured by one time measurement.

In this study, a micro plate reader, POWERSCAN HT (DS Pharma Biomedical, WA, USA), shown in Figure 2.6.1 was used.

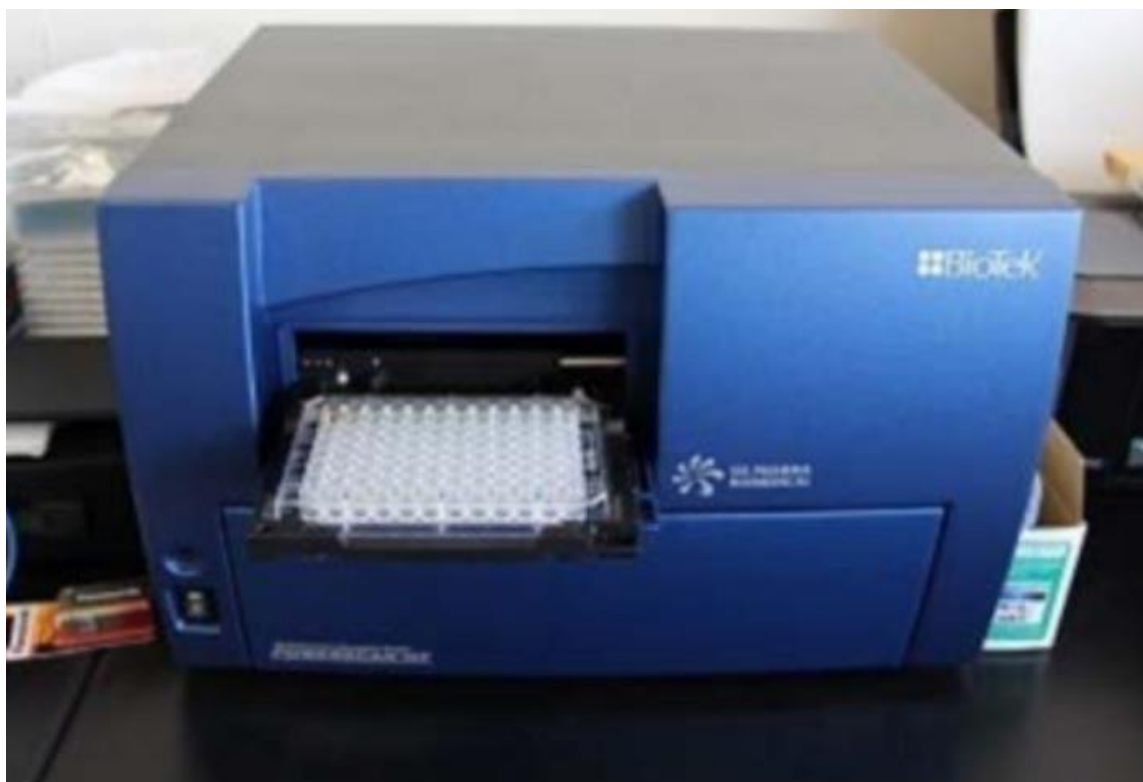


Figure 2.6.1 A picture of the micro plate reader with put a sample plate on.

§ 2.6.3 Hydrogen peroxide (H₂O₂)

In the study, Amplex[®] Red Hydrogen Peroxide/Peroxidase Assay Kit (Invitrogen, Carlsbad, CA, USA) was used as a chemical probe reagent detecting H₂O₂ concentration in the PAM.²⁰⁾

The chemical probe kit is composed of the Amplex[®] Red reagent, dimethyl sulfoxide (DMSO) as a solvent, 0.25 M of sodium phosphate buffer, horseradish peroxidase (HRP) as a catalyst and an H₂O₂ standard solution for making samples using to draw a standard curve.

The Amplex[®] Red reagent and HRP diluted to the sodium phosphate buffer is worked as a reagent solution. Except for samples, H₂O₂ standard solutions and a background samples were prepared. 0, 2.5, 5 and 10 μM of H₂O₂ diluted to pure water were prepared as H₂O₂ standard solutions and the initial medium diluted to degrees of each samples were prepared as background samples. 30 min after of the reagent addition, the absorbance of 560 nm light was measured.

The measured H₂O₂ concentration indicates the net amount since those were calculated from the absorbance of samples subtracted by the background. Each samples, H₂O₂ standard solutions and a background were prepared in triplicate.

The reagent, which contained reagent for measurements of 100 samples, should be used up by one time experiment because the absorbance of reagent itself is increasing with the lapse of time. Moreover, a micro plate reader, described in § 2.6.2, should be used for measurement of absorbance of the samples for the same reason.

The H₂O₂ detecting reaction by the reagent is shown in Figure 2.6.2. Amplex[®] Red reagent react with the H₂O₂ and produce a resorufin in presence of the HRP as a catalyst.

The resorufin is generated by the reaction between Amplex[®] Red and H₂O₂ and has absorbance of 490 nm wavelength light on the other hand Amplex[®] Red has no absorbance of a visible light. Therefore, the absorbance is proportional to the H₂O₂ concentration. The reagent is also detected by a fluorescence of 590 nm excited by 530-560 nm of light.

Figure 2.6.3 shows an example of the measurement provided from the maker. Even sub-pico molar of H₂O₂ was detected proportionally to the absorbance by the reagent.

On the other hand, the method is not suitable for the high H₂O₂ concentration, which is over several micro molar, because the absorbance of resorufin is saturated. In this study, samples were diluted 20 to 50 times by the sodium phosphate buffer.

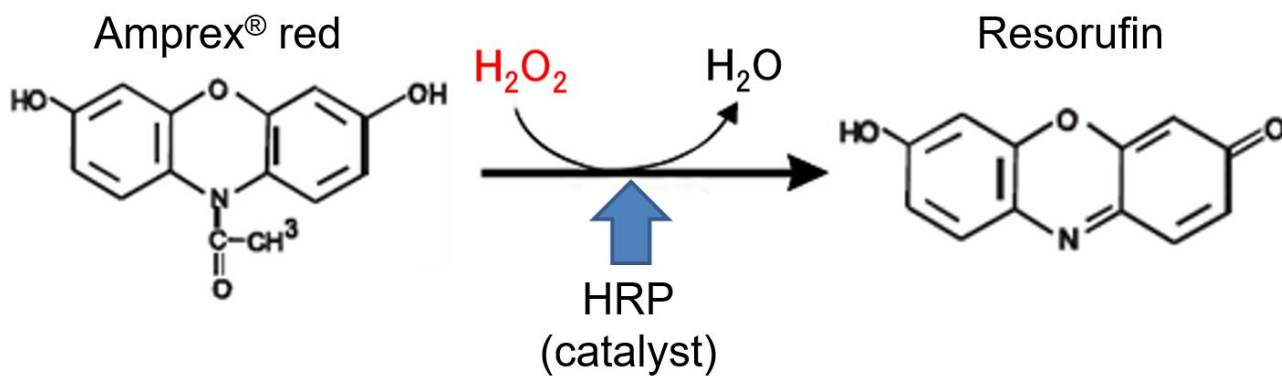


Figure 2.6.2 The H_2O_2 detecting reaction by using the Amplex® Red reagent.

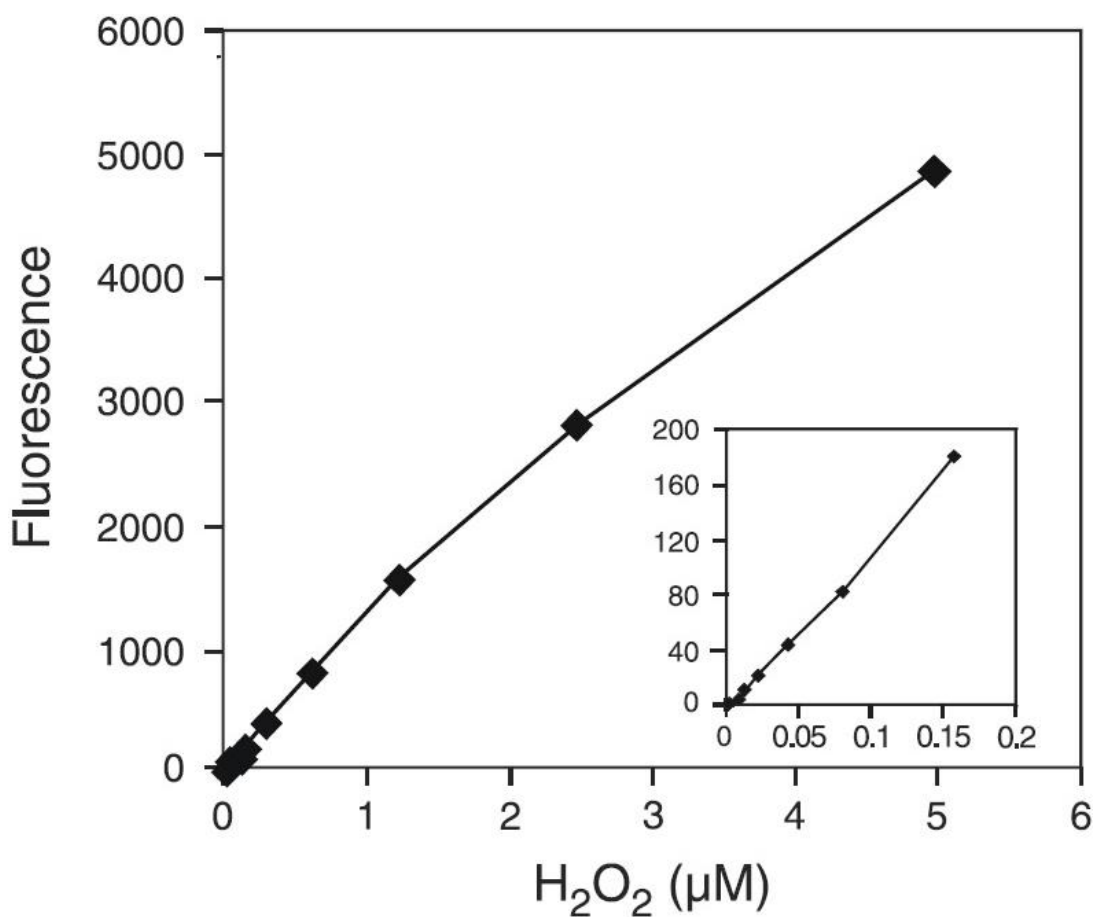


Figure 2.6.3 An example of the H_2O_2 measurement provided from the maker.²⁰⁾

§ 2.6.4 Nitrite and nitrate ion (NO_2^- / NO_3^-)

In this study, OxiSelect™ In Vitro Nitric Oxide (Nitrite/Nitrate) Assay Kit solution (Cell Biolabs Inc., San Diego, CA, USA) was used as a chemical probe reagent detecting H_2O_2 concentration in the PAM.²¹⁾

The NO_2^- and NO_3^- detection kit is composed of a solution of sulfanilamide, a solution of N-(1-naphthyl) ethylene diamine, catalyst of a decomposition of nitric acid and the solvent, and an NO_2^- and NO_3^- standard solution for making samples to draw a standard curve.

Concentrations of a nitrite ion and a sum of nitrite ion and nitrate ion can be measured, respectively. The nitrate concentration is calculated by a subtraction of the nitrate ion concentration from the sum of nitrite ion and nitrate ion.

Nitrate ion was decomposed to nitrite ion by mixing samples with the catalyst of a decomposition of nitric acid for an hour. After that, a DPBS was added to each samples, then a solution of N-(1-naphthyl) ethylene diamine was added to each samples immediate after an addition of a solution of sulfanilamide. Those samples were left to stand for 10 min and the absorbance of 540 nm light was measured. The NO_2^- detection reaction is shown in Figure 2.6.4.²¹⁾

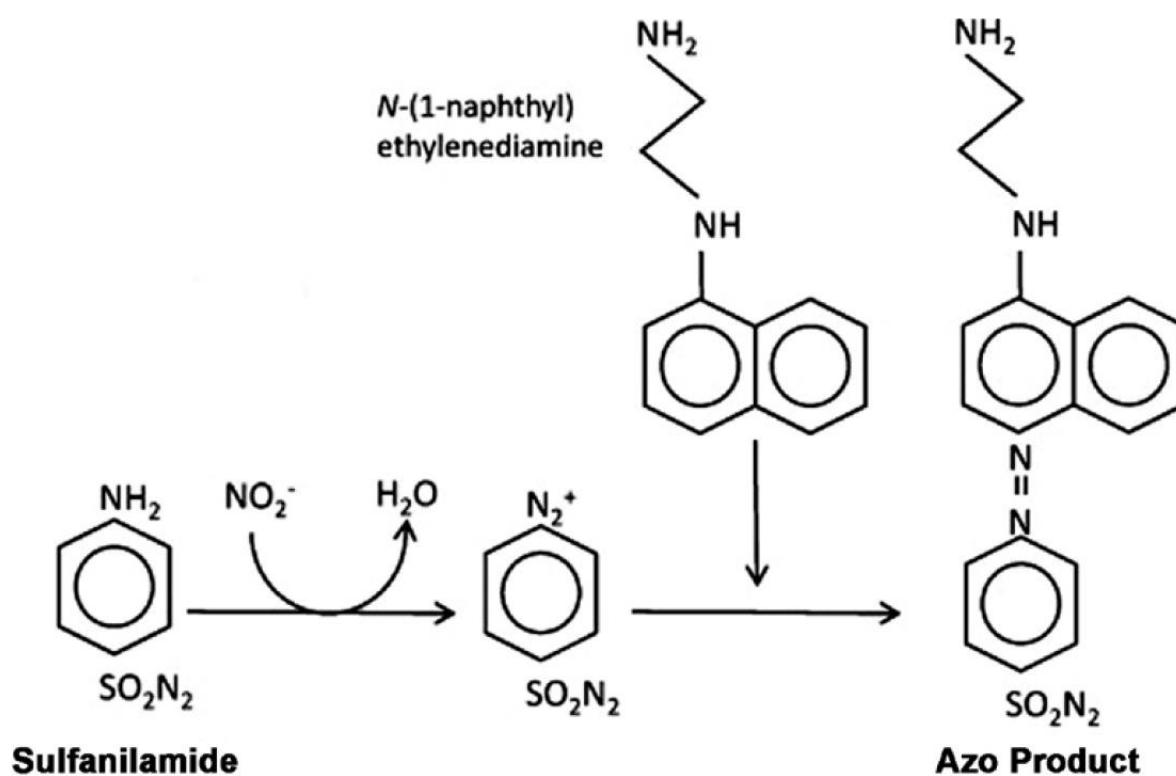


Figure 2.6.4 The NO_2^- detection reaction by using the OxiSelect™ reagent²¹⁾

An amino functional group ($-\text{NH}_2$) of the sulfanilamide is replaced to an azo functional group ($-\text{N}_2$) by a reaction with nitrite ions. Moreover, the product reacts with N-(1-naphthyl) ethylene diamine and an azo product, which absorbs a 540 nm light, is generated as shown in Figure 2.6.4.

A micro plate reader is not necessary for the measurement because the absorbance of azo product is stable at least several hours after mixing the reagent. The rest of the reagent can be restored by freezing immediate after used.

§ 2.7 Gas chromatography and mass spectrometry (GC-MS)

§ 2.7.1 Theory

Gas chromatography and mass spectrometry (GC-MS) is a combined measurement method of the gas chromatography (GC) which has high resolution and mass spectrometry (MS) which can analyze qualitative. GC-MS is fine measuring organic species in a liquid.

Figure 2.7.1 shows a schematic illustration of a mechanism of the GC-MS measurement.

In this study, a gas chromatography (HP6890, Agilent Technologies) with a separating column (HP19091S-433, Agilent Technologies) and a mass spectrometry (HP5973, Agilent Technologies) were used for detecting.

Before a sample injection, liquid samples were filtrated by a 0.22 μm filter for avoiding a clogging of the separating column. A 1 μL of sample injected to the GC was heated to 250°C and vaporized. The vaporized sample was sprit to 1:50 and injected to the separating column with 1.0 L/min of He gas flow.

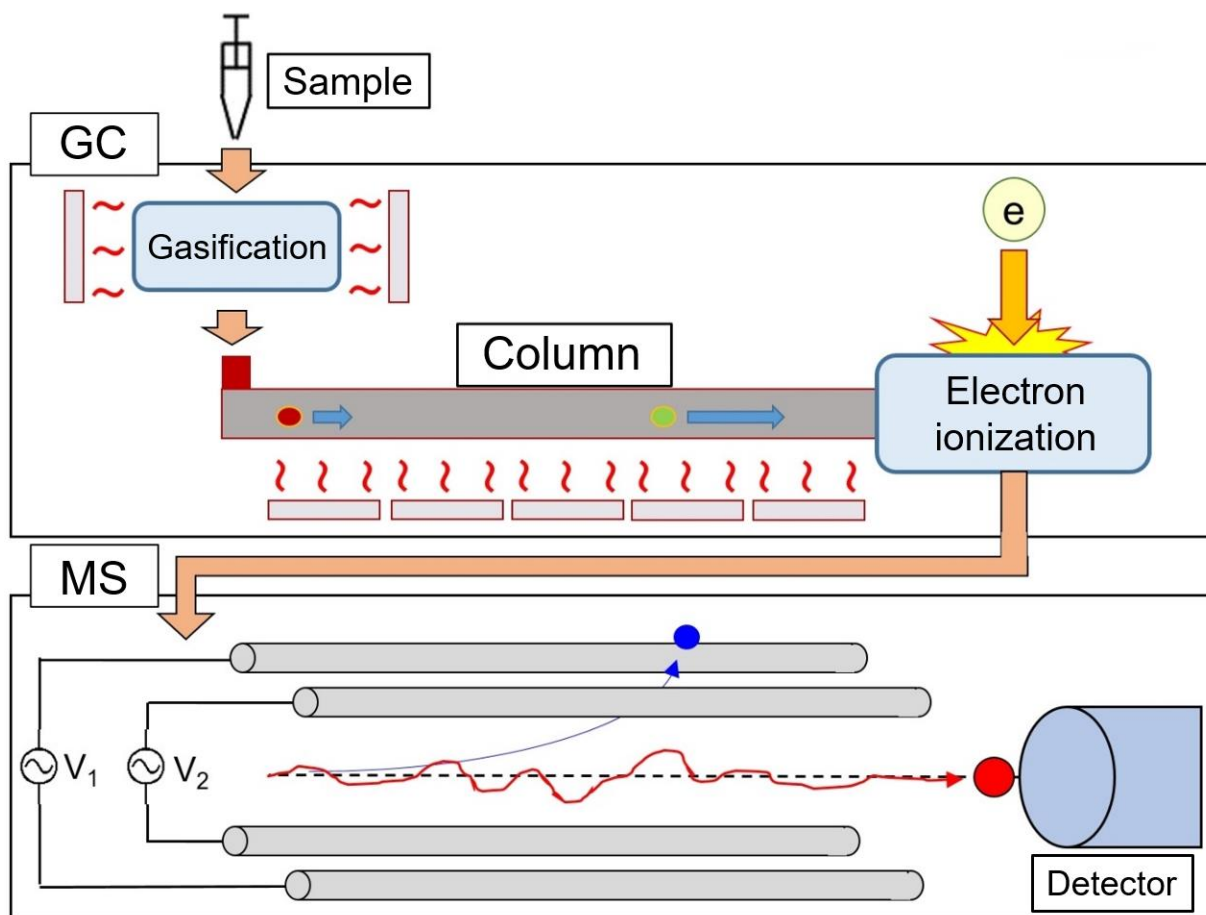


Figure 2.7.1 A schematic illustration of a mechanism of the GC-MS measurement.

The separation column, which is 1 m of length, filled with a loading material. Injected samples are separated by differences of a transaction between samples and the loading material. In this study, the author used the 5% phenyl – 95% methyl polysiloxane as the loading material.

By gradually increasing the temperature of the separating column, fine peaks were obtained samples having various boiling point. In addition, the obtained peak become sharp because the holding time is shortened. In this study, the column temperature was increased to 290°C form 40°C with the increasing rate of 10°C/min.

Samples separated by a GC system are injected to an electron ionization room in a MS system and then fragmented and ionized.

The MS used in this study is constructed by a quadrupole mass spectrometry. The quadrupole MS is composed of 4 electrode poles and a detector. Ac voltages of $V_1 = U + V\cos \omega t$ and $V_2 = -U - V\cos \omega t$ are applied to each 2 poles.

Then, the electric field is described as a formula (2.7.1).

$$\begin{aligned}
 E_x &= -\frac{\delta\varphi}{\delta x} = -(U + V\cos \omega t) \frac{2x}{r_0^2} \\
 E_y &= -\frac{\delta\varphi}{\delta y} = (U + V\cos \omega t) \frac{2y}{r_0^2} \\
 E_z &= -\frac{\delta\varphi}{\delta z} = 0
 \end{aligned}
 \tag{2.7.1}$$

Equation of motion of ions injected to the electric field is described as a formula (2.7.2).

$$\begin{aligned}
 m \frac{\delta^2 x}{\delta t^2} + 2e(U + V \cos \omega t) \frac{x}{r_0^2} &= 0 \\
 m \frac{\delta^2 y}{\delta t^2} - 2e(U + V \cos \omega t) \frac{y}{r_0^2} &= 0 \\
 m \frac{\delta^2 z}{\delta t^2} &= 0
 \end{aligned} \tag{2.7.2}$$

From the formula (2.7.2), injected ions receive a periodic forth in the direction of X and Y axis. Ions moves with a constant velocity in the direction of Z axis since no forth is received in the direction.

By changing of variables as shown in (2.7.3), the formula (2.7.2) is changed to a differential equation (2.6.4), which is known as the *Mathieu equation*.

$$\omega t = 2 \xi, \quad a = \frac{8eU}{mr_0^2 \omega^2}, \quad q = \frac{4eV}{mr_0^2 \omega^2} \tag{2.7.3}$$

$$\begin{aligned}
 \frac{\delta^2 x}{\delta t^2} + (a + 2q \cos 2 \xi) x &= 0 \\
 \frac{\delta^2 y}{\delta t^2} + (a + 2q \cos 2 \xi) y &= 0
 \end{aligned} \tag{2.7.4}$$

The equation has a stable solution and an unstable solution when the $\xi \rightarrow \infty$, namely, an infinite time passed.

Ions reach to the detector in only a condition obtaining a stable solution. Obtaining

a stable solution or not is decided by a function containing a and q .²²⁾

The requirements to obtain a stable solution is called as a stable diagram. Consequently, ions having various mass can be detected by changing the AC voltage with keeping the ratio of a and q .²²⁾

§ 2.7.2 Derivatization method

Generally, GC-MS can detect volatile organic species such as carbohydrate, aromatic compounds, terpene, ester, lactone, alcohol and so forth. In this study, hydrophilic low molecular weight organic compounds such as amino acid, organic acids, saccharides, nucleic acid bases and so on are also measured by a derivatization method generating a methoxime and a trimethylsilyl compounds.²³⁾

A reaction of treating with a methoxamine is shown in Figure 2.7.2.

A carbonyl group ($-C(=O)-$), which is a hydrophilic functional group, is changed to a volatile methoxime ($R-C(=NOCH_3)-R'$) by a dehydration generation with a methoxamine (CH_3ONH_2).

A reaction of treating with an N-methyl-N-trimethylsilyl-trifluoroacetamide (MSTFA) is shown in Figure 2.7.3.

A hydroxyl group ($-OH$), which is a hydrophilic functional group, is changed to a volatile trimethylsilyl ($R-O-Si(-CH_3)_3$) by reacting with a MSTFA.

From the above, samples are volatile by an addition of hydrophobic groups generated from hydrophilic groups with the derivatization method. Samples should be completely dried since the derivatization is prevented by a moisture.

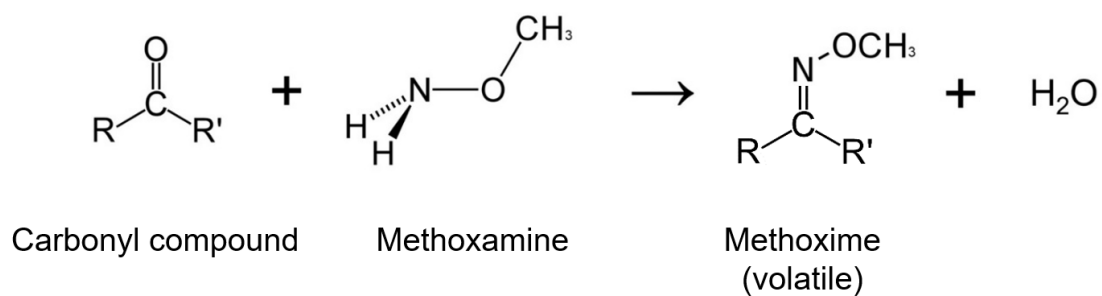


Figure 2.7.2 A reaction of treating hydrophilic compounds with a methoxamine.

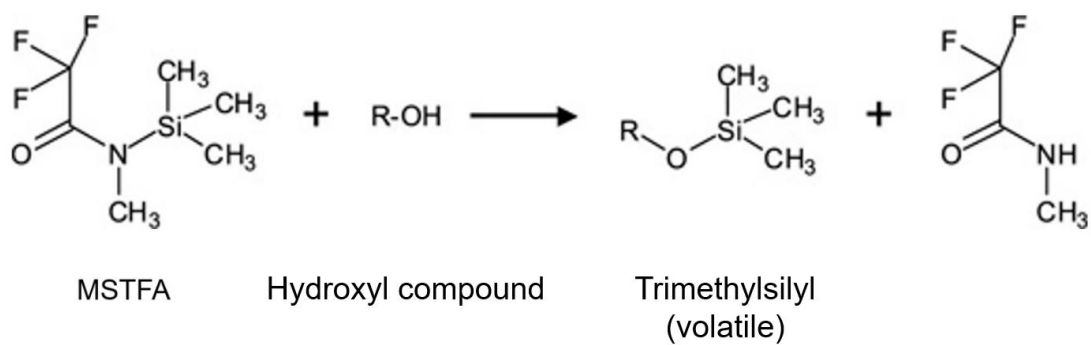


Figure 2.7.3 A reaction of treating hydrophilic compounds with a MSTFA.

Chapter 2 Experimental setup and evaluation methods of PAM and crystals

In this study, 50 μL of an O-methylhydroxylamine hydrochloride (Sigma) diluted with a pyridine (wako) (20 g/L) was mixed to the dried samples, then the sample incubated for 90 min at 37°C (cell incubator is preferred). After that, 100 μL of MSTFA plus 1 vol% 2,2,2-trifluoro-N-methyl-N-(trimethylsilyl)-acetamide, chlorotrimethylsilane (TMCS; wako) is mixed with the sample and then the sample incubated for 30 min at 27°C (thermostatic oven was used).²⁴⁾

The method was used for an analysis of oxalic acid generation by the NEAPP.

§ 2.8 Microscope observation

In this study, microscope was used for a differential interference contrast (DIC) observation and a fluorescence observation.

Images obtained by the DIC measurement reflect a refraction factor and a thickness of a sample. Therefore, the DIC measurement is preferred to measure a transparent sample such as cells and crystals. The measurement mechanism is shown in Figure 2.8.1.

A half part of observation light is polarized and transmit through the sample in parallel with the other light. Some light path difference is generated in a place which has a gradient of a refraction factor or a thickness and detected.

In the fluorescence measurement, exciting light was emitted to samples by using a halogen lamp (TH4-100, Olympus) with a blue light filter and a fluorescence light is observed.

In this study, the DIC and the fluorescence observation were done by an upright microscope (IX73, Olympus).

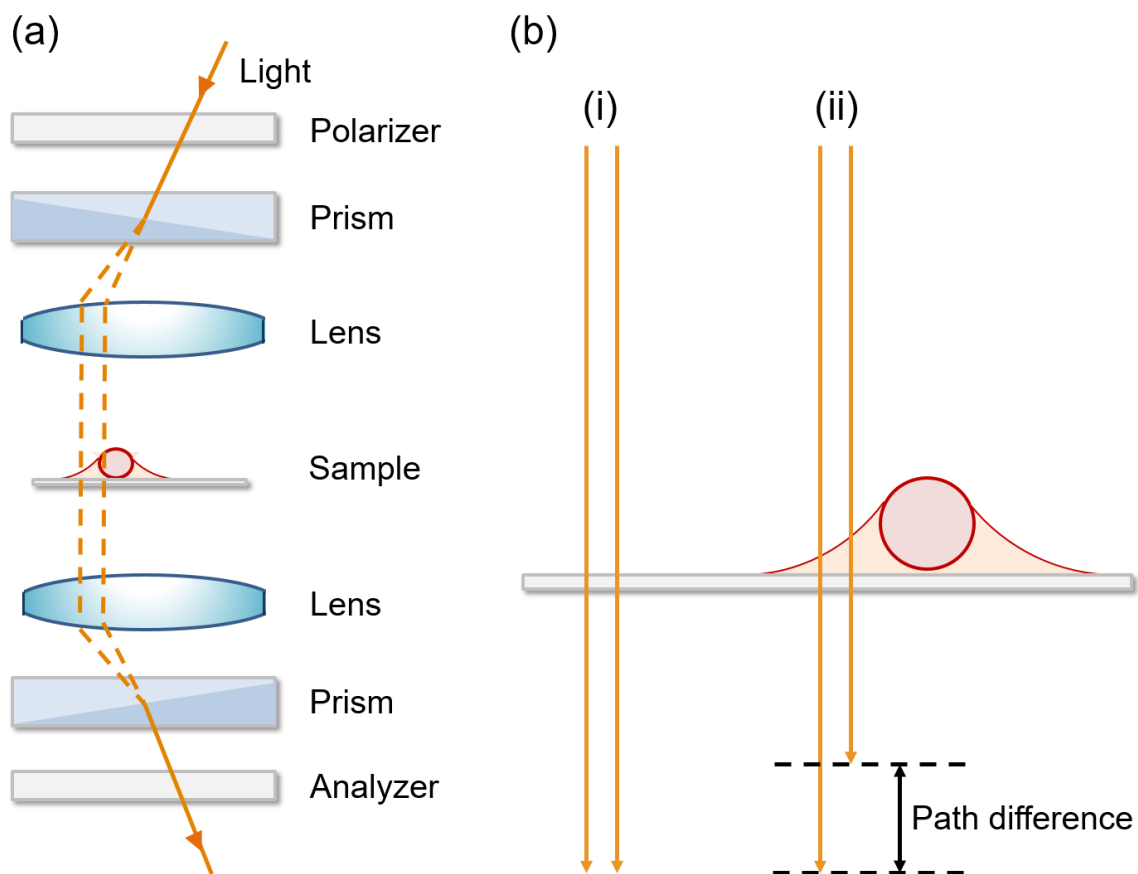


Figure 2.8.1 (a) A structure of DIC microscope and (b) a light transmission (i) without or (ii) with a sample.

§ 2.9 Analysis using cells

§ 2.9.1 Cell passaging

Cells need a regular passaging even when an experiment is not done because cells are living. In addition, experimental results are affected by properties of the passaging such as a passaging cycle and a cell confluence, which is a cell covering ratio of a bottom of cell culturing dish. Controlling of those properties by the regular passaging is very important for a repeatability of experiments using cells.

In this study, human glioblastoma cells (U251SP; Center for Advanced Medicine and Clinical Research, Nagoya univ.) and human breast epithelial cells (MCF10A; Center for Advanced Medicine and Clinical Research, Nagoya univ.) were cultured with a DMEM (plus FBS, P/S). All of cell dealings was done in a clean bench (MHE-132AJ, Panasonic) for preventing some bacteria contamination.

An old medium was aspirated from a cell culturing dish and then the cells were washed with 6 mL of DPBS. After aspirating the DPBS, the dish was incubated with 2 mL of a trypsin (Sigma) at 37°C, 5% of CO₂ concentration for several minutes until peeling off (U251SP: about 4 min, MCF10A: about 15 min). After that, the cell suspension mixing with 8 mL of DMEM was centrifuged by a centrifugal separator (KUBOTA2800; 22°C, 1300 rpm, 5 min) and then the supernatant was replaced to a new DMEM. The cell suspension diluted to a proper concentration with the DMEM was poured to a 25 cm² flask (Sigma) and re-incubated.

The passaging frequency depends on the cell type and the surroundings. In this study,

3×10^5 counts of U251SP cells were passaged every 2 days and 3×10^5 counts of MCF10A cells were passaged every 6 days.

A trypan blue solution (invitrogen) was used for counting cells. Cell living is also analyzed because living cells are dyed only the cell membrane, on the other hand died cells are also dyed inner of the cell.

In this study, only cells, whose cell survival was over 80% and confluence was 70-90%, were used for experiments.

§ 2.9.2 Cell survival assay

The CellTiter 96[®] AQueous One Solution Cell Proliferation Assay (Promega) has been used for measuring cell survivals.²⁵⁻²⁷⁾ The kit composed of the 3-(4,5-dimethylthiazol-2-yl)-5-(3-carboxymethoxyphenyl)-2-(4-sulfophenyl)-2H-tetrazolium, inner salt (MTS), which permeate cell membranes.

An intracellular reaction of the MTS is shown in Figure 2.9.1.²⁸⁾

The MTS is reduced to a formazan by an intracellular nicotinamide adenine dinucleotide (NADH), which is an evidence of the cell living judged by an aspect of cellular metabolism. Relative cell survivals were calculated by measuring an absorbance of 490 nm light; the wavelength light is absorbed by the formazan.

Micro plate reader is preferred to use in the experiment since the formazan generation continues as long as the cell living. In addition, the cell culture plate should be shaded because the absorbance of MTS is also increasing by a light emission.

The experiment takes 3 days. 200 μ L of cell suspension composed of 5000 cells was added to each wells of 96 well cell culturing plate (Falcon). Then the plate was incubated for 24 h at 37°C, 5% of CO₂ after 20 min of leaving to stand. The leaving to stand is done for enhancing cells to adherent because the distribution of cells are biased by a gas flowing in an incubator if cells incubated immediately after the cell suspension pouring. The cell distributions of each experiments should be similar since gathered cells are likely to be difficult to be killed compared with distributed cells.

After the incubation, the medium replaced to 200 μ L of samples and then 24 h incubation was done. After that, the samples replaced to 100 μ L of the CellTiter 96[®] reagent diluted 10 times by the DMEM and then 490 nm absorbance was measured after

1 h of incubation.

In this study, cell survival is calculated by $100 \times ((\text{absorbance of samples}) - (\text{background}) / (\text{absorbance of initial}) - (\text{background}))$. The initial represents cells incubated with the initial medium and the background represents only the CellTiter 96[®] reagent.

Samples are the PAM and RONS, whose concentration is same as the PAM, added medium. H₂O₂, NO₂⁻ and NO₃⁻ is added with H₂O₂ solution (invitrogen), NaNO₂ solution (Wako) and NaNO₃ solution (Wako). An effect of the dilution of the DMEM could be neglected because only less than 1 vol% of those solutions were added to the DMEM.

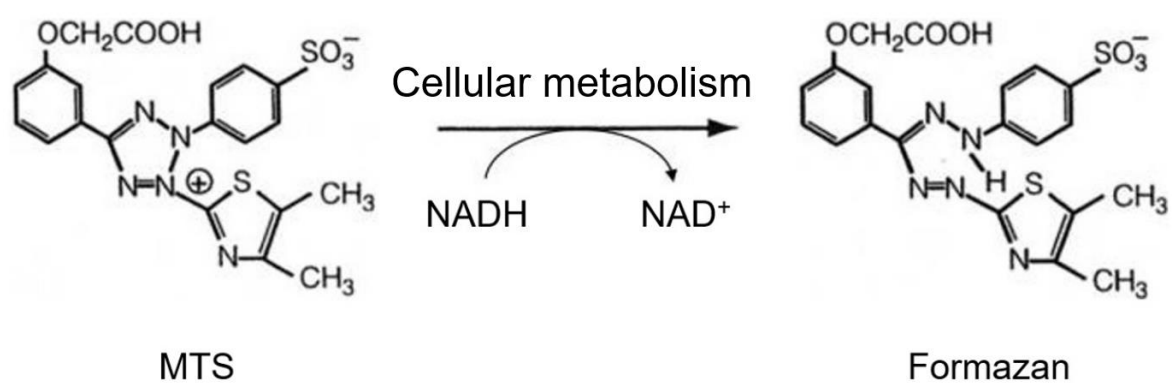


Figure 2.9.1 An intracellular reaction of the MTS reduced to a formazan.²⁸⁾

§ 2.9.3 Fluorescence probe

5-(and-6)-chloromethyl-2',7'-dichlorodihydrofluoresceindiacetate, acetyl ester (CM-H₂DCFDA) (Invitrogen) has been used for measuring a whole intracellular RONS.²⁹⁾ The reagent detect RONS, nonselectively. The detection reactions inside a cell is shown in Figure 2.9.2.³⁰⁾

A CM-H₂DCFDA permeated to an inside of a cell changed to 2', 7'-Dichlorodihydrofluorescin (DCFH) by an intracellular esterase catalyzing. Then DCFH changed to 2', 7'-dichlorodifluorescin (DCF) by an oxidation induced by intracellular RONS. The DCF was excited by a 492-495 nm light and emitted 517-527 nm fluorescence.

In this study, 200 μ L of cell suspension composed of 5000 cells was added to each wells of 8 well culture slide (Falcon). Then the plate was incubated for 24 h at 37°C, 5% of CO₂ after 20 min of leaving to stand. After that, 10 μ M of CM-H₂DCFDA solution of DPBS replaced each wells for loading the reagent to cells and the culture slide was incubated for 1 h. After that, 200 μ L of samples replaced each wells and the fluorescent was observed after 2 h of an additional incubation.

The obtained fluorescent images were merged with the DIC image of the cells.

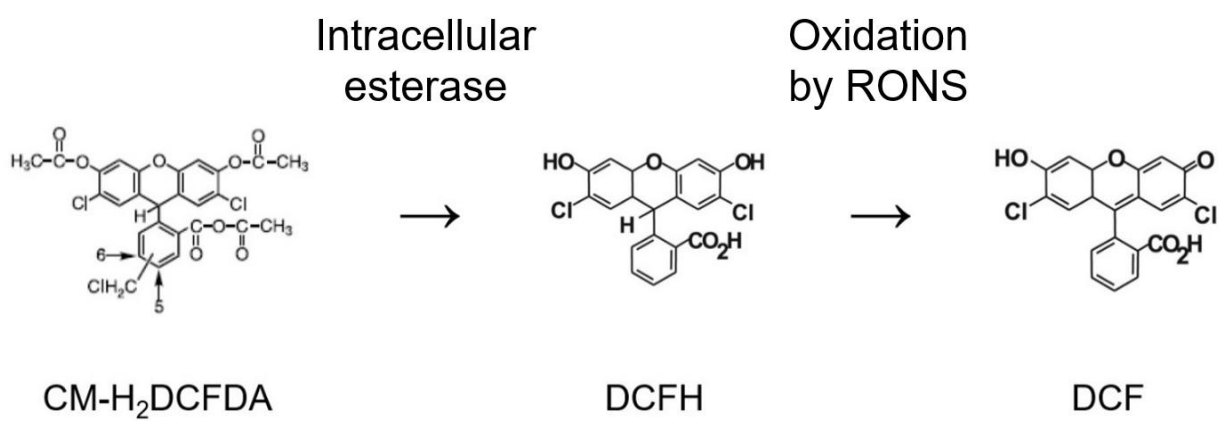


Figure 2.9.2 A detection reactions of CM-H₂DCFDA inside a cell.²⁸⁾

§ 2.10 Metabolomics

§ 2.10.1 Theory

Metabolomics is one of the *Omic*s, which elucidates an intracellular mechanisms by analyzing the changing of intracellular proteins, genes, metabolomes and so forth.³¹⁾

Metabolomics has many advantages from other *Omic*s, for example, the few analysis targets, the fine reflection of a phenotype, the high and fast sensitivity for a disorder. Therefore, there are many reports described about the metabolism analysis. The number is increasing gradually. Over 1000 reports are published per year now. There are reports of wide topics from a fundamental analysis of cell metabolism,³²⁾ to an investigation of the effect of an anticancer drug.³³⁾

One of the causes of the public interest is a new discovery about aspect of cancers, a dysbolism.³⁴⁾ Namely, a metabolism difference between cancer cells and normal cells is attracted attentions. For example, most cancer cells predominantly produce energy and other species, which used for cell proliferation, by *glycolysis* rather than oxidative phosphorylation via the tricarboxylic acid (TCA) cycle, even in the presence of an adequate oxygen supply, which is known as *Warburg effect*.³⁵⁾ Actually, most famous recent topics of the metabolome are related with the *Warburg effect*, which are glucose, insulin and mitochondria.

In this study, 1×10^6 counts of U251SP cells mixed with 10 mL of DMEM in 100 mm cell culture dish (Falcon) were incubated (37°C, 5% of CO₂) for 24 h. After that, the medium replaced to 10 mL of samples, which is an initial medium, the PAM and RONS,

whose concentration is as long as the PAM, added medium, and the samples were incubated for 30 min. Then, after washing cells with 10 mL of 5w% D-mannitol solution, metabolomes in the cell were abstracted by mixing with 800 μL of ethanol and then 550 μL of a standard solution was mixed. After that, an ultrafiltration of the 1000 μL of the sample was performed ($2300 \times g$, 4°C , 5 min). Then, only the supernatant was analyzed by CE-MS method.

§ 2.10.2 Capillary electrophoresis and mass spectrometry (CE-MS)

CE-MS is one of the mass spectrometry method. CE-MS was generally used for analysis of metabolomes of cancer cells because of the high quantitativity and the applicability for various type species weather volatile or not.³²⁾ The difference from GC-MS explained in § 2.7 is the mechanism of a separation of samples. Electric field is applied to the both ends of a capillary through a sample solution. Samples were separated by the difference of the velocity of samples decided by electric charges, viscosities and radius of ions. The method is prefer to use for a metabolomics because it can detect ionic compounds, which is composed of many of metabolomes.

In this study, 52 kinds of cations and 64 kinds of anions were measured. Agilent CE-TOFMS system (Agilent Technologies) was used for detecting cations with the voltage of a positive, 27 kV and Agilent CE system for CE and Agilent 6460 TripleQuad LC/MS Machine No. QqQ1 for MS were used for detecting anions with the voltage of a positive, 30 kV. In both measurements, Fused silica capillary (50 μm \times 80 cm) was used as the capillary.

The measured 116 of metabolomes were listed to Table 2.10.1.

Table 2.10.1 List of 116 metabolomes measured by the CE-MS analysis.

2,3-Diphosphoglyceric acid	Creatinine	IMP	Spermine
2-Hydroxyglutaric acid	Cys	Inosine	Succinic acid
2-Oxoglutaric acid	Cystathionine	Isocitric acid	Thr
2-Oxoisovaleric acid	Dihydroxyacetone phosphate	Lactic acid	Trp
2-Phosphoglyceric acid	Erythrose 4-phosphate	Leu	Tyr
3-Phosphoglyceric acid	Folic acid	Lys	UDP-glucose
6-Phosphogluconic acid	Fructose 1,6-diphosphate	Malic acid	Urea
Acetoacetyl CoA	Fructose 1-phosphate	Malonyl CoA	Uric acid
Acetyl CoA	Fructose 6-phosphate	Met	Val
Adenine	Fumaric acid	Mevalonic acid	Xanthine
Adenosine	Galactose 1-phosphate	N,N-Dimethylglycine	XMP
Adenylosuccinic acid	GDP	N-Acetylglutamic acid	Xylulose 5-phosphate
ADP	Gln	NAD+	β -Ala
ADP-ribose	Glu	NADH	γ -Aminobutyric acid
Ala	Glucose 1-phosphate	NADP+	
AMP	Glucose 6-phosphate	NADPH	
Arg	Glutathione (GSH)	N-Carbamoylaspartic acid	
Argininosuccinic acid	Glutathione (GSSG)	Ornithine	
Asn	Gly	Phe	
Asp	Glyceraldehyde 3-phosphate	Phosphocreatine	
ATP	Glycerol 3-phosphate	Phosphoenolpyruvic acid	
Betaine	Glycolic acid	Pro	
Betaine aldehyde	Glyoxylic acid	PRPP	
cAMP	GMP	Putrescine	
Carbamoylphosphate	GTP	Pyruvic acid	
Carnitine	Guanine	Ribose 1-phosphate	
Carnosine	Guanosine	Ribose 5-phosphate	
cGMP	His	Ribulose 5-phosphate	
Choline	HMG CoA	S-Adenosylhomocysteine	
cis-Aconitic acid	Homocysteine	S-Adenosylmethionine	
Citric acid	Homoserine	Sarcosine	
Citrulline	Hydroxyproline	Sedoheptulose 7-phosphate	
CoA	Hypoxanthine	Ser	
Creatine	Ile	Spermidine	

§ 2.10.3 Principal component analysis (PCA)

Principal component analysis (PCA) is one technique for reducing a dimensionality of large multivariate datasets.³⁶⁾ In the case of the study, 116 of dimensionality by each measured metabolomes are reduced to 11 axis from PC1 to PC11.

When the samples plotted to those axis, each quantities of measured 116 metabolomes are weighted and summed. The PC1 axis is decided so that the dispersion of values are maximum as described in formula (2.10.1),

$$I_{PC1} = x_1 I_1 + x_2 I_2 + x_3 I_3 + \dots + x_{116} I_{116} \quad (2.10.1)$$

where x_n represents weighting and I_n represents quantities of metabolomes. After that, PC2 to 11 axis also plotted same method. The proportion of variances indicated information amounts of each axis and calculated by a formula (2.10.2),

$$P_{PCn} = l_i / \sum_{i=1}^{11} l_i \quad (2.10.2)$$

where l_i represents each characteristic values.

§ 2.11 X-ray diffraction (XRD)

§ 2.11.1 Theory

X-ray diffraction (XRD), whose wavelength and strength is specific to the crystal structure, is obtained by a monochrome X-ray irradiation to the crystal sample as shown in Figure 2.11.1. The d represents a distance between atoms constructing the crystal. A composition, structure and crystallinity of measured sample are obtained from the XRD spectrum. The analysis method has been used for films and crystals.³⁷⁻³⁹⁾

In this study, a powder sample mashing the particles synthesized by the NEAPP irradiation was analyzed by the XRD. D8 ADVANCE (Brucker AXS) was used with a $\text{CuK}\alpha$ line filtered by a Ni filter.

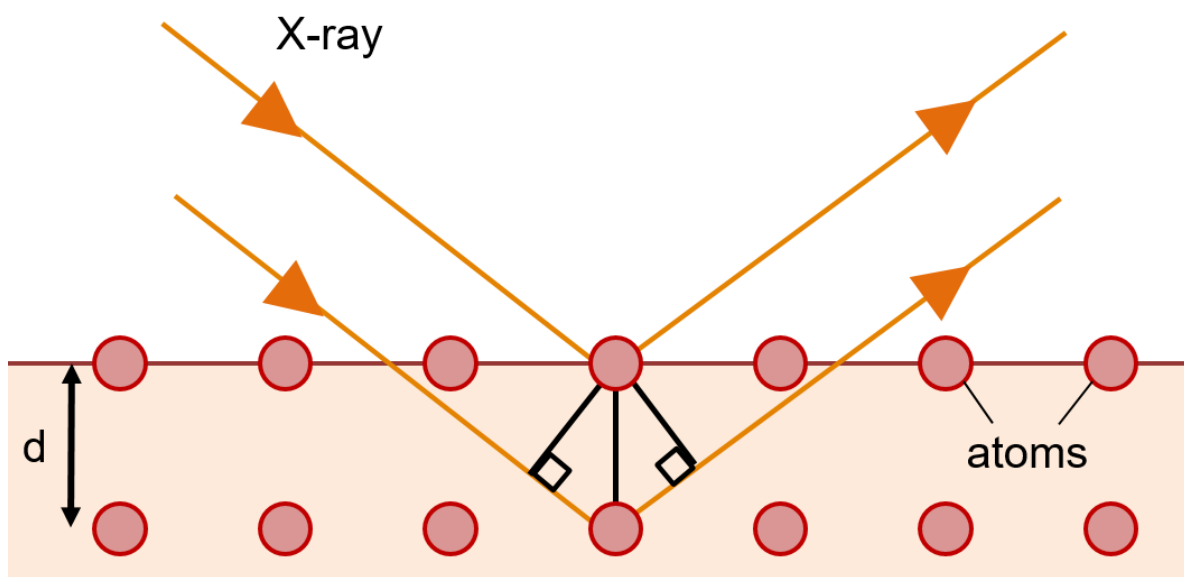


Figure 2.11.1 A scheme of an X-ray irradiation to a crystal surface for the XRD analysis.

§ 2.11.2 Rietveld analysis

Rietveld analysis, which is a whole pattern fitting structure refinement invented by Hugo Rietveld, is now widely accepted to be an exceptionally valuable method for structural analysis of nearly all classes of crystalline materials not available as single crystals.⁴⁰⁾

By using the method, parameters of a crystal structure and a form of peaks are refined with a fitting to a theory or a standard spectrum by a least squares method.

In this study, Rietveld refinement of the XRD data was performed using the EXPO2014 package.⁴¹⁾ standard XRD cards were acquired from a powder diffraction file database (PDF-2/PDF-4).

§ 2.12 Scanning electron microscope and energy dispersive X-ray spectrometry (SEM-EDX)

Scanning electron microscope and Energy dispersive X-ray spectrometry (SEM-EDX) has been used for various structural analysis such as polymer composition.⁴²⁻⁴⁴⁾

In the SEM a stream of primary electrons is focused onto the sample surface resulting in a number of different particles or waves being emitted such as secondary electrons, back-scattered electrons, X-rays, photons, Auger electrons and so forth.

Characteristic X-ray is emitted from X-ray irradiated atom as shown in Figure 2.12.1. An inner shell electron is excited by the X-ray irradiation and a hole is generated. Then an outer shell electron fill in the hole and the rest energy is emitted as a characteristic X-ray.

The characteristic X-rays give characteristic chemical information of the emitting atoms. The probed depth in EDX analysis is around 1-3 μm , which is decided by the escape depth of a characteristic X-ray.

In this study, S-3400N (Hitachi high-tech) was used for the SEM with 20 kV of acceleration voltage and EDAX genesis (EDAX) was used as for the XMA. Some disturbance, mainly C and O, was likely to be also measured except of the signals of samples since the samples were fixed on an organic adhesive agent.

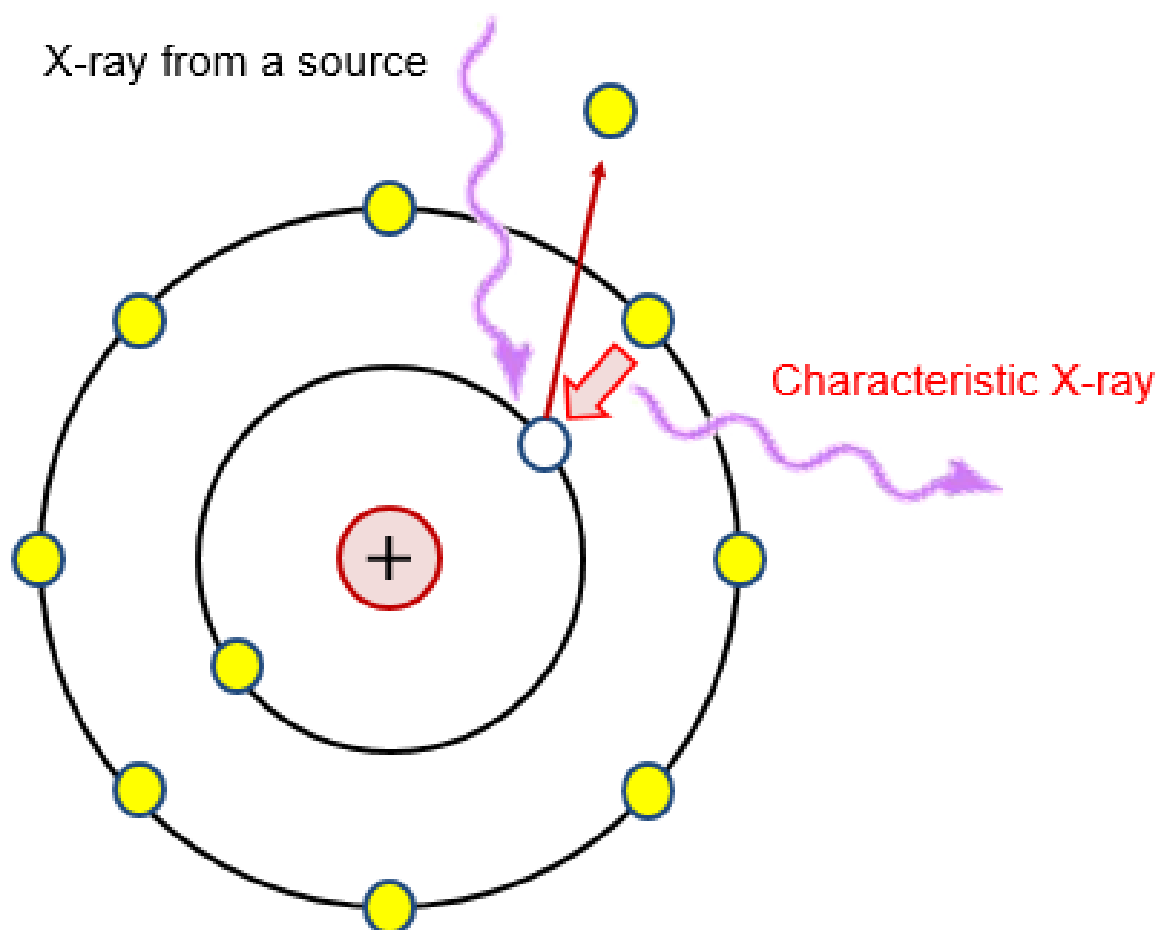


Figure 2.12.1 A scheme of an X-ray irradiation to an atom of sample for the EDX analysis.

§ 2.13 Fourier Transform infrared (FT-IR)

FT-IR is an important technique in organic chemistry. It is an easy way to identify the presence of certain functional groups in a molecule. Also, one can use the unique collection of absorption bands to confirm the identity of a pure compound or to detect the presence of specific impurities.⁴⁵⁻⁴⁷⁾

Functions of a sample is analyzed by measuring an infrared absorbance by bindings consisted in samples as listed in Table 2.13.1.

In the FT-IR measurement, disturbing spectra of a water (4000 cm^{-1} to 3400 cm^{-1} , 2000 cm^{-1} to 1300 cm^{-1}) and carbon dioxide (around 2400 cm^{-1}) were also observed. The water and carbon dioxide spectrum from vapor can be reduced by N_2 gas or dried air flowing to the measuring cavity. Samples should be also completely dried for preventing a water infrared absorbing.

In this study, the powder sample mixed with KBr powder (wako) and pressed was analyzed by the Continuum (Thermofisher scientific). The number of accumulation was 1024 and the resolution was 8 cm^{-1} .

Table 2.13.1 List of FT-IR peaks from organic functions.

Functional group	Mode	Position (cm ⁻¹)	Strength
<i>Alkane</i>	C-H stretch	3000-2840	Middle
	C-H bending	1600-1400	Middle
<i>Alkene</i>	C=C stretch	1647-1640	Middle
	C-H stretch	3150-3050	Middle
	C-H out-of-plane bending	1000-650	Strong
<i>Alkyne</i>	C-C stretch	2260-2100	weak
	C-H stretch	3340-3270	Strong
	C-H bending	700-600	Strong
<i>Aromatic</i>	C-H stretch	3100-3000	Middle
	C-H out-of-plane bending	900-675	Middle
	C-H stretch	1450-1400	Weak
<i>Alcohol</i> (associative) (not associative)	O-H stretch	3650-3580	Strong
	O-H stretch	3550-3200	Strong
	C-O stretch	1260-1000	Strong
<i>Ether</i> (fatty) (aromatic)	C-O stretch	1260-1000	Strong
	C-O-C antisymmetric stretch	1150-1080	Strong
	C-O-C antisymmetric stretch	1275-1020	Strong
	C-O-C symmetric stretch	1075-1020	Strong
<i>Ketone</i>	C=O stretch	1740-1690	Strong
<i>Aldehyde</i>	C=O stretch	1720-1740	Strong
<i>Carbonic acid</i>	O-H stretch	3300-2500	Strong
	C=O stretch	1720-1700	Strong
	O-H bending	100-850	Middle
<i>Ester, Lactone</i> (fatty) (formic acid, aromatic)	C-O stretch	1300-1000	Strong
	C=O stretch	1750-1735	Strong
	C=O stretch	1730-1715	Strong
<i>Amide</i>	C=O stretch	1650-1515	Strong
<i>Amine</i> (weak solution) (liquid)	N-H stretch	3500, 3400	Strong
	N-H stretch	3400-3350	Strong
		3330-3250	Strong

§2.14 Statistics

Statistical analysis. All assays were performed in duplicate and the empirical standard deviations were calculated.

Empirical standard deviations demonstrate the reproducibility of parallel assays but do not allow statistical analysis of variance. The t-test was used for the statistical determination of significances ($p < 0.05$ = significant; $p < 0.01$ = high significant).

Asterisks (* = significant; ** = high significant) signifying statistical significance are shown in the figures.

References for Chapter 2

- 1) M. Iwasaki, H. Inui, Y. Matsudaira, H. Kano, N. Yoshida, M. Ito, and M. Hori, Nonequilibrium atmospheric pressure plasma with ultrahigh electron density and high performance for glass surface cleaning. *J. Appl. Phys.* **92**, 081503 (2008).
- 2) H. Tanaka, M. Mizuno, K. Ishikawa, K. Nakamura, H. Kajiyama, H. Kano, F. Kikkawa, and M. Hori, *Plasma Medicine*. **1**, 265-277 (2011).
- 3) H. Tanaka, M. Mizuno, K. Ishikawa, K. Nakamura, F. Utsumi, H. Kajiyama, H. Kano, S. Maruyama, F. Kikkawa, and M. Hori, *Plasma Medicine*. **2**, 207-220 (2012).
- 4) S.S. Martin, and P. Leder, *Mol. Cell. Biol.* **21**, 6529-6536 (2001).
- 5) Sigma-Aldrich. "Dulbecco's Modified Eagle's Medium (DME) - Formulation". (<http://www.sigmaaldrich.com/content/dam/sigma-aldrich/docs/Sigma/Formulation/d5796for.pdf>).
- 6) K. Takeda, Y. Miyawaki, S. Takashima, M. Fukasawa, K. Oshima, K. Nagahata, T. Tatsumi, and M. Hori, *J. Appl. Phys.* **109**, 033303 (2011).
- 7) J.W. Coburn and M. Chen, *J. Appl. Phys.* **51**, 3134-3136 (1980).
- 8) Y. Kawai, K. Sasaki and K. Kadota, *Jpn. J. Appl. Phys.* **36**, L1261 (1997).
- 9) R.E. Walkup, K.L. Saenger and G.S. Sewyn, *J. Chem. Phys.* **84**, 2668 (1986).
- 10) H.M. Katsch, A. Tewes, E. Quandt, A. Goehlich, T. Kawetzki and H.F. Döbele, *J. Appl. Phys.* **88**, 6232 (2000).
- 11) S. F. Durrant and M.A.B. Moraes, *J. Vac. Sci. Technol. A*. **13**, 2513 (1995).
- 12) S. F. Durrant and M.A.B. Moraes, *J. Vac. Sci. Technol. A*. **16**, 509 (1998).
- 13) A. Gicquel, M. Chenevier, Kh. Hassouni, A. Tserepi and M. Dubus, *J. Appl. Phys.* **83**, 7504 (1998).

- 14) W. John, "Electron Spin Resonance: Elementary Theory and Practical Applications", *Springer Netherlands*. (1986).
- 15) K. Makino, *Kagaku to seibutsu*. **27**, 529-532 (1989).
- 16) T. Kondo, V. Misik, and P. Riesz, *Ultrason. Sonochem.* **3**, S193-S199 (1996).
- 17) A. Tani, Y. Ono, S. Fukui, S. Ikawa, and K. Kitano, *Appl. Phys. Lett.* **100**, 254103 (2012).
- 18) H. Wu, P. Sun, H. Feng, H. Zhou, R. Wang, Y. Liang, J. Lu, J. Zhang, and J. Fang, *Plasma Process. Polym.* **9**, 417-424 (2012).
- 19) T. Azma, K. Fujii, and O. Yuge, *Life Sciences*. **54**, 185-190 (1994).
- 20) M. Zhou, Z. Diwu, N.P. Voloshina, and R.P. Haugland, *Analyt. Bioc.* **253**, 162-168 (1997).
- 21) L.C. Green, D.A. Wagner, J. Glogowski, P.L. Skipper, J.S. Wishnok, and S.R. Tannenbaum, *Analyt. Biochem.* **126**, 131-138 (1982).
- 22) K. Fuwa, and T. Fujii, *Shijyu-kyoku Shituryoubunsekikei -Genri to Ohyo- [Quadruple Mass Spectrometer -Principle and Application-]*, Tokyo, Koudansha, (1977).
- 23) Y. Zhou, Z. Wang, and N. Jia, *J. Environ. Sci.* **19**, 879-884 (2007).
- 24) <http://www.an.shimadzu.co.jp/gcms/support/lib/pdf/c146-0261.pdf>
- 25) G. Malich, B. Markovic, and C. Winder, *Toxicology*. **124**, 179-192 (1997).
- 26) P. Wang, S.M. Henning, and D. Hever, *PLOS ONE*. **5**, e10202 (2010).
- 27) H. nakagami, K. Maeda, R. Morishita, S. Iguchi, T. Nishikawa, Y. Takumi, Y. Kikuchi, Y. Saito, K. Tamai, T. Ogihara, and Y. Kaneda, *Arterioscler. Thromb. Vasc. Biol.* **25**, 2542-2547 (2005).
- 28) J.A. Barltrop, and T.C. Owen, *Bioorg. Med. Chem. Lett.* **1**, 611-614 (1991).

- 29) T. Sato, M. Yokoyama, K. Johkura, *J. Phys. D: Appl. Phys.* **44**, 372001 (2011).
- 30)
https://tools.thermofisher.com/content/sfs/manuals/Reactive_Oxygen_Species_ROS_Detection_Reagents_J1_10Jan2006.pdf
- 31) C. Knox, V. Law, T. Jewison, P. Liu, S. Ly, A. Frolkis, A. Pon, K. Banco, C. Mak, V. Neveu, Y. Djoumbou, R. Eisner, A.C. Guo, and D.S. Wishart, *Nucl. Acids Res.* **39**, D1035-D1041 (2011).
- 32) A. Hirayama, K. Kami, M. Sugimoto, M. Sugawara, N. Toki, H. Onozuka, T. Kinoshita, N. Saito, A. Ochiai, M. Tomita, H. Esumi, and T. Soga, *Cancer Res.* **69**, 4918-4925 (2009).
- 33) H. Makinoshima, M. Takita, K. Saruwatari, S. Umemura, Y. Obata, G. Ishii, S. Matsumoto, E. Sugiyama, A. Ochiai, R. Abe, K. Goto, H. Esumi, and K. Tsuchihara, *J. Biol. Chem.* **290**, 17495-17504 (2015).
- 34) D. Hanahan, and R.A. Weinberg, *Cell.* **144**, 646-674 (2011).
- 35) O. Warbug, On the origin of cancer cells. *Science.* 123, 309-314 (1956).
- 36) I. Jolliffe, "Principal Component Analysis".
DOI: 10.1002/9781118445112.stat06472 (2014).
- 37) H.S.C. O'Neill, and W.A. Dollase, *Phys. Chem. Minerals.* **20**, 541-555 (1994).
- 38) M.H. Yao, R.J. Baird, F.W. Kunz, and T.E. Hoost, *J. Catal.* **166**, 67-74 (1997).
- 39) K. Thamaphat, P. Limsuwan, and B. Ngotawornchai, *Kasetsart J. (Nat. Sci.)* **42**, 357-361 (2008).
- 40) H.M. Rietveld, "The Rietveld Method", *Energy Research Foundation.* (1993).
- 41) EXPO2014 <http://www.ba.ic.cnr.it/content/expo>; A. Altomare, C. Cuocci, C. Giacobuzzo, A. Moliterni, R. Rizzi, N. Corriero, and A. Falcicchio, *J. Appl. Cryst.*

46, 1231-1235 (2013).

42) K. Suzuki, *Atmos. Environ.* **40**, 2626-2634 (2006).

43) N. Thaulow, U.H. Jakobsen, and B. Clark, *Cement. Concrete. Res.* **26**, 309-318 (1996).

44) F. Scala, and R. Chirone, *Biomass and Bioenergy.* **32**, 252-266 (2008).

45) D. Naumann, D. Helm, and H. Labischinski, *Nature.* **351**, 81-82 (1991).

46) B.L. Frey, and R.M. Corn, *Anal. Chem.* **68**, 3187-3193 (1996).

47) M. Kacurakova, P. Capek, V. Sasinkova, N. Wellner, and A. Ebringerova, *Carbohydr.*

Polym. **43**, 195-203 (2000).

Chapter 3

Quantitative measurement of RONS in the PAM

§ 3.1 Introduction

The mechanism of an antitumor effect of the PAM is unclear. Relatively long-lived RONS generated by NEAPPs are likely to contribute for the antitumor effect of the PAM.^{1,2)} Moreover, short-lived RONS is also important since it has been considered as a precursors of the long-lived RONS in a NEAPP irradiated water.³⁾ However, quantitative measurements of those RONS generated in the NEAPP irradiated medium has not been performed.

Therefore, the author measured comprehensive RONS generation in the PAM and compared with other reported NEAPP sources.

In this Chapter 3, a short-lived RONS were detected using ESR with a trapping method and long-lived RONS were detected by using chemical probe methods, respectively.

§ 3.2 Short-lived RONS

Figure 3.2.1 shows an ESR spectrum of the PAM mixed with DMPO before the NEAPP irradiation. DMPO-OH (◆ in Figure 3.2.1), DMPO-H (● in Figure 3.2.1), and other six-lines (▼ in Figure 3.2.1) signals were detected by those hyperfine structures.⁴⁾

Figure 3.2.2 shows the expanded spectrum for 3472-3482 G, where the DMPO-H signal was observed. The DMPO-H signal was 100 times weaker than the DMPO-OH signal. Six-lines seemed to be derived from impurities in the DMPO. DMPO-OH, DMPO-H indicated the generation of hydroxyl radical ($\cdot\text{OH}$) and hydrogen radical ($\cdot\text{H}$) in the PAM during the NEAPP treating.

Those results indicates $\cdot\text{OH}$, which is one of the important short-lived RONS as a precursor of long-lived RONS in the PAM was likely generated by a light dissociation reaction, $\text{H}_2\text{O} + h\nu \rightarrow \cdot\text{OH} + \cdot\text{H}$. The more detailed discussion is described in the Chapter 4.

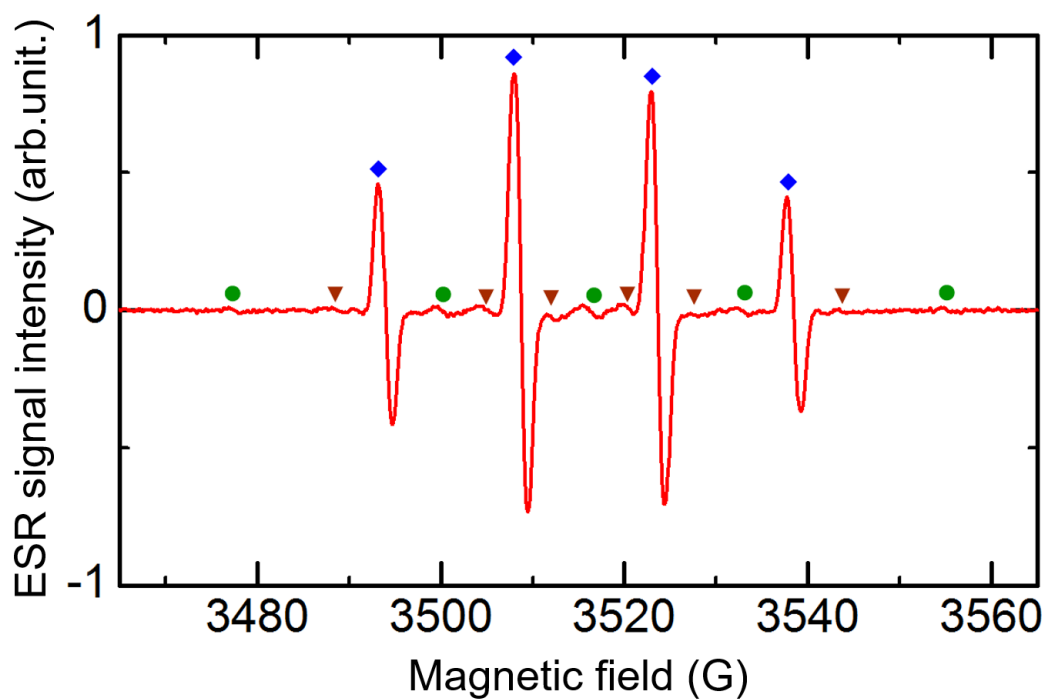


Figure 3.2.1 ESR spectrum of the PAM mixed with DMPO before the NEAPP irradiation; DMPO-OH (◆), DMPO-H (●), and other six-lines (▼).

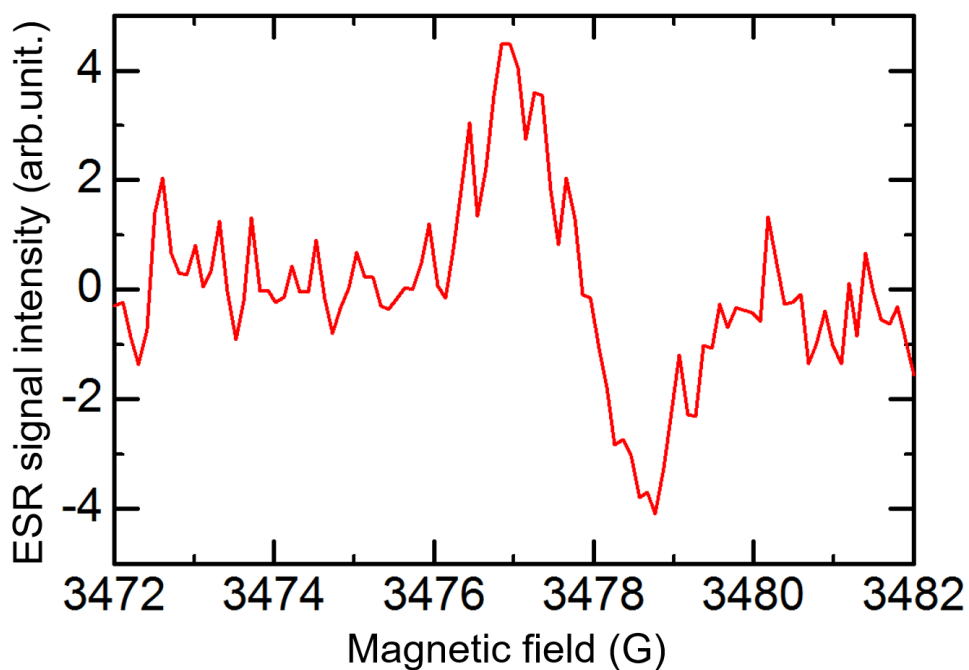


Figure 3.2.2 ESR spectrum of the PAM mixed with DMPO expanded a region from 3472 to 3482 G.

Figure 3.2.3 shows ESR signals of the PAM and a medium added $\cdot\text{NO}$ generating reagent as a positive control. For trapping generated $\cdot\text{NO}$, c-PTIO was pre-added to mediums before starting the NEAPP irradiation or adding $\cdot\text{NO}$ generation reagent.

Absorption spectra of c-PTIO (\bullet in Figure 3.2.3), with signal ratios of 1:2:3:2:1 and hyperfine splitting of N nuclei with 0.82 mT were detected. Four major peaks associated with c-PTI signals (\blacktriangledown in Figure 3.2.3) were also observed, representing adducts of $\cdot\text{NO}$ trapping, with nine lines exhibiting hyperfine splitting of N nuclei of 0.98 and 0.44 mT.

As shown in Figure 3.2.3(a) (i) and (ii), c-PTI signal was observed by more than 10 μM of $\cdot\text{NO}$ generation in a medium. On the other hand, as shown in Figure 3.2.3(a) (iii), no C-PTI signals were detected in the PAM.

It is notable that C-PTI signals were detected in buffer to which NOC7 was added and in which NO radicals were generated to a concentration of at least 10 μM . These observations indicate that NO radicals at concentrations greater than 10 μM dissolve poorly in bulk medium. Therefore, NO radicals produced as a result of NEAPP irradiation might react and be consumed on the liquid surface or in the gas phase.

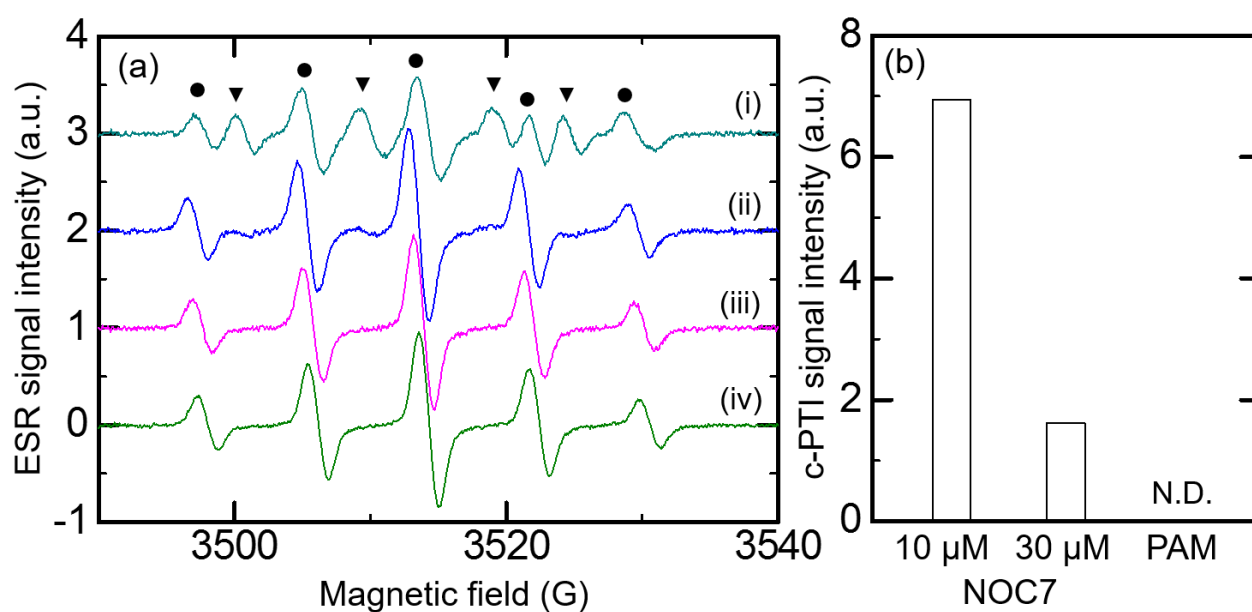


Figure 3.2.3 (a) ESR spectra of 250 μL of 20 mM HEPES buffer solution composed of (i) 30 μM , (ii) 10 μM NOC7 (NO generator). ESR spectra of (iii) PAM, (iv) initial medium. c-PTIO was added to all samples at a concentration of 25 μM . (b) Bar graph depicting the intensity of c-PTI peak (3500 G).

Figure 3.2.4 shows an ESR spectrum of the PAM mixed with the CYPMPO before the NEAPP irradiation obtained 4 min after from finished the NEAPP irradiation.

CYPMPO-OH adduct (\blacktriangledown in Figure 3.2.4) indicating an existence of $\cdot\text{OH}$ was detected in the PAM immediately after the NEAPP irradiation. The result corresponded to the result of a measurement by DMPO shown in Figure 3.2.1. On the other hand, no CYPMPO-OOH adduct (\blacklozenge in Figure 3.2.4) indicating an existence of super oxide anion ($\cdot\text{O}_2^-$) was detected. The $\cdot\text{O}_2^-$ generation by a NEAPP has been reported in the plasma activated water (PAW) and the it was also reported the pH lowering induced by the NEAPP enhanced the generation.⁵⁾ Therefore it was considered that a cause of no $\cdot\text{O}_2^-$ generation that the irradiation target, DMEM, was buffered to around neutral.

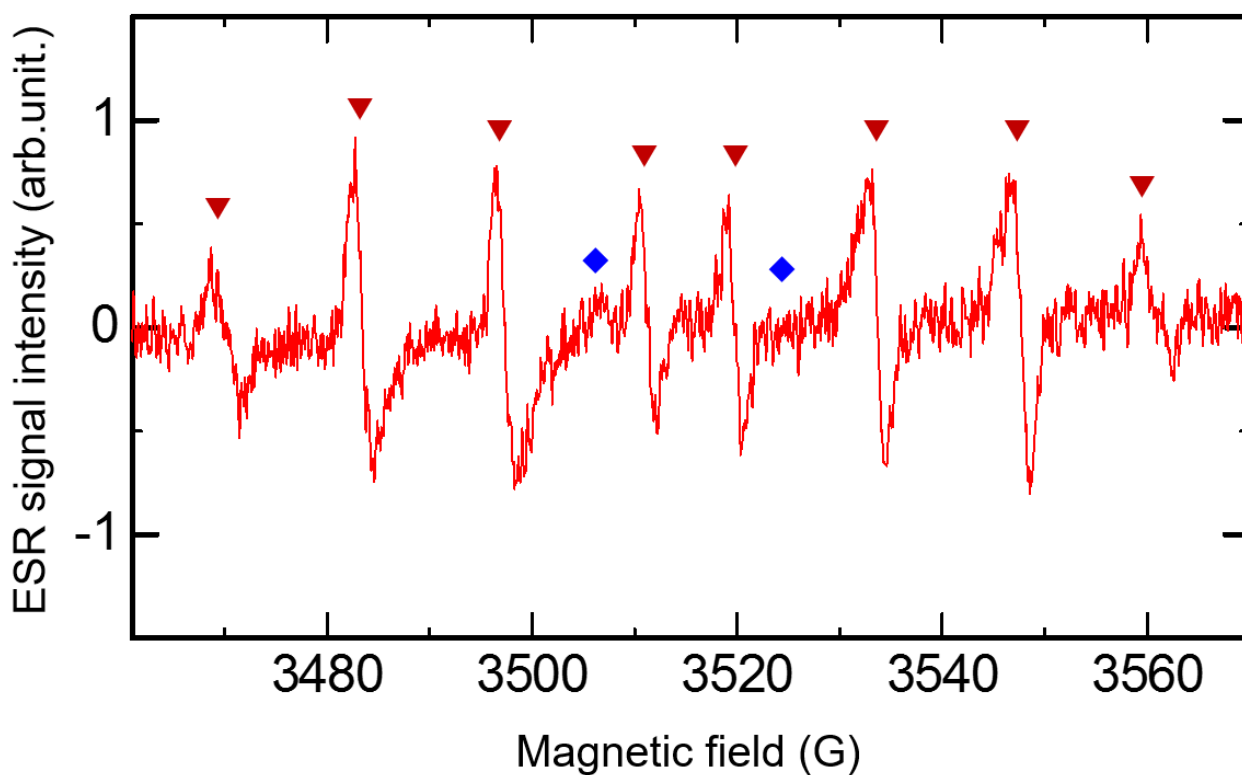


Figure 3.2.4 ESR spectrum of the PAM obtained 4 min after the NEAPP irradiation to CYPMPO added DMEM.

§ 3.3 Long-lived RONS

The result of measurements of long-lived RONS, hydrogen peroxide (H_2O_2), nitrite ion (NO_2^-) and nitrate ion (NO_3^-) were measured by chemical probe methods. Measurement targets were DMEM and DMEM (plus FBS, P/S) irradiated with the NEAPP.

The dependence of H_2O_2 generation on the irradiation period is shown in Figure 3.3.1. The H_2O_2 generated concentrations were proportional to the NEAPP irradiation period at least up to 300 s. The generation rates were $0.3528 \mu\text{M/s}$ and $0.2987 \mu\text{M/s}$ in the DMEM and the DMEM (plus FBS, P/S), respectively. It is considered that H_2O_2 generation rate of the DMEM (plus FBS, P/S) is 1.18 times lower than the DMEM due to the prevention of H_2O_2 generation by anti-oxidants consisted in the FBS.

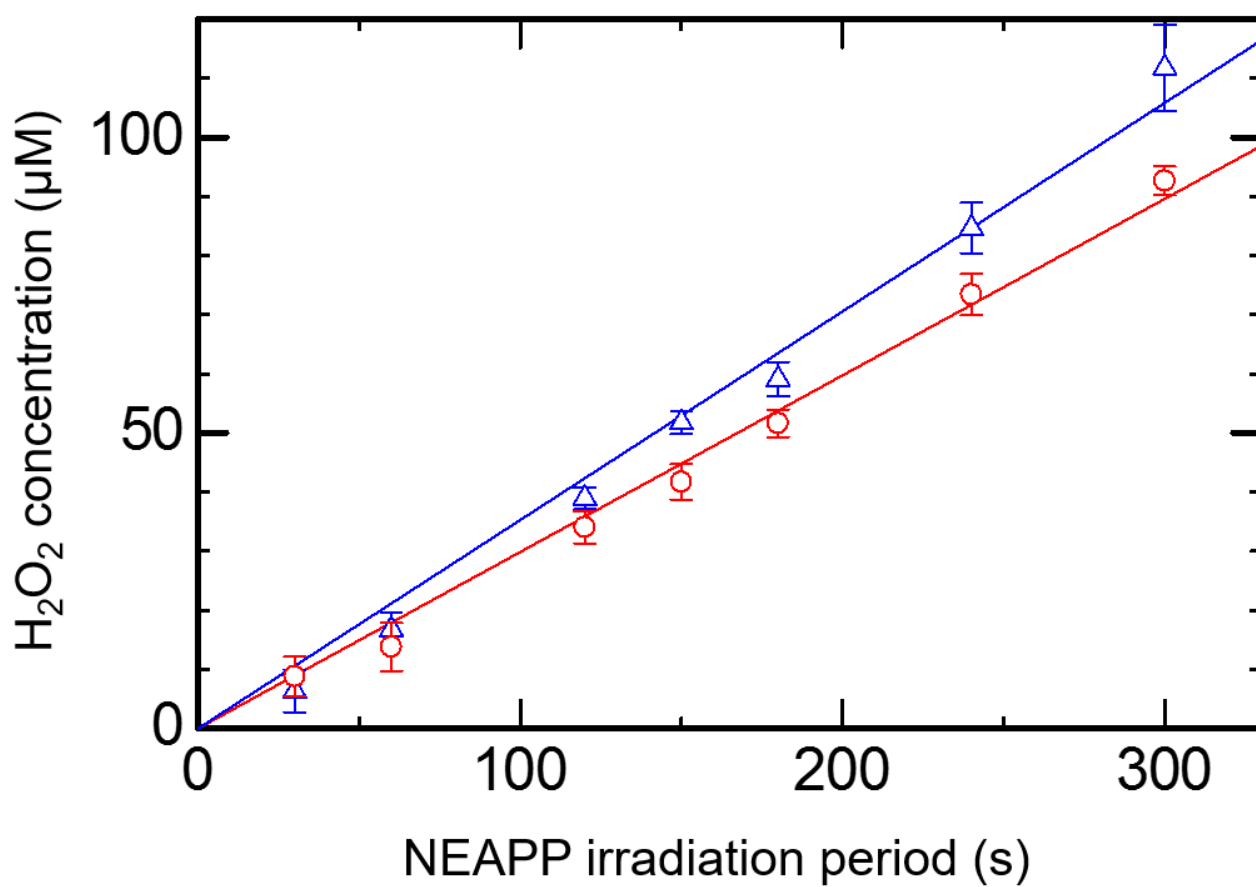


Figure 3.3.1 The dependence of H_2O_2 generated concentrations in the NEAPP irradiated (Δ) DMEM and (\circ) DMEM (plus FBS, P/S) on the irradiation period.

The dependence of NO_2^- generation on the irradiation period is also shown in Figure 3.3.2. The NO_2^- generated concentrations were proportional to the NEAPP irradiation period at least up to 300 s similar to the H_2O_2 . The generation rates were $10.4 \mu\text{M/s}$ in both the DMEM and the DMEM (plus FBS, P/S). Contrary to the H_2O_2 , the result indicates liquid components, such as FBS, were rarely contributed to the NO_2^- generation. This is an evidence of the dominant NO_2^- generation in the gaseous phase, which is discussed in detail at § 4.3.

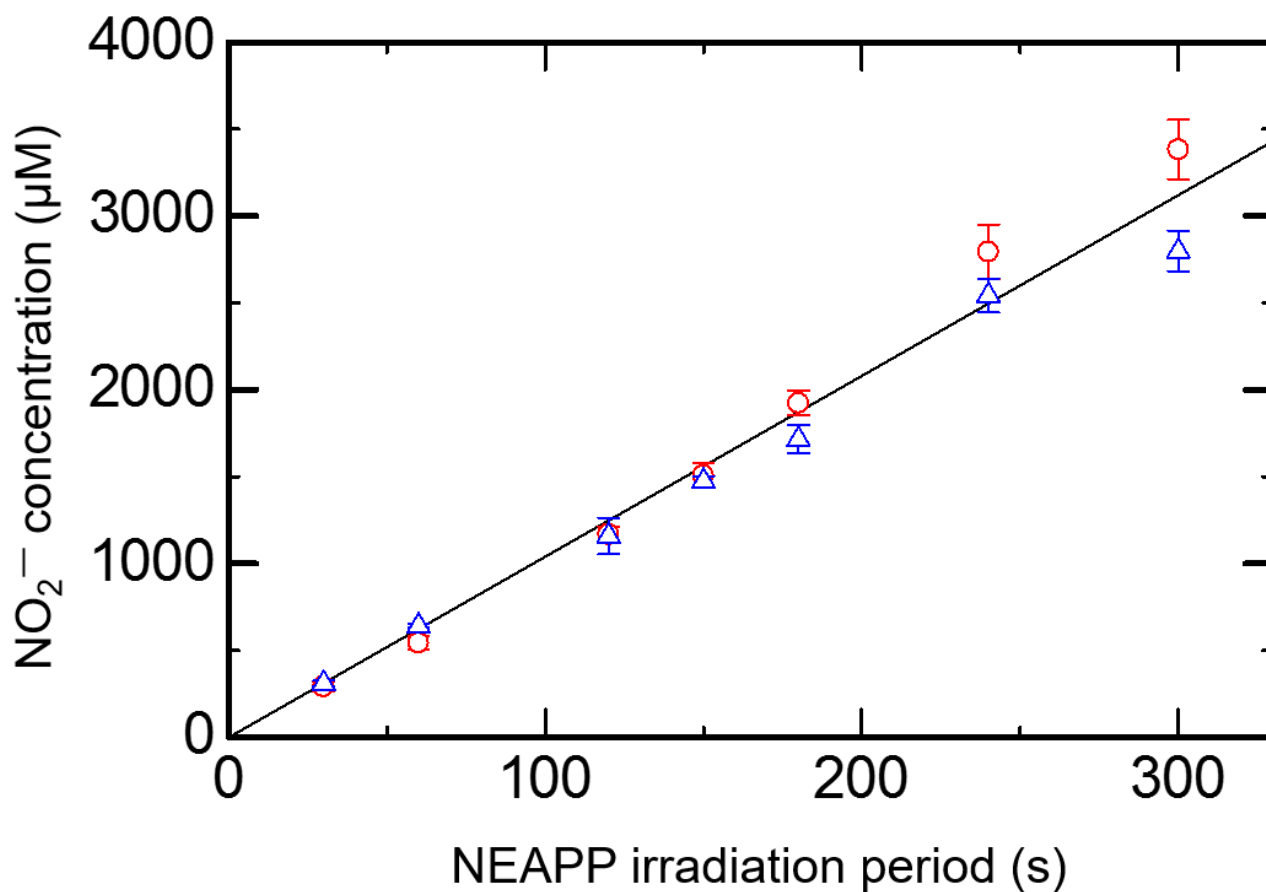


Figure 3.3.2 The dependence of NO₂⁻ generated concentrations in the NEAPP irradiated (△) DMEM and (○) DMEM (plus FBS, P/S) on the irradiation period.

Finally, the dependence of NO_3^- generation on the irradiation period is also shown in Figure 3.3.3.

Several hundreds of micro molar of NO_3^- generation was detected. However, a proportion to the irradiation period was not shown in the measurement in comparison with the H_2O_2 and the NO_2^- measurements and the errors of the concentrations tend to be bigger than the other species.

It is considered that some species prevent an activity of the catalyst for NO_3^- decomposition and the result should be discussed carefully.

Consequently, the generated concentrations of hydrogen peroxide (H_2O_2), nitrite ion (NO_2^-) and nitrate ion (NO_3^-) in NEAPP irradiated liquids were listed to Table 3.3.1 with some previously reported data.

The NEAPP used in this study generates relatively large amount on NO_2^- compared with other NEAPPs for the generated concentration ratio of $\text{NO}_2^-/\text{H}_2\text{O}_2$. The characteristic contributed to the antitumor effect synergistically with other RONS described in Chapter 5.

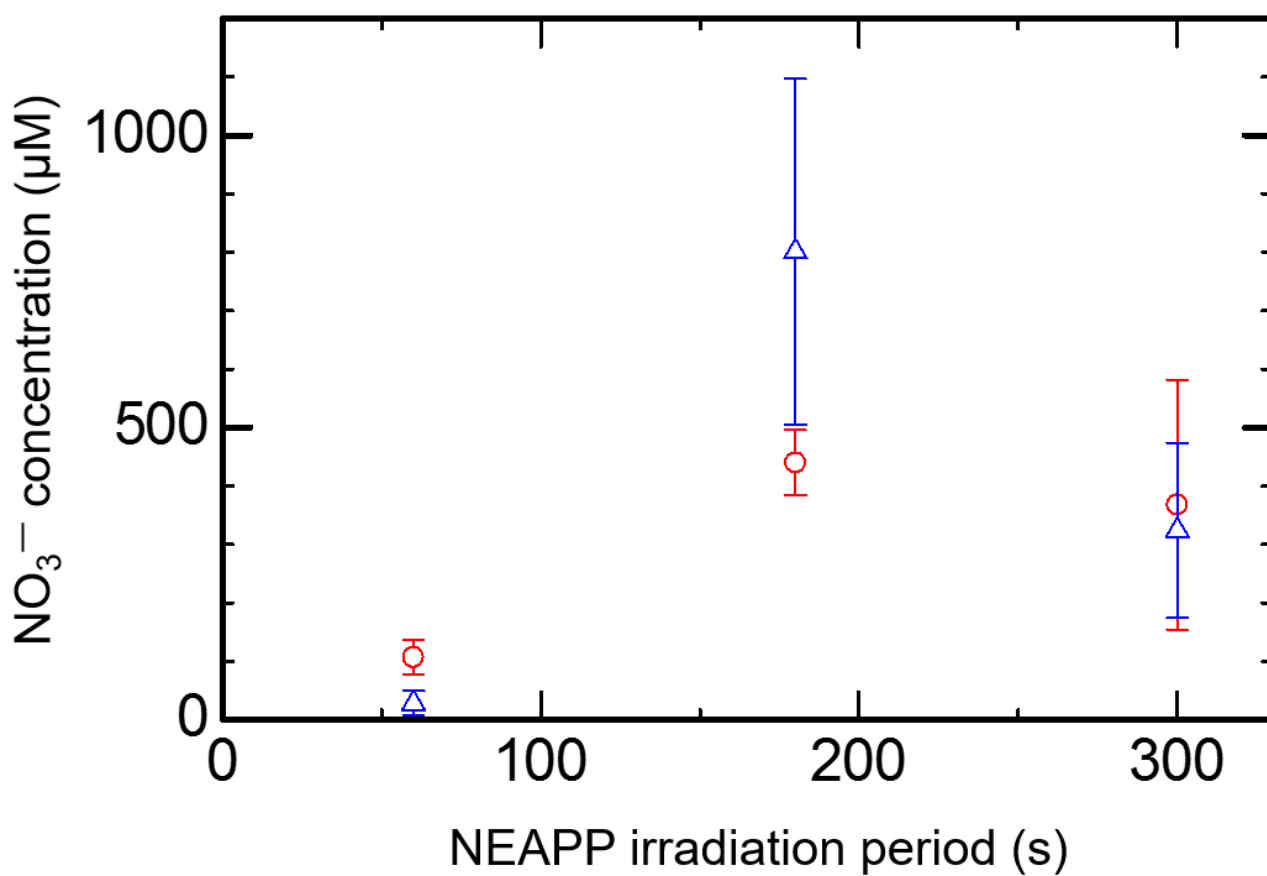


Figure 3.3.3 The dependence of NO₃⁻ generated concentrations in the NEAPP irradiated (△) DMEM and (○) DMEM (plus FBS, P/S) on the irradiation period.

Table 3.3.1 Concentration of H₂O₂, NO₂⁻ and NO₃⁻ generated by 60 s plasma compared with other plasma sources and simulation results.

	H ₂ O ₂ (μM)	NO ₂ ⁻ (μM)	NO ₃ ⁻ (μM)	Notes
<i>Culture media</i>				
Ar 60Hz NEAPP ^a (L = 13 mm)	17 ± 3	642 ± 10	n.a.	DMEM #5796 ^b This study, ~Chapter 6
Ar 60Hz NEAPP (L = 3 mm)	227 ± 42	265	n.a.	DMEM #5796 ⁶⁾ This study, Chapter 7~
Ar 1MHz plasma jet (kinpen GmbH)	33	n.a.	n.a.	RPMI +FBS(8%)+P/S(1%) ⁷⁾
Ar 1.1 MHz plasma jet (kinpen 09 GmbH)	60	26	n.a.	RPMI +FBS(10%)+P/S(2%) +glutamine(1%) ⁸⁾
5 kHz 7.5 kV Liquid surface	87	n.a.	n.a.	MEM +FBS(10%) +P/S ²⁾
300 Hz 10 kV DBD	59 ± 16	69 ± 10	374 ± 85	Agar surface ⁹⁾
320 Hz 15 kV DBD	221 ± 33	74 ± 6	790 ± 38	Agar surface ⁹⁾
He + 0.3%O ₂ 13.56MHz parallel plates	n.a.	7.4 ± 1	n.a.	RPMI +FCS(10%) ¹⁰⁾
<i>Water</i>				
Ar (RF plasma jet)	14.5	21	11	Distilled water ¹¹⁾
Air (27 kV DC)	3.6	7.4	5	¹²⁾
Air (DC electro spray)	170	990	740	with NaH ₂ PO ₄ (7.5 mM) ¹³⁾
Air (Simulation DBD)	280	0.11	76	¹⁴⁾
Air (Glidarc)	2 ± 2	320 ± 40	26 ± 4	Distilled water ¹⁵⁾
Ar (Gas-liquid plasma)	147 ± 30	n.a.	n.a.	Suspension of bacteria ¹⁶⁾

^a NEAPP: Non equilibrium atmospheric pressure plasma

^b DMEM#5796: DMEM composed of a high concentration of glucose

§ 3.4 Reactive organic species

The medium, which is a target of the NEAPP irradiation, composed of various kinds of organics such as glucose, amino acids and vitamins. NEAPP could react with those organics.

Figure 3.4.1 shows GC-MS spectrum of DMEM only, DMEM irradiated with the NEAPP for irradiation distance of 13 mm or 3 mm. Molecular structures of a part of detected species are shown in Figure 3.4.2. In the 3 mm of irradiation distance, the NEAPP plume was touched to the medium surface and not touched when the distance was 13 mm.

As shown in Figure 3.4.1 (a), glutamine in the PAM was decreased by 3 mm or 13 mm of NEAPP irradiation. A similar decreasing is also observed in other amino acids and glucoses. Therefore, the NEAPP was likely to affect to amino acids and some chemical modification was performed whether the NEAPP plume attaching or not. Amino acids changing by an oxidation effect of NEAPPs was reported.¹⁷⁾

However, candidates of the products by the NEAPP irradiation were detected only in the case of attaching NEAPP irradiation as shown in Figure 3.4.2 (b)-(d).

D-gluconic acid is synthesized by an oxidation of glucose. Generally, the process is performed by using a biosynthesis with *Aspergillus niger*.¹⁸⁾ The product indicates glucose oxidation by the attaching NEAPP irradiation. Acetic acid and propanoic acids could be generated from glucose or amino acids by cutting the C-C bond sited a carbonyl group.

Charged particles such as electrons and ions were likely to contribute to the generation since those species could affect to liquid species only when the NEAPP plume

attaching. Short-lived RONS (e.g. $\cdot\text{OH}$, $\cdot\text{H}$) or light emission ($< 339\text{ nm}$) from the NEAPP are candidate of the generation because both effect in an attached irradiation is also bigger than a remote irradiation.

In the case of remote NEAPP irradiation, the decreased organic components was not detected by a GC-MS measurement. Therefore, volatile species such as alcohol is the candidate. It was an evidence that a bad smell was came when the NEAPP irradiated to the medium.

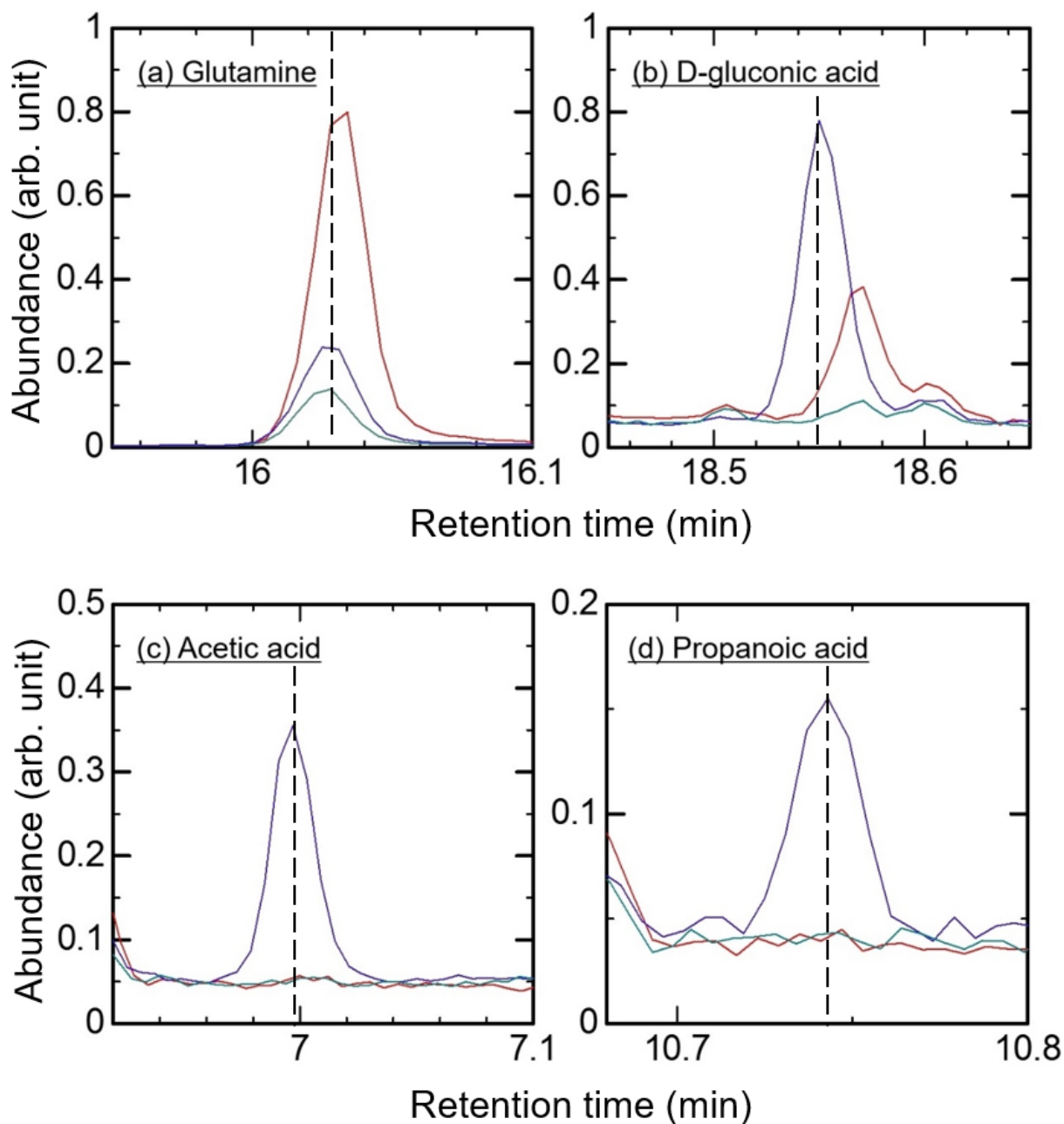


Figure 3.4.1 GC-MS spectrum of DMEM only (red line), DMEM irradiated with the NEAPP, which irradiation distance 13 mm (green line) or 3 mm (blue line).

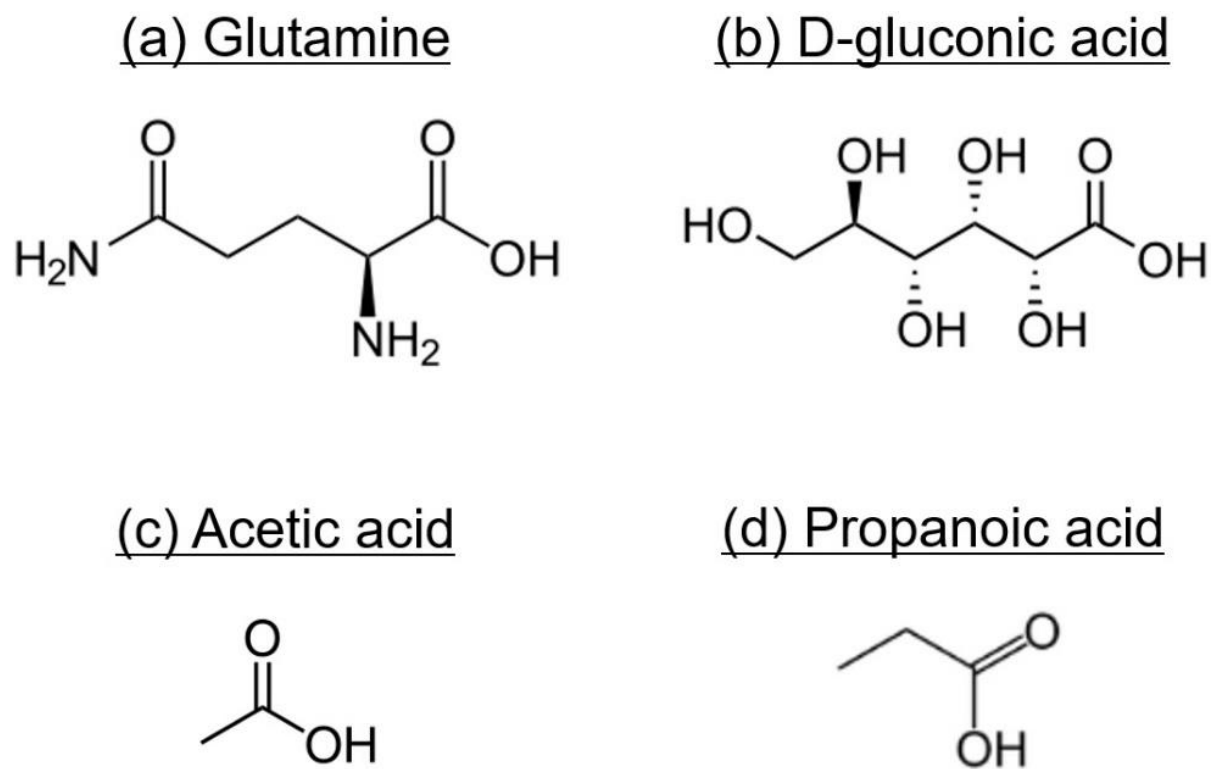


Figure 3.4.2 Structures of a part of detected species by GC-MS.

§ 3.5 Summary

In this Chapter 3, short-lived and long-lived RONS generations in a NEAPP irradiated medium were comprehensively measured.

In short-lived RONS, hydroxyl radical ($\cdot\text{OH}$) and Hydrogen radical ($\cdot\text{H}$) was generated in the PAM immediately after the NEAPP irradiation against super oxide anion ($\cdot\text{O}_2^-$) and nitric monoxide ($\cdot\text{NO}$). Therefore, it is likely that $\cdot\text{OH}$ and $\cdot\text{H}$ was worked as precursor of long-lived species in the PAM generated in the liquid phase and the reactions were investigated in Chapter 4.

In long-lived RONS, hydrogen peroxide (H_2O_2), nitrite ion (NO_2^-) and nitrate ion (NO_3^-) generations were quantitatively detected in the PAM. Therefore, those contributions for the antitumor effect of the PAM were analyzed in Chapter 5. Since H_2O_2 and NO_2^- generations were proportion to the NEAPP irradiation period, those species generated by the NEAPP irradiation certainly. Characteristically, the NO_2^- generation rate was higher than other previous reported NEAPP sources. The result indicated that the NEAPP source susceptible to the ambient air composed of nitrogen molecules.

In organic species, some change occurred by the NEAPP irradiation. Since organic acids was induced in the PAM only for direct irradiation case, no reactive organics has antitumor effect that is observed in the PAM made by remote NEAPP irradiation.

References for Chapter 3

- 1) H. Tanaka, M. Mizuno, K. Ishikawa, K. Nakamura, H. Kajiyama, H. Kano, F. Kikkawa, and M. Hori, *Plasma Medicine*. **1**, 265-277 (2011).
- 2) T. Sato, M. Yokoyama, and K. Johkura, *J. Phys. D: Appl. Phys.* **44**, 372001 (2011).
- 3) W. Tian, and M.J. Kushner, *J. Phys. D: Appl. Phys.* **47**, 165201 (2014).
- 4) H. Nishikawa, and T. Yoshikawa, “ESR and free radical”, Nihon igakukan, (1989).
- 5) A. Tani, Y. Ono, S. Fukui, S. Ikawa, and K. Kitano, *Appl. Phys. Lett.* **100**, 254103 (2012).
- 6) T. Adachi, H. Tanaka, S. Nonomura, H. Hara, S. Kondo, and M. Hori, *Free Radical Biol. Med.* **79**, 28-44 (2014).
- 7) J. Winter, H. Tresp, M.U. Hammer, S. Iseni, S. Kupsch, A.S. Bleker, K. Wende, M. Dunnbier, K. Masur, K.D. Weltmann, and S. Reuter, *J. Phys. D: Appl. Phys.* **47**, 285401 (2014).
- 8) S. Bekechus, J. Kolata, C. Winterbourn, A. Kramer, R. Turner, K.D. Weltmann, B. Broker, and K. Masur, *Free Radical Research*. **48**, 542-549 (2014).
- 9) N. Mertens, M. Mahmoodzada, A. Helmke, P. Grunig, P. Laspe, S. Emmert, and W. Viol, *Plasma Process. Polym.* **11**, 910-920 (2014).
- 10) A.R. Gibson, H.O. McCarthy, A.A. Ali, D. O’Connell, and W.G. Graham, *Plasma Process. Polym.* **11**, 1142-1149 (2014).
- 11) P. Sun, Y. Sun, H. Wu, W. Zhu, J.L. Lopez, W. Liu, J. Zhang, R. Li, and J. Fang, *Appl. Phys. Lett.* **98**, 021501 (2011).
- 12) P. Lukes, E. Dolezalova, I. Sisrova, and M. Clupek, *Sci. Technol.* **23**, 015019 (2014).
- 13) Z. Machala, B. Tarabova, K. Hensel, E. Spetlikova, L. Sikurova, and P. Lukes,

- Plasma Process. Polym.* **10**, 649-659 (2013).
- 14) C.A.J van Gils, S. Hofmann, B.K.H.L. Boekema, R. Brandenburg, and P.J. Bruggeman, *J. Phys. D: Appl. Phys.* **46**, 175203 (2013).
- 15) M. Naitali, G.K. Youbi, J.M. Herry, M.N.B. Fontaine, and J.L. Brisset, *Appl. Environ. Microbiol.* **76**, 7662-7664 (2010).
- 16) J. Shen, Q. Sun, Z. Zhang, C. Cheng, Y. Lan, H. Zhang, Z. Xu, Y. Zhao, W. Xia, and P.K. Chu, *Plasma Process. Polym.* **12**, 252-259 (2015).
- 17) E. Takai, T. Kitamura, J. Kuwabara, S. Ikawa, S. Yoshizawa, K. Shiraki, H. Kawasaki, R. Arakawa, and K. Kitano, *J. Phys. D: Appl. Phys.* **47**, 285403 (2014).
- 18) P. Buzzini, M. Gobbetti, J. Rossi, and M. Ribaldi, *Biotechnol. Lett.* **15**, 151-156 (1993).

Chapter 4

H_2O_2 and NO_2^- generation mechanism in the PAM

§ 4.1 Introduction

In the case of the PAM, the antitumor species are enough stable to remain in the PAM for several hours. However, those generation mechanisms in the PAM have not been fully elucidated yet as described in § 1.2.4.

The RONS generation mechanism is discussed in the Chapter 4. Especially, the author focused H_2O_2 and NO_2^- which are generated in the PAM proportionally to the NEAPP irradiation period. Moreover, H_2O_2 is known as a key species of the antitumor effect of the PAM, ¹⁾ and a characteristic large amount of NO_2^- is generated in the PAM as listed in Table 3.3.1.

The generation reaction phase is separated in gaseous phase and liquid phase. In this study, the liquid phase reaction analysis was mainly discussed. Gaseous reactions were discussed with referring some previous reports.

In the Chapter 4, hydrogen peroxide (H_2O_2) and nitrite ion (NO_2^-) are especially focused and those generating mechanisms in the PAM are analyzed.

§ 4.2 Hydrogen peroxide (H₂O₂)

§ 4.2.1 H₂O₂ generation in gaseous phase

The NEAPP measurements of the gaseous species have been performed previously.^{2,3)} Consequently, gaseous hydroxyl radical($\cdot\text{OH}$) and triplet oxygen atom ($\cdot\text{O}({}^3\text{P})$) were likely to contribute for the H₂O₂ generation.

Figure 4.2.1 shows a gaseous $\cdot\text{OH}$ distribution during the NEAPP irradiation to a medium, which has been measured by laser induced fluorescence (LIF) method.²⁾ Since the NEAPP plume length was about 5 mm, an $\cdot\text{OH}$ radical distribution is concentrated to the inside of the NEAPP plume region. Inside of the NEAPP plume, where VUV and high energy electrons could contribute for the reactions.

In addition, however an absorbing of VUV light by a mixed ambient air was small up to 2 mm from the NEAPP spouting slit, in remote region, VUV light was strongly absorbed by oxygen molecules came from ambient air.²⁾

From the above, it is considered that $\cdot\text{OH}$ radicals is generated by gaseous or in-liquid reactions of a water molecule dissociation of (4.2.1).



Aqueous $\cdot\text{OH}$ recombination to H₂O₂ is well known as a predominant reaction of aqueous $\cdot\text{OH}$ generated by ultrasound or gamma-rays irradiating to water.^{4,5)} Even in gaseous phase, H₂O₂ can be generated from $\cdot\text{OH}$ by a three-body reaction of (4.2.2),⁶⁾



Where M represents a collision partner (e.g. Argon).⁶⁾ Actually, it has been reported that a gaseous H₂O₂ concentration generated by an Ar plasma jet was proportion to a humidity of the discharging Ar gas flow.⁷⁾

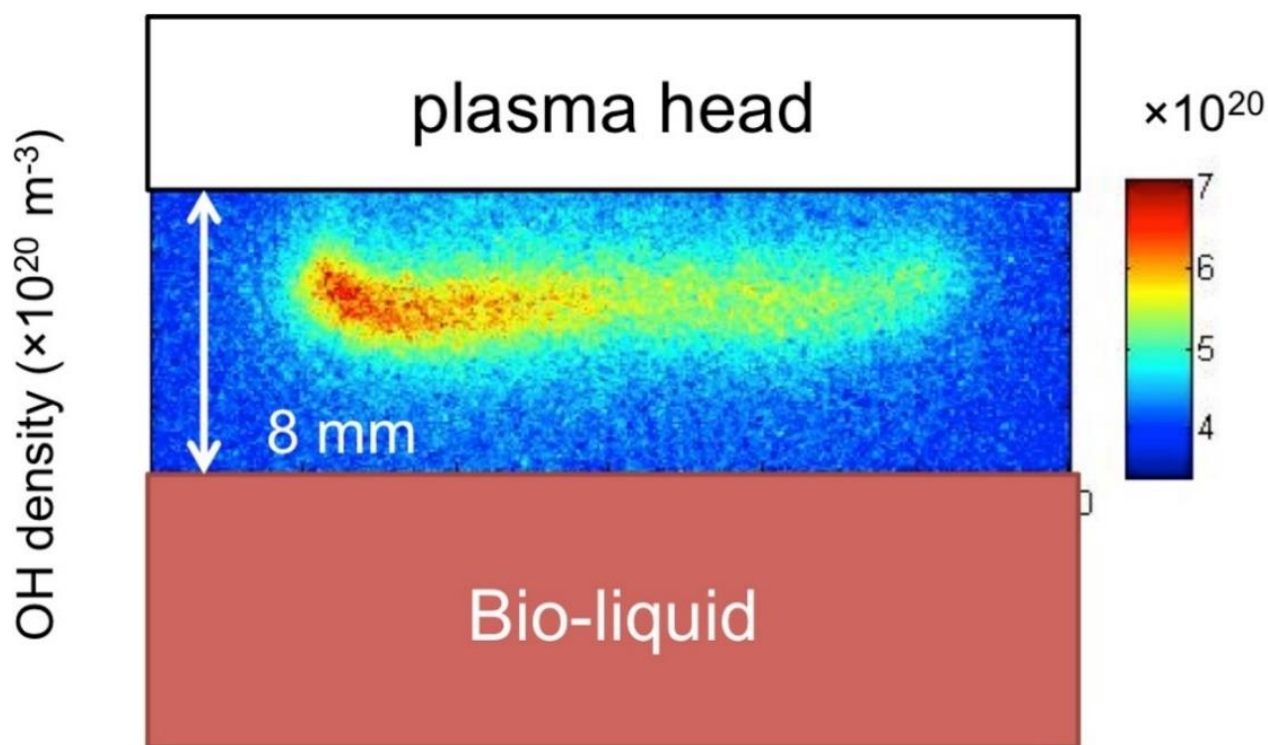


Figure 4.2.1 A gaseous $\cdot\text{OH}$ distribution during the NEAPP irradiation to a bio liquid.²⁾

The another considered way of gaseous H₂O₂ generation is derived from a triplet oxygen atom ($\cdot\text{O}({}^3\text{P})$). Figure 4.2.2 shows the dependence of gaseous densities of N and O atoms on the distance from the NEAPP spouting slit.³⁾ However the $\cdot\text{O}({}^3\text{P})$ density was decreased with the distance being off, $\cdot\text{O}({}^3\text{P})$ reached the treated liquid surface, which correspond to 13 mm of the distance.³⁾ The result is likely to be an evidence of H₂O₂ generation from the $\cdot\text{O}({}^3\text{P})$ at the surface of the irradiation target solution by a reaction of (4.2.3).



Actually, it also has been reported that an H₂O₂ generation in a water irradiated with a radical source, FPA10 (Fuji machine), which supplies only radical without lights, electrons and ions.⁸⁾ The result indicates radicals from the NEAPP, such as $\cdot\text{O}({}^3\text{P})$, contribute to the H₂O₂ generation. Consequently, it has been discovered that gaseous hydroxyl radical($\cdot\text{OH}$) and triplet oxygen atom ($\cdot\text{O}({}^3\text{P})$) are likely to contribute the gaseous H₂O₂ generation and the gaseous H₂O₂ could dilute in the PAM.

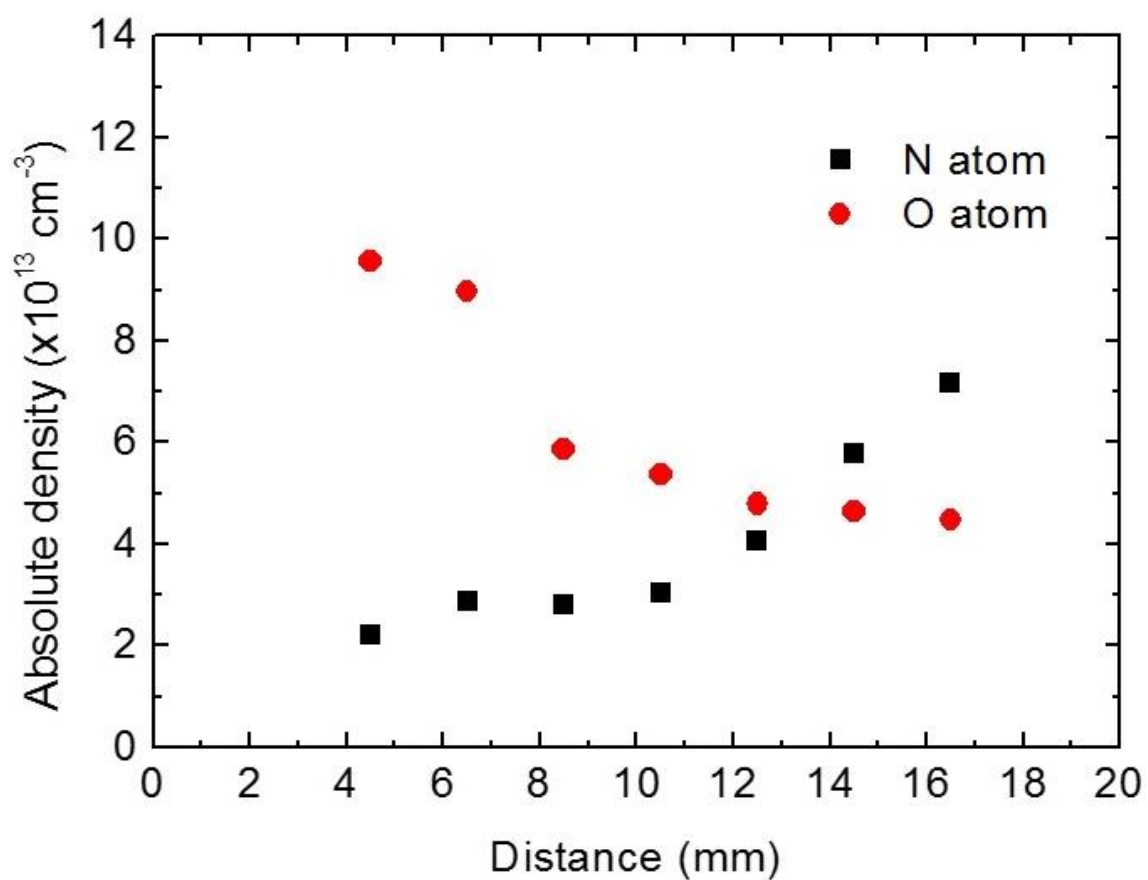


Figure 4.2.2 The dependence of gaseous densities of N and O atoms on the distance from the NEAPP spouting slit.³⁾

§ 4.2.2 H₂O₂ generation in liquid phase

Relatively short-live species generated in the liquid phase were measured. Figure 4.2.3 shows the ESR spectra of DMPO adducts with or without the MgF₂ covering above the medium.

Both DMPO-OH and DMPO-H signals were detected even with MgF₂ covering. As discussed regarding the photo-dissociation of water, it was not surprising that DMPO adducts were detected in the culture medium by ESR spectroscopy. When medium was irradiated with light at >115 nm, DMPO-OH and DMPO-H were generated by photo-dissociation at 62 and 52%, respectively, of the amounts generated by whole-spectrum NEAPP irradiation. Therefore, it is considered that aqueous ·OH was predominantly generated by irradiation of light from the NEAPP. Although ·OH was also detected in the gas phase, in the case of the remote irradiation from the target surface, the gaseous ·OH may hardly reach the liquid phase because of the short lifetime.

Both DMPO-OH and DMPO-H were generated by irradiation with the optical emissions from the NEAPP source. This indicates that photo-dissociation of water is the dominant reaction leading to the generation of OH and H radicals by a reaction of (4.2.4).⁹⁾



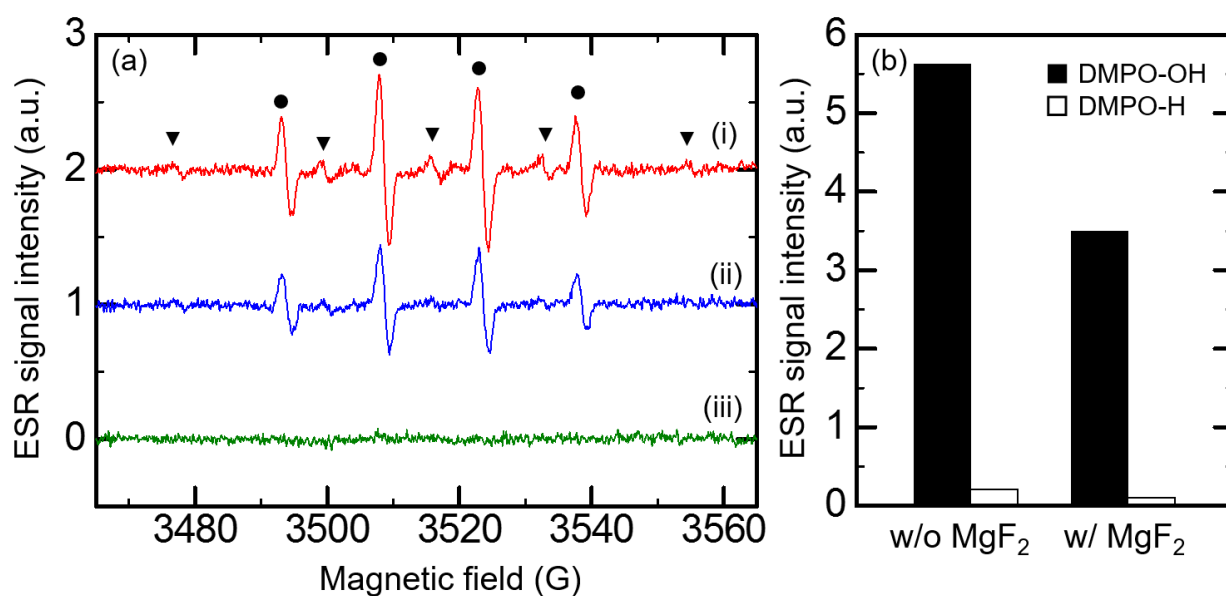


Figure 4.2.3 (a) ESR spectra of 290 mM DMPO added to 250 μL of medium irradiated with NEAPP with (i) and without (ii) the glass tube covered with an MgF_2 plate. Spectra were acquired 90 s after the NEAPP irradiation. (iii) Initial culture medium. (b) Bar graph depicting the intensities of the DMPO-OH (3494 G) and DMPO-H (3500 G) peaks.

Emission of NEAPP involving VUV light irradiation of the medium was measured using OES. Figure 4.2.4 shows the optical emission spectrum at VUV region. In the VUV emission, spectral peaks originating from N (120.0 nm, 174.3 nm), and H (121.6 nm) were identified. Spectrum from O radical might be absorbed by ambient oxygen molecules.

Under ambient atmospheric conditions, water molecules are contained in the gas phase as humidity. In addition, the gas phase is in contact with the liquid surface. The water molecules evaporate into the gas phase in the vicinity of the liquid surface. Subsequent illumination with intense VUV emissions induces the formation of OH radicals at the liquid surface via a well-known photo-dissociation reaction.¹⁰⁾

The UV light emission spectrum is also shown in Figure 4.2.5 and the peaks were also identified as emissions originating from $\cdot\text{OH}$ ($\text{A}^2\Sigma^+ \rightarrow \text{X}^2\Pi$). Consequently, VUV/UV light emitted from chemical species such as $\cdot\text{O}$, $\cdot\text{N}$, $\cdot\text{H}$, and $\cdot\text{OH}$, which generated in the NEAPP plume region, supplied to the gas/liquid interface and predominantly generated $\cdot\text{OH}$ radical by water dissociation.

H_2O_2 generation in water by a recombination of OH radicals is well known.¹⁰⁾ However, in this study, H_2O_2 below the detection limit, which is several micro molar, was detected in the medium irradiated with MgF_2 covering even aqueous OH radicals were generated (data not shown). In addition, H_2O_2 generation was also analyzed under conditions in which OH radicals were scavenged by the addition of D-mannitol (OH radical scavenger), given that $\cdot\text{OH}$ radicals are generally considered H_2O_2 precursors. Surprisingly, when D-mannitol was added (final concentration of 1 mM) prior to irradiation, no notable change in H_2O_2 concentration in the PAM was observed, which are $108.9 \pm 10.8 \mu\text{M}$ and $103.9 \pm 6.6 \mu\text{M}$ by 300 s of the NEAPP irradiation and there are no

significant difference analyzed by the t-test.

Those result suggests that the generation of H_2O_2 in PAM does not primarily proceed via the pathway involving OH radicals generated by photo-dissociation during NEAPP irradiation. Therefore, it was indicated that contributions of gaseous species, such as ($\cdot\text{O}({}^3\text{P})$) and gaseous H_2O_2 , was dominant for the H_2O_2 generation. OH radicals generated in the PAM could contribute to modification organic components of the medium shown in § 3.4 by its high oxidation power.

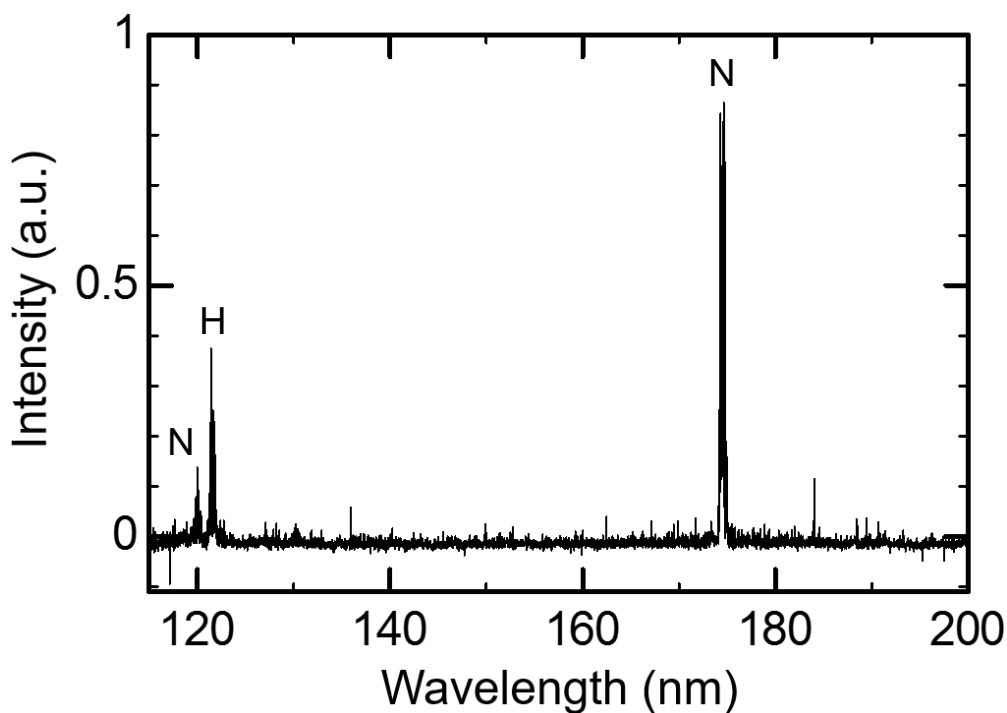


Figure 4.2.4 Spectrum of 115 to 200 nm light emitted from the NEAPP source observed at 7 mm below the NEAPP slit using optical emission spectroscopy.

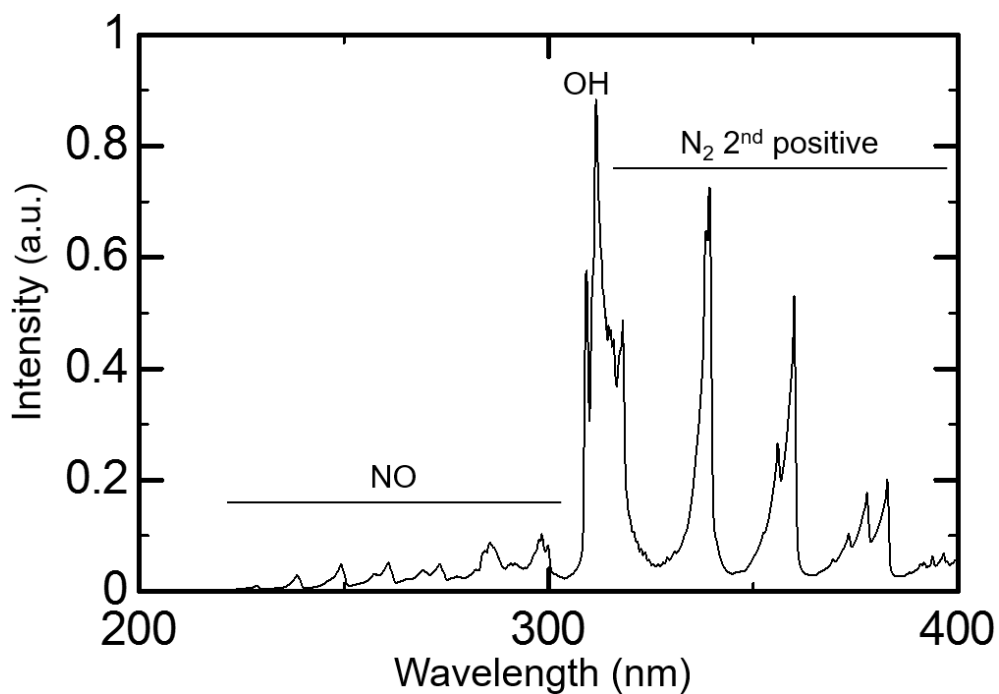
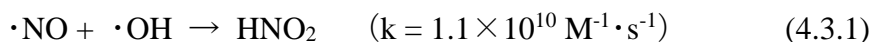


Figure 4.2.5 Spectrum of 200 to 400 nm light emitted from the NEAPP source observed at 7 mm below the NEAPP slit using optical emission spectroscopy.

§ 4.3 Nitrite ion (NO₂⁻)

§ 4.3.1 NO₂⁻ generation in gaseous phase

In the case of the nitrite ion (NO₂⁻), NO is an important precursor. The generation reaction with ·NO is shown in (4.3.1).



Since the reaction rate constant is relatively high, the reaction occurs very fast.

A gaseous ·OH generation was shown in Figure 4.2.1. A gaseous ·NO distribution has been measured by OES as shown in Figure 4.3.1.²⁾

The ·NO generation in the gaseous phase is explained by two theory, which are deriving from nitrogen or oxygen atoms electrically or vibrationally excited by an electron impact, or deriving from a reaction between a nitrogen atom and an excited oxygen molecule. Those reactions are shown in below (4.3.2) to (4.3.5)



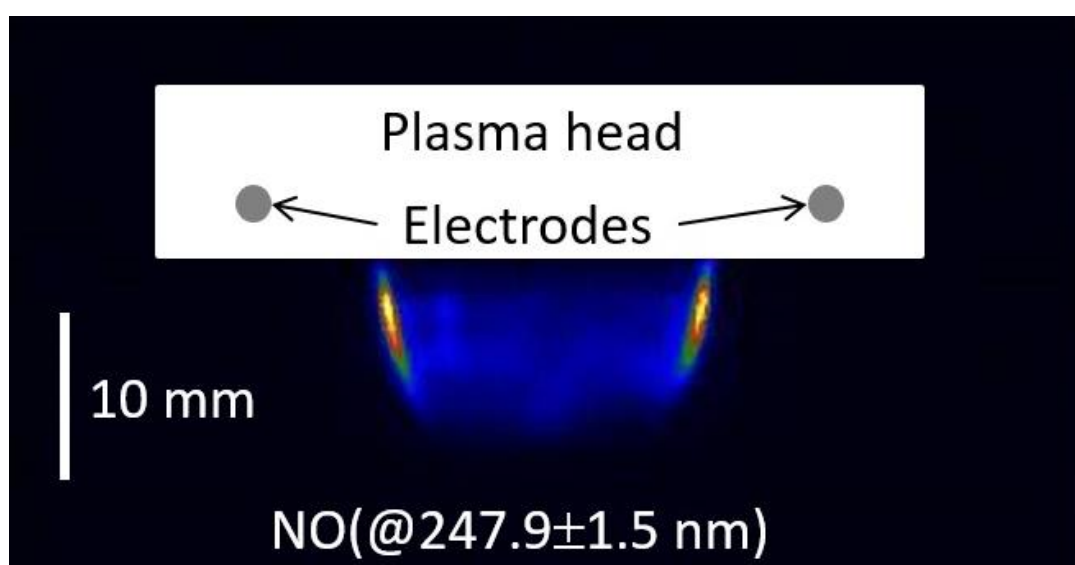


Figure 4.3.1 An gaseous $\cdot\text{NO}$ distribution identified by $247.9 \pm 1.5 \text{ nm}$ of light observed by OES. (Intensity is stronger from blue to red).²⁾

Next, the author tried to control the ambient gas by using a chamber. Figure 4.3.2 shows NO_2^- concentrations in PAMs generated with Ar discharge gas in the air or Ar atmosphere, and with Ar 99% + N_2 1% of discharge gas in Ar atmosphere.

Significant low NO_2^- concentration was observed in the PAM generated in Ar atmosphere. This result indicates that the mixing of air involving N_2 is necessary for the generation of NO_2^- . On the other hand, NO_2^- concentration is obviously increased by a mixing 1% N_2 to the discharge gas. The result also supports the nitrogen involved in the NEAPP region dominantly contribute to the NO_2^- generation.

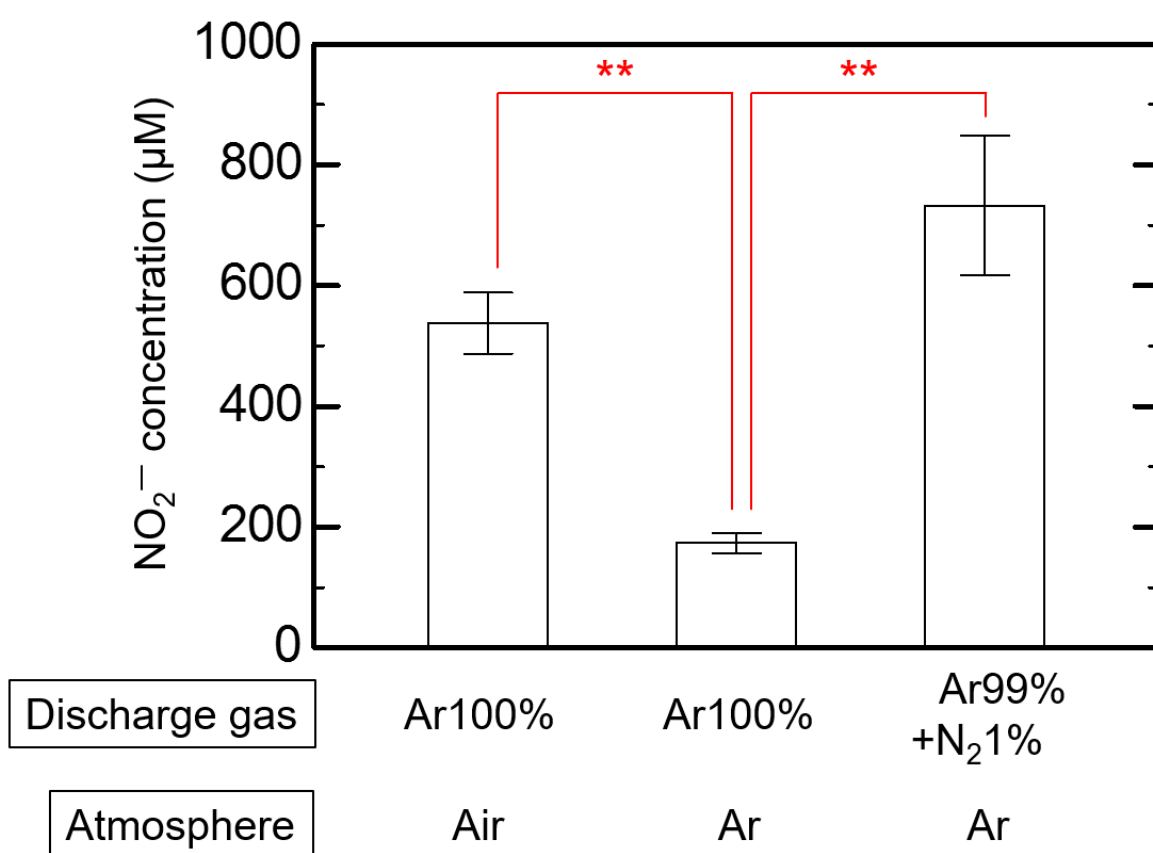


Figure 4.3.2 NO₂⁻ concentrations in PAMs generated with Ar discharge gas in the air or Ar atmosphere, and with Ar 99% + N₂ 1% of discharge gas in Ar atmosphere (p < 0.05 = *; p < 0.01 = **).

§ 4.3.2 NO₂⁻ generation in liquid phase

A relative gaseous ·NO density dependence on the distance from the NEAPP spouting slit has been reported as shown in Figure 4.3.3.²⁾ The gaseous ·NO density was increasing with the distance from the spouting slit and the gaseous ·NO was reached 13 mm under from the NEAPP exit slit, where are an NEAPP irradiating liquid surface. Nevertheless, no ·NO was detected in the PAM as shown in Figure 3.2.3.

A reason of the ·NO absence in the liquid phase was considered as the low solubility of ·NO. In a simulation of RONS generation in a NEAPP irradiated water, ·NO, which generated from ambient nitrogen molecules, came from gaseous phase. Therefore, A dissolving of ·NO to the liquid phase is needed for ·NO existence in the liquid phase. The solubility of RONS has been decided by the *Henry's raw constants* and the solubility is calculated by the formula (4.3.6).¹⁰⁾

$$D_{ij} = D_i \left(\frac{hn_i - n_j}{hn_i} \right) \quad (4.3.6)$$

D_{ij} represents a diffusion factor from gaseous phase to liquid phase, D_i represents a diffusion factor in gaseous phase and n_i , n_j represent gaseous and liquid molecular concentrations, respectively, Then h is called as the *Henry's raw constant* and the constant characterize as solubility.

As shown in Table 1.2.2, *Henry's raw constants* of ·NO and HNO₂ are 4.4×10^{-2}

and 1.15×10^3 and $\cdot\text{NO}$ has very low value.^{11,12)} From the consideration, $\cdot\text{NO}$ could change to HNO₂ in gaseous phase and then dilute to the PAM rather than $\cdot\text{NO}$ direct dilution to liquid phase. The conclusion is also supported by detection of no $\cdot\text{NO}$ in the PAM bulk region shown in Figure 4.2.3.

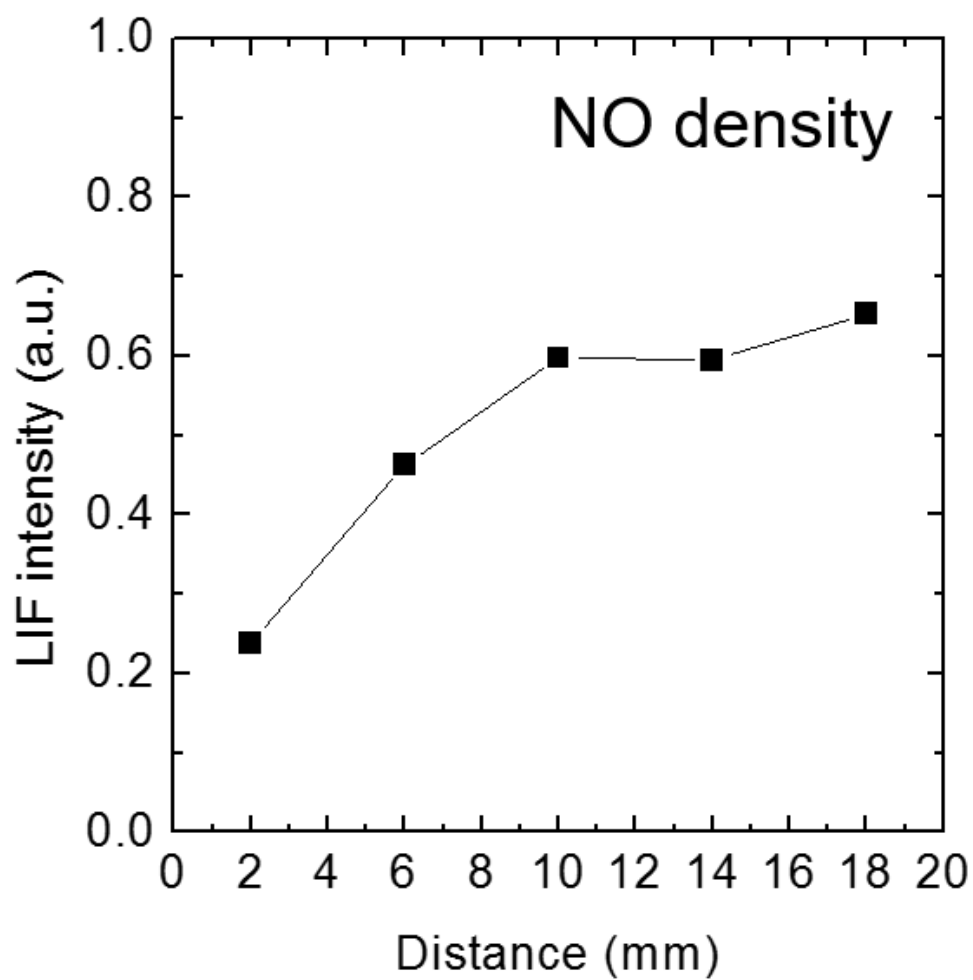


Figure 4.3.3 A relative gaseous $\cdot\text{NO}$ density dependence on the distance from the NEAPP spouting slit.²⁾

§4.4 Summary

In this Chapter 4, H₂O₂ and NO₂⁻ generation mechanisms in the PAM were elucidated. In the case of a NEAPP irradiated water, the RONS generation mechanism was examined by a simulation. As a result, H₂O₂ and NO₂⁻ generation model in water was described as shown in Figure 4.2.1(a). In this chapter, aqueous phase reactions in the case of the PAM were mainly investigated. As a result, H₂O₂ and NO₂⁻ generation mechanisms in the PAM were elucidated as shown in Figure 4.2.1(b).

In the H₂O₂ analysis, the main precursor is $\cdot\text{OH}$. However aqueous $\cdot\text{OH}$ was dominantly generated by a light emission from the NEAPP, only very little concentration of H₂O₂ was detected in the medium irradiated only light from the NEAPP. Therefore, gaseous reactions is dominant for H₂O₂ generation in the PAM. Namely, a reaction of gaseous oxygen atoms with water in the medium surface, which is $\text{H}_2\text{O} + \cdot\text{O}({}^3\text{P}) \rightarrow \text{H}_2\text{O}_2$, or a dissolving of H₂O₂ generated in the NEAPP region, where exists a large amount of $\cdot\text{OH}$, with an $\cdot\text{OH}$ recombination reaction of $2\cdot\text{OH} \rightarrow \text{H}_2\text{O}_2$. On the other hand, the aqueous $\cdot\text{OH}$ could be react with the medium components such as organic species. The estimation is corresponding to the result described in § 3.4.

In the NO₂⁻ analysis, no $\cdot\text{NO}$ was dissolved to the medium even though $\cdot\text{NO}$ was exist in the gaseous phase. It is well known that gaseous $\cdot\text{NO}$ was generated from mixed ambient air involving N₂ and O₂, through $\cdot\text{O}$ and $\cdot\text{N}$ generations and N₂ and O₂ excitations. One of a cause is estimated as the low solubility of $\cdot\text{NO}$ and a gaseous generation of NO₂⁻ was also indicated. Gaseous $\cdot\text{NO}$ could react with gaseous $\cdot\text{OH}$ with a reaction of $\cdot\text{NO} + \cdot\text{OH} \rightarrow \text{HNO}_2$. After that the HNO₂ was dissolved to the PAM and NO₂⁻ was generated by an ionization.

From the above discussions of the RONS generations, a schematic representation of the generation reaction model in the PAM was made up into shown in Figure 4.4.1(b). In particular, a behavior of photo-generated OH radicals, which generation is indicated by a red x-mark in Fig. 4.4.1(b), was characteristic to the PAM. Those $\cdot\text{OH}$ could contribute to an oxidization of aqueous organic species instead of an H_2O_2 generation. The interaction between the NEAPP and organic species composed of the medium is discussed in detail in Chapter 7 and 8.

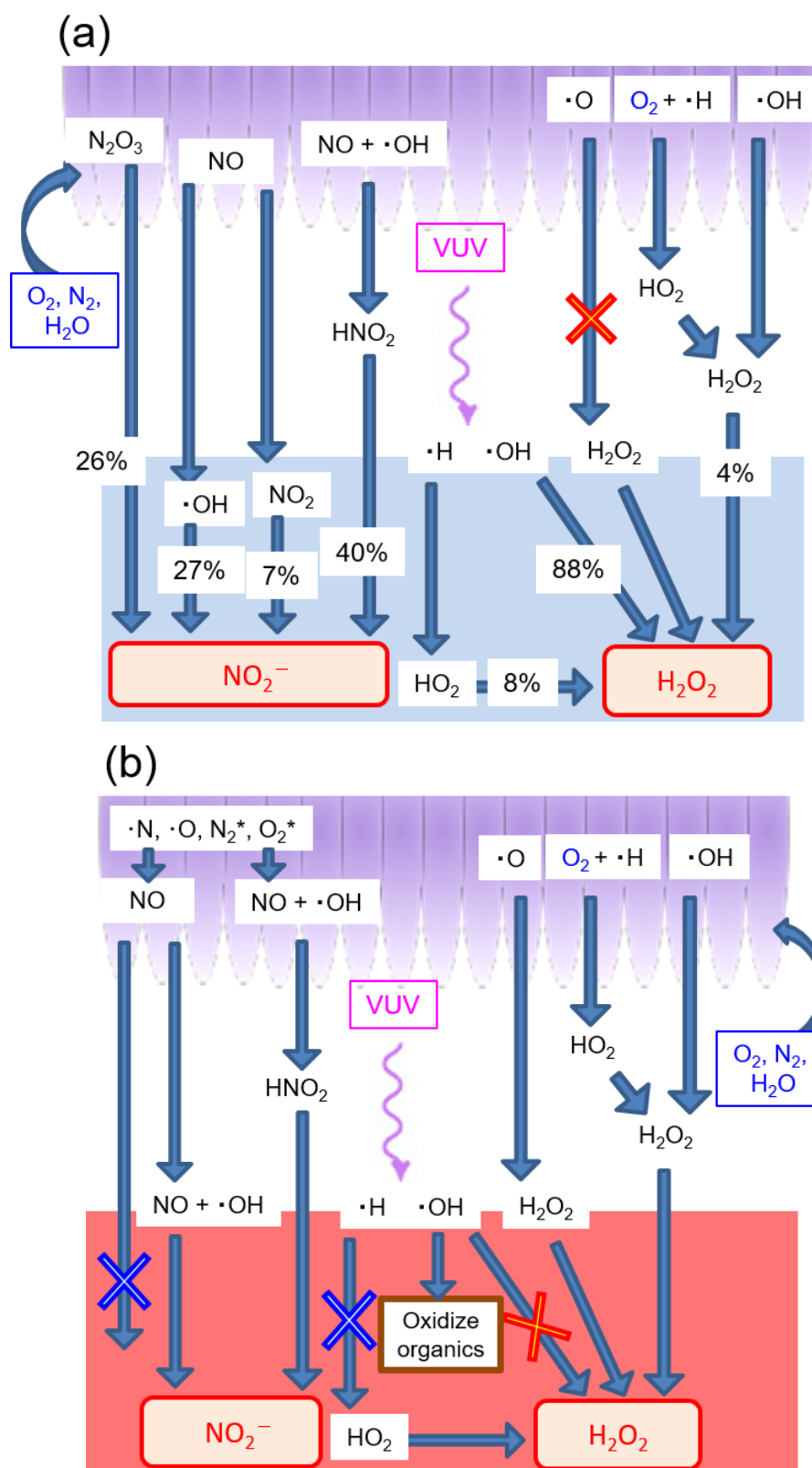


Figure 4.4.1 Schematic representations of RONS generation reaction model in (a) a NEAPP irradiated water¹⁰⁾ and (b) the PAM.

References for Chapter 4

- 1) T. Sato, M. Yokoyama, and K. Johkura, *J. Phys. D: Appl. Phys.* **44**, 372001 (2011).
- 2) S. Liang, Bio-iryousousei ni muketa AC reiki hiheikou taikiatu plasma thu no kasseishu seisei kikou no kaimei [Elucidation of reactive species generation mechanism in AC driven non-equilibrium atmospheric pressure plasma for establishing plasma medicine], *Master thesis of Nagoya Univ.* (2015).
- 3) K. Takeda, K. Ishikawa, H. Tanaka, M. Sekine, and M. Hori, Behaviors of activated species generated by AC power excited non-equilibrium atmospheric pressure Ar plasma jet in atmosphere. *The 60th JSAP Spring Meeting*. 29p-B9-13 (2016).
- 4) T. Kondo, C. M. Krishna, and P. Risez, *Int. J. Radiat. Biol.* **53**, 891-899 (1988).
- 5) T. Kondo, J. Gamson, J. B. Mitchell, and P. Risez, *J. Radiat. Biol.* **54**, 955-962 (1988).
- 6) P. Bruggeman, and D.C. Schram, *Plasma Sources Sci. Technol.* **19**, 045025 (2010).
- 7) J. Winter, H. Tresp, M.U. Hammer, S. Iseni, S. Kupsch, A.S. Bleker, K. Wende, M. Dunnbier, K. Masur, K.D. Weltmann, and S. Reuter, *J. Phys. D: Appl. Phys.* **47**, 285401 (2014).
- 8) T. Towatari, Taikiatsu sanso radical-gen wo mothiita ekithu sakkin mechanism ni kansuru kenkyu [Study of sterilization mechanism in liquid by using atmospheric pressure oxygen radical source], *Master thesis of Meijo univ.* (2015).
- 9) Y. Iwazawa, Kagaku binran [Chemical handbook] Tokyo, Maruzen, 2004.
- 10) W. Tian, and M.J. Kushner, *J. Phys. D: Appl. Phys.* **47**, 165201 (2014).
- 11) R. Sander, *Atmos. Chem. Phys.*, **15**, 4399-4981, (2015).
- 12) D. Mackay, and W. Y. Shiu, *J. Phys. Chem. Ref. Data.* **10**, 1175 (1981).

Chapter 5

Long-lived RONS contribution to antitumor effect of the PAM

§ 5.1 Introduction

Long-lived species could remain in the PAM and contribute for the antitumor effect of the PAM. As elucidated in § 3.4, since no organic reactive components were detected in the PAM, the author focused on RONS. However, H_2O_2 antitumor effect is confirmed by a kind of cancer cells,¹⁾ the synergistic effect with other RONS is not elucidated. In addition, NO_2^- , which is dominantly generated long-lived RONS in the PAM, was hardly attracted attentions because it has a little toxicity for cancer cells. Therefore, the individual and synergistic antitumor contributions of H_2O_2 , NO_2^- and NO_3^- , which are long-lived RONS detected in § 3.3, should be elucidated.

In the Chapter 5, the antitumor effect of those RONS generated by the NEAPP was evaluated by incubating actual human cancer and normal cells with the PAM or RONS added medium. For investigating the antitumor effect, the cell survival was measured and the amount of RONS integrated in cells was also measured.

§ 5.2 Selective antitumor effect of the PAM

Figure 5.2.1 shows observed images of U251SP (glioblastoma; a, b) and MCF10A (normal cells; c, d) after incubation with a medium (b, d) and the PAM (a, c) irradiated with the NEAPP for 180 s. However the same PAM was used for the incubation of U251SP and MCF10A, only U251SP cells shrunk against MCF10A cells seem normal. The shrinking shape is one of evidences of apoptotic death. From those results, The PAM induced selective apoptotic killing of only cancer cells against normal cells.

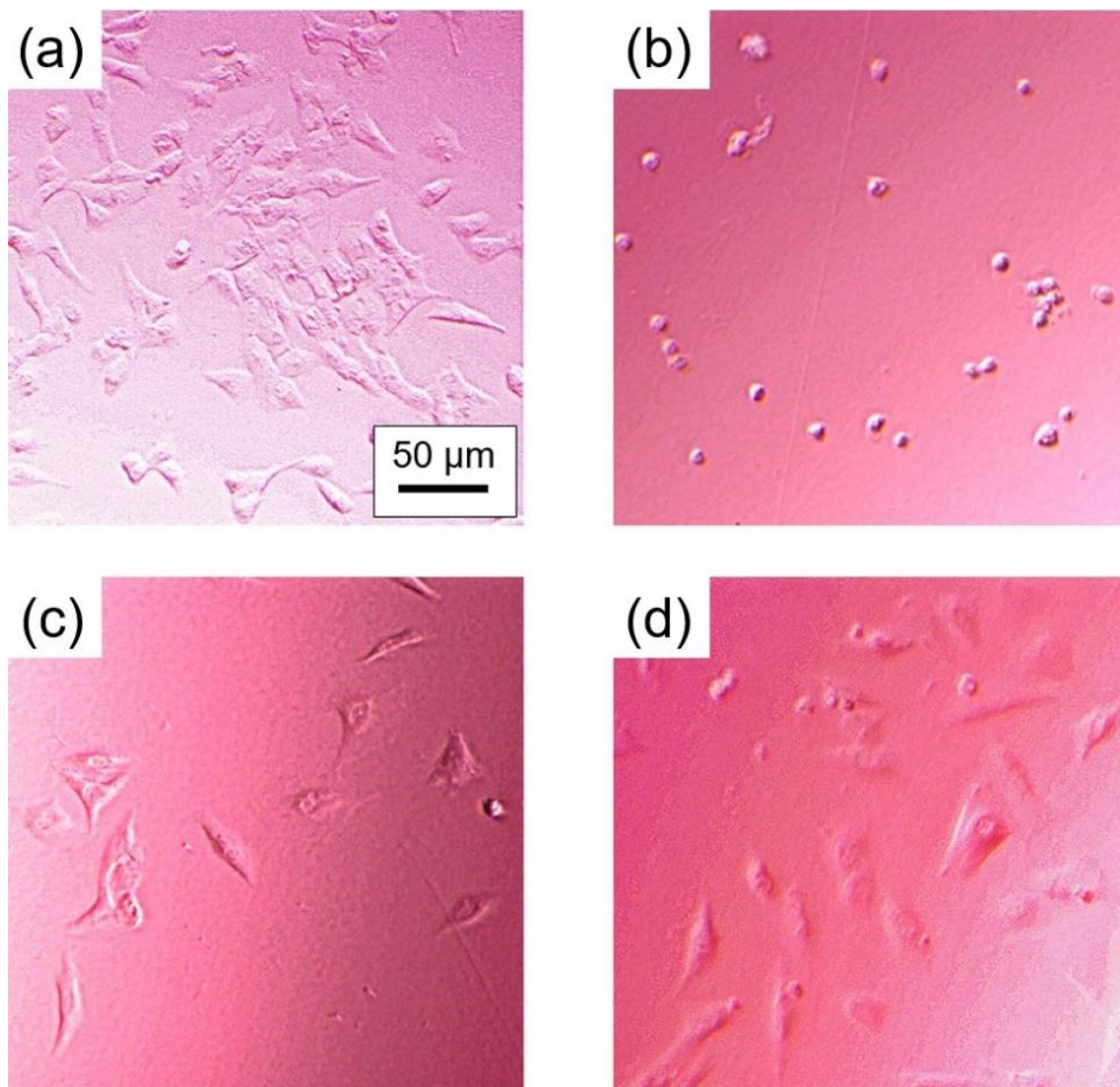


Figure 5.2.1 Observed images of U251SP (glioblastoma; a, b) and MCF10A (normal cells; c, d) after incubation with a medium (b, d) and the PAM, which is irradiated with the NEAPP for 180 s (a, c).

Figure 5.2.2 and 5.2.3 shows cell survivals of U251SP and MCF10A after incubating with PAM, which are measured by MTS assay.

As shown in Figure 5.2.2, a difference of cell survivals between U251SP and MCF10A is about 80% with a strong significance.

In addition, as shown in Figure 5.2.3, the cell survivals of U251SP were lower than those of MCF10A, regardless of the plasma irradiation period. The induction of apoptosis in the tumor cells depended on the plasma irradiation period. Similarly, the RONS concentration in the plasma-irradiated medium was proportional to the plasma irradiation period by a comparison to results of Chapter 3. Therefore, RONS is likely to contribute for the antitumor effect of the PAM.

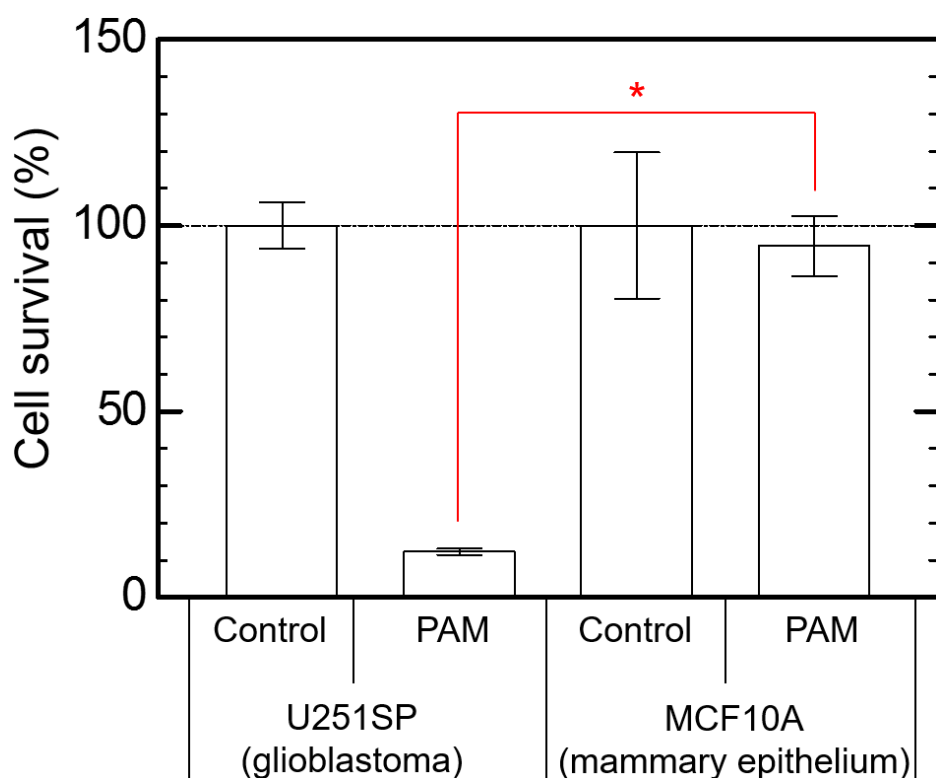


Figure 5.2.2 Cell survivals of U251SP and MCF10A after incubating with PAM, which is irradiated with the NEAPP for 180 s ($p < 0.05 = *$; $p < 0.01 = **$).

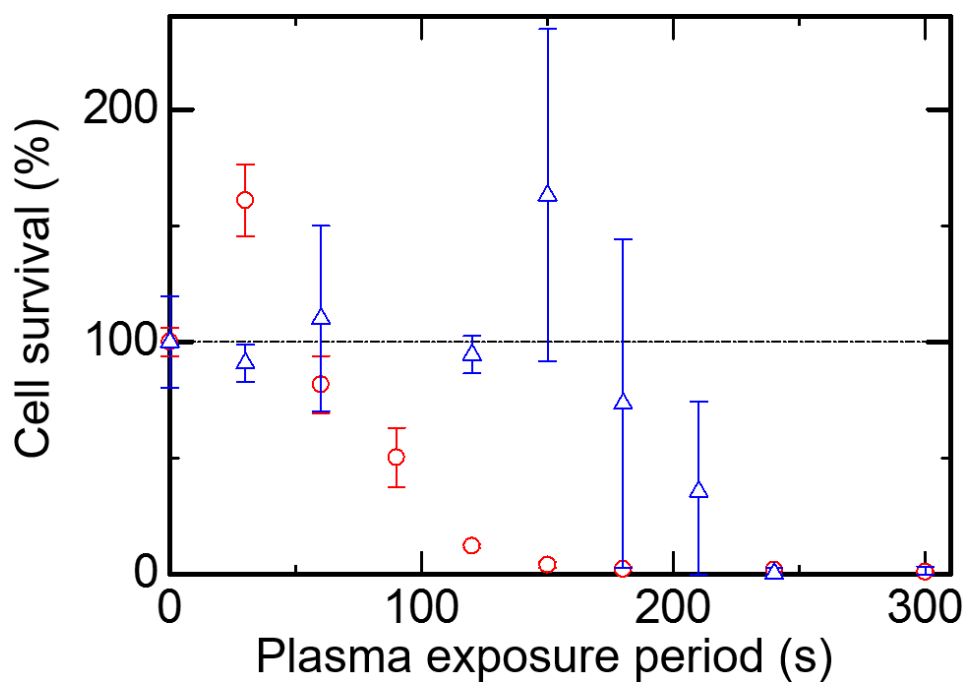


Figure 5.2.3 Cell survivals of U251SP (○) and MCF10A (△) after incubating with PAM, which is irradiated with the NEAPP up to 300 s.

§ 5.3 Intracellular RONS

The whole amount of intracellular RONS was detected by a fluorescent reagent.

Figure 5.3.1 shows merged images of fluorescent images and DIC images. U251SP (glioblastoma) cells were incubated with (a) a medium, (b) the PAM, (c) H_2O_2 and NO_2^- added medium (d) NO_2^- added medium. Those added concentrations were equivalent to the PAM.

The monochrome round images are U251SP cells. Nevertheless no fluorescent was observed in the control sample shown in Figure 5.3.1 (a), most cells incubated with the PAM show a fluorescent and the result indicates the PAM induce an accumulation of RONS in cells.

The accumulation of RONS in the PAM could induced by the RONS diluted in the medium since the fluorescence was also observed by the RONS added medium shown in the Figure 5.3.1 (c). Especially, RONS, which has a permeability of cell membrane, such as H_2O_2 , was likely to contribute to increasing the RONS level in cells.

However, little fluorescence was observed in the NO_2^- added medium as shown in Figure 5.3.1 (d). Therefore, the accumulation of RONS is dominantly contributed by an H_2O_2 individual effect and a synergistic effect of H_2O_2 and NO_2^- , which is described in § 5.4.2 in detail.

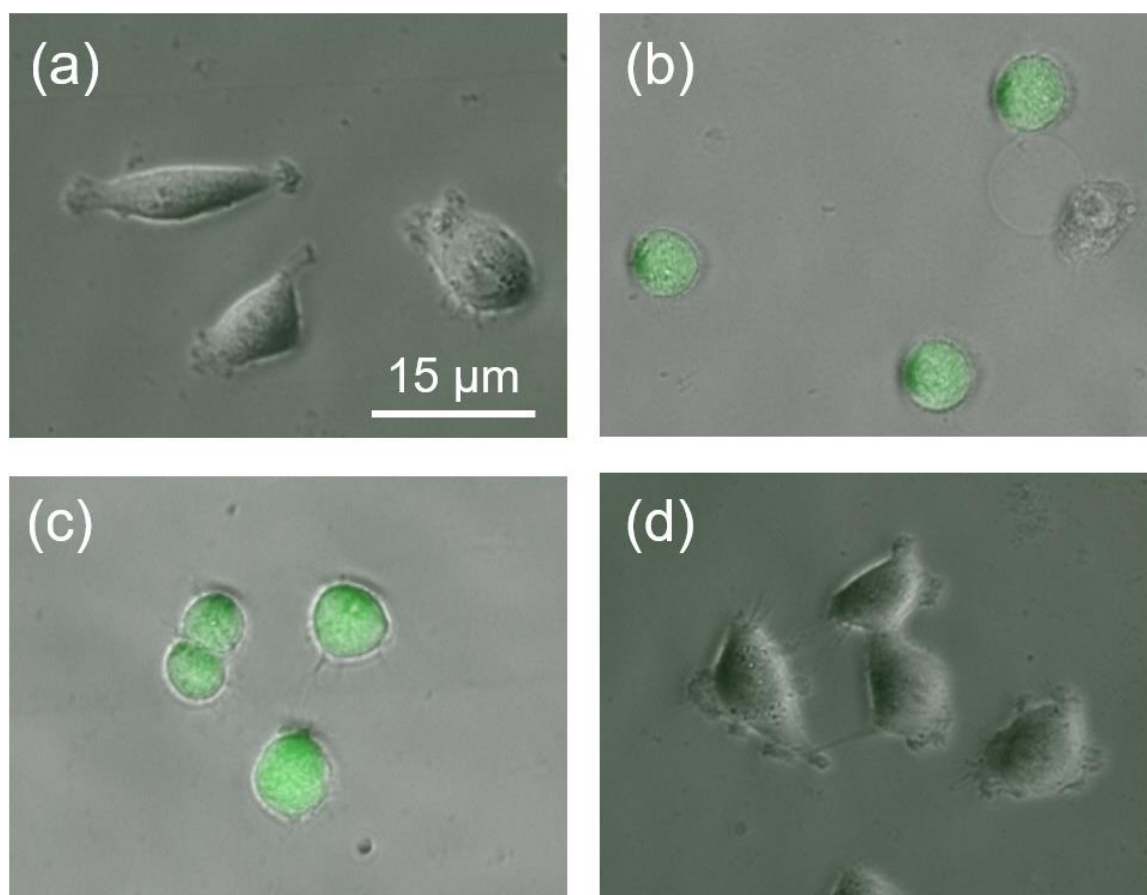


Figure 5.3.1 Merged images of fluorescent images and DIC images of U251SP (glioblastoma) cells were incubated with (a) medium, (b) PAM, (c) H_2O_2 and NO_2^- added medium (d) NO_2^- added medium.

§ 5.4 Antitumor effect of antitumor species generated by the NEAPP

§ 5.4.1 Nitrate ion (NO_3^-)

An individual or synergistic antitumor effect of RONS were analyzed. Figure 5.4.1 shows cell survivals of U251SP (glioblastoma) after incubation with 2000 μM of nitrate ion added DMEM or DMEM (plus FBS, P/S). The cell survival of U251SP was not changed by an addition of 2000 μM of nitrate ion regardless of with or without the FBS addition. The measured concentrations of NO_3^- in the PAM was up to 1000 μM with or without the FBS addition. Therefore, an individual NO_3^- antitumor effect didn't exist in the PAM in every cases of previously examination of PAM.

Figure 5.4.2 shows the dependence on the amount of the H_2O_2 addition of cell survivals of U251SP after incubation with 1000 μM of NO_3^- and H_2O_2 (▼ in Figure 5.4.2) or only H_2O_2 (▲ in Figure 5.4.2) added medium. The amount of H_2O_2 is normalized by a NEAPP irradiation period for the amount of H_2O_2 generation.

There is no difference on cell survivals between NO_3^- and H_2O_2 or only H_2O_2 added medium. The result indicates the NO_3^- in the PAM also has no synergy with H_2O_2 .

Therefore, NO_3^- concentration in the PAM can be negligible in the antitumor effect of the PAM. NO_3^- might be contribute for a plant growth enhanced by NEAPPs since the NO_3^- is known as a nutrient and signal for plant growth.²⁾

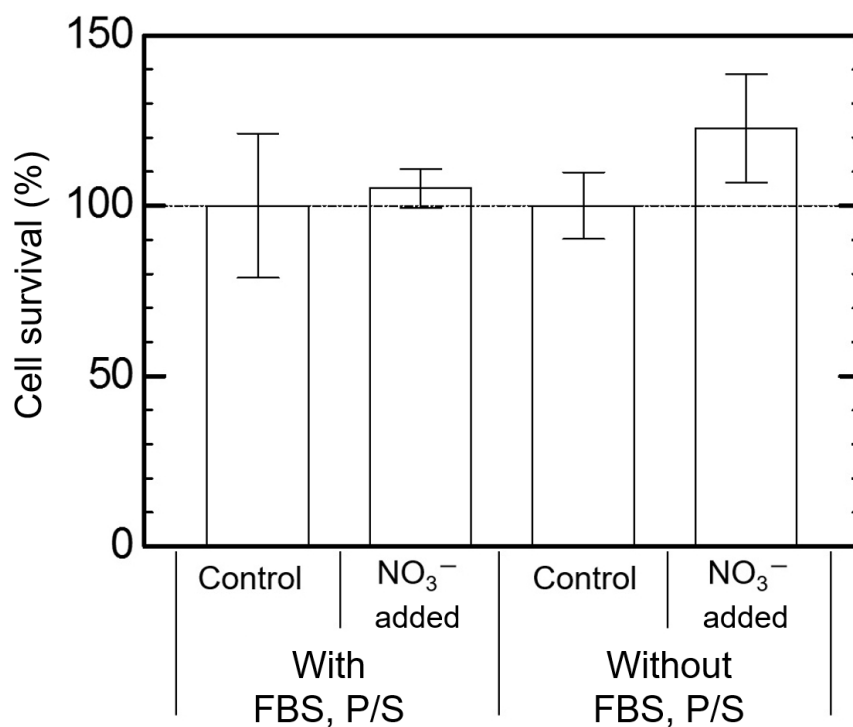


Figure 5.4.1 cell survivals of U251SP (glioblastoma) after incubation with $2000 \mu\text{M}$ of nitrate ion added DMEM or DMEM (plus FBS, P/S).

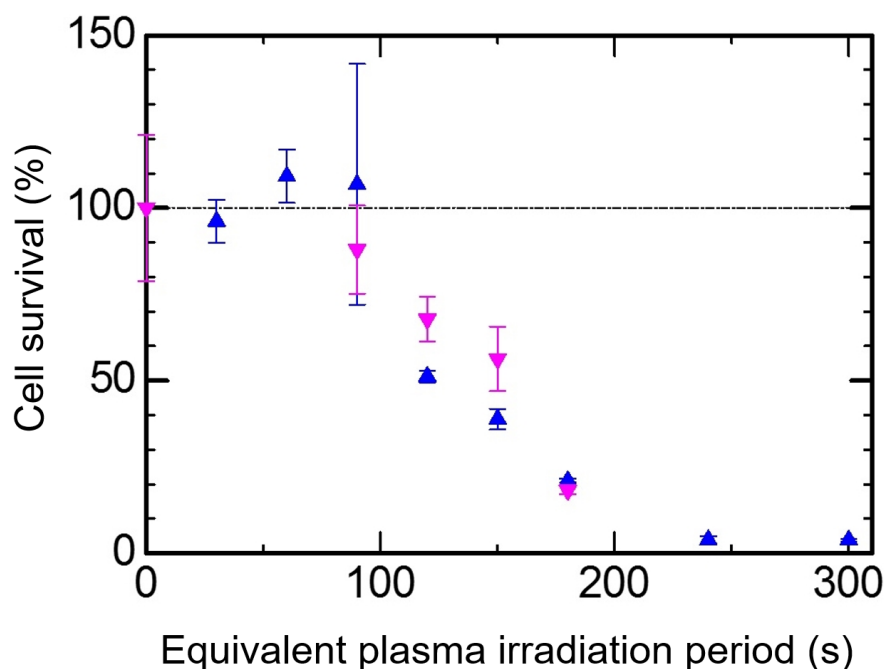


Figure 5.4.2 The dependence on the amount of the H_2O_2 addition of cell survivals of U251SP after incubation with $1000 \mu\text{M}$ of NO_3^- and H_2O_2 (\blacktriangledown) or only H_2O_2 (\blacktriangle) added medium.

§ 5.4.2 Synergistic antitumor effect of H_2O_2 and NO_2^-

An individual and synergistic effect induced by NO_2^- were also elucidated by a cancer cell incubation. Figure 5.4.3 shows cell survivals of U251SP (glioblastoma) cells after incubation for 24 hours in culture media with added H_2O_2 , added NO_2^- , added H_2O_2 and NO_2^- , or in PAM. Each concentration of RONS added corresponded with the concentration measured in PAM after 180 s irradiation.

The cell survival in NO_2^- added medium was the same as that of the control, whereas the survival decreased in the H_2O_2 -added medium and decreased even more in medium with added H_2O_2 and NO_2^- . This indicates that NO_2^- enhanced synergistically the cancer cell killing effect of H_2O_2 . The cell survival of cells cultured in PAM decreased in most samples compared to the corresponding control, indicating that the antitumor effects of H_2O_2 and NO_2^- are different from those of PAM.

Figure 5.4.4 shows in detail the dependence of cell survivals of U251SP on the NEAPP irradiation period or the amount of added RONS after an incubation with (i) PAM, (ii) NO_2^- added medium, (iii) H_2O_2 added medium or (iv) both H_2O_2 and NO_2^- added medium. The horizontal axis is normalized by RONS concentrations in those samples. The lethal dose (LD_{50}) indicates the point where half of cells were killed.

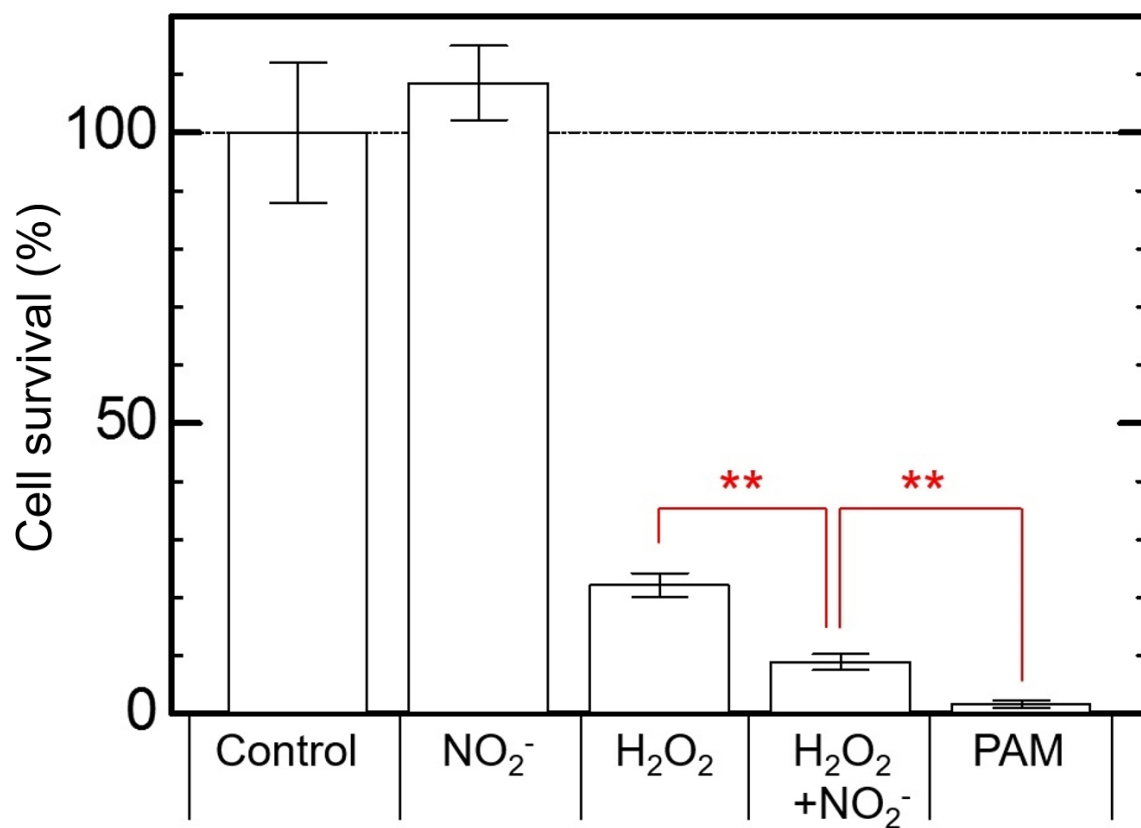


Figure 5.4.3 Cell survivals of U251SP (glioblastoma) cells after incubation with added H_2O_2 , added NO_2^- , added H_2O_2 and NO_2^- , or in PAM. Each concentration of RONS added corresponded with the concentration measured in PAM after 180 s irradiation ($p < 0.05 = *$; $p < 0.01 = **$).

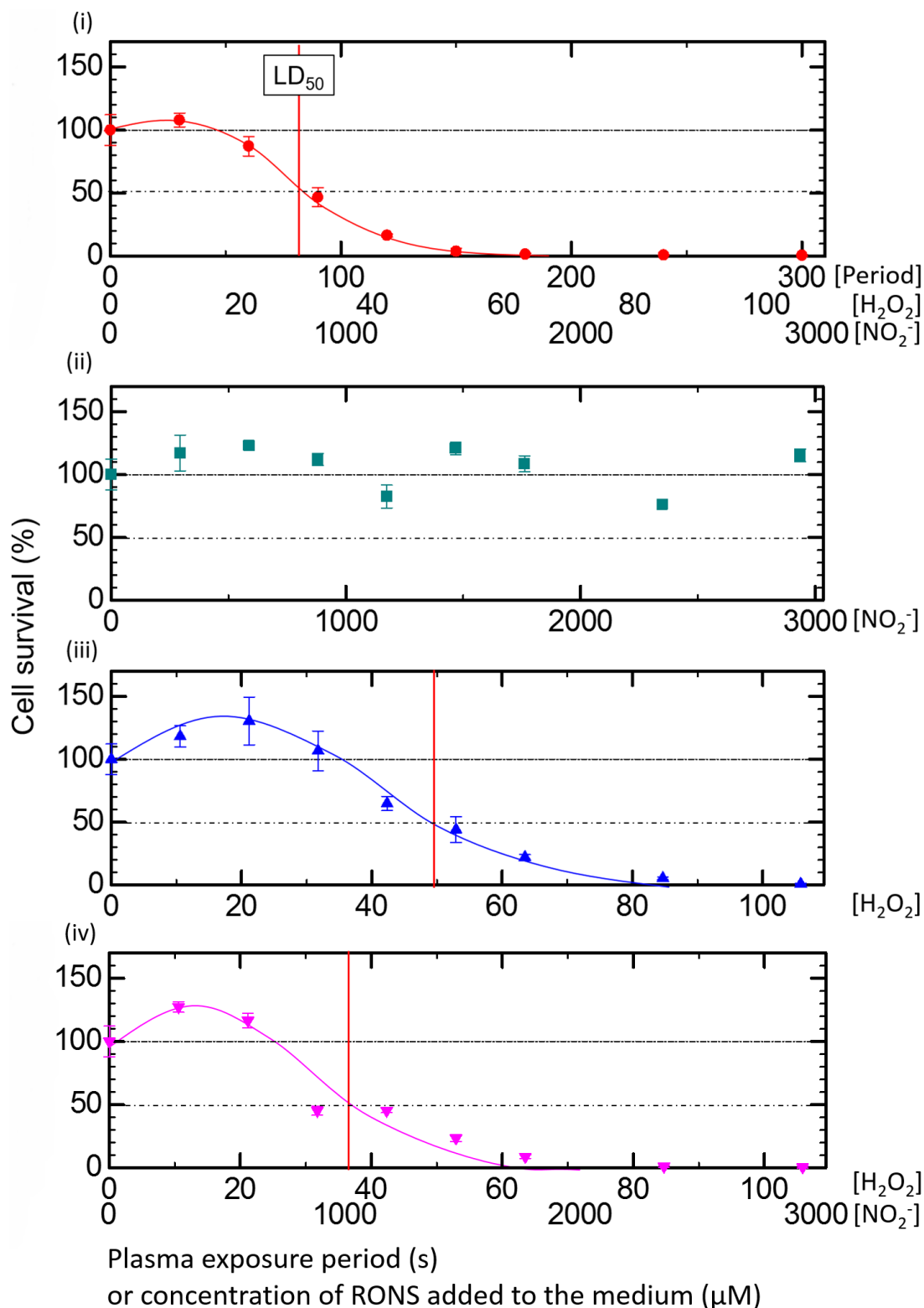


Figure 5.4.4 Dependence of cell survivals of U251SP on the NEAPP irradiation period or the amount of added RONS after an incubation with (i) PAM, (ii) NO_2^- added medium, (iii) H_2O_2 added medium or (iv) both H_2O_2 and NO_2^- added medium.

The LD_{50} level follows the order as $\text{PAM} < \text{H}_2\text{O}_2 + \text{NO}_2^- < \text{H}_2\text{O}_2$. No cancer cell killing effect was observed using NO_2^- added medium, regardless of the NO_2^- concentration, showing that nitrites exhibit very little cell toxicity. The result also shows an unknown antitumor effect except the synergistic antitumor effect of H_2O_2 and NO_2^- . For example, H_2O_2 and NO_2^- are believed to generate peroxynitrite (ONOOH) which is toxic to cells and is formed by the reaction $\text{H}_2\text{O}_2 + 2\text{NO}_2^- \rightarrow 2\text{ONOOH}$.^{3,4)} Previously, ONOOH was determined in plasma activated water (PAW) at pH 3.3.⁴⁾ It is stable at basic pH or otherwise it immediately decomposes to NO_3^- . If generated ONOOH in the PAM, it may remain in the PAM because the medium is buffered slightly basic (approximately pH 7.8 during a cell incubation).

DMEM, a medium used in this study, comprises over 30 components such as inorganic salts, amino acids and vitamins and the effect of NEAPP irradiation on these compounds is unknown. Therefore, unknown reactive species could be generated during the irradiation of DMEM and the synergism of H_2O_2 and NO_2^- the author mentioned in this thesis is certainly prominent as one of the antitumor effects, appeared with respect to PAM.

§ 5.5 Summary

In the Chapter 5, the antitumor effect of the PAM induced by RONS generated by the NEAPP was elucidated.

The selectivity of the antitumor effect is appeared in cell lines for U251SP (human glioblastoma) against MCF10A (human breast epithelial cell).

Since intracellular RONS were detected in the PAM and H_2O_2 and NO_2^- added medium, the intracellular RONS was likely to come from surroundings of cells and RONS could contribute for the antitumor effect of the PAM.

In the analysis of H_2O_2 , some decreasing of cancer cell survival was appeared.

In the analysis of NO_3^- , neither individual nor synergistic effect were detected. Therefore, NO_3^- is negligible when discussing the antitumor effect of the PAM.

In the analysis of NO_2^- , However no antitumor effect was induced by individual effect, the cell survival decreasing of H_2O_2 was enhanced by NO_2^- existence. The result indicates synergistic antitumor effect of H_2O_2 and NO_2^- . Since the PAM shows more antitumor effect than H_2O_2 and NO_2^- added medium, other antitumor effects were exit in the PAM. Namely, a synergistic antitumor effect of H_2O_2 and NO_2^- existence was successfully elucidated.

References for Chapter 5

- 1) T. Sato, M. Yokoyama, and K. Johkura, *J. Phys. D: Appl. Phys.* **44**, 372001 (2011).
- 2) N.M. Crawford, *The Plant Cell*. **7**, 859-868 (1995).
- 3) S. Hippeli, and E.F. Elstner, *Zeitschrift für Naturforschung C*. **52**, 555-563 (1997).
- 4) P. Lukes, E. Dolezalova, I. Sisrova, and M. Clupek, *Plasma Sour. Sci. Technol.* **23**, 015019 (2014).

Chapter 6

Intracellular metabolism pathways disordered by the PAM

§ 6.1 Introduction

It is considered that cancer cells incubated with the PAM was killed by downregulating intracellular pathway, which involves proteins, enzymes, metabolomes and so forth.¹⁾ In previous study, intracellular proteins and RONS were analyzed and a signaling pathway (e.g. AKT-PI3K pathway) inducing the apoptotic death by the PAM was successfully elucidated.¹⁾ However, to understand the mechanism comprehensively, other cell components must be analyzed. Especially, Metabolomes is important because it reflect cellular phenotype responsively. Actually, active *glycolysis* pathway in cancer cells has been used as a noninvasive tumor detection by positron emission tomography (PET).²⁾ Since the responsibility of metabolomes is high, it is preferred to an analysis of the cell death induced by the PAM for several hours.

Therefore, in the Chapter 6, the 116 kinds of metabolomes of cancer cells incubated with the PAM were analyzed.

§ 6.2 Sample preparation

Before the metabolomics analysis, a cell culturing was performed with the experimental properties for searching a preferred incubation time.

Figure 6.2.1 shows cell survivals of U251SP as a function of the incubate period with the PAM (○ in Figure 6.2.1) or the RONS (equivalent concentration of H₂O₂ and NO₂⁻ to the PAM) added medium (△ in Figure 6.2.1). At the origin of the horizontal axis, a medium incubating cancer cells was replaced to samples and each time incubated before a cell counting.

Cell survivals were gradually decreased as a function of the cell incubation period and cell survivals were almost zero by both samples after 24 h of incubation (data not shown). From the result of cell survival measurements, a schematic model was considered as shown in Figure 6.2.2. Because of individual specificity of cells, some cells were started to be killed by the PAM when cells incubated 2 h. In 0.5 h of incubation, however cell survival was not changed, the cells were dying and metabolomes might be changed. Since metabolites of killed cells can't be measured, the dying cells is preferred to measure metabolomes reflect an effect of an incubation with the PAM.

Actually, an activation mechanism of antitumor drugs (AZD9291, PKI-587) was investigated *in vivo* by an metabolomics analysis.³⁾ In the previous study, to measuring dying cancer cells, the metabolites after 6 h of drug treatment was measured however the drugs affect after 72 h of incubation.³⁾ Therefore, even in this study, the incubation time was decided as 0.5 h and the author tried to analyze a metabolism of dying cells by the PAM incubation.

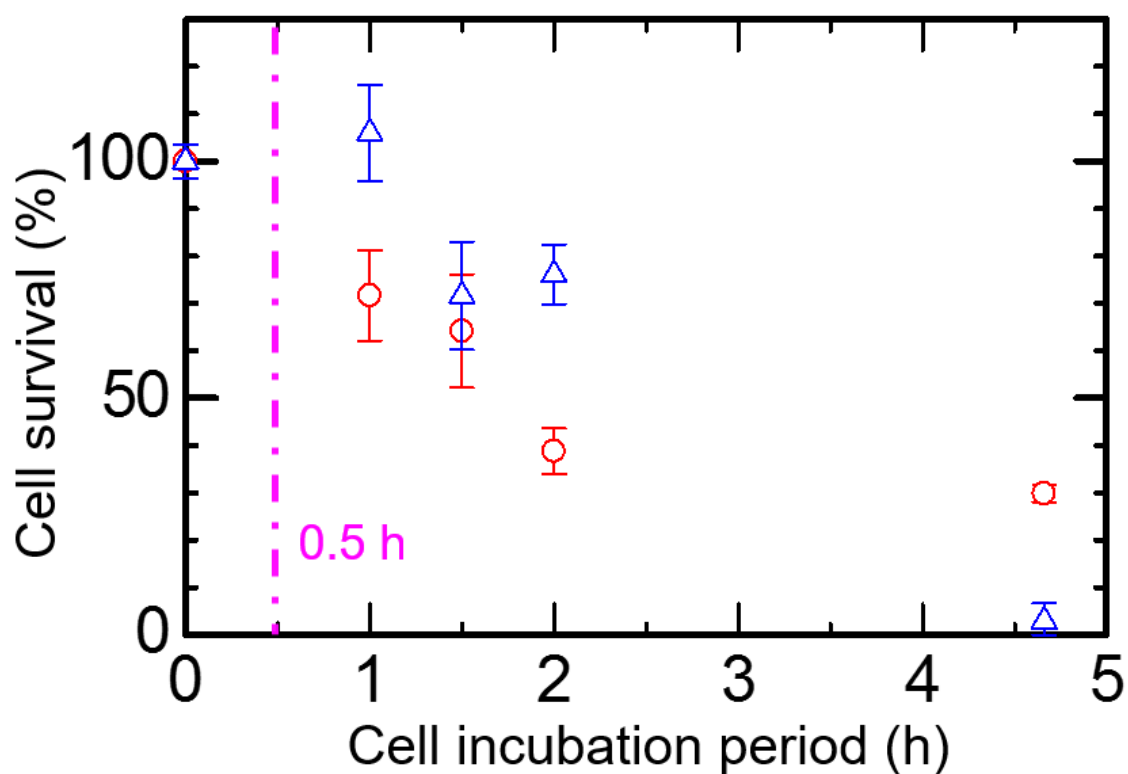


Figure 6.2.1 Cell survivals of U251SP as a function of the incubate period with (○) the PAM or (△) the RONS added medium.

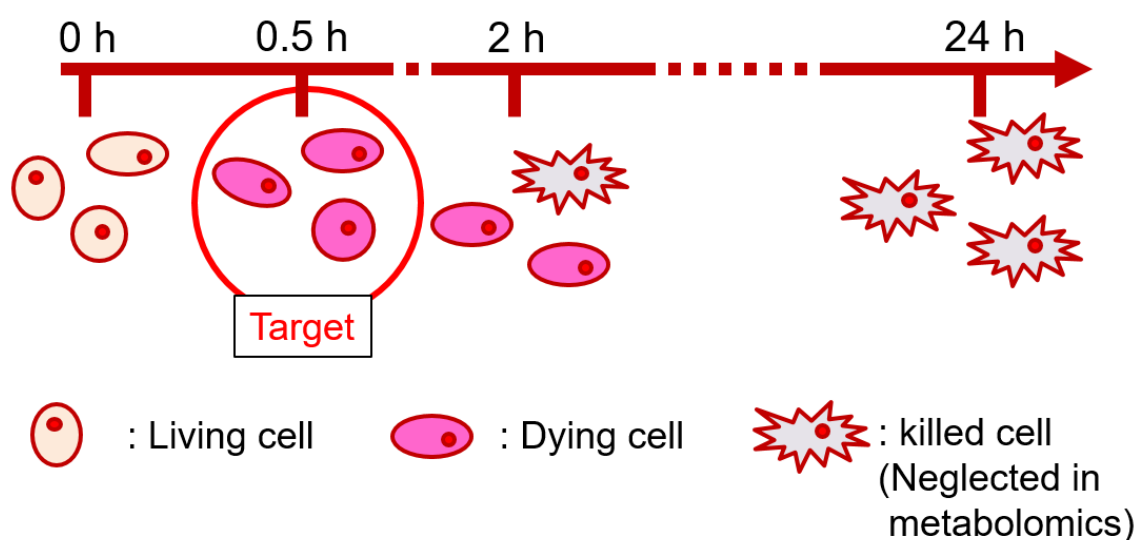


Figure 6.2.2 a schematic model of the gradual decreasing of U251SP cell survivals as a function of the cell incubation period.

§ 6.3 Statistical analysis

Table 6.3.1 shows the quantitative measurement result of 116 metabolites in cancer cells.

Figure 6.3.1 shows a *heatmap* of 116 metabolites. The color indicates the amount of each metabolite. Metabolites, which measured as similar quantitative characteristic, were arranged around of each other.

By the cluster analysis, the *heatmap* was separated (i) – (iii) regions. In the (i) region, metabolites decreased by the effect of PAM and RONS added medium since metabolites decreased in only PAM and RONS. NAD^+ , which is a coenzyme of *glycolysis*, and ATP, which is an energy source of cell proliferation, were involved in the region.

In the (ii) region, metabolomes decreased by the 30 min of cell incubation except for an initial. Metabolites, which are related with tricarboxylic acid cycle (TCA cycle), such as acetyl CoA, malic acid, fumaric acid and so forth were involved in the region. A role of the TCA cycle is a destination of branched chain amino acids (BCAA) metabolism. Estimated by the result, TCA cycle received little effect from the PAM and RONS and worked as destination of BCAA metabolism. Actually, little difference was appeared in levels of total intracellular amino acids of cancer cells incubated with a control medium, the PAM and RONS added medium as shown in Figure. 6.3.2. Total amino acids was calculated by the formula (6.3.1)

$$\begin{aligned} \text{Total Amino Acids} = & [\text{Ala}] + [\text{Arg}] + [\text{Asn}] + [\text{Asp}] + [\text{Cys}] + [\text{Gln}] + [\text{Glu}] + [\text{Gly}] + \\ & [\text{His}] + [\text{Ile}] + [\text{Leu}] + [\text{Lys}] + [\text{Met}] + [\text{Phe}] + [\text{Pro}] + [\text{Ser}] + \\ & [\text{Thr}] + [\text{Trp}] + [\text{Tyr}] + [\text{Val}] \end{aligned} \quad (6.3.1)$$

In the (iii) region, metabolomes increased by the effect of PAM and RONS added medium since metabolomes increased in only PAM and RONS. The region composed of Glyceraldehyde 3-phosphate (G3P) and Fructose 1,6-diphosphate (F1,6P), which involved in the first portion of *glycolysis*, or Ribulose 5-phosphate (Ru5P) and Ribose 5-phosphate (R5P), which is involved in *pentose phosphate pathway (PPP)*. The increasing of *glycolysis* and *pentose phosphate pathway (PPP)* were discussed in § 6.4.

However the drastic change of metabolomes was observed by the PAM, only little difference between the PAM and the RONS added medium was observed even by the analysis.

Chapter 6 Intracellular metabolism pathways disordered by the PAM

Table 6.3.1 Quantities of 166 metabolites in cancer cells (unit: pmol/10⁶ cells)

Compound name	initial			Control			PAM			RONS		
	1	2	3	10	11	12	4	5	6	7	8	9
NAD ⁺	2,244	2,305	2,242	1,540	1,714	1,481	451	524	442	301	290	302
cAMP	2.6	3.6	2.9	2.0	2.1	1.9	2.7	2.8	3.0	2.4	2.1	2.0
cGMP	N.D.	N.D.	N.D.	N.D.	N.D.	N.D.	N.D.	N.D.	N.D.	N.D.	N.D.	N.D.
NADH	168	182	180	140	N.D.	130	213	N.D.	N.D.	N.D.	N.D.	N.D.
Xanthine	26	19	16	N.D.	N.D.	N.D.	18	18	23	18	21	N.D.
ADP-ribose	11	14	15	5.8	4.1	5.9	5.5	5.8	3.6	3.7	2.8	3.1
Mevalonic acid	N.D.	N.D.	N.D.	N.D.	N.D.	N.D.	N.D.	N.D.	N.D.	N.D.	N.D.	N.D.
UDP-glucose	790	768	713	540	522	483	272	367	353	315	262	235
Uric acid	N.D.	N.D.	N.D.	N.D.	N.D.	N.D.	N.D.	N.D.	N.D.	N.D.	N.D.	N.D.
NADP ⁺	45	48	48	34	39	38	32	46	45	34	33	32
IMP	29	33	26	18	18	19	62	72	72	72	60	71
Sedoheptulose 7-phosphate	N.D.	N.D.	N.D.	N.D.	N.D.	N.D.	N.D.	104	58	134	97	135
Glucose 6-phosphate	424	454	561	244	314	274	67	64	69	71	81	93
Fructose 6-phosphate	116	122	137	70	75	67	75	111	121	102	91	134
Fructose 1-phosphate	N.D.	N.D.	N.D.	N.D.	N.D.	N.D.	204	765	1,259	1,443	1,702	1,753
Galactose 1-phosphate	126	167	156	54	116	71	N.D.	78	55	85	53	51
Glucose 1-phosphate	43	54	29	24	N.D.	5.6	6.3	N.D.	N.D.	N.D.	11	21
Acetoacetyl CoA	N.D.	N.D.	N.D.	N.D.	N.D.	N.D.	N.D.	N.D.	N.D.	N.D.	N.D.	N.D.
Acetyl CoA	20	18	20	10	12	13	12	15	12	13	13	13
Folic acid	7.0	6.8	6.5	6.8	5.5	5.0	7.7	10	7.7	6.5	6.6	7.0
Ribose 5-phosphate	57	60	73	60	45	48	1,023	1,290	832	1,390	1,052	962
CoA	34	37	32	23	N.D.	24	18	16	17	13	12	13
Ribose 1-phosphate	N.D.	N.D.	N.D.	N.D.	N.D.	N.D.	N.D.	18	13	40	34	16
Ribulose 5-phosphate	32	32	26	21	31	16	670	927	885	1,023	837	801
Xylulose 5-phosphate	N.D.	N.D.	N.D.	N.D.	N.D.	N.D.	1,567	2,737	1,910	1,930	1,524	1,638
Erythrose 4-phosphate	N.D.	N.D.	N.D.	N.D.	N.D.	N.D.	N.D.	N.D.	N.D.	N.D.	N.D.	N.D.
HMG CoA	9.3	14	11	6.6	8.2	8.0	16	24	21	22	19	22
Glyceraldehyde 3-phosphate	N.D.	N.D.	N.D.	N.D.	N.D.	N.D.	987	673	654	1,330	820	1,019
NADPH	N.D.	N.D.	N.D.	N.D.	N.D.	N.D.	N.D.	N.D.	N.D.	N.D.	N.D.	N.D.
Malonyl CoA	3.9	3.6	2.6	N.D.	1.6	1.3	N.D.	N.D.	N.D.	N.D.	N.D.	N.D.
Phosphocreatine	4,401	5,399	4,027	2,841	4,100	3,219	195	450	278	384	269	180
XMP	N.D.	N.D.	N.D.	N.D.	N.D.	N.D.	49	67	69	38	34	45
Dihydroxyacetone phosphate	220	217	155	301	342	204	2,738	4,961	3,643	4,252	3,407	3,748
Adenylosuccinic acid	15	16	16	12	N.D.	11	21	23	23	17	15	16
Fructose 1,6-diphosphate	620	628	571	624	580	499	10,252	15,764	18,159	16,714	16,759	18,758
6-Phosphogluconic acid	131	128	110	135	129	126	80	88	88	100	79	69
N-Carbamoylaspartic acid	155	175	174	62	63	68	12	15	12	9.5	7.3	6.3
PRPP	84	86	77	65	81	88	21	36	36	43	46	43
2-Phosphoglyceric acid	37	39	35	28	20	22	N.D.	N.D.	N.D.	3.4	N.D.	N.D.
2,3-Diphosphoglyceric acid	206	274	287	163	172	174	47	61	40	N.D.	N.D.	N.D.
3-Phosphoglyceric acid	276	284	261	184	160	177	N.D.	63	35	34	21	20
Phosphoenolpyruvic acid	N.D.	N.D.	N.D.	N.D.	N.D.	N.D.	N.D.	N.D.	N.D.	N.D.	N.D.	N.D.
GMP	67	N.D.	69	49	N.D.	N.D.	84	95	N.D.	81	74	78
AMP	94	73	80	65	70	60	362	575	555	435	366	387
2-Oxoisovaleric acid	N.D.	N.D.	N.D.	N.D.	N.D.	N.D.	N.D.	N.D.	N.D.	N.D.	N.D.	N.D.
GDP	120	116	123	88	122	82	120	105	120	101	96	110
Lactic acid	7,124	5,399	3,677	3,612	4,511	2,096	N.D.	N.D.	N.D.	N.D.	N.D.	N.D.
ADP	563	518	555	415	417	413	462	706	689	632	538	587
GTP	1,696	1,829	1,784	1,206	1,341	1,179	351	359	366	306	294	304
Glyoxylate	N.D.	N.D.	N.D.	N.D.	N.D.	N.D.	N.D.	N.D.	N.D.	N.D.	N.D.	N.D.
ATP	9,728	9,446	9,377	6,500	7,694	6,182	738	817	784	729	688	697
Glycerol 3-phosphate	171	200	172	118	162	140	39	45	70	64	44	60
Glycolic acid	N.D.	N.D.	N.D.	N.D.	N.D.	N.D.	N.D.	N.D.	N.D.	N.D.	N.D.	N.D.
Pyruvic acid	357	544	N.D.	N.D.	N.D.	145	N.D.	N.D.	N.D.	N.D.	N.D.	N.D.
N-Acetylglutamic acid	N.D.	N.D.	N.D.	N.D.	N.D.	N.D.	N.D.	N.D.	N.D.	N.D.	N.D.	N.D.
2-Hydroxyglutaric acid	54	34	38	N.D.	29	15	N.D.	17	23	13	17	N.D.
Carbamoylphosphate	N.D.	N.D.	N.D.	N.D.	N.D.	N.D.	N.D.	N.D.	N.D.	N.D.	N.D.	N.D.
Succinic acid	N.D.	157	167	124	95	73	59	N.D.	181	N.D.	132	162
Malic acid	1,582	860	658	N.D.	N.D.	N.D.	N.D.	N.D.	N.D.	N.D.	N.D.	N.D.
2-Oxoglutaric acid	N.D.	N.D.	N.D.	N.D.	N.D.	N.D.	N.D.	N.D.	N.D.	N.D.	N.D.	N.D.
Fumaric acid	199	N.D.	N.D.	N.D.	N.D.	N.D.	N.D.	N.D.	N.D.	N.D.	N.D.	N.D.

Chapter 6 Intracellular metabolism pathways disordered by the PAM

Compound name	initial			Control			PAM			RONS		
	1	2	3	10	11	12	4	5	6	7	8	9
Citric acid	1,725	1,891	2,002	288	345	257	678	1,070	1,023	856	814	979
<i>cis</i> -Aconitic acid	13	20	15	N.D.	N.D.	N.D.	N.D.	N.D.	N.D.	N.D.	N.D.	N.D.
Isocitric acid	N.D.	N.D.	N.D.	N.D.	N.D.	N.D.	N.D.	N.D.	N.D.	N.D.	N.D.	N.D.
Urea	N.D.	N.D.	N.D.	N.D.	N.D.	N.D.	N.D.	N.D.	N.D.	N.D.	N.D.	N.D.
Gly	15,794	16,284	16,081	10,638	11,758	10,335	7,754	11,919	12,526	11,531	11,059	12,065
Putrescine	100	105	89	70	50	35	109	103	114	65	82	85
Ala	6,675	7,203	7,132	518	816	599	N.D.	N.D.	158	93	52	34
β -Ala	717	741	749	461	541	427	261	516	506	452	423	524
Sarcosine	N.D.	N.D.	N.D.	N.D.	N.D.	N.D.	N.D.	N.D.	N.D.	N.D.	N.D.	N.D.
<i>N,N</i> -Dimethylglycine	N.D.	N.D.	N.D.	N.D.	N.D.	N.D.	N.D.	N.D.	N.D.	N.D.	N.D.	N.D.
γ -Aminobutyric acid	306	366	366	196	249	211	137	222	221	200	194	229
Choline	N.D.	N.D.	N.D.	N.D.	N.D.	N.D.	685	1,558	1,935	1,918	1,809	2,132
Ser	8,590	8,923	9,583	6,590	7,640	6,858	5,328	8,230	8,603	8,065	8,165	8,619
Carnosine	N.D.	N.D.	N.D.	N.D.	N.D.	N.D.	N.D.	N.D.	N.D.	N.D.	N.D.	N.D.
Creatinine	102	113	95	39	47	33	19	43	52	41	32	39
Pro	7,325	7,672	8,188	4,800	6,056	4,909	439	2,135	2,668	2,357	1,961	2,903
Betaine	N.D.	N.D.	N.D.	N.D.	N.D.	N.D.	N.D.	N.D.	N.D.	N.D.	N.D.	N.D.
Val	1,232	1,217	1,157	630	745	513	1,040	2,011	1,853	1,684	1,902	1,815
Thr	17,394	18,407	17,693	12,619	13,960	12,207	8,749	13,799	14,331	14,476	14,031	14,354
Homoserine	N.D.	N.D.	N.D.	N.D.	N.D.	N.D.	N.D.	7.4	14	N.D.	N.D.	N.D.
Betaine aldehyde	N.D.	N.D.	N.D.	N.D.	N.D.	N.D.	N.D.	N.D.	N.D.	N.D.	N.D.	N.D.
Cys	186	135	154	135	129	131	241	281	245	162	155	170
Hydroxyproline	314	340	325	75	99	82	122	119	113	118	76	97
Creatine	8,069	8,564	7,771	5,799	6,197	5,233	8,109	11,708	12,874	10,613	10,805	11,489
Leu	2,694	2,825	2,744	1,645	1,773	1,424	1,959	3,139	3,022	2,655	2,789	2,668
Ile	745	782	789	594	606	380	871	1,326	1,136	951	1,196	1,116
Asn	370	427	364	155	186	165	41	N.D.	N.D.	5.1	N.D.	N.D.
Ornithine	85	83	84	N.D.	39	N.D.						
Asp	14,339	15,011	13,979	9,604	11,862	10,018	10,652	16,715	18,754	16,963	16,809	18,445
Homocysteine	N.D.	N.D.	N.D.	N.D.	N.D.	N.D.	N.D.	N.D.	N.D.	N.D.	N.D.	N.D.
Adenine	N.D.	N.D.	N.D.	N.D.	N.D.	N.D.	2.4	8.6	37	32	36	29
Hypoxanthine	N.D.	N.D.	N.D.	N.D.	N.D.	N.D.	N.D.	N.D.	14	16	N.D.	16
Spermidine	N.D.	3.7	5.2	N.D.	N.D.	N.D.	N.D.	14	11	3.8	19	15
Gln	45,640	47,203	47,004	32,782	37,141	33,639	27,774	41,450	44,093	39,251	39,594	41,130
Lys	1,394	1,484	1,478	1,177	1,306	997	1,406	2,413	2,368	2,133	2,399	2,360
Glu	57,157	60,625	58,213	35,658	41,071	35,200	19,605	28,014	27,314	23,605	20,886	21,601
Met	2,547	2,836	2,513	1,471	1,682	1,500	1,012	1,323	1,312	1,664	1,674	1,546
Guanine	N.D.	N.D.	N.D.	N.D.	N.D.	N.D.	N.D.	N.D.	N.D.	N.D.	N.D.	N.D.
His	2,645	2,759	2,747	1,542	1,856	1,591	1,331	2,110	2,264	2,159	2,070	2,385
Carnitine	N.D.	N.D.	N.D.	N.D.	N.D.	N.D.	N.D.	N.D.	N.D.	N.D.	N.D.	N.D.
Phe	988	984	989	700	745	601	724	1,122	1,063	989	1,043	1,106
Arg	652	675	677	626	615	521	1,076	1,270	1,234	1,143	1,266	1,262
Citrulline	159	163	179	77	89	89	42	60	76	98	91	75
Tyr	851	895	887	615	710	521	665	1,076	988	934	1,068	1,046
S-Adenosylhomocysteine	N.D.	N.D.	N.D.	N.D.	N.D.	N.D.	N.D.	N.D.	N.D.	N.D.	N.D.	N.D.
Spermine	N.D.	N.D.	N.D.	N.D.	N.D.	N.D.	N.D.	N.D.	N.D.	N.D.	N.D.	N.D.
Trp	159	168	153	119	113	94	113	194	173	160	191	187
Cystathionine	155	143	160	80	111	97	60	78	103	99	87	96
Adenosine	N.D.	N.D.	N.D.	N.D.	N.D.	N.D.	N.D.	N.D.	N.D.	N.D.	N.D.	N.D.
Inosine	N.D.	N.D.	N.D.	N.D.	N.D.	N.D.	N.D.	N.D.	N.D.	N.D.	N.D.	N.D.
Guanosine	N.D.	N.D.	N.D.	N.D.	N.D.	N.D.	N.D.	N.D.	N.D.	N.D.	N.D.	N.D.
Argininosuccinic acid	47	N.D.	28	N.D.	N.D.	N.D.	N.D.	N.D.	N.D.	N.D.	N.D.	N.D.
Glutathione (GSSG)	1,184	1,304	1,347	2,541	2,530	1,919	3,411	6,768	7,111	6,569	6,892	7,368
Glutathione (GSH)	24,385	25,492	25,100	14,138	16,830	15,441	3,682	2,646	2,383	3,413	2,313	2,423
S-Adosylmethionine	103	117	125	72	82	71	67	93	110	115	96	89

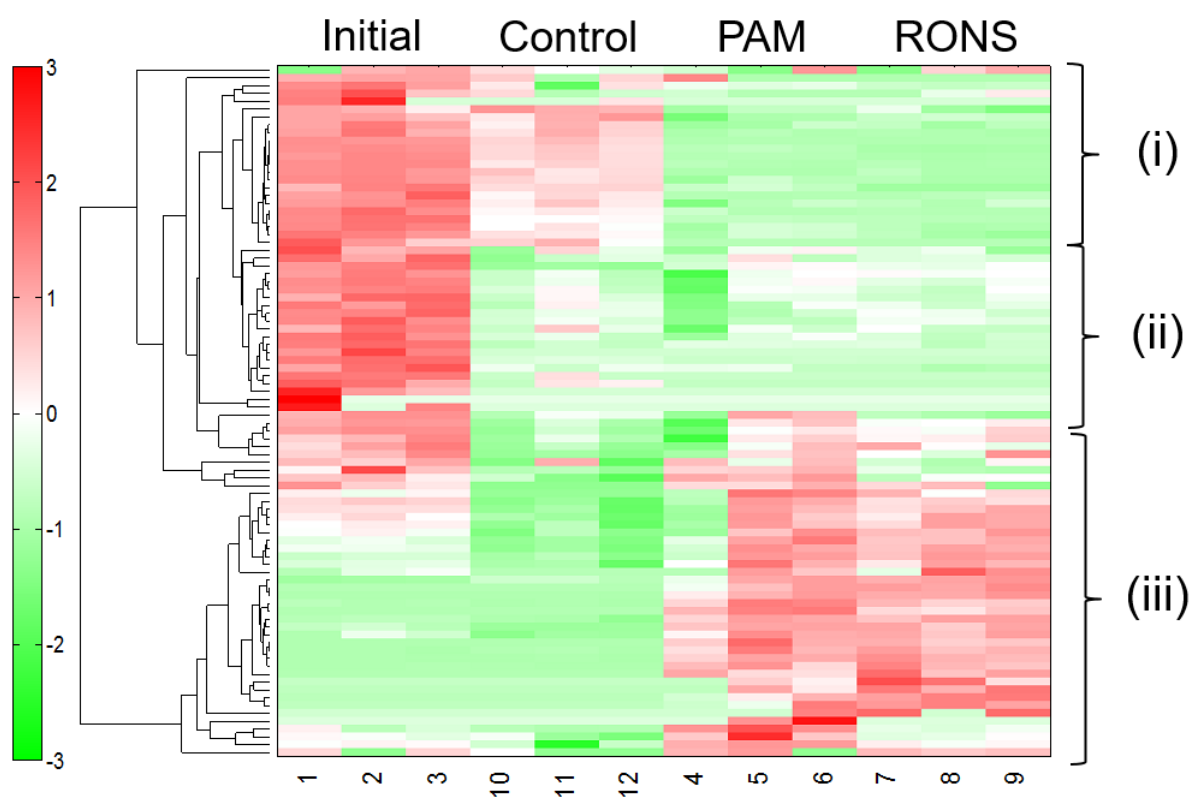


Figure 6.3.1 A *heatmap* of 116 metabolomes obtained after an incubation with an initial, a medium as a control, the PAM or the RONS added medium.

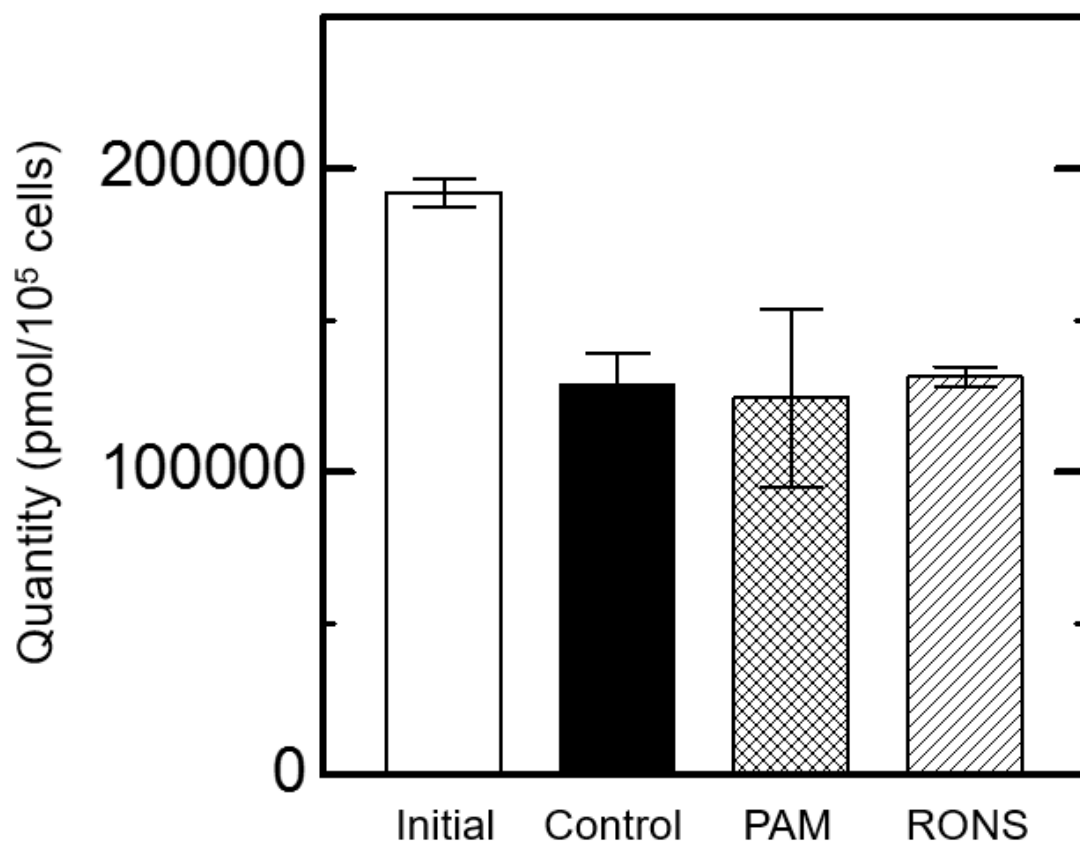


Figure 6.3.2 Total amino acids in in cells incubated with an initial, a control, the PAM and the RONS added medium.

The result of quantitative measurement of metabolomes was also analyzed with a statistical method.⁴⁾ Figure 6.3.3 shows PC1 and PC2 axis from the result of the principal component analysis (PCA). The analysis performed with triplicate samples.

The result of metabolism seems to be reliable because each triplicate samples were gathered. However a sample of PAM was varied, at least, PAM samples gathered in a point on the PC1 axis, which has highest contribution.

The samples were separated to 2 groups on the PC1 axis, which were initial, incubated with a medium, and incubated with the PAM, incubated with the RONS added medium. Since stimulus and control samples were clearly separated on the axis, a metabolome changing by stimulations of PAM or RONS certainly appeared.

Those samples also separated to 2 groups on the PC2 axis, which were incubated with a medium or an initial, an incubated with the PAM and an incubated with the RONS added medium. Therefore, the axis might reflect performing a normal cell cycle or not. It is considered that in stimulus cells, the normal cell cycle could not perform because of a cell metabolism disorder.

Contrary to drastic difference between stimulus and control samples, only little difference between the PAM and the RONS added medium was observed.

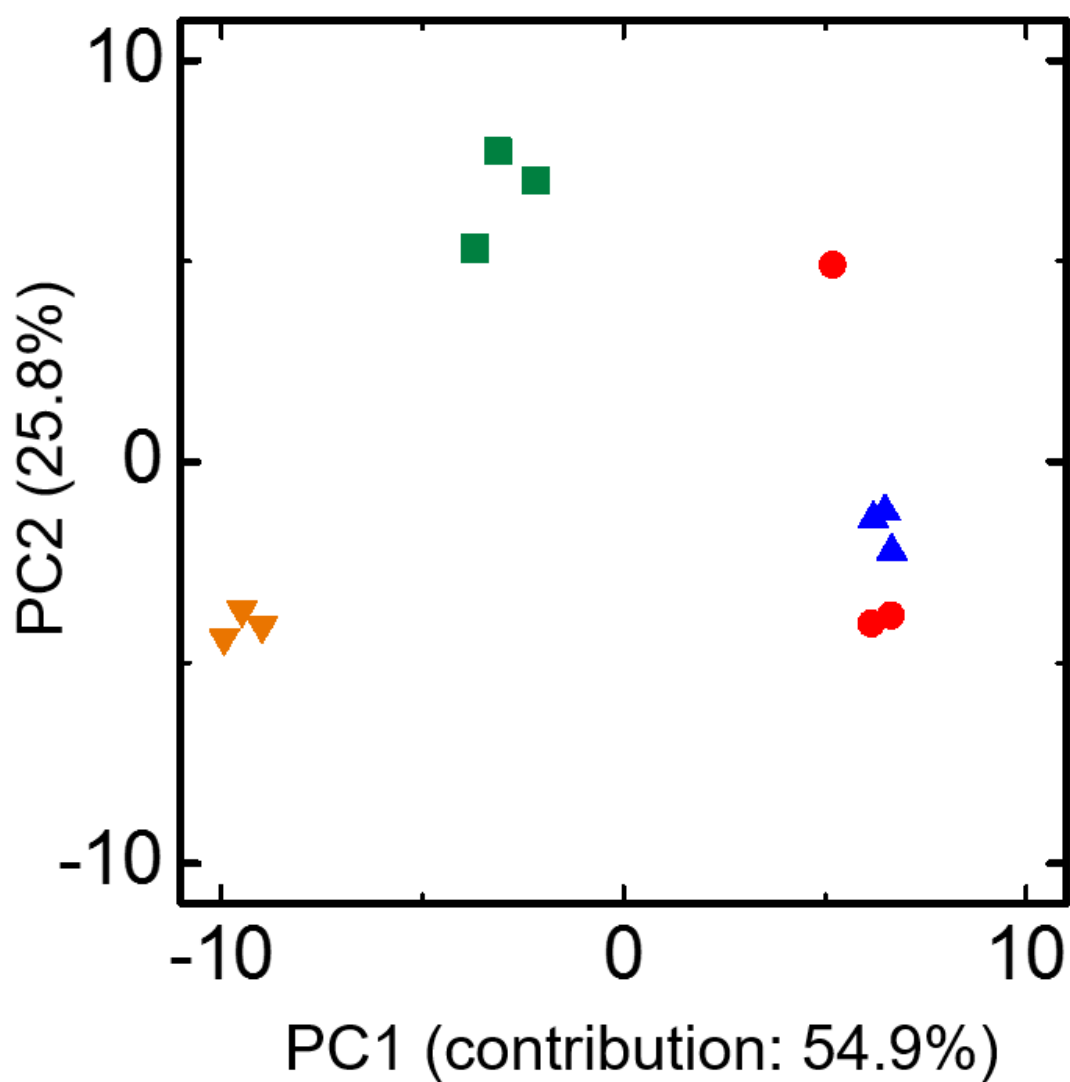
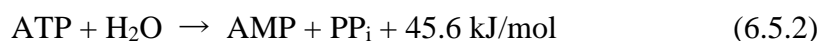


Figure 6.3.3 PC1 and PC2 axis from the result of the principal component analysis (PCA) obtained after an incubation with (▼) initial, (■) medium, (●) PAM or (▲) RONS added medium.

§ 6.4 Adenosine triphosphate (ATP) decreasing by the PAM

In this study, the author especially focused on *glycolysis* and linked pathways because the adenosine triphosphate (ATP), which is an energy source of cells proliferation depending on *glycolysis*. One of the important characteristics of cancer against normal cells is a dependence of ATP generation on *glycolysis*, which named as *Warburg effect*, as mentioned in § 2.9.1.

ATP generates energies by changing itself to adenosine diphosphate (ADP) or adenosine monophosphate (AMP) by a reaction of (6.5.1) and (6.5.2).



A characteristic part of *glycolysis* and *pentose phosphate pathway (PPP)* are shown in Figure 6.4.1. The measured samples are shown in the upside light of the Figure. In the Figure, the N.D. represents not detected, and the N.A. represents not available, which was not measured.

As shown in Figure 6.4.1, *glycolysis* generates 2 ATP by a cycle from a glucose transported to an inside of cells through a glucose transporter placed in a membrane. First, 2 ATP is used in the front half part and then 4 ATP is produced in the latter half part.

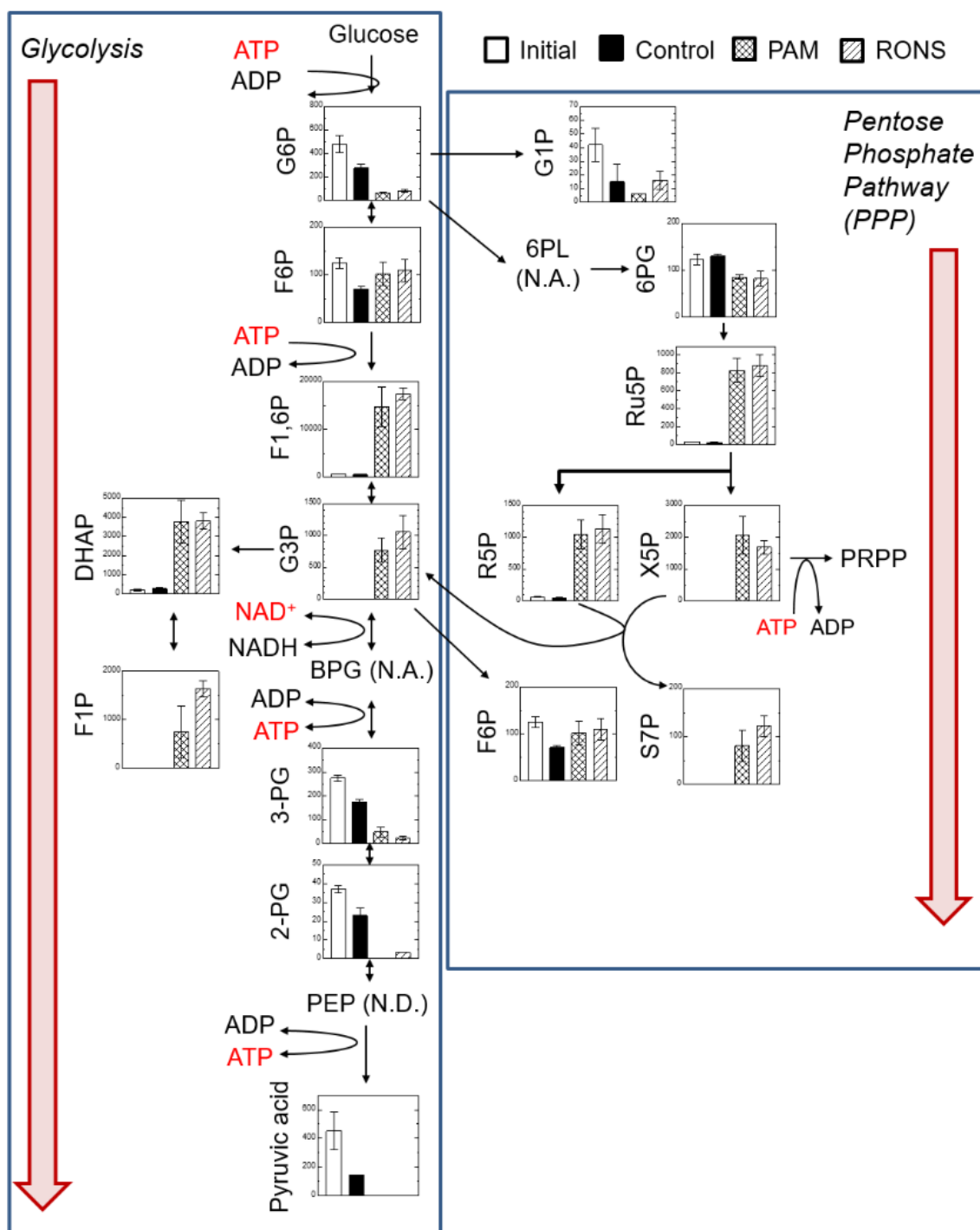


Figure 6.4.1 A characteristic part of *glycolysis* and *pentose phosphate pathway* (PPP); samples are shown in the upside light of the Figure the N.D. represents not detected, and the N.A. represents not available, which was not measured.

In the *glycolysis*, the amounts of metabolite were decreased in downflow of pathway of G3P and 3-PG after an incubation with the PAM or the RONS. The result indicates inducing short of 3-PG by damming of the *glycolysis* flow.

On the other hand, the *pentose phosphate pathway (PPP)* was considerably enhanced by an incubation with the PAM and the RONS. From the result, the overflow of G6P to the *PPP* was also indicated. The overflow has been reported as a resistant mechanism of cancer cells from an anticancer drug.⁵⁾ When *glycolysis* was down-regulated by a drug, glucose was supplied to *glycolysis* through *PPP*.⁵⁾ However, in the case of the PAM, the ATP synthesis through *PPP* was not occurred since *glycolysis* was stemmed in down-flow after G3P, where is supplying point from *PPP*.

A nucleotide, NAD^+ , is related to the reaction of the damming point, BPG synthesis from G3P. If the damming has occurred, the amount of ATP might be decreased since no ATP producing reactions in the *glycolysis*, which are the 3-PG synthesis from BPG and the Pyruvic acid synthesis from PEP, occurred. Moreover, only ATP consuming reactions, which are G6P synthesis from a glucose and F1,6P synthesis from F6P, occurred.

The amounts of (a) NAD^+ , (b) total NAD ($\text{NADH} + \text{NAD}^+$), (c) PRPP and (d) ATP in the incubated cells are shown in Figure 6.4.2.

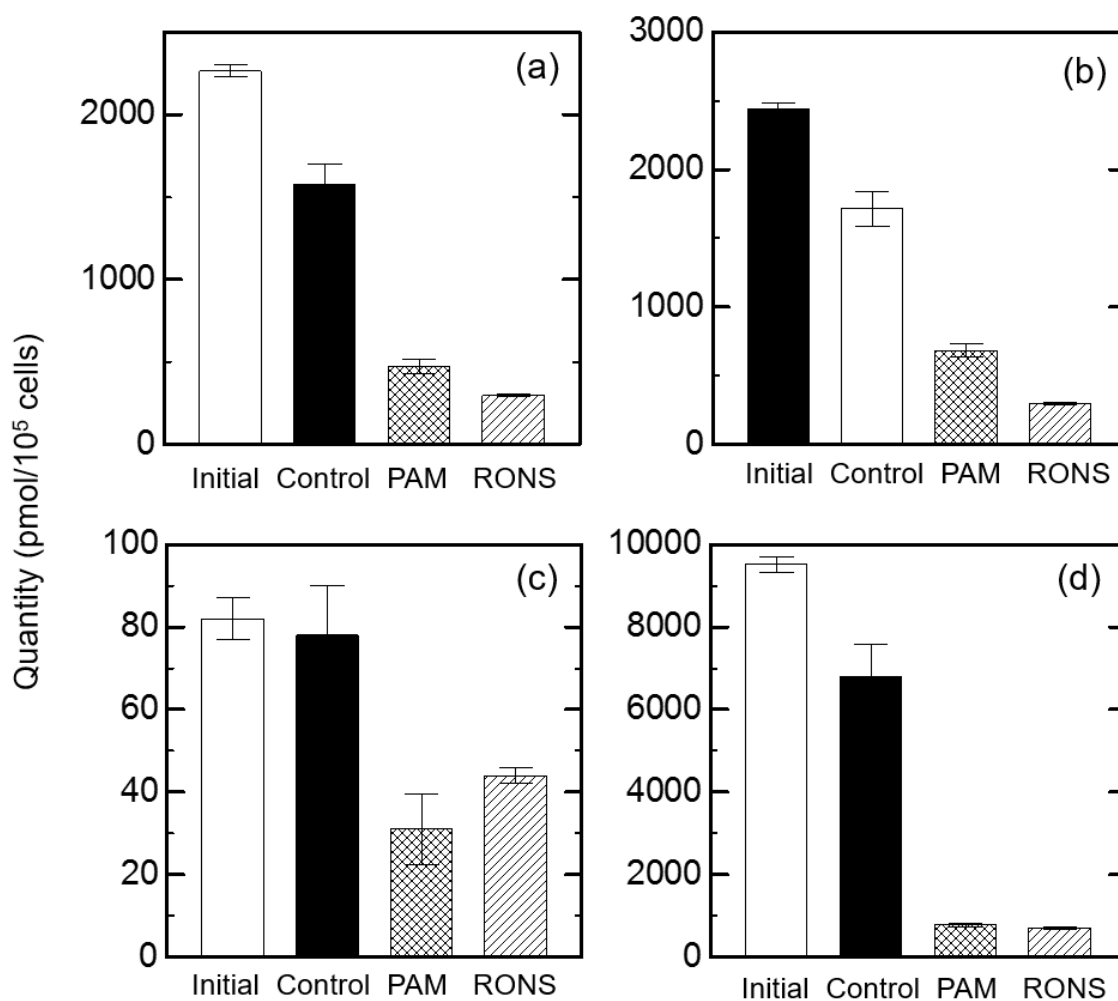


Figure 6.4.2 Amounts of (a) NAD⁺, (b) total NAD (NADH + NAD⁺), (c) PRPP and (d) ATP in cells incubated with an initial, a control, the PAM and the RONS added medium.

Actually as shown in Figure 6.4.2(a), NAD^+ level was decreased by incubating with the PAM. Characteristic much NAD^+ in cancer cells is consumed for the high proliferation and DNA repair rate.^{6,7)} Figure 4.6.3 shows pathways related to the part of *glycolysis* down-flow from G3P to BPG. As shown, the NAD^+ level decreasing could induce the *glycolysis* damming shown in Figure 6.4.1.

Since not only the NAD^+ level but also total NAD ($\text{NADH} + \text{NAD}^+$) was decreased as shown in Figure 6.4.2(b), the NAD^+ lack didn't derived from a failure of a reduction of intracellular NADH. If anything, the down-regulation of NAD^+ might be induced by a failure of total NAD generation. Tryptophan, nicotinamide (NAM), nicotinic acid (NA) and nicotinamide riboside (NR) are known as precursors of NAD^+ generation.⁸⁾ Actually, high NAM and NA levels protected cells against apoptosis.⁹⁾

In the case of mammal cells, NAM is a main source for generating NAD^+ .⁸⁾ As shown in Figure 4.6.3, NAM react with 5'-phosphoribosyl-1'-pyrophosphate (PRPP) and converted to nicotinamide mononucleotide (NMN) by an enzyme, nicotinamide phosphoribosyltransferase (NAMPT).¹⁰⁻¹³⁾ Then, NMN converted to NAD^+ by an enzyme, nicotinamide/nicotinic acid mononucleotide adenylyltransferase (NMNAT).⁸⁾

R5P, which is a kind of metabolites involved in *PPP*, is converted to PRPP. Figure 6.4.2(c) shows amount of PRPP in cells. PRPP is generated from R5P by consuming ATP.¹⁴⁾ Therefore, however the PRPP level in cells incubated with the PAM was decreased, it was considered as a result of the ATP decreasing induced by the PAM rather than a cause.

Therefore, it was considered as a reason of the NAD^+ decreasing that down-regulations of NAD^+ synthesis enzymes, NAMPT or NMNAT. Actually, NAM Because NAD^+ is rapidly consumed (approximately 1 h) and converted to NAM in cells, NAMPT

and NMNAT is necessary for retaining intracellular NAD^+ level.¹⁵⁾ It has been considered that NAD^+ decreasing induced by a down-regulation of NAMPT is one of cause of the symptoms of aging.¹⁶⁾ If the down-regulation was occurred, previously reported AKT kinase down-regulation could be also induced by a lack of NAMPT.¹⁾

The down-regulation of NAMPT has strongly drawn attentions as a target protein for cancer therapy. It is reported an accumulation of metabolites related to *Glycolysis* or *PPP*, which are fructose 1-phosphate (F1P), sedoheptulose 7-phosphate (S7P), fructose 1,6-diphosphate (F1,6P), and dihydroxyacetone phosphate (DHAP) were led by NAMPT inhibition.¹⁷⁾ The result in the study was properly corresponded to the reported characteristics of NAMPT inhibition.

It is also reported that NAMPT down-regulation led to alternation of *PPP* activity, which characterized by an activation of not only S7P also xylulose 5-phosphate (X5P), and the result shown in Figure 6.4.1 corresponded it well.¹⁸⁾ On the other hand, however it was also reported attenuations of α -ketoglutarate (2-OG), which is a part of TCA cycle, and serine were induced by NAMPT down-regulation,¹⁸⁾ in this study, undetectable 2-OG was detected in each samples and similar serine concentrations were detected with concentrations of 9032 ± 506 (initial), 7029 ± 545 (control), 7387 ± 1793 (PAM), and 8283 ± 295 (RONS) pmol/ 10^5 cells. Therefore, the discussion should be done carefully.

However, the downflow from G3P could be also induced by glyceraldehyde-3-phosphate dehydrogenase (GAPDH), which is a kind of protein. Actually, intracellular GAPDH was down-regulated by irradiating with a He + O₂ plasma jet.¹⁹⁾ RONS generated by NEAPP irradiation could contribute for the down-regulation since it is well known that NO donors such as SNGO and SNAP, peroxyxynitrite donors such as SIN-1, and hydroxyl radical donors such as H₂O₂ inhibit GAPDH activity as a cause of the GAPDH

down-regulation.²⁰⁻²³⁾ In the distinct effect, some oxidants, involving peroxynitrite and H₂O₂, induced a GAPDH aggregate formation and the aggregate might participate a neurotoxicity.²⁴⁾

On the other hand, in the case of an anticancer drug, AZD9291 which down-regulate Epidermal Growth Factor Receptor (EGFR), metabolites of G6P, 6-PG and P1,6P in *glycolysis* were also down-regulated.³⁾

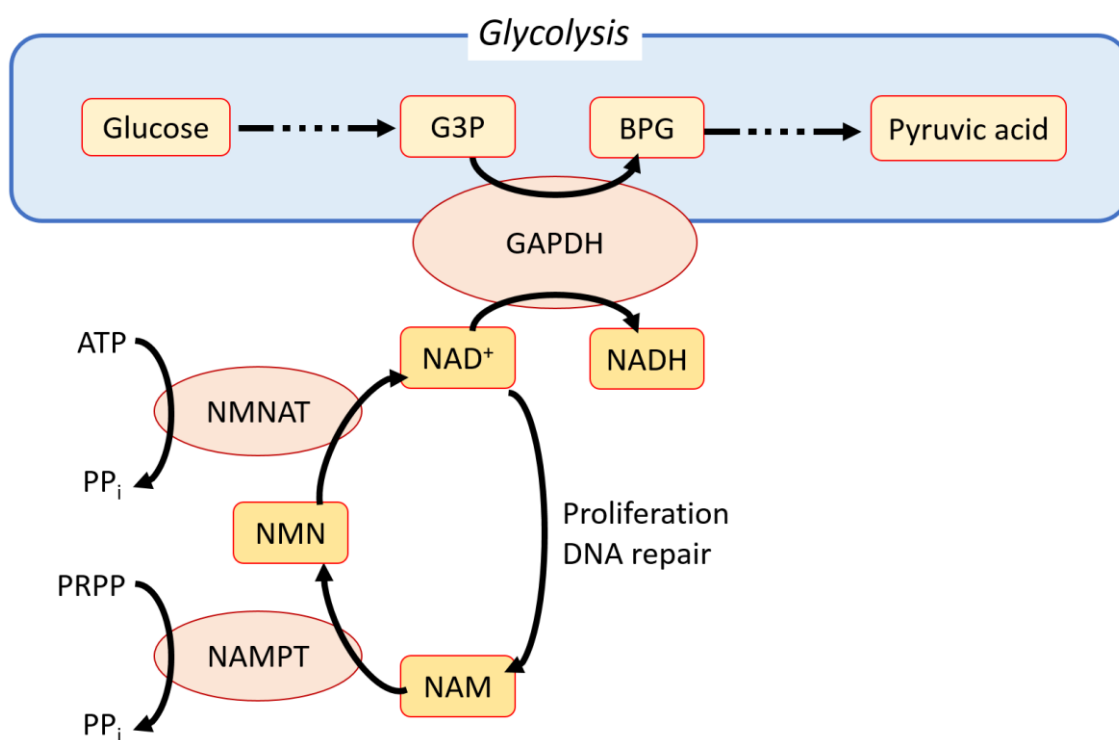


Figure 6.4.3 Pathways related to the part of glycolysis down-flow from G3P to BPG

As shown in Figure 6.4.2(d), ATP level was also drastically decreased over 10 times by the incubation with the PAM. The ATP shortage could be induced by the NAD^+ decreasing, which induced by the PAM, since the result is corresponding to the *glycolysis* damming.

The cellular energy shortage could be one of the cause of the antitumor effect of the PAM. Moreover, the cell killing mechanism has a selectivity of the killing for cancer cells against normal cells because the killing is deriving from a damming of *glycolysis*, which is the main energy source for cancers.

By the analysis of metabolism of incubated cells, little difference was observed between the PAM and the RONS added medium, which composed of H_2O_2 and NO_2^- . Therefore, the antitumor effect by disorder of a metabolism of cancer cells was dominantly induced by the synergistic antitumor effect of RONS generated in the PAM described in Chapter 5. Actually, RONS is likely to induce the ATP decreasing since ATP decreasing by H_2O_2 addition was previously reported in murine macrophage-like cell.²⁵⁾ However, in this case, the synergistic effect of H_2O_2 and NO_2^- were likely to contribute.

On the other hand, the uninvestigated antitumor effects, which is also described in the Chapter 5, could be working with the another mechanism.

§ 6.5 Summary

In previous chapters, RONS and other reactive species contribution for the cancer killing of the PAM was elucidated. However, effects of RONS for biological samples were unclear.

In the Chapter 6, an intracellular response was investigated by analyzing biological species in cancer cells. An intracellular metabolomics analysis for cancer cells was performed. Especially, *glycolysis*, which is the main ATP producing pathway of cancers, and liked pathways were analyzed. Since metabolism activities strongly depend on the cell type whether cancer cells or normal cells, the difference could induce the selectivity of cell killing induced by the PAM.

By the study, a change of metabolites by the PAM were appeared. Since the metabolite change was appeared before inducing cancer cell killing by the PAM, it might contribute for the cell killing mechanism of the PAM. However, it needed more study for clearly evaluation.

In an analysis of metabolome flow pathways, ATP decreasing was significantly appeared. In the cancer cells incubated by the PAM, *glycolysis* pathway consumed ATP rather than produced since the flow was stemmed at G3P. The damming could be contributed by NAD⁺ decreasing. Therefore, NAMPT and NMNAT, which are a generation enzyme of NAD⁺, might be down-regulated. If the down-regulation was occurred, previously reported AKT kinase down-regulation could be also induced. However, the downflow from G3P was also induced by GAPDH, which is a kind of protein, so that proteomics analysis was also needed for more clear elucidation of the damming mechanism.

The metabolism disorder dominantly induced by the synergistic antitumor effect of RONS generated in the PAM described in Chapter 5. However, it is still unclear that the effect was induced by whether individual effects of H_2O_2 and NO_2^- or unknown species generated by an interaction between the medium and RONS. Especially, organic species, which involved in the medium, could be changed by the NEAPP irradiation, for example, an oxidation was likely to occur as described in § 3.4.

Therefore, in this study also investigated an interaction between aqueous organic species and the NEAPP. Then, calcium oxalate crystal synthesis was appeared and the mechanism was examined as described in Chapter 7.

References for Chapter 6

- 1) H. Tanaka, M. Mizuno, K. Ishikawa, K. Nakamura, H. Kajiyama, H. Kano, F. Kikkawa, and M. Hori, *Plasma Medicine*. **1**, 265-277 (2011).
- 2) J.M. Ollinger, and J.A. Fessler, *IEEE Signal Processing Magazine*. **14**, 43-55 (1997).
- 3) H. Makinoshima, M. Takita, K. Saruwatari, S. Umemura, Y. Obata, G. Ishii, S. Matsumoto, E. Sugiyama, A. Ochiai, R. Abe, K. Goto, H. Esumi, and K. Tsuchihara, *J. Biol. Chem.* **290**, 17495-17504 (2015).
- 4) T. Sato, M. Yokoyama, and K. Johkura, *J. Phys. D: Appl. Phys.* **44**, 372001 (2011).
- 5) T. Yamamoto N. Takano, K. Ishikawa, M. Ohmura, Y. nagahata, T. Matsuura, A. Kamata, K. Sakamoto, T. Nakanishi, A. Kubo, T. Hishiki, and M. Suematsu, *Nat. Commun.* **5**, 3480 (2014).
- 6) A. Chiarugi, C. Dolle, R. Felici, and M. Ziegler, *Nature Reviews Cancer*. **12**, 741-752 (2012).
- 7) T-Q. Bi, and X-M. Che, *Cancer Biol. Ther.* **10**, 119-125 (2010).
- 8) S. Yamaguchi, and J. Yoshino, *J. J. Biochem. Soc.* **87**, 239-244 (2015).
- 9) C.L. Crowley, C.M. Payne, H. Bernstein, C. Bernstein, and D. Roe, *Cell. Death. Differ.* **7**, 314-326 (2000).
- 10) A. garten, S. Petzoid, A. Korner, S. Imai, and W. Kiess, *Trends Endocrinol Metab.* **20**, 130-138 (2009).
- 11) S. Imai, *Curr Pharm Des.* **15**, 20-28 (2009).
- 12) C. Peiro, T. Romacho, R. Carraro, and C.F. Sanchez-Ferrer, *Front. Pharmacol.* **1**, 135 (2010).
- 13) S. Schuster, M. Penke, T. Gorski, R. Gebhardt, T.S. Weiss, W. Kiess, and A. Garten,

- Biochem Biophys Res Commun.* **458**, 334-340 (2015).
- 14) D. Sampath, T.S. Zabka, D.L. Misner, T. O'Brien, and P.S. Dragovich, *Pharmacol. Ther.* **151**, 16-31 (2015).
- 15) M. Rechsteiner, D. Hillyard, and B.M. Olivera, *Nature.* **259**, 695-696 (1976).
- 16) S. Imai, *Cell Metab.* **6**, 363-375 (2007).
- 17) B. Tan, S. Dong, R.L. Shepard, L. Kays, K.D. Roth, S. Geeganage, M-S. Kuo, and G. Zhao, *J. Biol. Chem.* **290**, 25812-25824 (2015).
- 18) B. Tan, D.A. Young, Z-H. Lu, T.I. Meier, R.L. Shepard, K. Roth, Y. Zhai, K. Huss, M-S. Kuo, J. Gillig, S. Pathasarathy, T.P. barkholder, M.C. Smith, S. Geegenage, and G. Zhao, *J. Biol. Chem.* **288**, 3500-3511 (2013).
- 19) J-W. Lackmann, S. Schneider, E. Edengeiser, F. Jarzina, S. Brinckmann, E. Steinborn, M. Havenith, J. Benedikt, and J.E. Bandow, *J. R. Soc. Interface.* **10**, 20130591 (2013).
- 20) T. Ishii, O. Sunami, H. Nakajima, H. Nishio, T. Takeuchi, and F. Hata, *Biochem. Pharmacol.* **58**, 133-143 (1999).
- 21) S. Mohr, J.S. Stamler, and B. Brune, *FEBS Lett.* **348**, 223-227 (1994).
- 22) J. Rivera-Nieves, W.C. Thompson, R.L. Levine, and J. Moss, *J. Biol. Chem.* **274**, 19525-19531 (1999).
- 23) J.M. Souza, and R. Radi, *Arch. Biochem. Biophys.* **360**, 187-194 (1998).
- 24) H. Nakajima, W. Amano, T. Kubo, A. Fukuhara, H. Ihara, Y. Azuma, H. Tajima, Y. Inui, A. Sawa, and T. Takeuchi, *J. Biol. Chem.* **284**, 34331-34341 (2009).
- 25) R.G. Spragg, D.B. Hinshaw, P.A. Hyalop, I.U. Schraufstatter, and C.G. Cochrane, *J. Clin. Invest.* **76**, 1471-1476 (1985).

Chapter 7

Calcium oxalate crystal synthesis in plasma irradiated medium

§ 7.1 Introduction

In previous chapters, it was indicated that reactive species generation in the PAM except for RONS was performed, such as organic synthesis. New findings regarding the synthesis of the crystalline form of salts in culture medium irradiated with NEAPP are described in Chapter 7 and 8.

The author report that NEAPP irradiation induces the formation of calculus-like salts containing calcium oxalate, even if no oxalate is contained in the medium. Therefore, it was indicated that an organic synthesis and crystallization were occurred in the PAM.

In this chapter, Dulbecco's modified Eagle's medium (DMEM), which is widely used in cell culture composed of 32 kinds of inorganics, amino acids, vitamins, glucose and so forth shown in Table 2.1.1.¹⁾, was used for the irradiation target. Properties of crystal-like particles synthesized in the medium were analyzed and the synthesis dynamics was investigated.

§ 7.2 Synthesis of crystals in a NEAPP irradiated medium

The morphology of particles synthesized in the bottom of dish filled the medium irradiated with the NEAPP was observed. Figure 7.2.1 shows a morphology of the particulates, which were observed after a 24-hour incubation of the NEAPP irradiated medium. The NEAPP irradiation period was 10 min.

The morphology of particulates were octahedrons several tens of microns in size. Particulates generated in samples incubated at both 4 and 37°C exhibited the similar morphologies. Therefore, the incubation temperature was not considered as an important factor of the crystal synthesis. In contrast, a contact between the NEAPP plume and the medium surface was found to be essential for the particulate generation because no particulates were generated by remote NEAPP irradiation (i.e., with the medium surface located under 13 mm from the NEAPP source exit).

No particulates were detected in non-irradiated initial medium examined using the same microscopic parameters. In addition, no particles appeared when only Ar gas flowed from the instrument (i.e., no NEAPP irradiation). These results indicate that the particulates are synthesized as a result of the NEAPP irradiation.

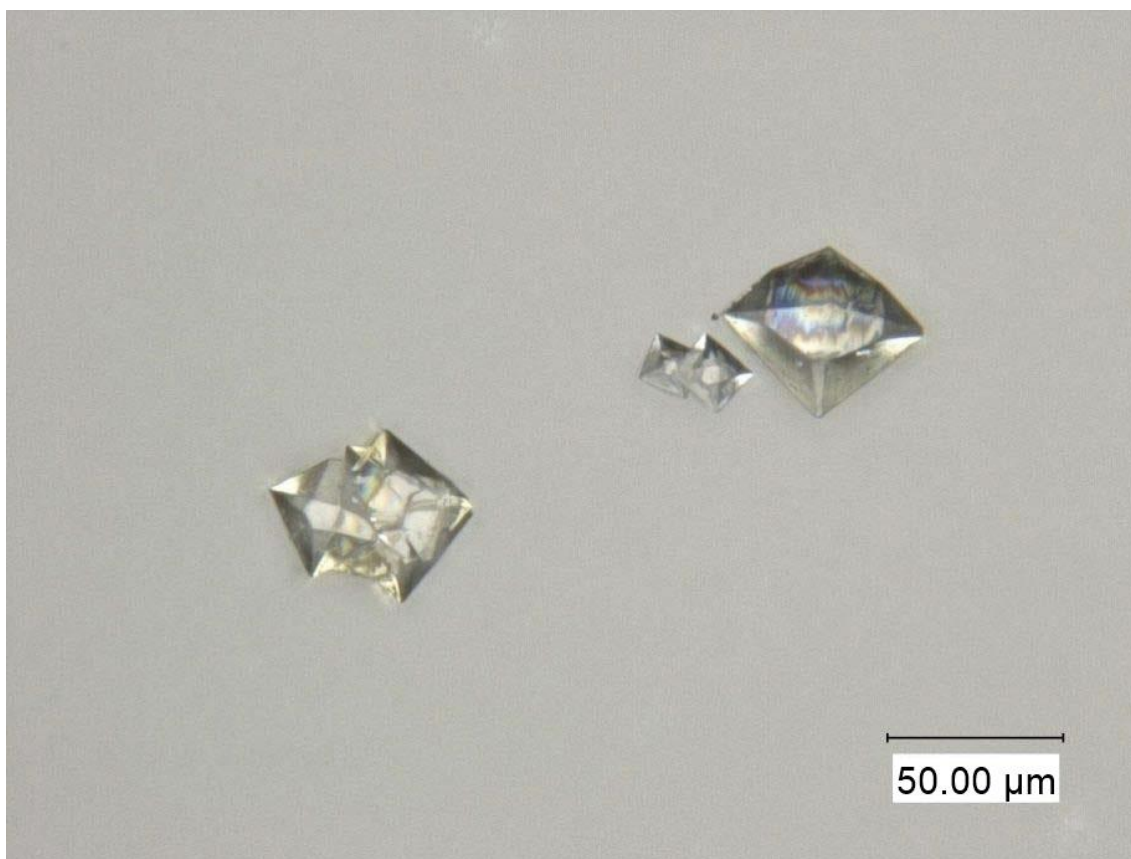


Figure 7.2.1 A microscopic image of the collected particulates, which were observed after the incubation of 10 min of NEAPP irradiated medium.

§ 7.3 Analysis of those particles structure

§ 7.3.1 Analysis of XRD

The structural measurement of the octahedral particles were performed by using XRD, SEM-EDX and FT-IR. Figure 7.3.1 (a) shows the powder XRD pattern of the particulate. All peaks are sharp with a minimal full-width at half maximum and no broad peaks were observed. These results indicate that the particulates are crystalline, with a minimal amorphous phase.

Analysis of a comparison with a powder diffraction file database (PDF card) showed that the main diffraction peak positions of the particulates corresponded with those of calcium oxalate dihydrate (COD, $\text{CaC}_2\text{O}_4 \cdot [2+x]\text{H}_2\text{O}$ [$x \leq 0.5$]) (JCPDS, 17-0541) crystals, as shown in Figure 7.3.1 (b). Calcium oxalates are represented by the general formula $\text{CaC}_2\text{O}_4 \cdot x\text{H}_2\text{O}$, where x represents the number of bound water molecules per molecule.²⁾

Notably, no patterns were observed corresponding to calcium oxalate anhydride (JCPDS, 77-4251), monohydrate (JCPDS, 20-0231), or trihydrate (JCPDS, 20-0232) or to calcium carbonate anhydride (JCPDS, 41-1475), monohydrate (JCPDS, 29-0306), or calcium phosphate (JCPDS, 9-0348). These data confirm that the particulates are primarily composed of a crystalline form of COD.

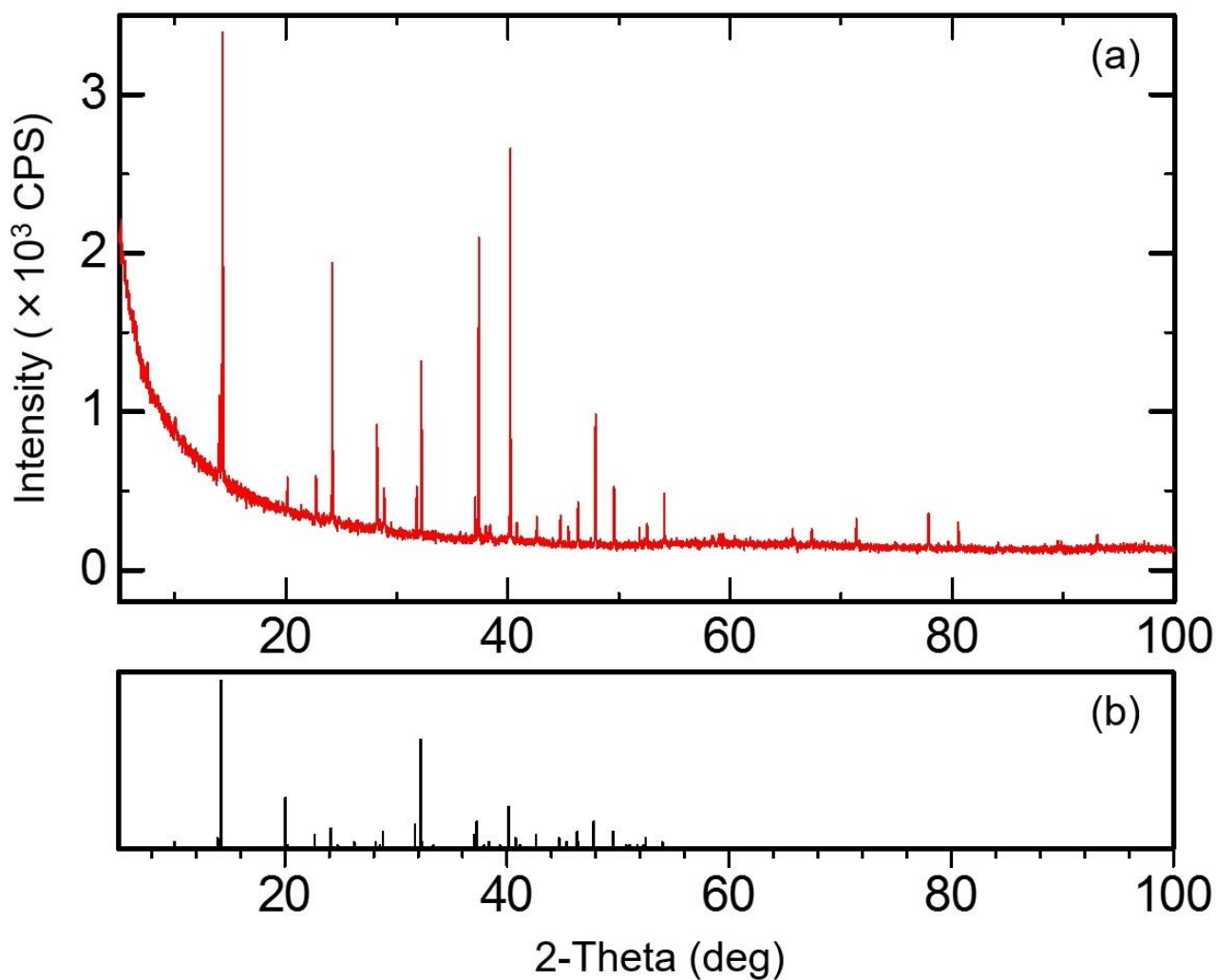


Figure 7.3.1 The powder XRD pattern of (a) the collected particulate material and (b) calcium oxalate dehydrate from a database (JCPDS, 17-0541).

To analyze the structure in detail, the background was subtracted and a Rietveld refinement was performed. The red line in Figure 7.3.2 (a) represents an observed XRD spectrum after subtraction of the background. Crystal structure data obtained from the joint committee on powder diffraction standards (JCPDS) database were subjected to Rietveld refinement using EXPO2014. Table 7.3.1 lists the crystal parameters for the particulates, and the blue line in Figure 7.3.2 (a) represents the calculated pattern for COD resulting from Rietveld refinement of the crystal diffraction data.

In general, calcium monohydrate (COM) is the predominant type of crystal formed in urine. COD dissolves and recrystallizes as COM within 24 hours.³⁾ Injection of a calcium chloride solution in the concentration range of 1 to 3 mol/L into a 250-mL sodium oxalate solution at pH 9 with concentrations varying between 0.01 and 0.1 M results in immediate precipitate formation.

The precipitate in homogenous samples contains thermodynamically stable COM. Enrichment of the thermodynamically unstable COD crystals is favored when the system is kept far from equilibrium due to concentration gradients.⁴⁾ These factors explain the formation of COD crystals rather than COM in this study.

Generation primarily of COD was reported following the injection of a contaminant such as tea extract, which is mainly composed of catechins.⁴⁾ It is possible that some contaminants could have played a role in the generation of primarily COD crystals in the present study, as several residuals observed in the XRD spectra (green line in Figure 7.3.2 (b)) have not yet been identified.

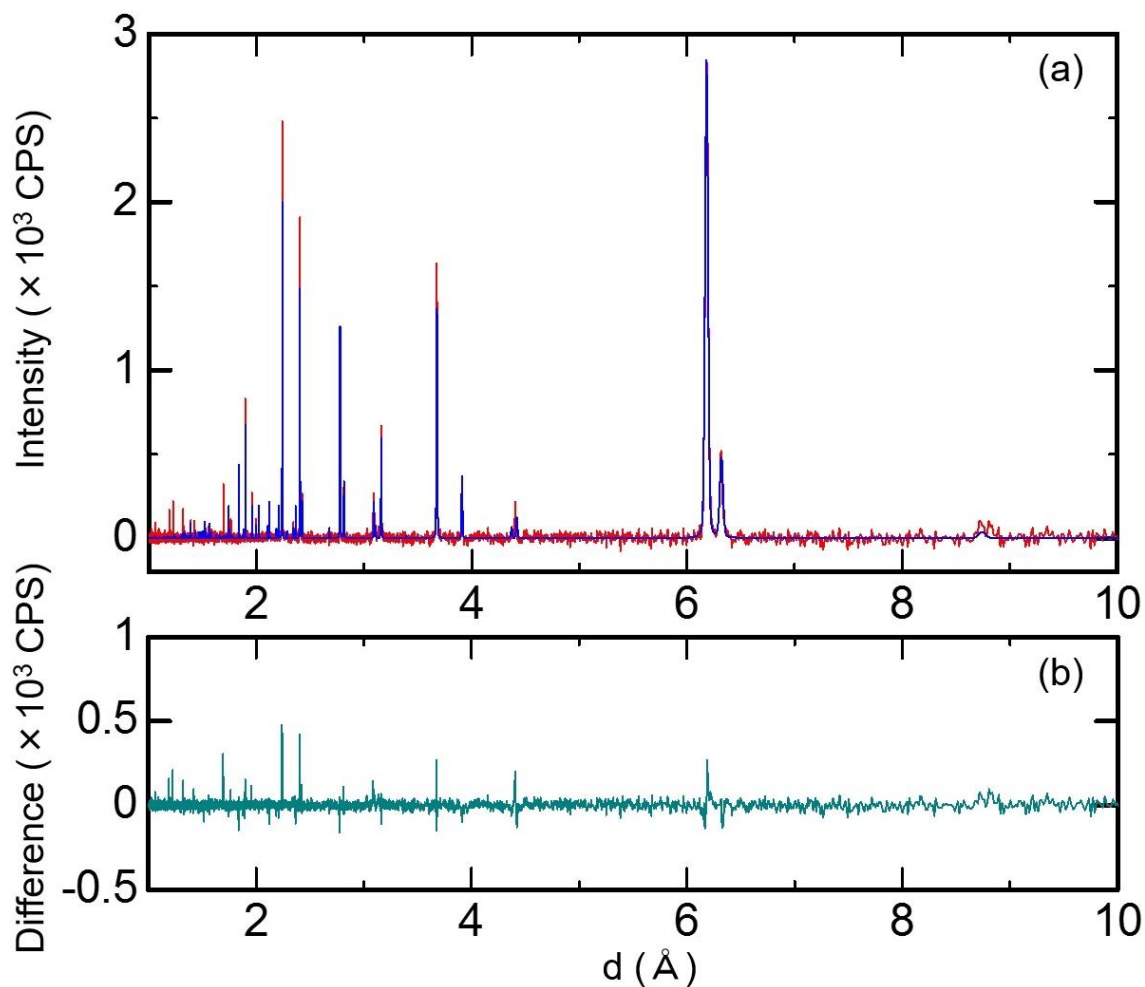


Figure 7.3.2 (a) Powder XRD pattern of collected particles (red line) and calculated pattern of calcium oxalate dihydrate after Rietveld refinement (blue line). (b) Difference pattern (green line). The background and $\text{Cu } K\alpha_2$ contributions have been subtracted.

Table 7.3.1 Results of Rietveld refinement and reliability estimates for the particulate material.

Phase	$\text{CaC}_2\text{O}_4 \cdot (2+x)\text{H}_2\text{O}$ ($x \leq 0.5$) (calcium oxalate dihydrate)
Crystal system	Tetragonal
Space group	I 4/m
Unit cell dimensions	$a=b=12.364(5) \text{ \AA}$, $c=7.353(0) \text{ \AA}$, $\alpha=\beta=\gamma=90.00(0)$
Cell volume	$1124.14(9) \text{ \AA}^3$
Density	3.14 g/cm^3
χ^2	1.849
S	1.360
R_e	5.871
R_{wp}	7.982

It can be found similarity with urinary stone formation. A crystallization in liquid is also observed in the half-way of the urinary stone generation process. In addition, the crystal was composed of calcium oxalate, which is mainly consisted in urinary stones.

Urinary stones are composed primarily of crystals of calcium salts (i.e., approximately 80% calcium oxalate or phosphate). Research conducted to date suggests that urinary stones are generated as follows: (1) the salt components become supersaturated in the urine, (2) crystallization occurs, (3) the crystals grow in size, and (4) the crystals form a concretion with non-crystalline matrix.

In this process, calcium ions, oxalate ions, and urea are required, as opposed to citric acid, magnesium, or pyrophosphate. Indeed, urolithiasis patients exhibit high levels of calcium and oxalate ions in their urine in comparison with healthy subjects.⁵⁾

Supersaturation is generally considered the driving force for the nucleation and growth of crystals, primarily due to the difference in chemical potential between the molecules in solution and those in the crystal phase. Thermodynamically, the solution is supersaturated, meaning that nucleation and/or crystal growth are possible.

Concentration distribution diagrams for species containing calcium and oxalate in the pH range 1 to 14 can be generated based on equilibrium calculations.⁶⁾ The medium's pH was maintained at about 8.5 using buffering agents in the present study, even during irradiation and incubation. Both precipitation and complex formation reactions involve the protonation of oxalate ions.⁶⁾

In short, the solubility of calcium oxalate is very low and depends on the pH: $[Ca^{2+}] [C_2O_4] = S([H^+] + K_a)/K_a$, where K_a is the acid dissociation constant of oxalic acid and S is the solubility constant of calcium oxalate.⁷⁾ At pH 8.5, the solubility (mg/mL) of calcium oxalate is less than 0.005,⁸⁾ and oxalic acid is electrolyzed into oxalate ion.⁹⁾

The initial medium contained 1.8×10^{-3} M CaCl_2 , which has a very high solubility of 74.5 (at 20°C) in water. As much as 10.8 μmol of calcium ion was present in the 6 mL of NEAPP-irradiated medium. Assuming that the structure of COD did not contain zeolitic water (i.e., $\text{CaC}_2\text{O}_4 \cdot 2\text{H}_2\text{O}$, which has a density of 3.14 g/cm^3), as listed in Table 7.3.1, approximately 0.16 pmol of calcium ion would be needed to generate one particle with a size of approximately 50 μm . The total number of experimentally generated particulates was typically around 1,000, which is consistent with the 10.8 μmol of calcium ion in the medium.

Calcium oxalate is poorly soluble in water and has a low acidic dissociation constant, pK_a , of 3.75 (at 25°C).¹⁰⁾ Thus, calcium cations and oxalate anions do not readily dissolve in the medium. As shown by the data listed in Table 2.2.1, the initial medium contained no oxalic acid or oxalate. In order to generate calcium oxalate, therefore, oxalic acid or oxalate would have to be synthesized in the medium.

The particulates isolated in this study did not dissolve in typical solvents such as water, ethanol, or dimethyl sulfoxide but dissolved completely in inorganic strong acids such as hydrochloric or nitric acid. These dissolution properties are consistent with calcium oxalate but not with any component of the initial medium.

In the gaseous phase of the plasma, only Ar flowed from the NEAPP source, and the air contained only nitrogen and oxygen. Therefore, no oxalic acid or oxalate could have been synthesized in the gaseous phase. However, NEAPP irradiation produces a variety of reactive oxygen and nitrogen species (RONS), such as superoxide anion,¹¹⁾ nitrous acid, and hydrogen peroxide.

Introduction of RONS into the liquid could result in the synthesis of oxalates from candidate organics in the medium. In addition, the emission of Vacuum UltraViolet

(VUV) from atoms such as $\cdot\text{N}$, $\cdot\text{O}$, and $\cdot\text{H}$ could have contributed to chemical bond breakage. VUV light travels only minimally through atmospheric air due to strong absorption by the air. If VUV was transmitted to the NEAPP irradiated solution surface, for example, water molecules substantially dissociate at O-H bonds to produce OH radicals.

In the study, since the crystals were synthesized in only a case of contacting of the NEAPP plume with the liquid surface, short-lived RONS such as OH radicals or charged particles such as electrons could participate in the promotion of chemical reactions leading to oxalate synthesis.

§ 7.3.2 Analysis of SEM-EDX

SEM-EDX analysis was performed for the powder made by mashing the crystals. An observed image of the mashed crystal by using SEM is shown in Figure 7.3.3. The acceleration voltage was 20 kV and the magnification was $\times 1700$.

The elements contained in the mashed crystal was analyzed by using EDX with the 20 kV of acceleration voltage and 200 s of accumulation period. Figure 7.3.4 shows the intensities of characteristic X-ray as a function of the characteristic X-ray energy. The characteristic X-rays deriving from C ($K\alpha$: 0.277 keV), O ($K\alpha$: 0.525 keV) and Ca ($K\alpha$: 3.69 keV, $K\beta$: 4.012 keV) were observed. Those peaks are corresponding to a calcium oxalate existence analyzed by XPS. In addition, some characteristic X-rays deriving Na ($K\alpha$: 1.041 keV) was also observed. This result indicates a few contaminations, as also shown in Figure 7.3.2 (b), were composed of Na^+ ion and that could come from a sodium component of the medium, such as NaCl, NaH_2PO_4 or NaHCO_3 .

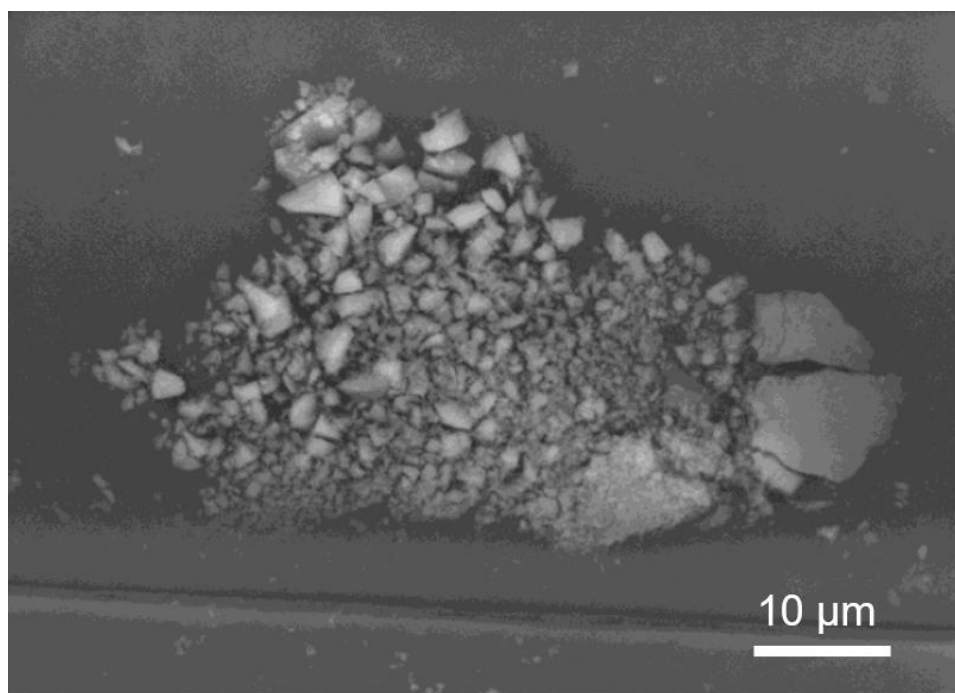


Figure 7.3.3 An observed image of the mashed crystal by using SEM.

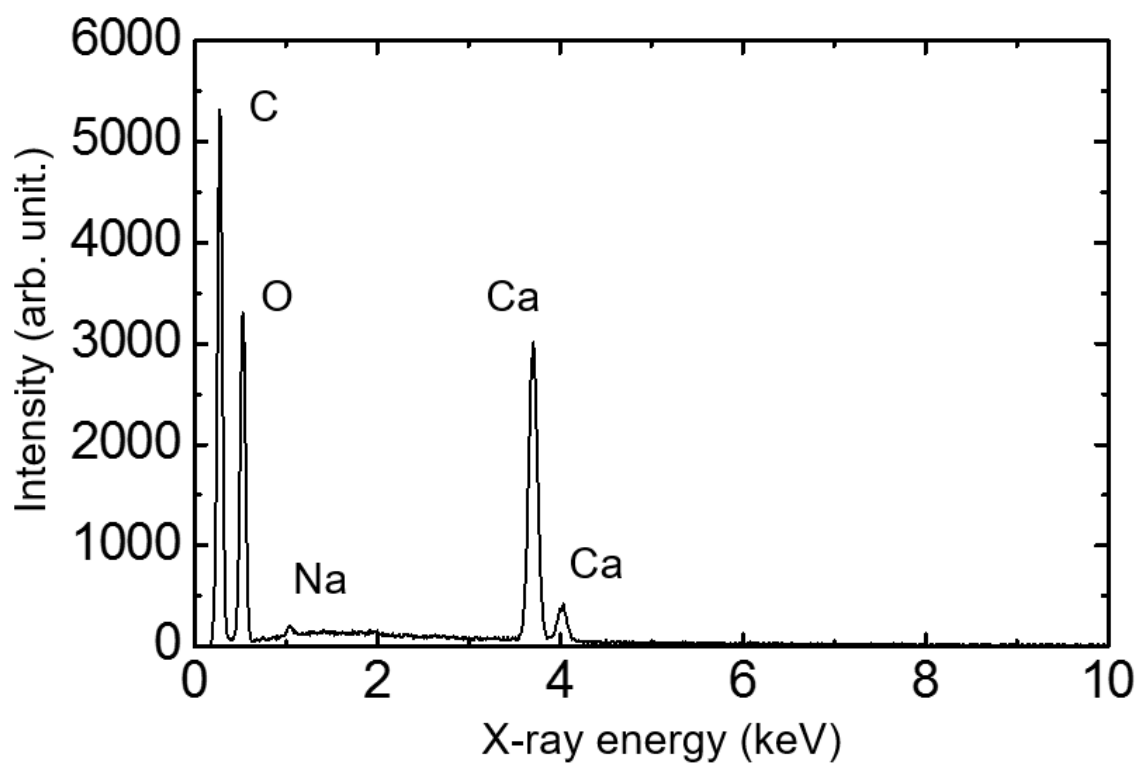


Figure 7.3.4 the intensities of characteristic X-ray from the crystal synthesized by the NEAPP as a function of the characteristic X-ray energy.

§ 7.3.3 Analysis of FT-IR

FT-IR analysis was performed for a pellet made by mixed KBr grains and a powder made by mashing the crystals. Figure 7.3.5 (a) shows the observed FT-IR spectrum. An absorbance of the vibration of a C=O binding (1647 cm^{-1}) was observed. In addition, IR absorbance characteristic of oxalates (1647 cm^{-1} , 1327 cm^{-1}), which is also observed in a standard spectrum of calcium oxalate with KBr solidifying shown in Figure 7.3.5 (b),¹²⁾ were also observed. Those results are corresponding to the result of XRD and an evidence of composing of oxalate.

A broad absorbance of the vibration of O-H binding ($4000\text{-}3400\text{ cm}^{-1}$) was also observed. The absorbance could derive from hydrated water consisted in the crystal and the result is corresponding to the crystal identification as dehydrate by the XRD analysis.

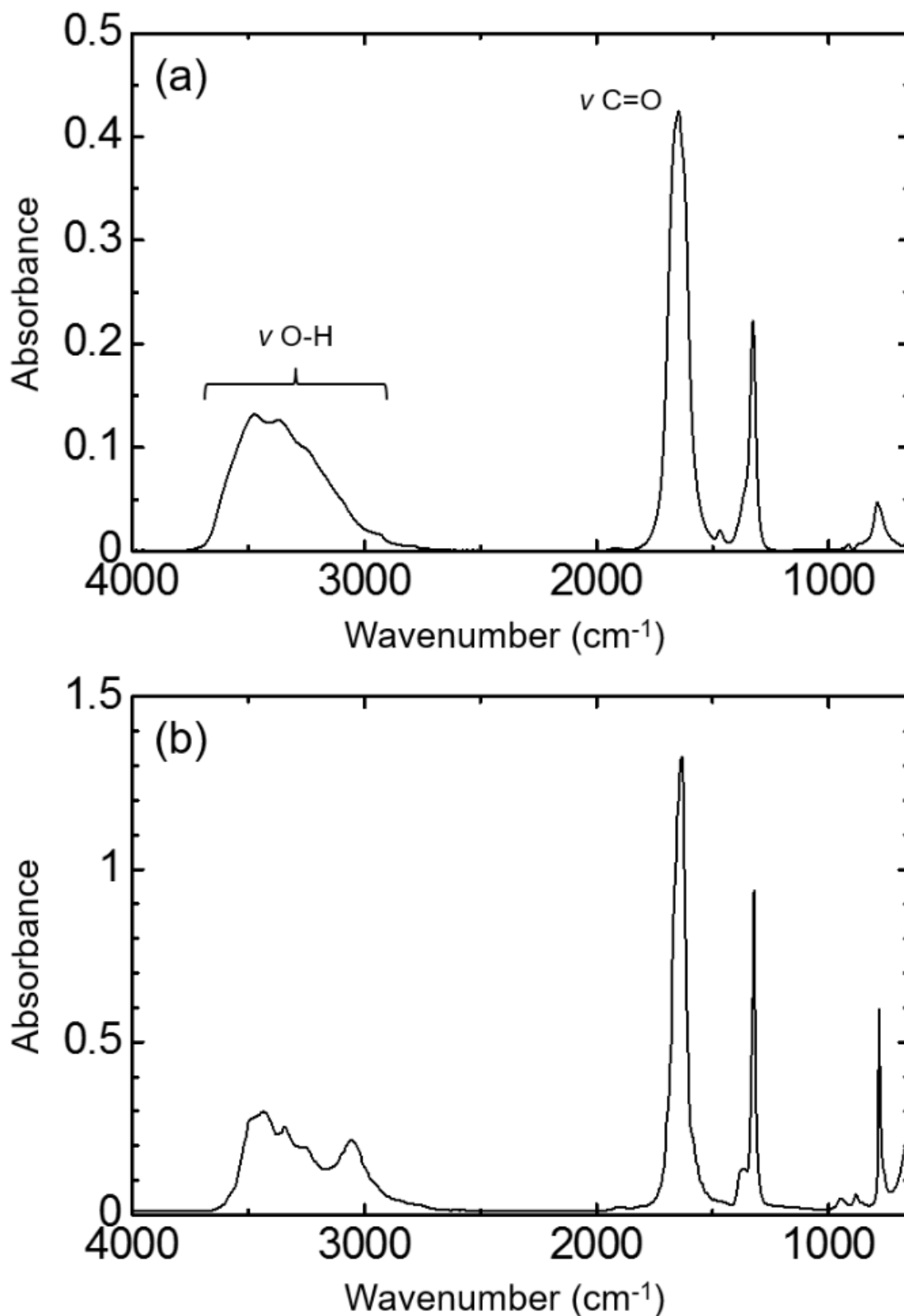


Figure 7.3.5 (a) FT-IR spectrum of the crystals synthesized by the NEAPP and (b) a standard FT-IR spectrum of calcium oxalate with KBr solidifying.

§ 7.4 Dynamics of the crystal growth

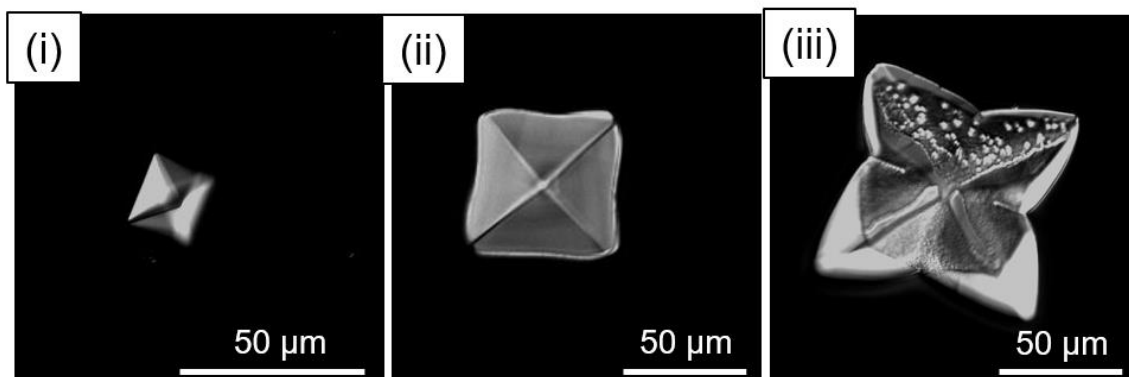
As described in §7.2, calcium oxalate crystals were synthesized in the medium irradiated with the NEAPP and the study may establish a new synthesis process of oxalic acid. For evaluating the productivity, the author measured the synthesis dynamics of the crystals over time.

After the NEAPP irradiation and 24 h incubation, crystalline shaped precipitates were synthesized in the solutions as shown in Figure 7.4.1 (a). By more than 120 s of the NEAPP irradiation, the crystal was synthesized and grown.

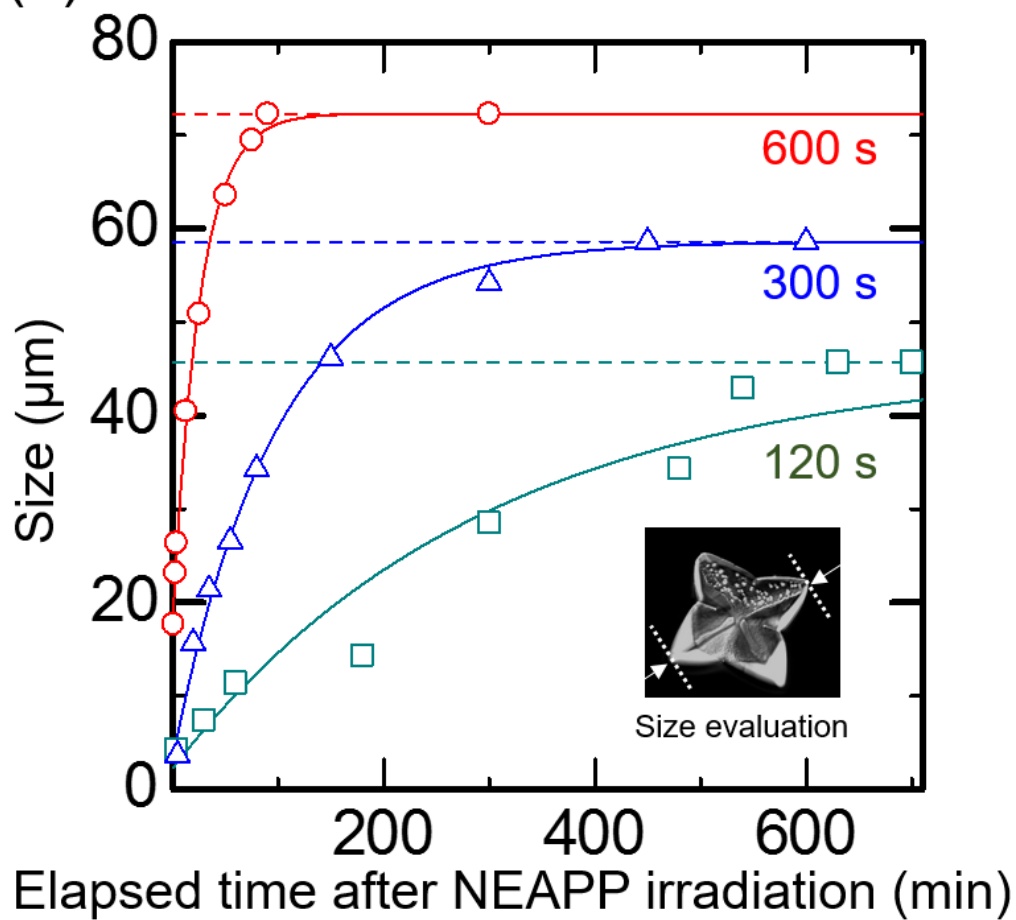
Figure 7.4.1 (b) shows the size of crystals synthesized in the medium irradiated with the NEAPP for 120 to 600 s as a function of elapsed time after the NEAPP irradiation. Approximate curves and saturation sizes of those crystals were also indicated by solid and dashed line. Bigger crystals were synthesized by longer time of NEAPP irradiation.

Figure 7.4.1 (c) shows the number of crystals was also increased by longer time of NEAPP irradiation. This result indicates the number of seed crystals was increased by the NEAPP. Therefore, the crystal synthesis was certainly occurred by the NEAPP irradiation and the NEAPP enhance the synthesis of crystal material and seed crystal.

(a)



(b)



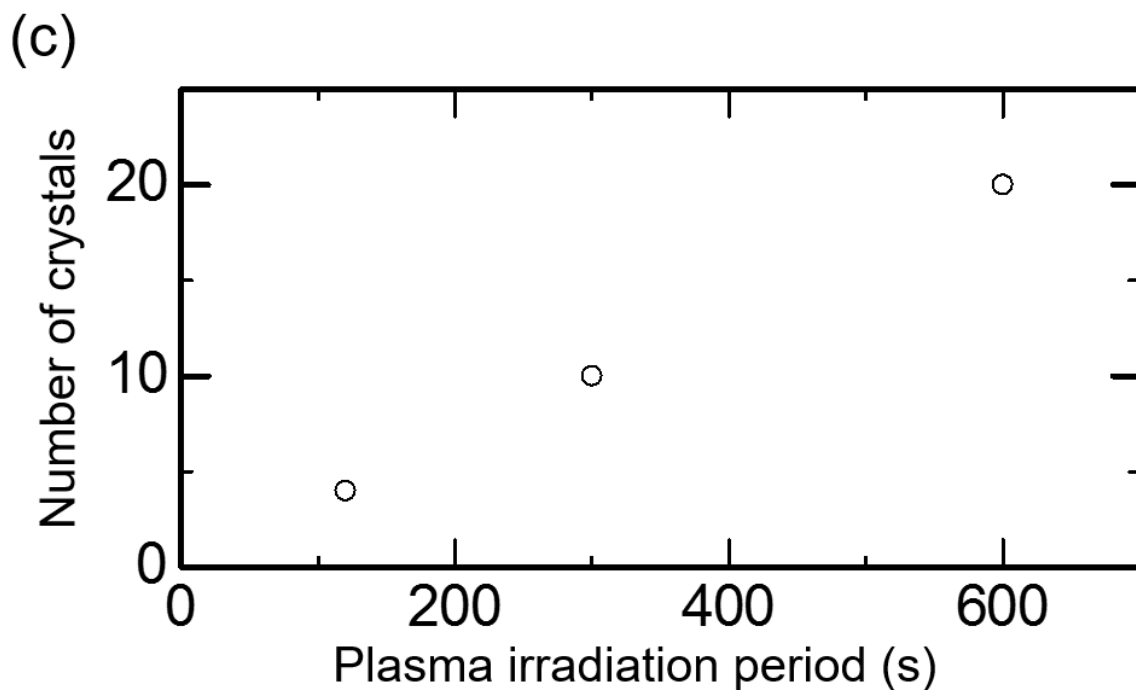


Figure 7.4.1 (a) morphologies of (i) 120 s, (ii) 300 s or (iii) 600 s irradiated samples after 24 h of incubation. (b) Size of crystals synthesized in the medium irradiated with the NEAPP for 120 s (square dots), 300 s (triangle dots) or 600 s (circle dots) or as a function of elapsed time after the NEAPP irradiation, those approximate curves (solid line) and saturation sizes (dashed line). (c) Numbers of crystals in a microscope sight after 24 h of incubation.

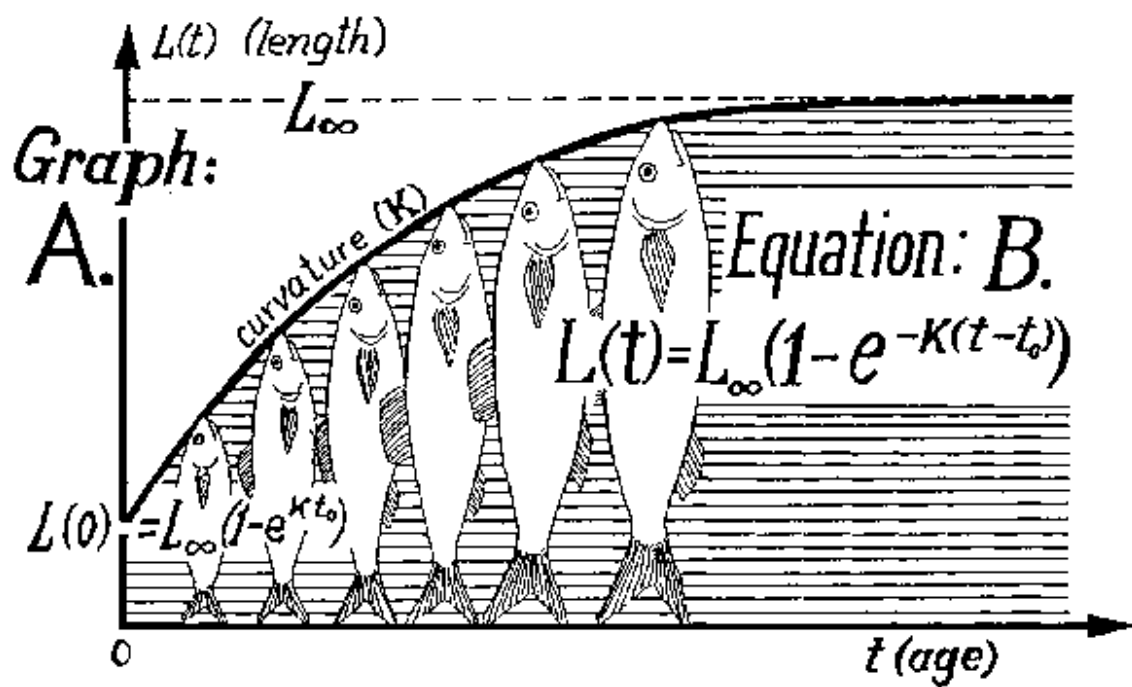


Figure 7.4.2 Conceptual scheme of von Bertalanffy model using in fisheries studies.¹³⁾

Finally, the author proposed the model for growth rate of crystals. The grown rate of the crystal size shown in Figure 7.4.1 (b) fitted well for the *von Bertalanffy* model, which is the most widely used growth curve and is especially important in fisheries studies shown in Figure 7.4.2.¹³⁾ The equation is $L_t = L_\infty(1-\exp(-K(t-t_0)))$, where L_∞ is a saturated size and K is a time constant.

By fitting for the *von Bertalanffy* model, K were 0.00336 (120 s), 0.0103 (300 s) and 0.0393 (600 s). Since the time constant was increased with increasing the irradiation time, some driving force of crystallization might be occurred by the NEAPP irradiation. Actually, Figure 7.4.1 (a) shows the crystal morphology differed by the irradiation time as (i) polyhedron, (ii) skeleton crystal and (iii) dendrite like. This morphological change is one of the evidence of driving force increasing.¹⁴⁾ The polyhedral form was obtained in near the equilibrium state. The macroscopic shape of the polyhedrons reflects the symmetry and the arrangement of the microscopic molecular lattice.¹⁴⁾ On the other hand, as the driving force increases, the growth rate is governed by heat transfer or mass diffusion, and then, the growing surface of the crystal becomes unstable in a diffusion field.¹⁴⁾ Because of the surface instability, it is considered that spikes or steps were generated on the surface of crystals and skeleton or dendrite like form were appeared.

Figure 7.4.3 shows a crystal morphologies synthesized in a medium after 300 s of NEAPP irradiation as a function of elapsed time after the NEAPP irradiation. The crystal shape was decided in the early stage of a crystal growth and grown with maintaining the shape. The result indicates that the increased driving force by the NEAPP was also maintained even after the NEAPP irradiation. Above the all, the NEAPP irradiation enhanced both seed crystals synthesis and the growth driving force.

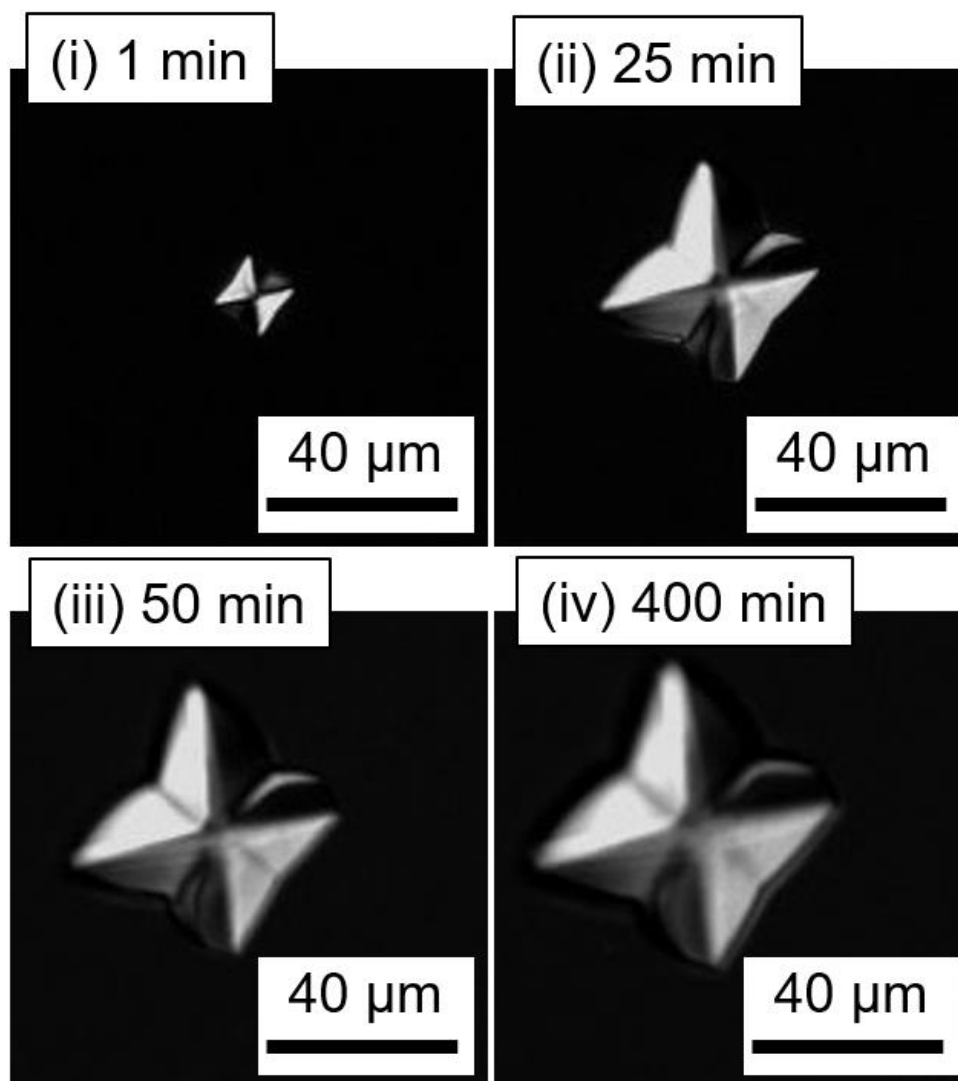


Figure 7.4.3 A crystal morphologies synthesized in a medium after 300 s of NEAPP irradiation as a function of elapsed time after the NEAPP irradiation.

§ 7.5 Summary

The irradiation of DMEM by contact with an NEAPP plume at a high electron density (on the order of 10^{16} cm^{-3}) resulted in the generation of particulates in the medium after incubation for 24 hours. The particulates were composed of octahedral crystals several tens of microns in size and primarily composed of COD. It is worth noting that NEAPP-induced synthesis of these oxalate crystals occurred in culture medium containing no oxalic acid or oxalate. Moreover, the NEAPP irradiation enhanced seed crystals synthesis and the growth driving force. The efficient calcium oxalate crystals synthesis process will contribute to establish fast and simple oxalic acid synthesis method.

References for Chapter 7

- 1) Sigma-Aldrich, (<http://www.sigmaaldrich.com/content/dam/sigmaaldrich/docs/Sigma/Formulation/d5796for.pdf>).
- 2) M.T.D. Orlando, L. Kuplich, D.O. de Souza, H. Belich, J.B. Depianti, C.G.P. Orlando, E.F. Medeiros, and P.C.M. da Cruz, L.G. Martinez, H.P.S. Corrêa, and R. Ortiz, *Powder Diffraction Suppl.* **23**, S59-S64 (2008).
- 3) M.A. Thrall, S.M. Dial, and D.R. Winder, *Vet. Pathol.* **22**, 625-628 (1985).
- 4) B. Bohner, G. Schuszter, O. Berkesi, D. Horvath, and A. Toth, *Chem. Commun.* **50**, 4289 (2014).
- 5) M. Daudon, R. Donsimoni, C. Hennequin, S. Fellahi, G.L. Moel, M. Paris, S. Troupel, and B. Lacour, *Urol. Res.* **23**, 319-326 (1995).
- 6) Z. Chen, C. Wang, H. Zhou, L. Sang, and X. Li, *Crys. Eng. Comm.* **12**, 845-852 (2010).
- 7) W. H. McComas, Jr, and W. Rieman III, *J. Am. Soc. Chem.* **64**, 2948 (1942).
- 8) S.L. Goss, K.A. Lemons, J.E. Kerstetter, and R.H. Bogner, *J. Pharm. Pharmacol.* **59**, 1485-1492 (2007).
- 9) M. Iwasaki, H. Inui, Y. Matsudaira, H. Kano, N. Yoshida, M. Ito, and M. Hori, *J. Appl. Phys.* **92**, 081503 (2008).
- 10) R. J. Ferguson, *Corrosion.* **399**, 1-9 (2002).
- 11) A. Tani, Y. Ono, S. Fukui, S. Ikawa, and K. Kitano, *Appl. Phys. Lett.* **100**, 254103 (2012).
- 12) The coblenz society, “*Coblentz Society Infrared Spectral Collection*”. **65**, (2009).
- 13) P. Sparre, and S.C. Venema, *FAO Fisheries Technical Paper.* **306**, 47-114 (1998).

- 14) H. Imai, Y. Oaki, and A. Kotachi, *Bull. Chem. Soc. Jpn.* **79**, 1834-1851 (2006).

Chapter 8

Essential components of the oxalate crystal synthesis by the NEAPP

§ 8.1 Introduction

A study about a useful calcium oxalate crystal synthesis method is described in Chapter 7. However, in the study, the calcium oxalate crystal synthesis was performed by the NEAPP irradiation to the DMEM, which is a cell culture medium composed of 32 organic and inorganic components as listed in Table 2.2.1 and it is considered that not all those components contribute for the oxalic acid crystal synthesis.

In this Chapter 8, the essential components for the crystal synthesis were elucidated by a screening method. The roles of those species were also elucidated and the model of the NEAPP induced crystal synthesis with minimum essentials was proposed.

§ 8.2 Screening of essential components for the crystal synthesis

For more efficient of the crystal synthesis and to controlling the synthesis, the elucidation of the mechanism of crystal synthesis is very important.

For the first approach to elucidate the mechanism, the author sifted minimum essentials from the solution as a necessary of the crystallization. First, components of the medium is classified to 4 parts, which are 7 organics, 1 saccharide, 15 amino acids, 8 vitamins and phenol red·Na.

In considering those concentrations in the medium, several grams per liter glucose and some organics were contained in the medium however less than several hundred milligrams per liter of amino acids and several milligrams per liter of vitamins contained in the medium.

Since the relative big and many crystals were synthesized, it was considered that the much essential components were also composed in the medium, like glucose and some organics. Therefore, the author tried that a solution composed of the 7 organics and the glucose was irradiated with the NEAPP and octahedral crystals synthesis was confirmed by a microscope after 24 h of incubation.

Next, the author tried the screening of the organic components by observing the NEAPP irradiated solution composed of the glucose and each organics after an incubation. However no crystals were observed in solutions composed of glucose and each 1 or 2 kinds of those organics, the octahedral crystals were synthesized in a solution composed of glucose, NaHCO₃ and CaCl₂.

Figure 8.2.1 shows crystals observed after 24 h in the solution composed of those 3 species irradiated with the NEAPP. Crystals which have very similar shape and size were observed in the bottom of the solution. Contrary to the results, no crystal was synthesized in a solution composed of any other 3 kinds of species. Those results indicated the minimum essential components are glucose, NaHCO_3 and CaCl_2 .

From the above screening, the author found candidates of those 3 kinds of species. The roles of those essential components were also examined in the next session.

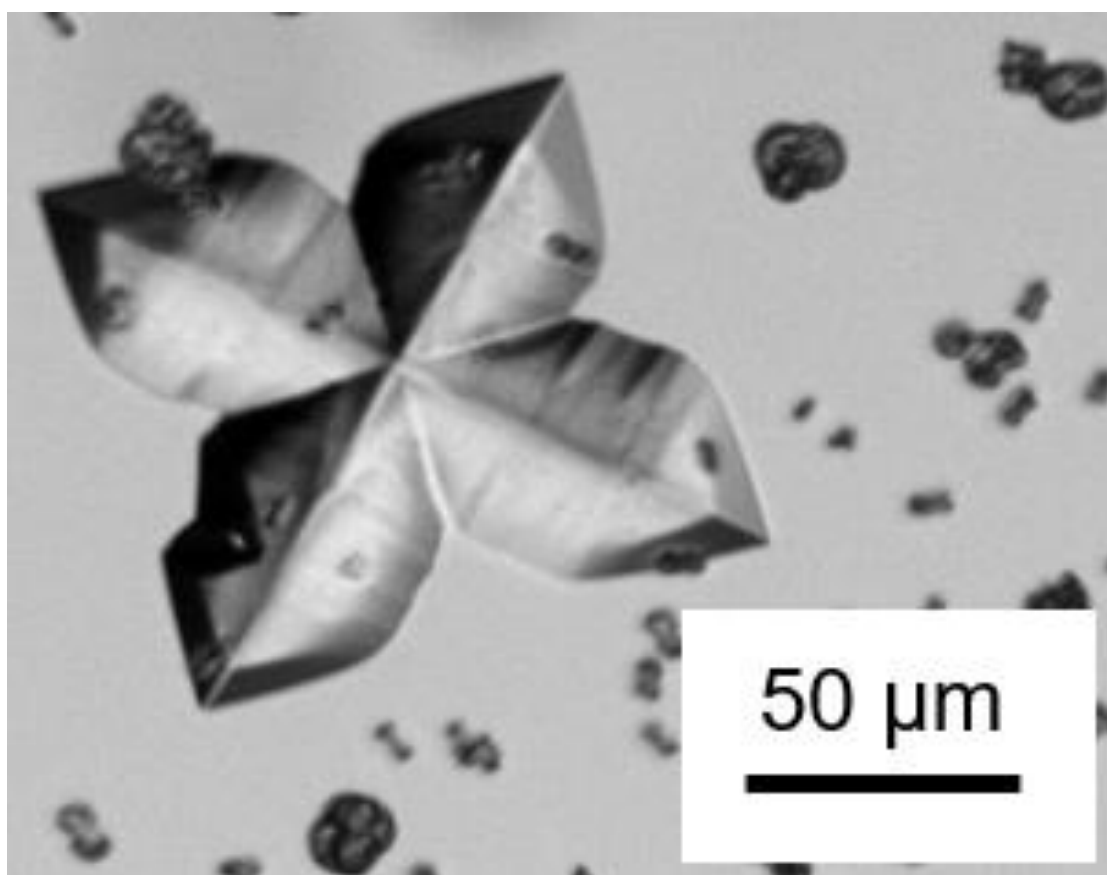


Figure 8.2.1 Morphology of the crystals synthesized during 24 h incubation of a solution composed of glucose, CaCl_2 and NaHCO_3 irradiated for 10 min with the NEAPP.

§ 8.3 Roles of essential components for the crystal synthesis

§ 8.3.1 Glucose

To investigate the role of glucose, a glucose solution irradiated with the NEAPP was analyzed by GC-MS method. Figure 8.3.1 (a) shows GC spectrum of the NEAPP irradiated the glucose solution, the glucose solution without the NEAPP irradiation and only the derivatization reagent as a background of the measurement.

A peak of the GC analysis, which indicated one of separated components of the NEAPP irradiated solution, was obtained at the retention time of 7.889. Broad peaks obtained at around 7.83 and 8.00 of retention time were identified as the background since same peaks also shown in similar retention time of the only derivatization reagent consisted solution.

Figure 8.3.1 (b) shows the MS spectrum at the retention time of 7.889. The obtained MS spectrum fitted well to a standard spectrum of Oxalic acid, bis(trimethylsilyl) ester (NIST MS# 352455), which is a result of MS analysis of a glucose solution derivatized by the same reagent used in the study, shown in Figure 8.3.1 (c).

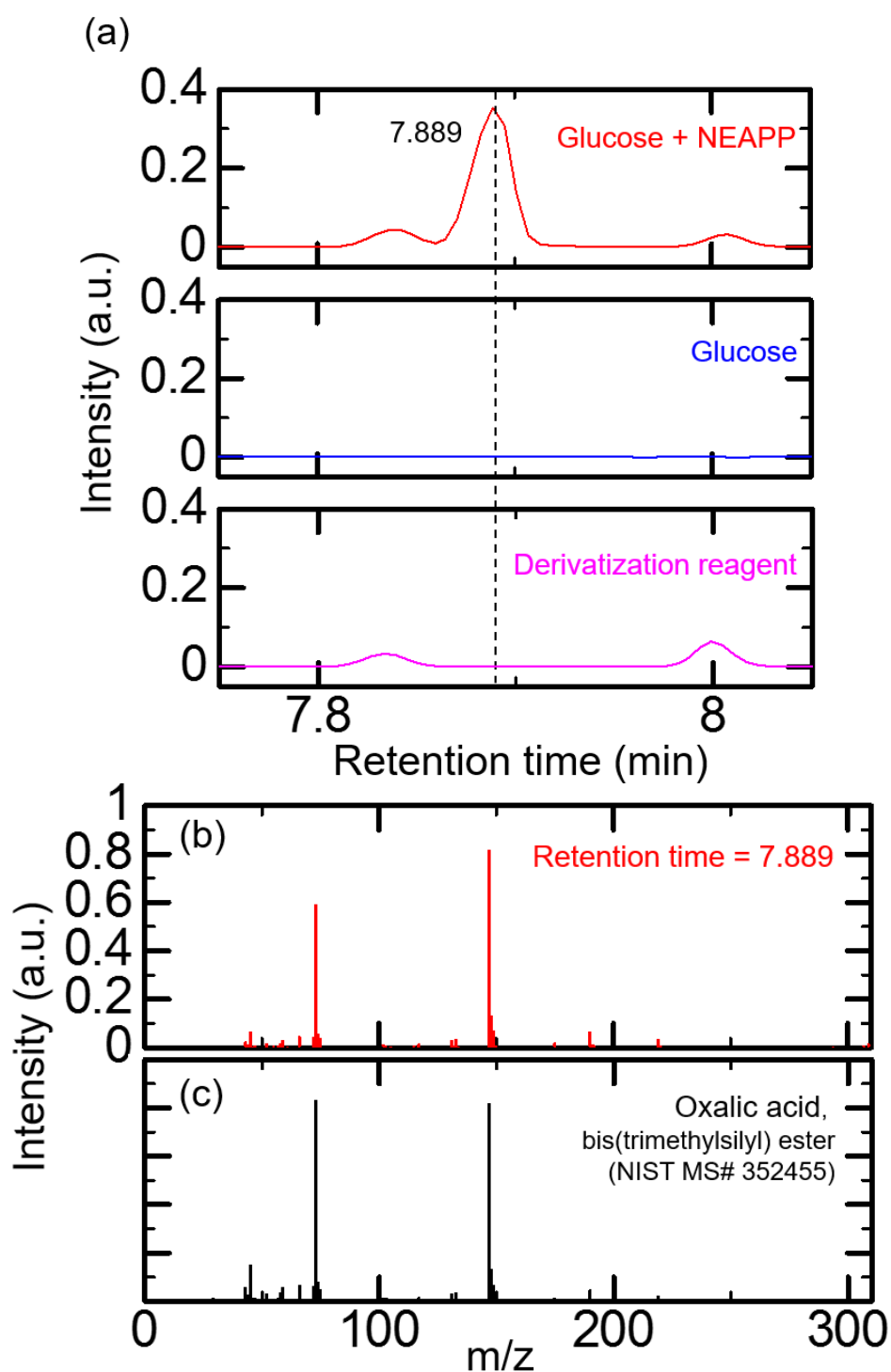


Figure 8.3.1 (a) The result of GC spectrum of the NEAPP irradiated glucose solution, the glucose solution without the NEAPP irradiation and only the derivatization reagent as a background, (b) the result of MS spectrum at 7.889 min of retention time of the NEAPP irradiated glucose solution, and (c) standard spectrum of Oxalic acid, bis(trimethylsilyl) ester (NIST MS# 352455).

Those results indicated that oxalic acid was synthesized from glucose by irradiation of the NEAPP and the oxalic acid could be a source reagent of calcium oxalate crystals.

In addition, gluconic acid was also observed in the solution by the GC-MS analysis. Gluconic acid is synthesized by oxidation of glucose using a catalyst such as gold particles,¹⁾ or biochemical synthesis of *Aspergillus niger*.²⁾ An oxidation effect of NEAPP might contribute to the synthesis.

Table 8.3.1 shows organic compounds detected by the measurement in the PAM and the NEAPP irradiated glucose solution. Glucose mainly played a role of the material of organic synthesis in the PAM since all of organic compounds synthesized in the PAM were also detected in the NEAPP irradiated glucose solution.

Therefore gluconic acid was also synthesized by the NEAPP irradiation, oxalic acid synthesis reaction from gluconic acid was estimated as a characteristic reaction of NEAPP. Since the crystals were synthesized only direct irradiation, reactive species existing in the NEAPP plume such as high energy electrons could contribute the synthesis. Therefore, this result indicates oxidation of the aldehyde group of glucose and oxalic acid synthesis reaction via gluconic acid was estimated as $C_6H_{12}O_6$ (glucose) + O \rightarrow $C_6H_{12}O_7$ (gluconic acid); $C_6H_{12}O_7$ (gluconic acid) + e (energetic) \rightarrow R + (COOH)₂.

Table 8.3.1 Organic compounds detected by the measurement in the PAM and the NEAPP irradiated glucose solution.

Compound name	Synthesis by the NEAPP irradiation	
	Medium	Glucose solution
<i>Oxalic acid</i>	Overlap ^a	yes
<i>Propanoic acid</i>	yes	yes
<i>Acetic acid</i>	yes	yes
<i>Propanoic acid</i>	yes	yes
<i>Threonic acid</i>	Overlap ^a	yes
<i>Tartaric acid</i>	yes	yes
<i>D-gluconic acid</i>	yes	yes
<i>Glucose</i>	yes	yes

^a Didn't detected because of Overlapping with other peaks

§ 8.3.2 Calcium chloride (CaCl₂)

Since the main crystal component was elucidated as calcium oxalate dehydrate, the calcium part of CaCl₂ seemed to be essential for the crystal synthesis and the author elucidated it.

To investigate the role of CaCl₂, solution composed of Ca(NO₃)₂ instead of CaCl₂ or minimum essentials except of CaCl₂ were irradiated with the NEAPP and then incubated for 24 h. Table 8.3.2 lists the elucidation result, which shows the pH of the solution after the NEAPP irradiation and the crystal synthesis occurred or not.

Crystals were also synthesized in the Ca(NO₃)₂ added solution, contrary to that no crystals were observed in the solution without any calcium salt addition. Those results indicate a calcium salt existence is necessary for the crystal synthesis by the NEAPP and CaCl₂ have been contributed to the crystal synthesis as calcium salt which works as a calcium ion provider.

Table 8.3.2. Dependence of the pH and the crystal synthesis on the solution components.

saccharide	Components		pH	Crystal synthesis
	pH buffer	Ca source		
glucose	NaHCO ₃	CaCl ₂	Neutral	yes
glucose	NaHCO ₃	Ca(NO ₃) ₂	Neutral	yes
glucose	NaHCO ₃	–	Neutral	no
glucose	HEPES (a neutral buffer)	CaCl ₂	Neutral	yes
glucose	–	CaCl ₂	Acid	no

§ 8.3.3 Sodium hydrogen carbonate (NaHCO_3)

Then, the author focused on the pH of the solution because all samples investigated above have almost neutral pH values. Empirically, pH value of a solution irradiated NEAPPs is lowered since some acids, may be mainly composed of nitric acid and nitrous acid generated from mixed N_2 in the ambient air. Since NaHCO_3 solution indicates basicity, the acid solution could be neutralized by the NaHCO_3 existence.

To investigate the role of NaHCO_3 , solution composed of a neutral buffer (HEPES) instead of NaHCO_3 or minimum essentials except of NaHCO_3 were irradiated with the NEAPP and then incubated for 24 h. the pH of solution was neutralized by NaHCO_3 or HEPES addition and crystals were synthesized in those solutions as shown in Table 8.3.1.

Those results indicate NaHCO_3 plays a role of neutralization of the pH to about 6 to 8 and supporting the crystal synthesis.

§ 8.4 Summary

From the elucidations in the Chapter 8, the mechanism of the crystal synthesis is described as shown in Figure 8.4.1.

Namely, it was discovered that the calcium oxalate crystals were synthesized in a solution composed of glucose, some neutral buffer and calcium ion irradiated with the NEAPP. Those components played a role of material and pH neutralizing.

Consequently, the synthesis of calcium oxalate crystals in a medium which is irradiated with the NEAPP was investigated. The minimum essentials for the crystal synthesis were detected as glucose, NaHCO_3 and CaCl_2 from over 30 species of medium components. In addition, those roles on the crystal synthesis were also investigated and a model of synthesis was established.

This study contribute for a new way of oxalic acid synthesis and this method may replace conventional methods, which take relatively long time and high cost. This study elucidated the NEAPP synthesis of organic; that is, oxalic acid synthesis from glucose.

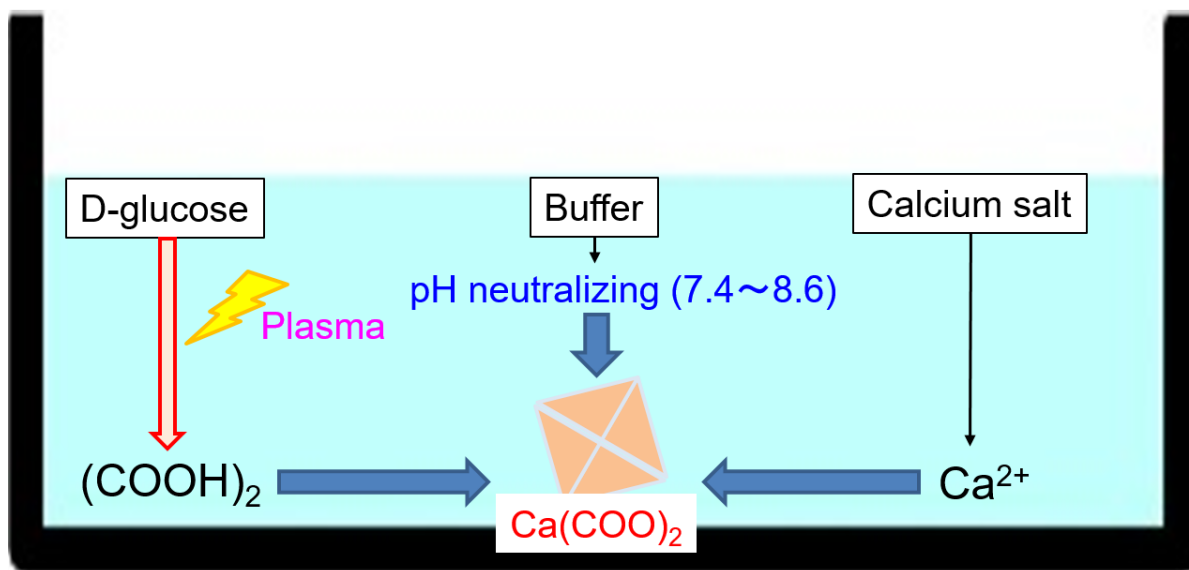


Figure 8.4.1 Model of the mechanism of calcium oxalate crystal synthesis in the solution composed of glucose and other minimum essential components.

References for Chapter 8

- 1) Y. Onal, S. Schimpf, and P. Claus, *Journal of Catalysis*. **223**, 122-133 (2004).
- 2) H. Znad, J. Markos, and V. Bales, *Process Biochemistry*. **39**, 1341-1345 (2004).

Chapter 9

Conclusions

§ 9.1 Summary of this thesis

NEAPP induces various useful reactions by reactive species generation. However, the mechanism has been not elucidated yet. The author tried to elucidate the mechanisms on major two types of applications, namely, indirect and direct NEAPP applications, which are a cancer therapy and an oxalic acid synthesis.

In the cancer therapy, plasma activated medium (PAM), which is a plasma irradiated cell culture medium, has shown a selective antitumor effect for cancer cells against normal cells. However, the mechanism is unclear.

Long-lived species, remaining in the PAM after the NEAPP irradiation, could be the antitumor species of the PAM, which are long-lived RONS and organic reactive species. In addition, Short-lived RONS, which play a role of a precursor of long-lived species, are also important for understanding

In Chapter 3, RONS concentrations were measured in the NEAPP irradiated medium at the beginning of the thesis. Short-lived RONS, which are $\cdot\text{OH}$, $\cdot\text{H}$, $\cdot\text{NO}$ and $\cdot\text{O}_2^-$, were measured and only $\cdot\text{OH}$ and $\cdot\text{H}$ were detected. $\cdot\text{OH}$ and $\cdot\text{H}$ could be generated by a water decomposition. Neither $\cdot\text{NO}$ and $\cdot\text{O}_2^-$ were detected because of the poor solubility and the weak acid pH value. Long-lived RONS, which are H_2O_2 , NO_2^- and

NO_3^- were quantitatively measured. H_2O_2 and NO_2^- were generated proportionally to the NEAPP irradiation period so that those species certainly generated by the NEAPP irradiation. Compared with NEAPP sources previously reported, NO_2^- concentration is relative high characteristically. The result is an evidence that the NEAPP source mixing the air, well. Reactive organic species, such as organic acid, were not detected in the PAM made with the remote NEAPP irradiation. On the other hand, in the case of attaching the NEAPP plume to the medium surface, some organic acids were observed. Therefore, organic species could be neglected in discussing the PAM.

In Chapter 4, the synthesis mechanism of H_2O_2 and NO_2^- , which are generated proportionally to the NEAPP irradiation period, were discussed by considering short-lived RONS, which are a precursor of long-lived RONS. Especially, $\cdot\text{OH}$ is a precursor of H_2O_2 and $\cdot\text{NO}$ is a precursor of NO_2^- . In the H_2O_2 analysis, however $\cdot\text{OH}$ was generated in the medium by a water decomposition reaction, no H_2O_2 was generated in the medium only by the light irradiation from the NEAPP. Therefore, the light-generated $\cdot\text{OH}$ reacted with other components such as organic components of the medium and gaseous reactions could mainly generate H_2O_2 . Namely, a reaction of gaseous oxygen atoms with water in the medium surface, which is $\text{H}_2\text{O} + \cdot\text{O}({}^3\text{P}) \rightarrow \text{H}_2\text{O}_2$, or a dissolving of H_2O_2 generated in the NEAPP region, where exists a large amount of $\cdot\text{OH}$, with an $\cdot\text{OH}$ recombination reaction of $2\cdot\text{OH} \rightarrow \text{H}_2\text{O}_2$.

In the NO_2^- analysis, no $\cdot\text{NO}$ was dissolved to the medium unless $\cdot\text{NO}$ was exist in the gaseous phase. One of a cause is estimated as the low solubility of $\cdot\text{NO}$ and a gaseous generation of NO_2^- was also indicated. Gaseous $\cdot\text{NO}$ could react with gaseous $\cdot\text{OH}$ with a reaction of $\cdot\text{NO} + \cdot\text{OH} \rightarrow \text{HNO}_2$. After that the HNO_2 was dissolved to the medium and NO_2^- was generated by an ionization.

In Chapter 5, the contributions of the long-lived RONS for the antitumor effect of the PAM were elucidated. The selectivity of the antitumor effect of the PAM was appeared in the cell line and intracellular RONS were detected in dead cells incubated with PAM and H₂O₂ and NO₂⁻ added medium. Therefore, the intracellular RONS was likely to come from surroundings of cells and RONS could contribute for the antitumor effect of the PAM.

In the analysis of H₂O₂, some decreasing of cancer cell survivals was appeared similarly to previous report. In the analysis of NO₃⁻, neither individual nor synergistic effect was detected. In the analysis of NO₂⁻, however no antitumor effect was induced individually, surprisingly, the cell survival decreasing of H₂O₂ was enhanced by NO₂⁻ existence. The result indicates synergistic antitumor effect of H₂O₂ and NO₂⁻. However, since the PAM shows more antitumor effect than that of medium with H₂O₂ and NO₂⁻, other antitumor effects were exist in the PAM. H₂O₂ and NO₂⁻ are believed to generate peroxyntirite (ONOOH) which is toxic to cells and is formed by the reaction $\text{H}_2\text{O}_2 + 2\text{NO}_2^- \rightarrow 2\text{ONOOH}$. Since the antitumor effect of the PAM was not repeated by only an addition of RONS, H₂O₂ and NO₂⁻ were likely only mediate factor and a research of the remaining unknown mechanism is important for the characteristic antitumor effect of the PAM.

In Chapter 6, intracellular metabolism of dying cancer cells by incubation with the PAM was analyzed. Metabolomics is preferred to analyze the antitumor effect of the PAM, which affect by several hours, since it has rapid response compared to other omics. The *glycolysis* decreasing occurred by NAD⁺ lack was introduced by the PAM. Therefore, NAMPT and NMNAT, which is a generation enzyme of NAD⁺, might be down-regulated. If the down-regulation was occurred, previously reported AKT kinase down-regulation

could be also induced.¹⁾ However, the downflow from G3P was also induced by GAPDH, which is a kind of protein, so that proteomics analysis was also needed for more clear elucidation of the damming mechanism. As a result of the decreasing, ATP in cancer cells was decreased and the cells were lacking in energy. The synergistic effect of H₂O₂ and NO₂⁻ could contributed to the decreasing since a similar disorder is also occurred by H₂O₂ and NO₂⁻ addition. The energy lack could also contribute to the selectivity of the PAM antitumor effect because the disorder energy generating pathway, *glycolysis*, is the main energy source of cancer cells.

In the oxalic acid synthesis, the author tried to synthesize calcium oxalate crystals in the NEAPP irradiated medium. If the calcium oxalate crystals were obtained, oxalic acid, which has great needs such as ablent for ships or large vehicles, is easily synthesized by mixing with sulfuric acid. Since the calcium oxalate crystal synthesis was tried for the first time, a fundamental knowledge and an understanding of the phenomenon is needed in the beginning.

In Chapter 7, particulates synthesized in the NEAPP irradiated medium were analyzed and those particulates identified as calcium oxalate dehydrate (COD) crystals. Generally, the crystals were certainly synthesized by the NEAPP irradiation, since the size and number of crystals were increased with extending the NEAPP irradiation period. Moreover, the driving force for the crystallization was also enhanced by the NEAPP irradiation. As described in above, the fundamental knowledge of the phenomenon and the dynamics of the crystal synthesis were understood. Since the medium is composed of 32 kinds of species, it is considered that only some of those components were essential for the calcium oxalate crystal synthesis. Therefore, finally, the author tried to identify the essential components for the crystal synthesis.

Chapter 9 Conclusions

In Chapter 8, a screening of the essential components from the medium was performed. Then Glucose, CaCl_2 and NaHCO_3 were successfully identified as the essential components. In the crystal synthesis, glucose played a role of the ingredient of oxalic acid for the organic synthesis by the NEAPP, CaCl_2 is a supplier of calcium ion and NaHCO_3 played a role of pH neutralizing. Consequently, it was elucidated that the calcium oxalate crystals are synthesized by the NEAPP irradiation to a buffer composed of glucose and calcium ion.

In conclusion of the thesis, the author examined reactions on NEAPP treated liquids from 2 aspects, direct and indirect NEAPP irradiations. The mechanisms of the effects of NEAPP irradiated medium were partly elucidated as the synergistic antitumor effect of H_2O_2 and NO_2^- in the PAM. In addition, those aqueous RONS generation model characteristic of the PAM was established. However, some PAM characteristic antitumor effects were still unclear. By an analysis of metabolomes of cancer cells incubated with the PAM, drastic change of the metabolites were appeared. However those change was also appeared by only RONS addition, another reactive species generation by an interaction of RONS and the medium was considered. Moreover, aqueous organic species were also affected by the NEAPP. In direct irradiation, it was found that organic components in the medium was changed to useful industrial organic species by the NEAPP irradiation and the crystallization might be also enhanced. However the mechanism was likely to be contributed by an oxidation power of the NEAPP, more examination is needed for clear elucidation of the organic synthesis by using NEAPP. Consequently, this thesis gives fundamental knowledge of useful effects and a mechanism of generating those factors when a medium irradiated with NEAPPs, which are attracted attentions to apply to various applications. The author believe that the knowledge become

a foundation of next examinations to develop the useful applications using an interaction between NEAPPs and mediums.

§ 9.2 Scope of future works

- *Cancer therapy*

There are many reports about antitumor effects of the PAM for various kinds of cancer cells and mice. In addition, the major parts of antitumor effect of the PAM is elucidated in this study. The next subject for clinical application is coexistence of biocompatibility and antitumor effect of the solution. The NEAPP cancer therapy is greatly processed to a clinical examination by solving the subject because the application proceed to a clinical phase. Side by side with this elucidation, mechanisms of an antitumor species generation should be also elucidated. If the mechanism is completely elucidated, antitumor effects of the NEAPP irradiated solution will be controlled and the applicability will be drastically increased.

1) Measurement of gaseous long-lived RONS

This study is mainly based on measurements of reactions in liquid phase. The author think gaseous long-lived RONS, which are H_2O_2 , NO_2^- and those related species such as NO_3^- or HO_2 , measurement are not enough compared to the short-lived RONS, which could be measured by relatively simple optical spectroscopic methods, such as vacuum ultra violet absorption spectroscopy (VUV-AS) or OES. For example, those gaseous species could be measured by FT-IR. However, it needs some ingenious designs de because of the low concentration.

2) Elucidation of an unclear part of the antitumor effect

As mentioned in Chapter 5, there are some unclear antitumor effects of the

PAM. Some unmeasured RONS, such as ONOO^- , HOCl and so forth, and organic reactive species deriving from organic components of the medium are candidates. For example, long-lived RONS could be measured by chemical probes and organic reactive species could be measured by GC-MS system.

3) Selecting the components of a solution irradiated with the NEAPP for clinical examination

In this study, a medium composed of 32 kinds of species was used as the NEAPP irradiated target solution for an evaluation of cell responses. For applying the medium to body, its components should be limited to several essential components. By preparing a biocompatible solution, more clinical investigation by animal experiments should be performed for a clinical examination.

- *Organic synthesis*

There are little studies of an organic synthesis by NEAPPs against many reports about the decomposition for treating volatile organic compounds (VOC). The organic species synthesis by using NEAPPs is a new field of science. Therefore, more basic knowledge of the reaction mechanism between the NEAPP and organic components is needed. By the elucidation, a new efficient organic synthesis theory using NEAPPs should be established for not only oxalic acid but also other useful organic compounds.

1) Elucidation of the basic reaction mechanisms for NEAPP organic synthesis

In this study, the essential components for calcium oxalate synthesis and those roles are identified. The oxalic acid is synthesized from glucose. However, the oxalic acid synthesis mechanism is unclear. The elucidation could be performed by analyzing other products shown in Chapter 8, for example, by using GC-MS analysis. The elucidation could open not only a new fundamental field but also a plan for the next study of NEAPP organic synthesis.

One of interesting organic species is tartaric acid $(\text{CH}(\text{OH})\text{COOH})_2$. It is also industrially valuable and only synthesized by biosynthesis now.

Acknowledgements

The present research was performed in Professor Hori and Professor Sekine Laboratory, Plasma Nanotechnology Research Center, Nagoya University, Author would like to appreciate his research adviser, Professor Masaru Hori, Institutes of Innovation for Future Society, Nagoya University, for his guidance, advices and encouragements through the course of this research. He is grateful to Professor Masaaki Mizuno, Center for Advanced Medicine and Clinical Research, Nagoya University. The author also would like to thank his vice-adviser, Professor Makoto Sekine, Plasma Nanotechnology Research Center, Nagoya University, for lots of valuable comments. At the same time, he wishes to express his gratitude to his vice-adviser, Specially Appointed Professor Kenji Ishikawa, Plasma Nanotechnology Research Center, Nagoya University, for his valuable suggestions and educational coaching. The author also would like thank to his vise-adviser, Specially Appointed Instructor Hiromasa Tanaka, Institutes of Innovation for Future Society, Nagoya University, for giving knowledge of a new ground.

The author express his gratitude feel grateful for Professor Masaru Hori, Institutes of Innovation for Future Society, Nagoya University, Professor Kazuo Nakazato, Department of Electrical Engineering and Computer Science, Nagoya University, Professor Hirotaka Toyoda, Department of Electrical Engineering and Computer Science, Nagoya University, Professor Motonobu Goto, Department of Chemical and Biological Engineering, Nagoya University, Professor Makoto Sekine, Plasma Nanotechnology Research Center, Nagoya University, Specially Appointed Professor Kenji Ishikawa, Plasma Nanotechnology Research Center, Nagoya University, Specially Appointed

Acknowledgements

Professor Satomi Tajima, Plasma Nanotechnology Research Center, Nagoya University, for grateful advises for editing the thesis.

The author is great thankful to Professor Masaaki Mizuno, Department of Medicine, Nagoya University, Professor Fumitaka Kikkawa, Department of Medicine, Nagoya University, Associate Professor Hiroaki Kajiyama, Department of Medicine, Nagoya University, Professor Yoko Yamanishi, Mechanical Engineering, Kyusyu University, Professor Takashi Kondo, Radiological Sciences, Toyama University, Instructor Kae Nakamura, Department of Medicine, Nagoya University, Mr. Shinya Sugiura, DENSO corporation, Mr. Akio Sugiura, DENSO corporation, Mr. Takashi Aoki, DENSO corporation, Mr. Shingo Kondo, DENSO corporation, Mr. Kazutoshi Ito, DENSO corporation, for their great advises of a new field.

The author is enormous grateful to Professor Masafumi Ito, Department of Electrical and Electronic Engineering, Meijo University, Associate Professor Hiroki Kondo, Plasma Nanotechnology Research Center, Nagoya University, Specially Appointed Assistant Professor Hiroshi Hashizume, Institutes of Innovation for Future Society, Nagoya University, Assistant Professor Keigo Takeda, Department of Electrical Engineering and Computer Science, Nagoya University, Specially Visiting Professor Toshio Hayashi, Plasma Nanotechnology Research Center, Nagoya University, Professor Takayuki Ota, Department of Electrical and Electronic Engineering, Meijo University, Specially Appointed Professor Hitoshi Ito, Plasma Nanotechnology Research Center, Nagoya University, Specially Appointed Professor Osamu Oda, Plasma Nanotechnology Research Center, Nagoya University, Specially Appointed Professor Naohiro Shimizu, Plasma Nanotechnology Research Center, Nagoya University, for their valuable advises for his thesis.

Acknowledgements

The author express obligation to Professors discussed in technological meetings, Professor Masaharu Shiratani, Electrical and Electronic Engineering, Kyusyu University, Professor Yuichi Setsuhara, Joining and Welding Research Institute, Osaka University, Toshiro Kaneko, Electronic Engineering, Tohoku University, Joe Ikehara Advanced Industrial Science and Technology, Associate Professor Ryugo Tero, Environmental and Life Sciences, Toyohashi University of Technology, Associate Professor Giichiro Uchida, Joining and Welding Research Institute, Osaka University, Assistant Professor Hirofumi Kurita, Environment and Biotechnology, Toyohashi University of Technology, for their precise indications.

The author also give his thank for co-worked students, Mr. Takuya Towatari, Mr. Mori, Mr. Jun Kobayashi, Mr. Hiroaki Sakakura, Mr.. Keisuke Ok, Mr. Tomoaki Sago, Mr. Satoshi Yuruzume, in Prof Ito and Prof Ota Laboratory and Mr. Pak, Mr. Atsushi Ando, Mr. Takusei Liu, Mr. Tomoki Amano, Mr. Takashi Kako, Mr. Yhang Cho, Mr. Yohei Takahashi, Mr. Masakazu Tomatsu, Mr. Borude Ranjit Rohidas, Mr. Atsuki Asano, Mr. Syunichi Sato, Mr. Shinnosuke Takai, Mr. Suiki Tanaka, Mr. Kenichi naito, Mr. Naoki Yoshitake, Mr. Masahito Imamura, Mr. Toshinari Ueyama, Mr. Tomonori Ichikawa, Mr. Katsumi Takeda, Mr. Kai, Ms. Kaku in Prof Hori and Prof Sekine Laboratory. Especially, great appreciation was given by the author to Mr. Shun Imai, Mr. Takumi Ito, Mr. Kazuki Iwamoto, Mr. Hirotsugu Sugiura, Mr. Kazuaki Kojima, Mr. Takumi Kumakura, Mr. Peter Pan, Mr. Yusuke Fukinaga, who are classmates of the author, and Mr. Kuangda Sun, Mr. Ryo Furuta, Mr. Takuya Tonami, Mr. Yukihiro Kuokawa, Mr. Daiki Kannno, Ms. Mika Takahashi, Mr. Ren Kuramashi, Ms. Kaede Katsuno, Mr. Yugo Hosoi, Mr. Kaiji Murakami, Mr. Soutaro Yamaoka, who was members of a study group of a plasma bio-application.

Acknowledgements

The author also appreciate to staffs of the laboratory, Dr. Takayoshi Tsutsumi, Dr. Ru Yu, Dr. Cho, Dr. Frank Wilson, Ms. Kuwabara, Ms. Teshigawara, Ms. Nishiyama, for their kindness.

Finally, the author would give his greatest thank to his family for their excellent supports and to Professor Hori for giving a chance and an environment for his drastic growth.

Naoyuki Kurake

February 2017

List of papers related to this thesis

1. Original papers

Title	Journal	Authors
1 Cell survival of glioblastoma grown in medium containing hydrogen Peroxide and/or nitrite, or in plasma-activated medium	Archives of Biochemistry and Biophysics, Vol.605, pp.102-108 (2016)	<u>N.Kurake</u> , H. Tanaka, K. Ishikawa, T. Kondo, M. Sekine, K. Nakamura, H. Kajiyama, F. Kikkawa, M. Mizuno, M. Hori
2 Synthesis of calcium oxalate crystals in culture medium irradiated with non-equilibrium atmospheric pressure plasma	Applied Physics Express, Vol.9, 096201 (2016)	<u>N.Kurake</u> , H. Tanaka, K. Ishikawa, K. Nakamura, H. Kajiyama, F. Kikkawa, M. Mizuno, Y. Yamanishi, M. Hori
3 Effects of $\cdot\text{OH}$ and $\cdot\text{NO}$ radicals in the aqueous phase on H_2O_2 and NO_2^- synthesized in plasma activated medium	Journal of Physics D: Applied Physics, Submitted	<u>N.Kurake</u> , H. Tanaka, K. Ishikawa, T. Kondo, K. Nakamura, H. Kajiyama, F. Kikkawa, M. Mizuno, K. Takeda, H. Hashizume, M. Hori
4 Synthesis of oxalate crystals from D-glucose diluted in an inorganic solution by irradiation of non-equilibrium atmospheric-pressure plasma	Journal of Applied Physics, Submitted	<u>N.Kurake</u> , H. Tanaka, K. Ishikawa, K. Nakamura, H. Kajiyama, F. Kikkawa, M. Mizuno, M. Hori
5 Quantitative metabolome profiling of glioblastoma disordered by antitumor effect of plasma activated medium (PAM)	To be submitted	<u>N.Kurake</u> , H. Tanaka, K. Ishikawa, K. Nakamura, H. Kajiyama, F. Kikkawa, M. Mizuno, M. Hori

List of papers related to this thesis

6	Dynamic Observation of Intracellular Changes and Structural Disruption in Plasma-irradiated Budding Yeast Cells Using Multiplex Coherent Anti-Stokes Raman Scattering Microscopy	Physical Chemistry Chemical Physics, Submitted	R. Furuta, <u>N. Kurake</u> , K. Ishikawa, K. Takeda, H. Hashizume, H. Kondo, T. Ohta, M. Ito, M. Sekine, M. Hori
7	Dynamic Changes of Lipid Droplets and Caspases in HeLa Cells Cultured in Plasma-Activated Medium: Analyses with Multiplex Coherent Anti-Stokes Raman Scattering (CARS) Microscopy	Biochimica et Biophysica Acta. Molecular Cell Research, Submitted	R. Furuta, <u>N. Kurake</u> , K. Ishikawa, K. Takeda, H. Tanaka, H. Hashizume, H. Kondo, T. Ohta, M. Ito, M. Sekine, M. Hori

2. International conferences

Title	Conference	Authors	
1	Chemical Analysis of Antitumor Effect of Plasma-Activated-Medium	COST Action TD1208 2 nd Annual Meeting, March 10-13, Lisbon(Portugal), (2014)	<u>N. Kurake</u> , H. Tanaka, K. Ishikawa, K. Nakamura, H. Kajiyama, F. Kikkawa, T. Kondo, M. Mizuno, K. Takeda, H. Kondo, M. Sekine, M. Hori
2	Electron spin resonance study of Plasma-Activated-Medium	5 th International Conference on Plasma Medicine, May 18-23, Nara(Japan), (2014)	K. Ishikawa, <u>N. Kurake</u> , H. Tanaka, T. Kondo, K. Nakamura, H. Kajiyama, F. Kikkawa, M. Mizuno, K. Takeda, H. Kondo, M. Sekine, M. Hori
3	Electron spin resonance study of plasma-liquid medium interactions	International Workshop on Diagnostics and Modelling for Plasma Medicine, May 23-24, Nara(Japan), (2014)	K. Ishikawa, <u>N. Kurake</u> , H. Tanaka, T. Kondo, K. Nakamura, H. Kajiyama, F. Kikkawa, M. Mizuno, K. Takeda, H. Kondo, M. Sekine, M. Hori
4	Chemical analysis of plasma-activated-medium for understanding mechanism of its antitumor effect	19th Korea-Japan Workshop on Advanced Plasma Processes and Diagnostics and 6th Workshop for NU-SKKU Joint Institute for Plasma-Nano Materials, July 6-7, Gunsan(Korea), (2014)	<u>N. Kurake</u> , H. Tanaka, K. Ishikawa, K. Nakamura, H. Kajiyama, F. Kikkawa, T. Kondo, M. Mizuno, K. Takeda, H. Kondo, M. Sekine, M. Hori

List of papers related to this thesis

Title	Conference	Authors
5 Electron spin resonance study of Plasma-Activated-Medium (PAM)	2014 Materials Research Society Fall Meeting and Exhibit, November 30-December 5, Boston(USA), (2014)	M. Hori, <u>N. Kurake</u> , H. Tanaka, K. Ishikawa, K. Nakamura, H. Kajiyama, F. Kikkawa, T. Kondo, M. Mizuno, K. Takeda, H. Kondo, M. Sekine
6 Chemical analysis of antitumor effect of Plasma-Activated-Medium	7 th International Symposium on Advanced Plasma Science and Its Applications for Nitrides and Nanomaterials / 8 th International Conference on Plasma-Nano Technology and Science, March 26-31, Nagoya(Japan), (2015)	<u>N. Kurake</u> , H. Tanaka, K. Ishikawa, K. Nakamura, H. Kajiyama, F. Kikkawa, T. Kondo, M. Mizuno, K. Takeda, H. Kondo, M. Sekine, M. Hori
7 Effects of long-lived reactive species in the Plasma-Activated-Medium	The 2 nd International Workshop on Plasma for Cancer Therapy, March 16-17, Nagoya(Japan), (2015)	<u>N. Kurake</u> , H. Tanaka, K. Ishikawa, K. Nakamura, H. Kajiyama, F. Kikkawa, T. Kondo, M. Mizuno, K. Takeda, H. Kondo, M. Sekine, M. Hori
8 Hydrogen peroxide and nitrous ion generated in culture media by irradiation of non-equilibrium atmospheric pressure plasmas	The 10 th Asian-European International Conference on Plasma Surface Engineering, September 20-24, Jeju(Korea), (2015)	<u>N. Kurake</u> , H. Tanaka, K. Ishikawa, K. Nakamura, H. Kajiyama, F. Kikkawa, T. Kondo, M. Mizuno, K. Takeda, H. Kondo, M. Sekine, M. Hori
9 Effects of Plasma-Activated Medium on Surface Morphologies of Lipid Bilayers	The 10 th Asian-European International Conference on Plasma Surface Engineering, September 20-24, Jeju(Korea), (2015)	T. Tonami, <u>N. Kurake</u> , H. Hashizume, H. Kondo, K. Ishikawa, K. Takeda, H. Tanaka, M. Sekine, M. Hori1, M. Ito, R. Tero
10 Antitumor effect of synergistic contribution of nitrite and hydrogen peroxide in the Plasma-Activated-Medium	68 th Gaseous Electronics Conference/9 th International Conference on Reactive Plasmas/33 rd Symposium on Plasma Processing, October 12-16, Honolulu(Hawaii), (2015)	<u>N. Kurake</u> , H. Tanaka, K. Ishikawa, K. Nakamura, H. Kajiyama, F. Kikkawa, T. Kondo, M. Mizuno, K. Takeda, H. Kondo, M. Sekine, M. Hori
11 Antitumor effect of Plasma-Activated-Medium (PAM) added with scavengers	8 th International Symposium on Advanced Plasma Science and Its Applications for Nitrides and Nanomaterials / 9 th International Conference on Plasma-Nano Technology and Science, March 6-10, Nagoya(Japan), (2016)	<u>N. Kurake</u> , H. Tanaka, K. Ishikawa, K. Nakamura, H. Kajiyama, F. Kikkawa, T. Kondo, M. Mizuno, K. Takeda, H. Kondo, M. Sekine, M. Hori

List of papers related to this thesis

Title	Conference	Authors
12 Enhancement of nitrite for cancer killing by hydrogen peroxide on the Plasma-Activated-Medium (PAM)	43 rd IEEE International Conference on Plasma Science, June 19-23, Banff(Canada), (2016)	<u>N. Kurake</u> , H. Tanaka, K. Ishikawa, K. Nakamura, H. Kajiyama, F. Kikkawa, T. Kondo, M. Mizuno, K. Takeda, H. Kondo, M. Sekine, M. Hori
13 Latent chemistry in plasma activated medium (PAM)	20th International Vacuum Congress, August 21-26, Busan(Korea), (2016)	<u>N. Kurake</u> , H. Tanaka, H. Mizuno, H. Hashizume, K. Takeda, H. Kondo, M. Sekine, T. Kondo, S. Ohnuma, M. Kato, K. Nakamura, H. Kajiyama, F. Kikkawa, M. Mizuno, M. Hori
14 Particulates generation in the plasma activated medium (PAM)	6 th International Conference on Plasma Medicine, September 4-9, Bratislava(Slovakia), (2016)	<u>N. Kurake</u> , H. Tanaka, K. Ishikawa, H. Hashizume, K. Nakamura, H. Kajiyama, F. Kikkawa, T. Kondo, M. Mizuno, K. Takeda, H. Kondo, M. Sekine, M. Hori
15 Metabolic profiles on glioblastoma (U251SP) modified in plasma-activated medium (PAM) cultivation	6 th International Conference on Plasma Medicine, September 4-9, Bratislava(Slovakia), (2016)	K. Ishikawa, <u>N. Kurake</u> , H. Tanaka, H. Hashizume, K. Takeda, K. Nakamura, H. Kajiyama, H. Kondo, M. Sekine, M. Kato, M. Mizuno, F. Kikkawa, M. Hori
16 Generation of active species in laser-induced-plasma activated medium	6 th International Conference on Plasma Medicine, September 4-9, Bratislava(Slovakia), (2016)	Y. Kurokawa, <u>N. Kurake</u> , K. Takeda, K. Ishikawa, H. Hashizume, H. Tanaka, H. Kondo, M. Sekine, M. Hori
17 Analysis of the crystal synthesized in the medium by the non-equilibrium atmospheric pressure plasma (NEAPP)	69 th Annual Gaseous Electronics Conference, October 10-14, Bochum(Germany), (2016)	<u>N. Kurake</u> , H. Tanaka, K. Ishikawa, H. Hashizume, K. Nakamura, H. Kajiyama, F. Kikkawa, T. Kondo, M. Mizuno, K. Takeda, H. Kondo, M. Sekine, M. Hori
18 Generation of Reactive Species in Medium Irradiated Laser-Induced-Plasmas	American Vacuum Society (AVS) 63 rd International Symposium and Exhibition, November 6-11, Nashville(USA), (2016)	Y. Kurokawa, <u>N. Kurake</u> , K. Takeda, K. Ishikawa, H. Hashizume, H. Tanaka, H. Kondo, M. Sekine, M. Hori

List of papers related to this thesis

Title	Conference	Authors
19 Synthesis and crystallization of oxalates in glucose-containing liquids irradiated with non-equilibrium atmospheric pressure plasmas	International Conference on Plasma Medical Science Innovation 2017(ICPMSI2017), February 27-28, Nagoya(Japan), (2017)	<u>N. Kurake</u> , H. Tanaka, K. Ishikawa, K. Nakamura, H. Kajiyama, F. Kikkawa, M. Mizuno, K. Takeda, H. Kondo, M. Sekine, M. Hori
20 A mechanism on generations of H ₂ O ₂ and NO ₂ ⁻ in plasma activated medium	International Conference on Plasma Medical Science Innovation 2017(ICPMSI2017), February 27-28, Nagoya(Japan), (2017)	<u>N. Kurake</u> , H. Tanaka, K. Ishikawa, K. Nakamura, H. Kajiyama, F. Kikkawa, T. Kondo, M. Mizuno, K. Takeda, H. Kondo, M. Sekine, M. Hori
21 Enhancement of cancer cell killing effect of hydrogen peroxide by nitrite existence in Plasma Activated Medium	International Conference on Plasma Medical Science Innovation 2017(ICPMSI2017), February 27-28, Nagoya(Japan), (2017)	<u>N. Kurake</u> , H. Tanaka, K. Ishikawa, K. Nakamura, H. Kajiyama, F. Kikkawa, M. Mizuno, K. Takeda, H. Kondo, M. Sekine, M. Hori
22 Antitumor Effects of LASER-Generated Plasma Activated Medium (LPAM) With and Without Catalase	International Conference on Plasma Medical Science Innovation 2017(ICPMSI2017), February 27-28, Nagoya(Japan), (2017)	Y. Kurokawa, <u>N. Kurake</u> , K. Takeda, K. Ishikawa, H. Hashizume, H. Tanaka, H. Kondo, M. Sekine, M. Hori
23 Antitumor effect of culture medium irradiated with non-equilibrium atmospheric pressure plasmas under purge of ambient by N ₂ and O ₂ mixtures	International Conference on Plasma Medical Science Innovation 2017(ICPMSI2017), February 27-28, Nagoya(Japan), (2017)	Y. Hosoi, R. Furuta, <u>N. Kurake</u> , K. Ishikawa, H. Hashizume, H. Tanaka, K. Takeda, H. Kondo, M. Sekine, M. Hori
24 Anti-Tumor Effects of Plasma-Activated Medium added with Fullerenol	International Conference on Plasma Medical Science Innovation 2017(ICPMSI2017), February 27-28, Nagoya(Japan), (2017)	D. Kanno, <u>N. Kurake</u> , H. Tanaka, H. Hashizume, K. Takeda, H. Kondo, K. Ishikawa, M. Sekine, and M. Hori
25 Elucidation of the Effects of Plasma-Activated Medium on Supported Lipid Bilayers by Employing High-Speed Atomic Force Microscopy	International Conference on Plasma Medical Science Innovation 2017(ICPMSI2017), February 27-28, Nagoya(Japan), (2017)	T. Tonami, <u>N. Kurake</u> , H. Hashizume, H. Kondo, K. Ishikawa, K. Takeda, H. Tanaka, M. Sekine, M. Ito, R. Tero, M. Hori
26 Effects of dielectric walls on atmospheric-pressure plasma discharges	International Conference on Plasma Medical Science Innovation 2017(ICPMSI2017), February 27-28, Nagoya(Japan), (2017)	K. Katsuno, <u>N. Kurake</u> , K. Ishikawa, H. Hashizume, H. Tanaka, H. Kondo, M. Sekine, M. Hori

List of papers related to this thesis

Title	Conference	Authors
27 Killing effects of HeLa cells in Laser-generated Plasma Activated Medium (LPAM)	9 th International Symposium on Advanced Plasma Science and Its Applications for Nitrides and Nanomaterials / 10 th International Conference on Plasma-Nano Technology and Science (ISPlasma 2017 / IC-PLANTS 2017), March 1-5, Nagoya(Japan), (2017)	Y. Kurokawa, <u>N. Kurake</u> , K. Takeda, K. Ishikawa, H. Hashizume, H. Tanaka, H. Kondo, M. Sekine, M. Hori
28 Effects of Reactive Oxygen and Nitrogen Species in Plasma-Activated Medium on Supported Lipid Bilayers	9 th International Symposium on Advanced Plasma Science and Its Applications for Nitrides and Nanomaterials / 10 th International Conference on Plasma-Nano Technology and Science (ISPlasma 2017 / IC-PLANTS 2017), March 1-5, Nagoya(Japan), (2017)	T. Tonami, <u>N. Kurake</u> , H. Hashizume, H. Kondo, K. Ishikawa, K. Takeda, H. Tanaka, M. Sekine, M. Ito, R. Tero, M. Hori

3. Awards

- **First prize**, *8th Plasma electronics incubation hall* (domestic), Aug. 31-Sept. 2, Shizuoka(Japan), (2014).
- **Student Award (gold prize)**, *The 10th Asian-European International Conference on Plasma Surface Engineering*, Sept. 20-24, Jeju(Korea), (2015).
- **Excellent Presentation Award**, *8th International Symposium on Advanced Plasma Science and Its Applications for Nitrides and Nanomaterials / 9th International Conference on Plasma-Nano Technology and Science*, March 6-10, Nagoya(Japan), (2016).
- **APEX spotlight 2016**, “Synthesis of calcium oxalate crystals in culture medium irradiated with non-equilibrium atmospheric-pressure plasma” *Applied Physics Express*, **9**, 096201 (2016).
- **Finalist of “GEC Student Award for Excellence”**, *69th Annual Gaseous Electronics Conference*, October 10-14, Bochum(Germany), (2016).